



City Research Online

City, University of London Institutional Repository

Citation: Forsyth, D. I. (2002). Fibre Optic Sensors Based on Fluorescence Techniques for Temperature and Strain Measurement. (Unpublished Doctoral thesis, City, University of London)

This is the accepted version of the paper.

This version of the publication may differ from the final published version.

Permanent repository link: <https://openaccess.city.ac.uk/id/eprint/30853/>

Link to published version:

Copyright: City Research Online aims to make research outputs of City, University of London available to a wider audience. Copyright and Moral Rights remain with the author(s) and/or copyright holders. URLs from City Research Online may be freely distributed and linked to.

Reuse: Copies of full items can be used for personal research or study, educational, or not-for-profit purposes without prior permission or charge. Provided that the authors, title and full bibliographic details are credited, a hyperlink and/or URL is given for the original metadata page and the content is not changed in any way.

City Research Online:

<http://openaccess.city.ac.uk/>

publications@city.ac.uk

**Fibre optic sensors based on
fluorescence techniques for
temperature and strain measurement**

David I. Forsyth

Thesis submitted for examination for the degree of

Doctor of Philosophy

at

City University

School of Engineering

July 2002

Table of Contents

Table of Contents.....	2
List of Tables.....	9
List of Figures.....	11
Acknowledgements.....	17
Copyright Declaration.....	20
Abstract.....	21
Symbols and Abbreviations.....	22
1. Optical Fibre sensors.....	24
1.1 Abstract.....	24
1.2 Introduction.....	25
1.3 Optical fibre sensor science.....	26
1.3.1 Historical steps.....	26
1.3.2 Structure of optical fibres.....	29
1.3.3 Characteristics, advantages and capabilities of optical fibre sensors.....	31
1.3.3.1 Characteristics.....	31
1.3.3.2 Advantages.....	33
1.3.3.3 Capabilities and significance.....	34
1.3.4 Physics of fibre optic sensing.....	35
1.3.4.1 Intensiometric fibre optic sensors.....	36
1.3.4.2 Interferometric fibre optic sensors.....	37
1.3.4.3 Polarimetric fibre optic sensors.....	40
1.3.4.4 Modalmetric fibre optic sensors.....	40
1.3.5 R&D trends in fibre optic sensor systems.....	41
1.3.6 Summary.....	44
1.4 Optical fibre temperature sensing.....	44

Table of Contents

1.4.1	Introduction.....	44
1.4.2	Industrial applications of fibre optic temperature sensors.....	45
1.4.3	Fibre temperature sensing techniques.....	46
1.4.4	Fluorescence-based techniques.....	52
1.4.4.1	Fluorescence lifetime-based techniques.....	54
1.5	Optical fibre strain sensing.....	65
1.5.1	Introduction and techniques of measurement.....	65
1.5.2	Recent advances in applications of fibre optic strain sensors.....	66
1.6	Summary and scope of the thesis.....	68
1.6.1	Aims and objectives.....	68
1.6.2	Structure of thesis.....	69
1.7	References.....	70
2.	Temperature-strain discrimination.....	80
2.1	Abstract.....	80
2.2	Introduction.....	81
2.3	Theory.....	82
2.4	Temperature-strain discrimination techniques.....	85
2.4.1	Previous work.....	85
2.4.1.1	General approaches.....	85
2.4.1.2	With relevance to the strain sensitivity of fluorescence lifetime.....	87
2.4.2	Other recent work.....	89
2.5	Summary.....	91
2.6	References.....	93

Table of Contents

3. Optical fibre temperature and strain sensors based on fluorescence lifetime monitoring	
3.1 Abstract.....	98
3.2 Introduction.....	99
3.3 Erbium doped fibre based sensors.....	99
3.3.1 200 ppm and 960 ppm doped fibres.....	100
3.3.1.1 Experimental arrangement.....	100
3.3.1.2 Results.....	102
3.3.1.3 Discussion.....	107
3.3.2 1050 ppm doped fibre.....	108
3.3.2.1 Experimental arrangement.....	108
3.3.2.2 Results.....	110
3.3.2.3 Discussion.....	112
3.3.3 4370 ppm doped fibre.....	112
3.3.3.1 Experimental arrangement.....	112
3.3.3.2 Results.....	114
3.3.3.3 Discussion.....	117
3.3.4 Erbium doped fibre based sensors – summary.....	118
3.4 Erbium/Ytterbium co-doped fibre based sensors.....	119
3.4.1 Introduction.....	119
3.4.1.1 Theory.....	119
3.4.1.2 Previous work.....	121
3.4.2 Photosensitively enhanced Er ³⁺ Yb ³⁺ co-doped fibre.....	121
3.4.2.1 Experimental arrangement.....	122
3.4.2.2 Results.....	123

Table of Contents

A) Temperature characteristics.....	123
B) Annealing.....	124
3.4.2.3 Discussion.....	126
3.5 Neodymium doped fibre based sensors.....	127
3.5.1 Previous work.....	127
3.5.2 1460 ppm Nd ³⁺ doped fibre.....	127
3.5.2.1 Experimental arrangement.....	127
3.5.2.2 Results.....	128
A) sensor 1.....	128
B) sensor 2.....	130
C) sensor 3.....	131
3.5.2.3 Discussion.....	132
3.6 Thulium/Holmium co-doped fibre based sensors.....	134
3.6.1 Introduction.....	134
3.6.2 4600 ppm/1100 ppm co-doped Tm ³⁺ /Ho ³⁺ fibre.....	136
3.6.2.1 Experimental arrangements.....	137
A) PLD system method.....	137
B) A/D card method.....	138
3.6.2.2 Results.....	143
A) PLD system.....	143
i) Temperature calibration.....	143
ii) Strain calibration.....	144
B) A/D card.....	145
i) Temperature calibration.....	145
ii) Strain calibration.....	147

Table of Contents

iii) High temperature calibrations and annealing effects...	149
a) High temperature calibration.....	149
b) Annealing effects.....	150
3.6.3 Tm ³⁺ /Ho ³⁺ co-doped fibre – conclusions.....	156
3.7 Tm ³⁺ in Y ₂ O ₃ powder probe sensor.....	156
3.7.1 Introduction.....	156
3.7.2 Previous work.....	158
3.7.3 Experimental method and results.....	160
3.7.3.1 Heat treatment.....	163
3.7.3.2 Fluorescence at 800 nm band.....	164
3.7.3.3 Fluorescence at 1.45 μm and 1.7 μm.....	165
3.7.4 Modelling of results.....	166
3.7.5 Discussion.....	168
3.7.6 Further probe analyses.....	169
3.8 Effects of sensor lengths and other parameters of interest.....	172
3.8.1 Introduction.....	172
3.8.2 Sample size.....	175
3.8.2.1 Erbium doped fibres.....	175
A) Experimental arrangement used.....	175
B) Results.....	176
i) 192 ppm doped Er ³⁺ fibre (4 μm /125 μm core/cladding).....	176
ii) 1000 ppm doped Er ³⁺ fibre (5.2 μm /125 μm core/cladding).....	177
iii) 4500 ppm doped Er ³⁺ fibre (6.2 μm /125 μm core/cladding).....	178
3.8.2.2 Er ³⁺ Yb ³⁺ co-doped fibre.....	179

Table of Contents

A) Experimental arrangement used.....	179
B) Results.....	179
3.8.2.3 Tm ³⁺ Ho ³⁺ co-doped fibre.....	180
A) Experimental arrangement used.....	180
B) Results.....	180
3.8.2.4 Conclusions.....	181
3.8.3 Pump power.....	182
3.8.3.3 Tm ³⁺ Ho ³⁺ co-doped fibre.....	182
3.8.3.4 Conclusions.....	183
3.8.4 Summary.....	183
3.9 Chapter summary.....	184
3.10 References.....	188
4. Fluorescence based temperature and strain measurement by the incorporation of Fibre Bragg gratings (FBGs).....	192
4.1 Abstract.....	192
4.2 Introduction.....	193
4.3 FBG background and sensing mechanism.....	194
4.3.1 Background.....	194
4.3.2 FBG sensing mechanism.....	196
4.4 Doped fibre based sensors combined with FBGs.....	196
4.4.1 4370ppm Erbium doped fibre with FBG as separate component.....	196
4.4.1.1 Experimental arrangement.....	197
4.4.1.2 Experimental results.....	200
4.4.1.3 Discussion.....	207
4.4.2 Doped fibres with FBGs written in.....	208

Table of Contents

4.4.2.1 Experimental Arrangement.....	208
4.4.2.2 Results and discussion.....	212
4.4.2.3 Means offset modelling.....	225
4.4.2.4 OSA spectra.....	227
4.4.2.5 Conclusions.....	228
4.4.3 High temperature FBG performance.....	229
4.4.4 High temperature annealing effects of Er ³⁺ :Yb ³⁺ co-doped photosensitive fibre.....	232
4.5 Conclusions.....	234
4.6 References.....	237
5. Conclusions and future work.....	241
5.1 Abstract.....	241
5.2 Summary of achievements.....	242
5.3 Current and future exponents of the fluorescent lifetime.....	244
5.3.1 Commercial uses.....	244
5.3.2 Academic uses.....	246
5.4 References.....	248
List of publications arising from thesis.....	251

List of Tables

Table 1.1 Some parameters and events which may be detected using fibre optic sensors....	32
Table 1.2 Advantages of fibre optic sensors.....	33
Table 1.3 Sensing parameters used for condition monitoring applications.....	35
Table 1.4 Strain and temperature sensitivities of various fibre optic sensors.....	43
Table 2.1 Summary of techniques and reported errors (rms) from various dual temperature/strain (T, ϵ) fibre-based sensor schemes (ranges used in brackets).....	92
Table 3.1 Comparison of performance of doped fibres for sensor use.....	108
Table 3.2 Comparison of performance from all dopant levels of Er^{3+} tested.....	118
Table 3.3 Strain and temperature sensitivity of fluorescence lifetimes ($^*\text{Tm}^{3+}/\text{Ho}^{3+}$ temperature sensitivity data at 20°C calculated from data).....	149
Table 3.4 Lifetime (μs) rms errors arising from fitting 3 rd order polynomial fits to the $\text{Tm}^{3+}/\text{Ho}^{3+}$ annealing data over each of the above ranges.....	153
Table 3.5 Temperature (°C) rms errors arising from fitting 3 rd order polynomial fits to the $\text{Tm}^{3+}/\text{Ho}^{3+}$ annealing data over each of the above ranges.....	154
Table 3.6 Lifetime (μs) rms errors arising from fitting 4 th order polynomial fits to the $\text{Tm}^{3+}/\text{Ho}^{3+}$ annealing data over each of the above ranges.....	154
Table 3.7 Temperature (°C) rms errors arising from fitting 4 th order polynomial fits to the $\text{Tm}^{3+}/\text{Ho}^{3+}$ annealing data over each of the above ranges.....	155
Table 3.8 Heat treatments for $\text{Tm}^{3+}:\text{Y}_2\text{O}_3$	163
Table 3.9 Comparative data from fibres tested so far.....	186
Table 3.10 Re-analysed comparative data from fibres tested so far.....	187
Table 4.1 Temperature and strain coefficients of the fluorescence lifetime and the FBG wavelength for all three sensors.....	214

List of Tables

Table 4.2 The standard deviation of differences between temperature (ΔT) and strain ($\Delta \epsilon$) values calculated using measurements from the optical sensors and the known parameters applied during the tests.....	216
Table 4.3 Average maximum (\hat{N}) non-linearity values (%) obtained from linear fits to lifetimes versus temperature data for all three sensors.....	217
Table 4.4 Lifetime standard deviation (rms) values and corresponding maximum non-linearity (\hat{N} %) values for all lifetime measurements at all applied strains.....	223
Table 4.5 Temperature standard deviation (rms) values and corresponding maximum non-linearity (\hat{N} %) values for all lifetime measurements at all applied strains.....	224
Table 4.6 Accuracies (rms) from the dual T, ϵ fibre-based sensor schemes tested here (shown in bold) compared with some others.....	235
Table 4.7 Comparison of the performances of all fibres.....	236

List of Figures

Fig.1.1 Cross-sectional view of a typical optical fibre.....	30
Fig.1.2 Fibre optic evanescent wave absorption technique.....	37
Fig.1.3 Response characteristics of a fibre optic Bragg grating.....	38
Fig.1.4 Schematic of the decay-time approach.....	56
Fig.1.5 Simplified schematic energy level diagram.....	61
Fig.3.1 Simplified schematic of experimental arrangement used in Er^{3+} doped fibre strain and temperature tests.....	100
Fig.3.2 Lifetime as a function of strain for 960 ppm Er^{3+} doped fibre at 125°C	103
Fig.3.3 Lifetime vs. temperature (without strain) for 960 ppm Er^{3+} doped fibre.....	104
Fig.3.4 Lifetime as a function of strain at 50°C for 200 ppm Er^{3+} doped fibre.....	104
Fig.3.5 Lifetime vs. temperature (without strain) plot for 200 ppm Er^{3+} doped fibre.....	105
Fig.3.6 Strain sensitivity of fluorescent lifetime to temperature for both fibres.....	105
Fig.3.7 Experimental arrangement used for temperature and strain calibration of 1050 ppm Er^{3+} doped fibre.....	109
Fig.3.8 Er^{3+} 1050 ppm temperature calibration (without strain).....	110
Fig.3.9 Er^{3+} 1050 ppm strain sensitivity of the fluorescent lifetime at 100°C	111
Fig.3.10 Er^{3+} 1050 ppm strain sensitivity of the fluorescent lifetime as a function of temperature.....	111
Fig.3.11 Experimental arrangement used for temperature and strain calibration of 4370 ppm Er^{3+} doped fibre.....	113
Fig.3.12 Er^{3+} 4370 ppm fluorescence spectra recorded from OSA.....	114
Fig.3.13 Er^{3+} 4370 ppm fluorescence spectral line broadening with temperature.....	115
Fig.3.14 Er^{3+} 4370 ppm fluorescent lifetime versus temperature.....	116
Fig.3.15 Er^{3+} 4370 ppm fluorescent lifetime strain effect at 40°C	116
Fig.3.16 Er^{3+} 4370 ppm fluorescent lifetime strain effect at 100°C	117

List of Figures

Fig.3.17 Energy levels involved in Er^{3+} Yb^{3+} energy transfer.....	120
Fig.3.18 Er^{3+} Yb^{3+} co-doped fibre experimental set-up for temperature measurement.....	122
Fig.3.19 Er^{3+} Yb^{3+} co-doped fibre initial temperature calibration.....	124
Fig.3.20 Er^{3+} Yb^{3+} co-doped fibre annealing at 800°C for 24 hrs.....	125
Fig.3.21 Er^{3+} Yb^{3+} co-doped fibre annealing effects.....	125
Fig.3.22 Results from previous work on Er^{3+} Yb^{3+} co-doped fibre.....	126
Fig.3.23 Experimental set-up for Nd^{3+} fibre temperature/strain calibration.....	127
Fig.3.24 Nd^{3+} temperature calibration data for sensor 1.....	128
Fig.3.25 Nd^{3+} temperature sensitivities of sensor 1.....	129
Fig.3.26 Nd^{3+} sensor 1 – effect of strain at 100°C.....	129
Fig.3.27 Nd^{3+} sensor 1: strain effect on lifetime at 35°C.....	130
Fig.3.28 Nd^{3+} sensor 2: lifetime versus strain for the minimum, middle and maximum temperatures.....	130
Fig.3.29 Nd^{3+} sensor 3: lifetime versus temperature calibration.....	131
Fig.3.30 Nd^{3+} sensor 3: lifetime versus strain at 30°C and 60°C.....	132
Fig.3.31 Energy level diagram of the Tm^{3+} and Ho^{3+} rare earth ions, showing the transitions previously used and lifetimes obtained in brackets from the relevant energy levels.....	135
Fig.3.32 Energy level diagram of the Tm^{3+} ion, showing transitions of interest.....	135
Fig.3.33 $\text{Tm}^{3+}/\text{Ho}^{3+}$ fibre absorption in the region of 780 nm wavelength (source: INO).136	
Fig.3.34 Schematic of PLD method (A).....	138
Fig.3.35 Experimental arrangement (B) used to measure the temperature and strain dependence of $\text{Tm}^{3+}/\text{Ho}^{3+}$ co-doped fibre.....	139
Fig.3.36 Optical Spectrum Analyzer (OSA) plot recorded at room temperature of 20.5°C (Resolution bandwidth, RBW of 10 nm).....	140

List of Figures

Fig.3.37 Multi-exponential form of $\text{Tm}^{3+}/\text{Ho}^{3+}$ co-doped fibre fluorescence, measured at 22°C.....	141
Fig.3.38 Set up for high temperature analysis of $\text{Tm}^{3+}/\text{Ho}^{3+}$ co-doped fibre.....	142
Fig.3.39 Temperature characteristics of $\text{Tm}^{3+}/\text{Ho}^{3+}$	143
Fig.3.40 Thermal characteristics of the fluorescence of 280 ppm Tm^{3+} -doped fibre.....	143
Fig.3.41 Temperature dependence of the intensities and fluorescent lifetimes of the $^3\text{F}_4$ and $^3\text{H}_4$ energy levels of $\text{Tm}^{3+}/\text{Ho}^{3+}$ co-doped fibre together with the single exponential Prony fit to the fluorescence decay. Solid lines are 3 rd order polynomial fits.....	145
Fig.3.42 $\text{Tm}^{3+}/\text{Ho}^{3+}$ co-doped fibre temperature sensitivities.....	146
Fig.3.43 $\text{Tm}^{3+}/\text{Ho}^{3+}$ co-doped fibre temperature dependent fluorescent intensities.....	147
Fig.3.44 Effect of applied strain on the $^3\text{F}_4$ fluorescence lifetime, measured at 200°C.....	148
Fig.3.45 Strain sensitivity of the $^3\text{F}_4$ and $^3\text{H}_4$ energy level lifetimes of $\text{Tm}^{3+}/\text{Ho}^{3+}$ co-doped fibre together with the single exponential Prony fit to the fluorescence decay at various temperatures.....	148
Fig.3.46 $\text{Tm}^{3+}/\text{Ho}^{3+}$ co-doped fibre high temperature characteristics (up to 900°C) of the energy levels involved (without any thermal annealing).....	150
Fig.3.47 $\text{Tm}^{3+}/\text{Ho}^{3+}$ co-doped fibre samples before and after annealing process (a) sample A and (b) sample B.....	151
Fig.3.48 Sample (a) annealing at 800°C for 28 hours.....	152
Fig.3.49 Sample (b) annealing at 900°C for 70 hours.....	152
Fig.3.50 Results from the previous work with Tm^{3+} in Y_2O_3	158
Fig.3.51 Tm^{3+} in Y_2O_3 energy level diagram showing the relevant electronic energy levels of Tm^{3+} in Y_2O_3 (data from RSTB's database of laser materials, MS474, NASA-LaRC, Hampton, VA23681-2199, USA).....	159
Fig.3.52 Experimental set-up used for Tm^{3+} in Y_2O_3	161

List of Figures

Fig.3.53 Fluorescence @800 nm band - all results.....	162
Fig.3.54 Lifetime of $Tm^{3+}:Y_2O_3$ fluorescence at 800 nm.....	164
Fig.3.55 Regression errors of lifetime data of $Tm^{3+}:Y_2O_3$ fluorescence at 800 nm.....	165
Fig.3.56 Lifetime data of $Tm^{3+}:Y_2O_3$ fluorescence at 1.45 μm and 1.7 μm induced by different wavelength sources.....	166
Fig.3.57 Thermal characteristics of Tm^{3+} fluorescence in Y_2O_3	168
Fig.3.58 Fluorescence at the 800 nm band probe B calibration results.....	170
Fig.3.59 Comparison of probe A and probe B results for fluorescence at the 800 nm band.....	170
Fig.3.60 Probe A and probe B comparisons and exchangeability for fluorescence at the 1 μm + band.....	171
Fig.3.61 Er^{3+} doped fibre experimental set-up for sensor length testing.....	175
Fig.3.62 192 ppm Er^{3+} doped fibre sensor length effects at 26.2°C.....	176
Fig.3.63 1000 ppm Er^{3+} doped fibre sensor length effects at 26.2°C.....	177
Fig.3.64 4500 ppm Er^{3+} doped fibre sensor length effects at 26.2°C.....	178
Fig.3.65 $Er^{3+} Yb^{3+}$ co-doped fibre sensor length effects at 26.2°C.....	179
Fig.3.66 Tm^{3+}/Ho^{3+} co-doped fibre experimental set-up for sensor length testing.....	180
Fig.3.67 Tm^{3+}/Ho^{3+} co-doped fibre experimental results on sensor lengths at 26.8°C.....	181
Fig.3.68 Tm^{3+}/Ho^{3+} co-doped fibre sensor (~10 cm) experimental results on pump power at 26.2°C.....	182
Fig.4.1 An example of a WDM system - the number of gratings depends on the FWHM of the source used.....	195
Fig.4.2 Simplified schematic of the experimental arrangement used for the temperature and strain test of the combined Er^{3+} -doped fibre/FBG sensor.....	197

List of Figures

Fig.4.3 Typical fluorescence spectrum and spectral feature due to the reflection by the FBG shown at three of the temperatures (note: OSA resolution of 1 nm for graph shown).....	200
Fig.4.4 Temperature calibration of the Er^{3+} -doped fibre element of the combined Er^{3+} -doped fibre/FBG sensor (i.e. with zero strain) compared with previous results from the same fibre without grating, both shown over the same temperature range.....	201
Fig.4.5 Strain effect on the lifetime of Er^{3+} -doped fibre element of the combined Er^{3+} -doped fibre/FBG sensor at 25°C, 60°C and 120°C.....	202
Fig.4.6 Strain sensitivity of the Er^{3+} -doped fibre lifetime versus temperature.....	203
Fig.4.7 Wavelength change as a function of temperature for the FBG at three different applied strains.....	204
Fig.4.8 Wavelength change as a function of applied strain for the FBG at three different temperatures.....	204
Fig.4.9 Temperature error in the combined Er^{3+} -doped fibre/FBG strain sensor.....	206
Fig.4.10 Strain error in the combined Er^{3+} -doped fibre/FBG strain sensor.....	206
Fig.4.11 Experimental arrangement used for the temperature and strain calibration of the sensors (sensors 1, 2 and 3 shown as insets).....	210
Fig.4.12 Fluorescence spectra from all three sensors showing intensity dips due to the FBG reflection.....	211
Fig.4.13 Fluorescent lifetime versus temperature calibration data for sensor 3 at minimum and maximum applied strains together with linear fits to the data.....	212
Fig.4.14 Shifts in the fibre Bragg grating wavelength with strain for sensor 3 for a range of temperatures tested.....	213
Fig.4.15 Comparison of the strain sensitivities of fluorescent lifetimes over the full temperature ranges for all three sensors.....	215

List of Figures

Fig.4.16 (a) Fluorescent lifetime versus temperature data obtained at minimum applied strain (221 $\mu\epsilon$) (b) difference between experimental data and linear fit for sensor 3.....	218
Fig.4.17 Graph showing the temperature characteristics of the fluorescent lifetime of all sensors for extended temperature range.....	219
Fig.4.18 (a) Fluorescent lifetime correction of Bragg shifts at constant temperature (30°C) and (b) at constant strain (221 $\mu\epsilon$) for sensor 3.....	220
Fig.4.19 (a) Fluorescent lifetime correction by Bragg shifts at constant temperature (30°C) and (b) at constant strain (221 $\mu\epsilon$) for sensor 3.....	221
Fig.4.20 Comparison of all sensor outputs over full temperature and strain ranges.....	222
Fig.4.21 Sensor 3 – means modelling of baseline values to achieve a combined minima for optimisation of use (over the range 30 –120°C).....	225
Fig.4.22 Sensor 3 – means modelling of baseline values to achieve a combined minima for optimisation of use (over the range 30 –150°C).....	226
Fig.4.23 Sensor 3 – OSA plots of the fluorescence intensity changes with temperature from 80 – 150°C with 150 g mass applied to the fibre (shown at 3 temperatures only).....	227
Fig.4.24 Sensor 3 – OSA plots showing the fluorescence intensity % decrease with increasing temperatures from 80°C with 150g mass applied to the fibre.....	227
Fig.4.25 Long term thermally induced decay effects on FBG performance.....	230
Fig.4.26 Normalised ICC of FBG at each annealing temperature with time.....	231
Fig.4.27 Er ³⁺ :Yb ³⁺ co-doped photosensitive fibre annealing effects.....	233
Fig.4.28 Er ³⁺ :Yb ³⁺ co-doped photosensitive fibre annealing at 800°C for 48 hrs.....	233

Acknowledgements

The work reported in this thesis was carried out under the supervision of Prof. K.T.V.Grattan, with the direction and assistance of various current and former Research Fellows in the *Optical Instrumentation Group* at *City University, London, UK* – namely Dr S.Wade, Dr T.Sun and Dr Z.Y.Zhang. I would, however, particularly like to thank Dr S.Wade (formerly Research Fellow at City University, now presently at the *Optical Technology Research Laboratory, Victoria University, Melbourne, Australia*) for sharing his time, talent and great team working skills in applied optics with me towards the latter part of the practical work, and also for the finesse he showed in getting some of our work published. I wish to also especially thank Prof. K.T.V.Grattan for his understanding and encouragement during my years of study at City, and an extra thanks to Dr T.Sun for her invaluable time and help during the writing-up process.

There are various other members of staff at City University whom I also want to thank for their constant encouragement - Dr W.Boyle, Mr W.Li and in particular Dr Y.M.Gebremichael for his friendliness and approachability. Also, K.T.V.Grattan's secretary Ms. Lecha Kowalska and the Electrical Engineering office staff at City University - Joan Rivellini and Linda Carr – thanks for all your help.

Also, several academic visitors from various parts of the world who assisted me in some of the work:

- A.Arnaud (*Instituto de Ingenieria Electrica, Facultad de Ingenieria, University of the Republic, Montevideo, Uruguay*)

Acknowledgements

- Dr S.J.Zhang (*Department of Physics, Northern Jiaotong University, Beijing 100044, PRC*)
- G.F.Qiu (*School of Mechanical Engineering, Nanjing University of Science and Technology, 200 Xiao Ling Wei, Nanjing 210094, PRC*)
- D.Perciante (*Facultad de Ingeniería, Instituto de Física, J. Herrera y Reissig 565, Montevideo, Uruguay*)
- X.Chen (*Changcheng Institute of Metrology, Beijing 100095, PRC*)

Their team-working contributions are much appreciated, and they have been referenced in some of the published work.

I wish to also thank the *Engineering and Physical Science Research Council (EPSRC)* in the UK for giving me financial support during my studies, and would also like to thank Prof. K.T.V.Grattan for giving me the opportunity to assist in some of the electronics labs and for some additional funding. Additional gratitude also to the *Worshipful Company of Scientific Instrument Makers* for giving me the SIM Prize in February 2000, an award which later enabled me to attend and present a paper at the *14th Optical Fiber Sensors Conference (OFS 2000)* held in Venice, Italy.

The author does not see this thesis as being the product of a period of lonely, isolated research sitting in dingy rooms and reading dusty old books; but as being the result of having had the opportunity to work within an excellent research team enabling him to make a practical contribution to knowledge and real-life measurement problems.

Acknowledgements

Finally, sincere gratitude goes to my family and friends for tolerating me during this busy period of time for me, and for their love and support - especially from my mother, Eve, without whom I would never have been able to achieve this thesis.

Copyright Declaration

The author hereby grants power of discretion to the City University Librarian to allow the thesis to be copied in whole or in part without further reference to the author. This permission covers only single copies made for study process, subject to normal conditions of acknowledgement.

Abstract

The author presents a thesis based upon the use of the fluorescent properties of rare earth doped materials. The thesis commences with a review of the current fibre sensor technology in the field, with special emphasis on those sensors designed for temperature and strain measurement. The use of the physical phenomena of fluorescence produced from rare earth doped optical fibre for temperature measurement is then introduced and explained in more detail, particularly with regard to utilisation of the fluorescence lifetime technique in such sensing, which is then compared to the other fluorescence-based methods for measuring temperature.

The recently discovered small strain sensitivity of the fluorescence lifetime is then introduced as a theoretical candidate for potential application to simultaneous temperature-strain sensing, using two different doped fibres in a single sensing element, and subsequently state-of-the-art temperature-strain discrimination techniques are then explored for the purposes of exploitation to dual measurement.

Results achieved from using the fluorescent lifetime approach for a range of rare earth materials are then presented, followed by further results obtained from combining the lifetime technique with Fibre Bragg gratings (FBGs) for the first time. Also, the irreversible effects upon FBG performance after exposure to long-term high temperatures are explored.

Finally, there is a summary of the work presented in this thesis and the author's opinions on achievements made. Current trends in fluorescence lifetime-based sensing are discussed, both commercially and academically, together with projected work for the future.

Symbols and Abbreviations

A	current, or initial fluorescence amplitude
Λ	pitch length of fibre Bragg grating
α	thermal expansion coefficient, or transition rate ratio
α, β	ratios of transition rates
A/D	analogue to digital
A-DSP	analogue to digital signal processor
ASE	Amplified Spontaneous Emission
CFBG	chirped in-fibre Bragg grating
CO ₂	carbon dioxide
CW	continuous-wave
c	velocity of light <i>in vacuo</i> , $2.9979... \times 10^8$ m/s, or centi-
C_1, C_2	radiation constants, $C_1 = 2\pi hc^2$ and $C_2 = hc/k$
°C	degrees Celsius
DFTS	Dispersive Fourier Transform Spectroscopy
δ	change in, or error
EFPI	extrinsic Fabry-Perot interferometric
$E, \Delta E$	energy and energy splitting between two different energy states
ϵ , or ε	strain
FBG	Fibre Bragg Grating
FIR	Fluorescence Intensity Ratio
f	frequency of a periodic signal
f.s.d	full scale deflection
G	giga, 10^9
g	gravitational constant, ~ 9.81 ms ⁻²
g	degeneracies of energy level
h	Planck constant, 6.625×10^{-34} J s
InGaAs	indium gallium arsenide
K	degrees Kelvin
K_{nT}	temperature coefficient
$K_{n\epsilon}$	strain coefficient
KrF	krypton fluoride
k	kilo, 10^3
k	Boltzmann constant, 1.38×10^{-23} J K ⁻¹
$\lambda, \Delta\lambda$	wavelength, and variance of wavelength
LD	Laser diode
LED	Light emitting diode
$\mu\epsilon$	microstrains (dimensionless 10^{-6} strain unit)
MCDV	Modified Chemical Vapor Deposition
μ	micro, 10^{-6}
MTF	mounted tube furnace
NA	numerical aperture
N	number of atoms occupying an energy level
\hat{N}	maximum non-linearity (expressed as a % of f.s.d)
n	nano, 10^{-9} , population of an energy state or refractive index

Symbols and Abbreviations

OSA	Optical Spectrum Analyser
OTDR	Optical time domain reflectometry
OTDA	Optical time domain analysis
PC	personal computer
POF	Plastic Optical Fibre
ppm	parts per million
PLD	phase-locked detection of fluorescence lifetime
%wt	percentage weight
P _o	maximum power
pH	measure of acidity
pε	picostrains (dimensionless 10 ⁻¹² strain unit)
p	pico, 10 ⁻¹²
RBW	Resolution bandwidth
ρ _e	photo-elastic constant
S/N	signal-to-noise ratio
σ, rms	standard deviation, or root-mean-square
s	seconds
<i>t</i>	time
φ _c	critical angle
<i>T</i> , or T	temperature
τ, L	Fluorescence lifetime, or the time-constant of an exponential signal
Δτ	change in fluorescence lifetime
TTL	Transistor-transistor logic
<i>V</i>	amplitude of a voltage signal
WDM	wavelength division multiplex
w, p, or P	power
<i>w</i>	radiant power per m ²
X ³⁺	trivalent rare earth ion X
ξ	thermo-optic coefficient
YAG	Yttrium Aluminium Garnet
<i>Y</i>	Young's Modulus
<i>z</i>	partition function
ZBLAN	heavy metal fluoride glass (ZrF ₄ , BaF ₂ , LaF ₃ , AlF ₃ , NaF)

Chapter 1

Optical fibre sensors

1.1 Abstract

This chapter presents an overview of current trends in optical fibre based sensing techniques, now used to detect a large range of measurands, with particular emphasis on temperature and strain measurement. It concludes with a consideration of the scope of the work to be presented in this thesis - the thesis structure and the aims and objectives of the work are discussed.

1.2 Introduction

As man inevitably improves the use of technology with time, his science of measurement does the same and this produces new and better ways to measure an increasing range of quantities. The importance of the obtaining of accurate and reliable data from measurements, industrial or otherwise, to any competitive world economy cannot be overlooked as it forms a basis of manufacturing improvement (e.g. quality assurance for better products), helps advance medical science (e.g. biosensors, medical devices etc.), can assist in matters of litigation (e.g. Forensic science, Health and Safety) and generally helps improve quality of life. A wide range of parameters usually need to be quantified on a daily basis with data being obtained from an ever increasing range of sensors - some more accurate, robust, smaller or perhaps simply cheaper than others. Numerous techniques have been developed over the years to achieve this end and are usually based on either electrical, chemical and/or optical principles.

Considerable recent progress has been made in the field of optical sensing, in particular in the field of fibre optical sensing - since its explosive [1] growth in the 1970s, allowing greater flexibility and many characteristic benefits over the then conventional electrical methods. The initial drive for the development of fibre optic sensors came from their potential use in military and aerospace applications, where the cost factors of the introduction of such a new technology were less rigid and the working environment often more hostile than is experienced with other areas of application. In many cases such as these, fibre optic techniques are preferred simply because of the convenience factor from the use of "open air path" optical approaches, through the channelling of the light to and from the region of interest (i.e. waveguide properties). Several possible accurate and reliable fibre

optical approaches are now well developed [2-4] and used to measure a large range of parameters, in many cases by out-performing non-fibre-based-sensors [5].

The more well known, indeed phenomenal recent advances in the fibre optics communications field are now firmly established, and these have not only overshadowed but also complimented the still developing, but somewhat smaller, fibre optic sensor industry. The US, Japan and most European countries now have extensive programs of fibre optic cabling for the main trunk networks of their telecommunications systems. The realisation of the now commonplace fibre-based computer data links and domestic data systems for the home are an example of the superior data handling capacity which fibre optics always possessed over conventional cabling. Consequently, this demand has resulted in the decreased costs of associated fibre optic components (fibres, sources, detectors), thus also benefiting the sensor industry.

1.3 Optical fibre sensor science

1.3.1 Historical steps

There are many significant developments [6] which have historically contributed to the advanced state of fibre optic science as we know it today:

- In 1854, John Tyndall demonstrated to the Royal Society that light could be conducted through a curved stream of water, proving that a light signal could be bent.
- In 1880, Alexander Graham Bell invented his 'Photophone', which transmitted a voice signal on a beam of light. Bell focused sunlight with a mirror and then talked into a

Chapter 1 Optical fibre sensors

mechanism that vibrated the mirror. At the receiving end, a detector picked up the vibrating beam and decoded it back into a voice in the same way a telephone did with electrical signals. Many things - a cloudy day for instance - could interfere with the Photophone, causing Bell to stop any further research with this invention.

- In 1880, William Wheeler invented a system of light pipes lined with a highly reflective coating that illuminated homes by using light from an electric arc lamp placed in the basement and directing the light around the home with the pipes.
- In 1888, the medical team of Roth and Reuss of Vienna used bent glass rods to illuminate body cavities.
- In 1895, French engineer Henry Saint-Rene designed a system of bent glass rods for guiding light images in an attempt at early television.
- In 1898, American David Smith applied for a patent on a bent glass rod device to be used as a surgical lamp.
- In the 1920s, Englishman John Logie Baird and American Clarence W. Hansell patented the idea of using arrays of transparent rods to transmit images for television and facsimiles respectively.
- In 1930, German medical student, Heinrich Lamm was the first person to assemble a bundle of optical fibers to carry an image. Lamm's goal was to look inside inaccessible

Chapter 1 Optical fibre sensors

parts of the body. During his experiments, he reported transmitting the image of a light bulb. The image was of poor quality, however. His effort to file a patent was denied because of Hansell's British patent.

- In 1954, Dutch scientist Abraham Van Heel and British scientist Harold. H. Hopkins separately wrote papers on imaging bundles. Hopkins reported on imaging bundles of unclad fibres while Van Heel reported on simple bundles of clad fibres. He covered a bare fibre with a transparent cladding of a lower refractive index. This protected the fibre reflection surface from outside distortion and greatly reduced interference between fibres. At the time, the greatest obstacle to a viable use of fibre optics was in achieving the lowest signal (light) loss.
- In 1961, Elias Snitzer of American Optical published a theoretical description of single mode fibres, a fibre with a core so small it could carry light with only one waveguide mode. Snitzer's idea was acceptable for a medical instrument looking inside the human body, but the fibre had a light loss equivalent to one decibel per metre. Communications devices needed to operate over much longer distances and required a light loss of no more than 10 or 20 decibels (measurement of the light power) per kilometre.
- In 1964, this critical (and theoretical) specification was identified by Dr. C.K. Kao for long-range communication devices, setting the maximum 10 or 20 decibels of light loss per kilometre standard. Kao also illustrated the need for a purer form of glass to help reduce light loss.

Chapter 1 Optical fibre sensors

- In 1970, one team of researchers began experimenting with fused silica, a material capable of extreme purity with a high melting point and a low refractive index. Corning Glass researchers Robert Maurer, Donald Keck and Peter Schultz invented fibre optic wire or "Optical Waveguide Fibers" (patent #3,711,262) capable of carrying 65,000 times more information than copper wire, through which information encoded on a pattern of light waves could be decoded at a destination even a thousand miles away. The team had solved the problems presented by Dr. Kao.
- In 1975, the United States Government decided to link the computers in the NORAD headquarters at Cheyenne Mountain using fibre optics to reduce interference.
- In 1977, the first optical telephone communication system was installed about 1.5 miles under downtown Chicago, and each optical fibre carried the equivalent of 672 voice channels.

Today more than 80 percent of the world's long-distance traffic is carried over optical fibre cables, and at least 25 million kilometres of the cable Maurer, Keck and Schultz designed has been installed world wide. Capacity now exceeds demand from telecom users.

1.3.2 Structure of optical fibres

Optical fibres are dielectric waveguiding devices [7] used to confine and then guide light. The majority of optical fibres used in sensing applications have silica glass cores but some special materials, such as sapphire, fluoride glasses and neodymium doped silica are utilised for specialised applications. The core is surrounded by a dielectric material called the

Chapter 1 Optical fibre sensors

cladding. The cladding refractive index must be lower than that of the core to satisfy Snell's Law for total internal reflection and thus propagation of the light along the fibre core. The cladding is generally made from silica glass, although for some applications a plastic or doped silica cladding is used. A barrier layer of plastic (the "buffer") is used to jacket the fibre; this provides the fibre with mechanical strength and protects it from damage or moisture absorption. In some sensing applications, a specialised buffer is used to enhance the fibre measurement sensitivity. Fig.1.1 illustrates a cross-sectional view of a standard optical fibre.

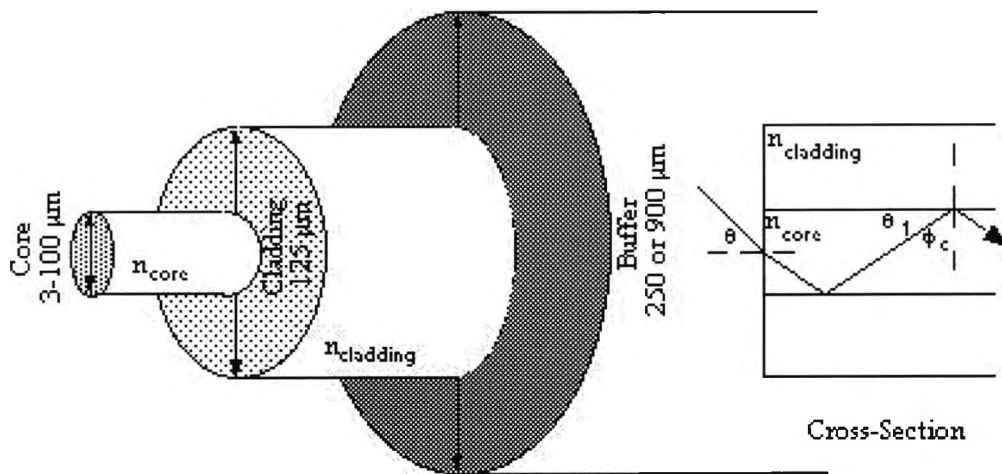


Fig.1.1 Cross-sectional view of a typical optical fibre [7].

A simplistic definition of the modes that are guided by an optical fibre can be explained by considering the locus of all the light rays which are launched at different entry angles into the core of the fibre. For any optical fibre, the number of modes that will be guided by the fibre is dependent on core size, the ratio of core/cladding refractive indices, and the wavelength of operation. Depending on the optical property utilised for the sensing application, the number of modes propagated by an optical fibre is an important parameter in fibre transmission.

1.3.3 Characteristics, advantages and capabilities of optical fibre sensors

1.3.3.1 Characteristics

As previously mentioned, the high expectations of optical fibres as information carriers in communication systems have been justified by their performance over the past two decades. Due to their high bandwidth, low attenuation and mechanical properties, each fibre is capable of replacing 1000 copper wires in telecommunication systems. With these characteristics it is no surprise that optical fibres have become the most affordable and efficient medium available in the field of telecommunications.

But optical fibres can be more than mere signal carriers. Light that is launched into and confined to the fibre core propagates along the length of the fibre unperturbed unless acted upon by an external influence. Any disturbance of the fibre alters the characteristics of the guided light; such alterations can be monitored, and related to the magnitude of the disturbing influence. The characteristics of the light which may be monitored in sensing applications include:

- amplitude
- polarisation
- phase
- modal distribution
- wavelength
- time-of-flight

Chapter 1 Optical fibre sensors

Such a modulation of the light makes possible the measurement of an ever-increasing and wide range of events and conditions, including:

strain	displacement	damage
residual strain	acceleration	cracking
vibration	deformation	wear
frequency	impact	corrosion
acoustic emission	liquid levels	pH levels
pressure	index of refraction	temperature
load	angular velocity	linear velocity
colour	mean ambient lighting	gaseous pollutants
holes in moving tapes	particle and energy measurement	fires and intruders
chemical composition	chemical reactions	electric fields

Table 1.1 Some parameters and events which may be detected using fibre optic sensors [7].

Fibre optic sensors may be *intrinsic* or *extrinsic*, depending on whether the fibre is the sensing element or the information carrier, respectively. They are designated “point” sensors when the sensing gauge length is localised to discrete regions. If the sensor is capable of sensing a measurand field continuously over its entire length, it is known as a “distributed” sensor; “quasi-distributed” sensors utilise point sensors at various locations along the fibre length. Fibre optic sensors can be transmissive or can be used in a reflective configuration by mirroring the fibre end-face.

1.3.3.2 Advantages

The principal advantages which fibre optic sensors possess over conventional sensors include:

small size	very wide frequency bandwidth response
low weight	simultaneous sensing of more than one parameter
robust	very wide operating temperature range
low unit cost	high tensile strength
high sensitivity	high fatigue life
high spatial resolution	fast response times
corrosion resistance	immunity to electromagnetic interference (EMI)
non-conductive	plus numerous systems-related advantages

Table 1.2 Advantages of fibre optic sensors [7].

There are some *disadvantages*, however, associated with using fibre optic sensors:

- there may be the need to isolate the sensor from unwanted effects
- the availability of suitable optical sources
- the cost and availability of suitable instrumentation
- the long-term stability of the installation needs to be examined
- the low general awareness of fibre optic sensor technology - the need for training of staff to use optical fibres

Comparing the advantages and disadvantages, it is clear that the advantages far outweigh the disadvantages. Many of the disadvantages can also be overcome in ways, depending on the specific application.

1.3.3.3 Capabilities and significance

Fibre optic sensors and systems have proven their advantages and capabilities in various applications and environments in the past. There is currently a growing interest in the potential for condition monitoring applications. Their significance for condition monitoring applications, coupled with their general fibre-optical advantages over other sensors stems from the fact that:

- they are made from a very durable material (i.e. silica) that is corrosion resistant and can withstand high tensile loading (can withstand up to 5% elongation - that is 50,000 $\mu\epsilon$)
- they can measure temperature from -200°C to 1100°C for silica, 2000°C for sapphire fibres, with better than 0.1°C resolution
- they are capable of having an extremely wide dynamic range (DC to MHz), with a uniform response characteristic
- they can be applied to complex surfaces and difficult-to-reach areas (i.e. around the circumference of a round object, around sharp corners or across welds)
- from point to long sensing lengths are possible (<1 mm to km)
- they offer immunity to EMI (can operate in electrically noisy environments and have no EMI noise pick-up over very long leads) and electrical isolation (they are non-conductive)
- they provide high spatial resolution (ie., 0.1 $\mu\epsilon$ easily achieved, 1 p ϵ demonstrated - that is one millionth of a $\mu\epsilon$)
- they can be used at any pressure, deep under the sea or in space, without adjustment

Chapter 1 Optical fibre sensors

- they can monitor the composition of gases or liquids, with an accuracy approaching parts per million
- they may be incorporated within many materials, structures, machines or components without significant modification of the environment or the fibre's own dielectric nature
- they can perform the sensing *in-situ*, at the location where a problem is expected or is actually occurring (i.e. they can be located much closer to the problem source)
- they are capable of monitoring different parameters simultaneously, thus reducing system cost and complexity
- they provide the ability for on-line analysis and the opportunity for feedback control
- they are already cost-competitive compared to many conventional sensors.

1.3.4 Physics of fibre optic sensing

The use of fibre optic sensors for condition monitoring applications primarily involves the sensing of the following parameters:

absorption	-->	chemical analysis
temperature	-->	performance monitoring
strain/vibration	-->	vibrational analysis & loading conditions
acoustic emission	-->	vibrational analysis and damage detection

Table 1.3 Sensing parameters used for condition monitoring applications [7].

Chapter 1 Optical fibre sensors

Fibre optic sensors can be categorised into four major groups: *intensiometric*, *interferometric*, *polarimetric*, and *modalmetric*. The category which a sensor falls under depends on the method by which the light is modulated in the fibre.

Several effective fibre optic sensing techniques have been developed for monitoring the condition of structures and machinery, as well as providing real-time analysis of chemical composition. Each method has its own unique characteristics and applications, providing several options available to the user depending on his/her requirements. The four major sensor groups are briefly described in more detail in the following sub-sections.

1.3.4.1 Intensiometric fibre optic sensors

Intensiometric fibre optic sensors are based on the modulation of light intensity in the fibre and are often configured as a distributed (i.e. spread across many locations) sensor. The variation in the light intensity can occur in the form of fracture loss, time-of-flight, refractive index, amplitude and wavelength. Fracture-loss techniques offer very simple and effective threshold sensors, but they are not useful for quantitative analysis. Absorption-based techniques, on the other hand, have significant potential for chemical analysis applications. Absorption techniques involve the monitoring of absorption of, for example, broadband light propagating through an absorbing medium. A spectrometer can be utilised to determine the absorption spectrum of the received light and hence the chemical species or concentrations present (they essentially represent chemical fingerprints) may be determined. Coupling optical fibres to a spectrometer permits remote, real-time monitoring. The optical air-path and sensing cell in the spectrometer may be replaced by optical fibres, provided that the fibres have sufficient optical transmission range in the infrared. The fibre optic sensor may

Chapter 1 Optical fibre sensors

then be configured extrinsically, delivering the light to/from a test chamber, or intrinsically by configuring the optical fibre in such a way that the light which passes along the fibre is not wholly constrained by the fibre, but part of it (the evanescent wave) propagates a short distance beyond the bounding surface of the glass core. This evanescent wave is modified by absorption in the contiguous medium and can thus be used to convey analytical information. Fig.1.2 illustrates the fibre optic evanescent wave absorption technique used in some fibre optic sensors.

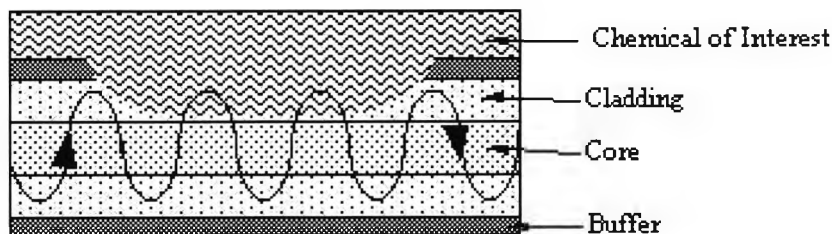


Fig.1.2 Fibre optic evanescent wave absorption technique [7].

1.3.4.2 Interferometric fibre optic sensors

Interferometric fibre optic sensors are a large class of extremely sensitive fibre optic sensors. Fibre optic interferometers are analogous to their respective classic bulk optic interferometers. They are typically used when ultra-high sensitivities are required and/or in applications of localised measurements, although sensor lengths longer than 1 metre are sometimes possible. This sensing technique is based primarily on detecting the optical phase change induced in the light as it propagates along the optical fibre. Fibre optic interferometers are generally intrinsic sensors in which light from a source is equally divided to follow two (or more) fibre-guided paths. The beams are then recombined to mix coherently and form a “fringe pattern” which is directly related to the optical phase

Chapter 1 Optical fibre sensors

difference experienced between the different optical beams. Singlemode fibre and associated components are used because they maintain the spatial coherence of the light beam, whereas multimode fibres do not. The most common configurations of the interferometers are the Mach-Zehnder, Michelson and Fabry-Perot fibre optic sensors.

The *Bragg grating* fibre optic sensor (sometimes called FBG) is a relatively new type of fibre optic sensor and is generally classed as an interferometer. In this technique a stable Bragg grating is permanently impressed (photo-etched) into the core of a suitable photosensitive fibre by exposure to a two-beam ultraviolet interference pattern. The region of periodic variation in the index of refraction of the fibre core then acts as a very narrowband reflection filter. The reflection signal is therefore a narrow spike with a centre wavelength that is linearly dependent on the backreflected Bragg wavelength and the mean index of refraction of the core. Fig.1.3 illustrates the working principles of a fibre optic Bragg grating.

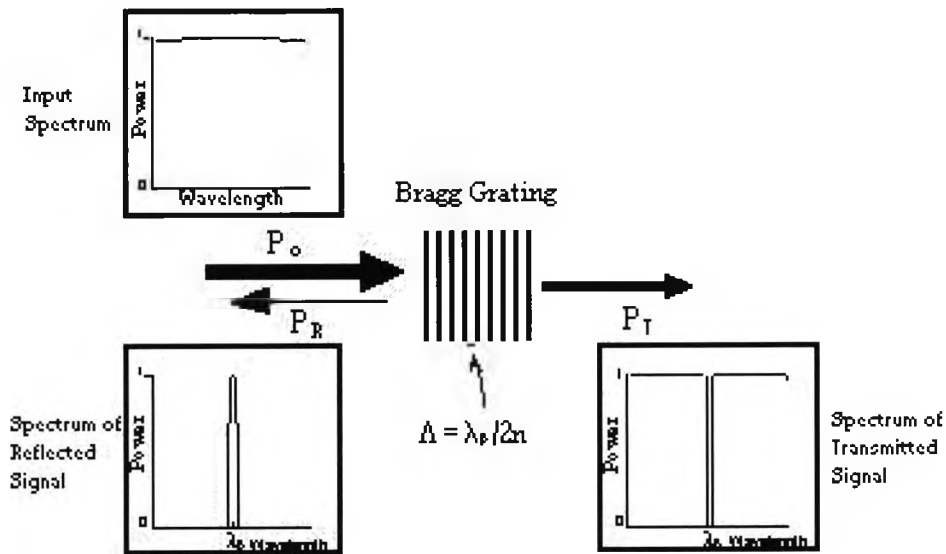


Fig.1.3 Response characteristics of a fibre optic Bragg grating [7].

Chapter 1 Optical fibre sensors

Consequently, any external parameters which act to alter the grating characteristics result in a shift in the reflected Bragg wavelength and this constitutes the mode of measurement. A strain resolution of $0.1 \mu\epsilon$ and temperature resolution of 0.1°C are readily achievable.

The Bragg sensor has several advantages over all other fibre optic sensors; it is constructed from a single, unweakened fibre, its response is highly linear to the measurand and temperature compensation is possible by overlaying two gratings. All other interferometers have a sinusoidal response characteristic, requiring calibration on initialisation (i.e. following power interruption). The Bragg sensor, on the other hand, is initially calibrated (determined from the grating characteristics) and any deviations from the Bragg wavelength are proportionately related to an exact parameter (i.e. strain). Other negative aspects of using the FBG as a sensor lie in its limited temperature range (and consequently the reduction in resolution at high temperatures) and the necessary optical system costs involved - since a quality grating has to be manufactured in the first place (or be bought), some sort of interrogation system is used and then the response is measured with some form of instrument e.g. an OSA. More details on aspects of using FBGs are discussed later in this thesis.

Bragg fibre optic sensors could be particularly useful when the Bragg gratings are arranged along the fibre length such that the gratings are written into the core of the optical fibre at various Bragg wavelengths. Each of the reflected wavelength signals from the corresponding gratings could be monitored by the use of a coupler, detector and tuneable optical filter, thus achieving single-fibre multiplexing of the sensors.

1.3.4.3 Polarimetric fibre optic sensors

Polarimetric fibre optic sensors are an attractive alternative to interferometric sensors when ultra-high sensitivity is not required, and longer sensor gauge lengths are desired. The principal of polarisation sensing is related to birefringence within the fibre. A polarised light beam is launched at 45° to the principal axis of a singlemode fibre, and thus the two orthogonal polarisation eigenmodes are equally excited and are degenerate. When an external force acts on the fibre the degeneracy is lifted and a phase difference is induced in the two eigenmodes. Consequently, a measurement of a change of the state of polarisation in the fibre is directly related to the measurand. The polarimetric fibre optic sensor is sometimes referred to as a differential interferometer.

The polarimetric fibre optic sensor is capable of detecting most parameters previously listed with the advantage of being configured as a point or distributed sensor. Drawbacks of this sensor include the high cost of components and the overall complexity of the system.

1.3.4.4 Modalmetric fibre optic sensors

Optical fibres were found to be very microphonic quite early in the development of fibre optic sensors. Research revealed this sensitivity to be based on the modulation in the distribution of modal energy in the optical fibre. This finding resulted in the first truly intrinsic fibre optic sensor; the modalmetric fibre optic sensor. Although this type of sensor is very sensitive, the modulation of the modal pattern is generally non-linearly related to all disturbances, resulting in deep fading and drifting of the output signal. This behaviour limits the use of this sensor for quantitative strain measurements, but nonetheless it can be used as a threshold-type sensor.

More complex techniques overcome this random behaviour by involving modal interferometry in a single, circular or elliptic core, two-mode optical fibre. Modalmetric sensors are capable of sensing most parameters; however, their sensitivities are generally far lower than interferometric sensors and the localisation of the sensing region is difficult. Usually, these sensors are employed in conjunction with other techniques, such as microbending, polarimetry, and optical time domain reflectometry (OTDR).

1.3.5 R&D trends in fibre optic sensor systems

The first practical temperature sensors were based on intensimetric techniques, utilising refractive index changes and/or fluorescence. Several commercially available products have been available over the past two decades and have been mainly utilised for hot-spot temperature measurements in high voltage equipment and in monitoring the cure process of composite materials. In recent years, researchers have used interferometric-based temperature sensors for monitoring combustion parameters inside engines, although no commercial products are yet available.

To date, chemical analysis is most effectively accomplished by Fourier Transform Infrared (FTIR) spectroscopy and index of refraction matching.

Multimode fibre optic sensors generally suffer from optical signal fading and drift. The optical fibre industry has overcome the inherent signal transmission weaknesses of multimode fibres by the use of singlemode fibre systems, but these are more difficult to handle, and utilise quite expensive components. This significant disadvantage offsets the

Chapter 1 Optical fibre sensors

multimode fibre's advantages of low cost and ease of application. However, some companies have developed different systems using these effects, e.g. *Future Fibre Technologies Pty. Ltd.* have developed the Foptic™ Vibration sensor. Based on a unique fibre optic modalmetric sensor configuration, it overcomes the inherent weaknesses of multimode fibre optic sensors, is easy to fabricate and costs relatively little to assemble.

The development of practical interferometric sensors, based on the principles mentioned earlier, started with two-arm interferometers with single-arm interferometers soon prevailing. The most common types now used are the Michelson and Fabry-Perot interferometers, the polarimetric differential interferometer and the Bragg grating sensor. The Michelson interferometer is a two-arm device used mainly in intrinsic vibration and acoustic emission detection. The Fabry-Perot and polarimetric fibre optic sensors are the most common for strain, extrinsic-vibration, and temperature measurements. The polarimetric sensor is used when ultra-high sensitivity is not required or if quasi-distributed sensing is desired. However, its high sensitivity to temperature is a significant disadvantage. The Bragg grating sensor is the newest and most promising technique developed. No initialisation or calibration is required as a change in the grating spacing (i.e. as the fibre is stretched) results in an absolute measurement. This offers clear advantages over other techniques as single, usually unweakened (no fibre splices or joins are required) fibres are used and complex phase demodulation signal processing schemes are not required.

A comparison of typical fibre optic sensor sensitivities is given below. The comparison is given in units of phase change (making it meaningless to include the Bragg grating sensor here), since its sensitivity is given in units of wavelength change.

Chapter 1 Optical fibre sensors

sensitivity	interferometer	polarimeter	modalmetric
strain ($^{\circ}/\mu\epsilon\cdot\text{cm}$)	6.5	0.06	0.02
temperature ($^{\circ}/\text{K}\cdot\text{cm}$)	23	2.5	0.2
T/S ($\mu\epsilon/\text{K}$)	3.6	41.7	10

Table 1.4 Strain and temperature sensitivities of various fibre optic sensors [7].

The ultimate sensitivity and resolution of the techniques included in the table are limited by the effectiveness of the phase demodulation signal processing techniques used to interrogate the sensors (i.e. it is essentially an instrumentation issue). Consequently, in recent years, many research and industry groups have been concentrating on developing practical and cost-effective instrumentation for these techniques. To date, only a few commercial products are available.

It has been shown that the Bragg sensor sensitivity and resolution approaches that of the interferometers considered, and may even surpass them with special instrumentation arrangements. Fundamentally, the sensitivity of the Bragg sensor is limited by the ability to monitor very small wavelength changes. The huge potential of Fibre Bragg gratings will be demonstrated in the following sections and will be discussed extensively in Chapter 4, where FBGs have been incorporated into rare earth doped fibres for the first time for the purposes of dual temperature and strain monitoring.

Recent years have seen the emergence of *plastic* optical fibres (POFs) intended for a wide variety of uses. These types of fibre sensors employ polymer materials for both the core and

the cladding of the fibre - the idea effectively being “spun off” from the communications industry to compliment the ubiquitous use of silica fibres in sensing. A short but comprehensive review of their sensor capabilities has been given by Grattan & Sun [3], which reports applications such as the determination of the refractive index of liquids or dynamic pressure sensing. They have been doped with rare earth ions (mainly Nd^{3+}) and have proven their application potential to lasers and amplifiers using luminescent effects such as fluorescence [8] or amplified spontaneous emission (ASE) [9]. They can also be doped with organic dyes to produce lasing action [10], or with materials which respond to short wavelength radiation for scintillation [3]. Such doped POFs are now be used in many sensing arrangements to detect a number of interesting parameters - such as mean ambient lighting, spatial detection with high-resolution or in some molecular biology sensing applications. Recent research has also shown POF uses in water quality monitoring [11, 12] and humidity sensing [13].

1.3.6 Summary

Optical fibre sensors have been widely exploited to monitor a range of parameters for various applications. However, temperature and strain are of a particular interest in this thesis and the following sections will review recent developments in these fields.

1.4 Optical fibre temperature sensing

1.4.1 Introduction

Temperature monitoring has been [14] a most important concern in various industries for many years, and the temperature compensation of other measurands e.g. strain, pressure and

flow is essential if accurate and reliable data are to be recorded. Several methods of temperature sensing have been used and the thermocouple is still a cheap and effective device for many simple sensor applications. However, in some situations where simple electrical monitoring is perhaps ineffective or impractical it may then be possible that optical fibre techniques are preferred. Temperature sensors probably still constitute the largest class of commercially available fibre-optical sensors [15].

1.4.2 Industrial applications of fibre optic temperature sensors

Numerous advantages of fibre optical sensors have been discussed previously in section 1.3.3.3, and a number of applications have been [4, 14] discussed in the literature where the fibre-optical approach to the measurement of temperature has proved to be of particularly value. Positive attributes such as immunity to electromagnetic interference (as opposed to thermocouples) and good accuracies (unlike pyrometry) over a large working range (0 to 2000°C) could well outweigh potential problems such as installation, probe flexibility and higher costs depending upon the particular requirements. Main applications currently in use include:

- *electrical power systems* e.g. transformer monitoring to recognise “hot spots” by winding a fibre optic sensor within the transformer, or retrofitting the sensor into the device e.g. in the transformer oil or in overhead cables
- *engine combustion monitoring*, particularly in turbine engines, to improve efficiency and lifetime
- “*smart structures*” and *structural integrity*, to determine structural changes with temperature, in monitoring processes such as concrete curing and to compensate other optical strain or pressure measurements for changing temperatures

- *furnaces* and *kilns* to improve combustion efficiency and possibly increase the lifetime of linings, whilst minimising the furnace “down-time” and consequent production loss
- *fire alarm systems* to monitor conditions of rapid temperature excursions, due to fire, by the detection of “hot spots” occurring within a length of fibre for the purposes of fire prevention
- *process industries* where the efficiency and safety of a plant can depend upon receiving reliable temperature data, especially a “non-spark” approach
- *sewers* and *drains* where the “non-spark” approach is essential because of the possibility of gas explosion
- *temperature compensation* for systems which depend upon being corrected for differentials with ambient temperatures, possibly over very wide ranges.

1.4.3 Fibre temperature sensing techniques

Many different physical phenomena are used to perform temperature sensing, each with attributes suitable for a particular application, but no single technique can, however, accommodate the entire range of temperatures and resolutions required for different applications [15]. The six main optically-based physical techniques currently in use are:

- remote *pyrometry* (or more commonly called *blackbody radiation* monitoring)
- *interferometry* to measure optical path-length changes in a material
- *intrinsic scattering* – namely *Raman*, *Rayleigh* and *Brillouin* techniques usually using optical-time-domain-reflectometry (OTDR) techniques in distributed temperature sensing

Chapter 1 Optical fibre sensors

- *luminescence* – usually *fluorescence* from rare earth doped fibres, powders, crystals or ceramic phosphors
- *absorption* – predominantly in semiconductor or rare earth doped materials
- *Bragg gratings* (FBGs) – written into optical fibres, sensitive to both temperature *and* strain

The range of operation for all these techniques is very broad, with reported values ranging from the cryogenic (down to 1 K) region [16] to 4000°C [17] in some commercially available devices. The techniques can be explained in more detail:

1) *Remote pyrometry*. This technique uses optical fibres to telemeter the *blackbody* spectrum of a small piece of material such as sapphire to an appropriate measurement site. The spectrum of pure blackbody radiation is described by Planck's radiation law. It is often written in terms of radiant power emitted per unit surface area i.e. in terms of irradiance (W_λ) as a function of wavelength [1]:

$$W_\lambda = \frac{C_1}{\lambda^5} \frac{1}{\exp(C_2 / \lambda T) - 1} \quad (1.1)$$

where λ is the wavelength, T the absolute temperature (K) and C_1 and C_2 are two radiation constants. However, the levels of thermal radiation are known to reduce at the lower temperatures and typically the method is used for higher-temperature applications. There are reports in the literature of some commercially available devices that currently utilise this technique (e.g. the *Luxtron Accufiber® models 10 & 100*), some of which can now measure up to 4000°C [18]. An excellent discussion of the technique is given by Nicholas and White [19], where the practical aspects of blackbody-based sensors are discussed in more detail and

fibre optic thermometers currently using this approach, including the Accufiber fibre optic sensor previously mentioned, are referenced.

2) *Interferometry*. This type of fibre temperature sensor measures the change in optical path length of a short piece of material whose thermal expansion coefficient and refractive index as a function of temperature are known. In some cases, multiple wavelengths are used to null out secondary effects such as strain or pressure in the material being measured. The most common type now used, the *Fabry-Pérot* (FP) interferometer, is often fabricated in materials such as glass, calcite, or zinc selenide (ZnSe). However, because of material choices in packaging, these sensors have limited upper temperature reaches. Interferometric fibre sensing techniques have been extensively reviewed recently by Grattan & Sun [21, 22], Rao & Jackson [3] and previously by many others [23, 24]. These types of sensors have very high sensitivities (often being too sensitive for many uses) and wide dynamic ranges, and consequently can be used for the sensing of several measurands as well as temperature [25].

3) *Intrinsic scattering* – *Raman*, *Rayleigh* and *Brillouin* scattering techniques have been greatly discussed in the literature and are actually luminescent effects [1, 3, 5, 21, 22, 25]. They are basically caused by [5] an interaction between the light transmitted by an optical fibre and the molecules in that fibre, and they have been shown to be temperature dependent. These effects are usually measured using a technique called *optical time domain reflectometry* (OTDR), which offers the advantage of distributed sensing. Distributed intrinsic scattering temperature measurement techniques are constantly improving. For example, Odic *et al* [26] have recently developed a sophisticated, real-time early fire detection and monitoring system for aeronautical applications, based on *Raman* scattering using OTDR techniques. They report the advantages of minimal false warnings, faster

retrieval of information from more aircraft locations, and ease of installation and substitution. Fellay *et al* [16] have recently extended the lower temperature limit of *Brillouin* scattering techniques by demonstrating distributed Brillouin-based temperature sensing in optical fibres right down to the cryogenic region of 1 K, for use in a real life installation at CERN in Geneva, Switzerland.

4) *Luminescent optical fibre sensing*. These sensors exploit the phenomena of luminescence (a term which also includes intrinsic scattering), occurring mainly as photoluminescence (or *fluorescence*) in rare earth doped materials or thermographic phosphors. Grattan and Zhang [1] have extensively exploited the phenomena of fluorescence from various materials for thermometric applications, mainly using a fluorescence *lifetime* technique. This method utilises time-coded changes in the fluorescent properties of certain materials with temperature. There are also several other approaches - fluorescent *intensity ratio*, *wavelength shift* and *amplified spontaneous emission* (ASE) - to name the major ones currently in operation. The fluorescent lifetime technique used previously [1], however, is also used as the basic measuring technique throughout this thesis. In this method, the temperature can be determined [15] by measuring fluorescence emission decay times from rare earth doped fibres/crystals or transition metal-doped phosphors. The technique has a proven large measurement range, having previously been used to measure temperature from the cryogenic [17] regions ($\sim 77\text{K}$) to 1400°C [27] in rare earth doped fibres and crystals, and up to 2000°C using certain phosphor techniques. It can also compliment the deficiencies mentioned previously in blackbody techniques at the lower temperatures. This was shown by Zhang *et al* [1, 20], who discussed the feasibility of optical thermometry based on the cross-referencing between blackbody radiation and the fluorescence lifetime technique in a prototype scheme which combined the two thermometric techniques together for the first

time, with the aim of producing a single fiber optic sensor possessing an extremely wide temperature range. Satisfactory results were achieved over the range from room temperature to 900°C at the time. The potential to achieve a much higher temperature range, given the more recent improvements in both techniques, still remains today. A detailed analysis of the fluorescence lifetime temperature measurement technique, and other fluorescence-based methods of temperature measurement, occurs in the following section.

5) *Absorption*. This technique uses the variation in the absorption spectrum with temperature of various materials, predominantly from semiconductor or rare earth doped materials [5]. There are several references in the literature [1, 5] to a commercial fibre device developed by Kyuma and co-workers (in 1982) at the Mitsubishi Electric Corporation, Japan, based on this technique using either polycrystalline CdTe or gallium arsenide as the absorbing crystal material. They tested over the region from -10°C to 300°C and reported an accuracy of $\pm 1^\circ\text{C}$. They also found gallium arsenide to be the more sensitive sensor at lower temperatures (<150°C). Currently there is very little work reported in the literature on using similar fibre absorption techniques for temperature measurement - probably the relatively high expense involved in the method are a key factor in this.

6) *Fibre Bragg grating (FBG) devices*. Inexorable progress has been made in this most popular area of fibre sensing since these devices were first discovered in 1978 by Hill and fellow workers [28, 29]. The distinct advantages that FBGs offer over several other fibre temperature sensors are now well known e.g. they can be easily multiplexed into arrays for distributed temperature sensing, they have inherent self-referencing capabilities etc. Several extensive reviews have appeared over recent years [3, 4, 21, 22, 30, 31] providing details on all aspects of FBG principles, fabrication, signal processing capabilities and usage. The theory of basic sensing mechanism has been previously discussed in section 1.3.4.2 of

this thesis, but a more detailed explanation occurs in section 4.4 where FBGs are combined with fluorescence generated from rare earth doped fibres and their sensing properties are exploited. Regarding the latter - the *temperature sensitivity* of a FBG in general is well known from the above review papers to be $\sim 10 \text{ pm}/^\circ\text{C}$, this being a factor of 10 more than the *strain sensitivity* ($\sim 1 \text{ pm}/\mu\epsilon$).

From all six of the preceding categories of fibre temperature sensors, it is the last one, i.e. the FBGs, which have recently begun to dominate fibre temperature sensing research. For example, they are currently being evaluated for structural integrity testing and temperature monitoring in the nuclear industry - recent work by Fernandez *et al* [32] has investigated radiation tolerances of several FBGs intended for temperature measurements in the presence of ionising radiations, including in-reactor core distributed temperature sensing using multiplexed FBGs. They found that those FBG temperature sensors written into photosensitive fibre, without any pre- or post-writing treatment, exhibited the highest radiation tolerances to both pure gamma and mixed gamma-neutron environments.

If there were to be any weaknesses regarding temperature measurement pointed out in the current “FBG-crazed sensor climate” then these could be highlighted by problems of range such as:

- their apparent inability to measure in the *cryogenic* regions – James *et al* [33, 34] recently discovered that FBG temperature sensitivity drops to almost zero at temperatures less than 100 K, whereas the strain sensitivity remains unaffected.
- their long term performance (*thermal erasure*) at high temperatures, a fact echoed in some recent research. For example, Winz and co-workers [35] at Oregon State

University have developed a process to fabricate FBGs which they claim shows no decrease in FBG performance over 10 days at 600°C. Also, McCreadie *et al* [36] have proposed fabricating surface relief long-period gratings into *sapphire* fibres for the purposes of achieving stability in very high temperatures in FBG sensing. They report stability up to 1100°C. However, their expectations in achieving stability right up to the melting point of sapphire (~ 2000°C) remain to be seen.

Related research into the high temperature annealing effects on the performance of a grating written into photosensitively-enhanced co-doped fibre has been performed in Chapter 4 of this thesis, and the results obtained on tests carried out over periods as long as 7 weeks are reported there. Workers at City University, London, UK are currently characterising FBGs written into various hosts for similar purposes in on-going work.

1.4.4 Fluorescence-based techniques

Historically, fibres doped with *luminescent* materials were first used by Snitzer [3] in the 1960s for work on lasers and optical amplification, then using a 300 µm core diameter neodymium doped fibre. Subsequent development of the idea, “spun off” from extensive use in the communications field, has been the major reason for the production of a range of different types of *fluorescent* optical fibre sensors which have been doped with these luminescent materials. Their increasingly varied sources of supply, both in the form of bulk optical systems and fibres, have contributed to the development over the years of a series of fluorescence-based sensors, some now commercialised (e.g. *Luxtron*®), and these techniques have been reported to cover a very wide temperature range, from the cryogenic [17] regions (~77K) up to 1400°C (potentially 1500°C) [27]. These include:

- Cr^{3+} [1] in ruby [37] and alexandrite [38]
- Pr^{3+} in ZBLAN glasses [39, 40]
- Nd^{3+} in glasses [41], garnets (YAG) [42] and fibres [43]
- powder probes e.g. Tm^{3+} in Y_2O_3 [44]
- Er^{3+} [45], Yb^{3+} [46], Tm^{3+} [47], $\text{Er}^{3+} \text{Yb}^{3+}$ [48] and $\text{Tm}^{3+} \text{Ho}^{3+}$ [49] doped silica fibres
- Eu^{3+} [50], Yb^{3+} [50], Sm^{3+} [50], Dy^{3+} [50] Pr^{3+} and Nd^{3+} [50] doped fibres (various hosts) using fluorescent intensity ratio techniques
- sapphire-ruby single crystal fibre [27]

These techniques (which do not include the use of thermographic phosphors - these are not actually fibre sensors but will be described later) are shown to be self-referencing i.e. they are largely immune to changes in excitation source (pump wavelength, intensity) and fibre bend losses. Some of these factors are investigated further for their effect on the measured fluorescent lifetime in Chapter 3 of this thesis, and the results shown there.

The term *fluorescence* is generally defined as the emission of light or other electromagnetic radiation of longer wavelengths by a substance as a result of the absorption of some other radiation of shorter wavelengths, provided the emission continues only as long as the stimulus producing it is maintained. In other words, fluorescence is the luminescence that persists for less than about 10^{-8} s after excitation. There are now several types of fluorescent temperature measurement approaches: the fluorescence *wavelength shift* and *amplified spontaneous emission* (ASE) approaches mentioned previously are both seldom used now to

measure temperature alone, but the two most popular methods of optical fibre fluorescence-based thermometry now in use are the fluorescence *intensity ratio* and the fluorescence *lifetime decay-time* based approaches. These techniques are readily comparable in the sense that they use the same physical principles to detect temperature change i.e. the thermalisation of closely spaced energy levels, from usually similar materials [5]. In the fluorescent lifetime scheme, the temperature-dependent lifetime of the fluorescence emitted from certain energy levels of certain materials are utilized [1]. In the fluorescence intensity ratio (FIR) technique, fluorescent decays in rare-earth-doped optical fibres from two closely-spaced levels to a common final state are monitored at the appropriate wavelengths and then the ratio of the two emission intensities is calculated, to form a quantity which is independent of the source intensity. The comparative performance characteristics of the two schemes have been discussed in detail by Wade [5], Sun [21] and by Collins *et al* [51] from the *Optical Technology Research Laboratory, Victoria University, Melbourne, Australia* who have undertaken extensive research on the technique. An interesting feature of the fluorescence intensity ratio temperature sensing technique is that it has recently been proved to be almost strain insensitive by Wade *et al* [52 - 56]. It has also recently been successfully combined with a FBG to achieve dual temperature-strain sensing in on-going work [57].

1.4.4.1 Fluorescence lifetime-based techniques

The work on temperature (and indeed strain) sensing in this thesis utilises the *fluorescence lifetime decay-time technique* [1] using the fluorescence generated from materials called the *rare earths* in either silica optical fibre or powder hosts, this being slightly different from some previous work done by Cates *et al* [58] who used the same technique but with fluorescence generated from $\text{La}_2\text{O}_2\text{S}:\text{Eu}$ and $\text{Mg}_4\text{FGGeO}_6:\text{Mn}$ *phosphors* to measure

Chapter 1 Optical fibre sensors

temperatures in the cryogenic regions. Phosphors are classed as being those fluorescent materials in a group which includes inorganic oxides, oxysulfides, orthophosphates and vanadates of the rare earth metals. Other metals, notably zinc, manganese, and a few others, are also constituents of numerous phosphors. Fluorescence in these types of materials arises from excited ions, maintained in low concentrations in the crystal lattice, which have a high probability of de-excitation by a photon emission instead of through other processes in the lattice itself. Experimental methods using phosphors usually employ fibres in the measurement system to relay the fluorescence, but the actual phosphor sensors are commonly surface mounted for remote measurements and the instrumentation required to achieve this is often cumbersome. An excellent review of remote fluorescence thermometry using thermographic phosphor techniques has been given by Allison & Gillies [59].

A detailed description of the rare earth elements used for work in this thesis (and also the luminescent properties that make them suitable for use as dopants in silica optical fibre or powder hosts) for application to fluorescence-based temperature sensing has been given by Wade [5] in a review in Chapter 2 of his thesis. Also, an excellent overview of the Modified Chemical Vapor Deposition (MCDV) process used in silicon rare earth doped fibre fabrication has been given by Nagel *et al* [60], and more recently by Digonnet [61], where in the latter the current manufacturing methods are described and appear not to have altered much in the last 20 years or so.

The fluorescence lifetime temperature measurement technique, as previously used by Grattan and Zhang [1], has proven to be practically simple to operate and relatively inexpensive in its use of electronic-based components, the most expensive item of any such

measurement system usually being the laser source used. Fluorescence may be excited in a doped fibre through the use of a pulse of light from an appropriate laser diode source. It is found that following the termination of the excitation light pulse, the fluorescence decay signal can be written as an exponential as a function of time, t , by

$$I = I_0 \exp(-t/\tau) + I_{\text{offset}} \quad (1.2)$$

where I_0 corresponds to the initial fluorescence amplitude (i.e. at $t = 0$), τ is the corresponding fluorescence lifetime (which is temperature dependent) and I_{offset} is the signal baseline offset. This can be more clearly seen from Fig.1.4. The excitation spectrum of a fluorescent material, illustrating the incident radiation spectral region which may be used for the induction of fluorescence, is determined by the absorption spectrum of the fluorescent material [1] which it often closely resembles, and by the efficiency with which the absorbed energy is transformed into fluorescence.

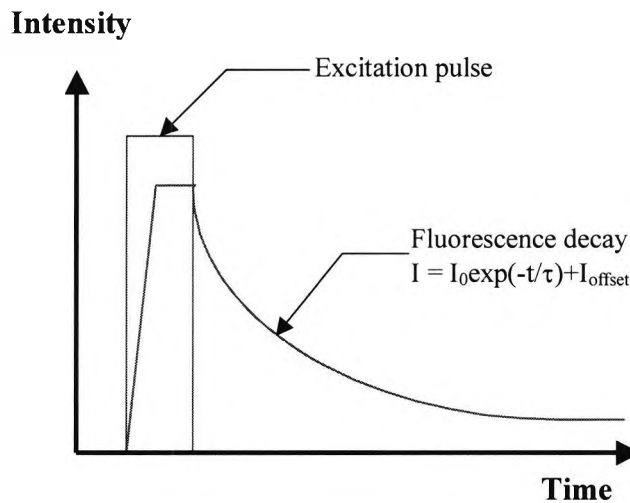


Fig.1.4 Schematic of the decay-time approach.

The initial persistence of fluorescent emission following the removal of excitation depends on the lifetime of the excited state, i.e. the average time that a molecule spends in that state

before emitting a photon and returning to the ground state, and this is an important and unique feature of an excited state. The emission usually decays in a manner that can be categorized by an exponential form and the time-constant (i.e. τ in equation 1.1) of such an exponential decay may be used as the measure of the lifetime of the excited state, often termed the *fluorescence lifetime* or *fluorescence decay time*. Therefore, mathematically speaking, we can say that the fluorescent decay time (or the lifetime of the material) is that time in which the amplitude of an exponentially decaying quantity reduces to e^{-1} (36.8%) of its original value.

In fluorescence lifetime thermometry, most materials used have relatively long lifetimes ($> 10^{-6}$ s), compared to many laser dyes, for example. This means that the fluorescence corresponds to the weakly allowed transitions between electronic energy levels of the fluorescent material. The material emits light because that is one of the ways for the electron, once excited by incident radiation, to give up its energy and to return from the excited to the ground state. Any reasonably effective competitive relaxation process can shorten the lifetime of the excited state. A variety of such competitive processes, some radiative and some non-radiative, exist. Hence all luminescent materials can be expected to exhibit a temperature-dependent fluorescence lifetime, and temperature-dependent fluorescence intensity to some degree, over some part of the temperature spectrum. These are the thermal properties which are most efficacious for fluorescence thermometry.

Lifetime-based methods have been, on the whole, one of the most successful schemes for fibre optic temperature sensing [62]. Reported accuracies vary from about $\pm 0.1^\circ\text{C}$ in the case of a Cr:LiSAF-based thermometer [1] to $\pm 5^\circ\text{C}$ using erbium [45], and are dependent

upon the ranges - these were 20 to 135°C in the former and 0 to 1100°C in the latter. The method has been shown to be more favourable for use with short wavelength emission, where both the cost of a sensor probe and the sensitivity are better, than for the longer wavelengths [63]. Nd^{3+} , Er^{3+} and Yb^{3+} can all be pumped at wavelengths in the near infrared, with convenient emission wavelengths at around 800 nm to 1000 nm. There are also several inherent advantages of the lifetime method - such as providing intensity independent, time coded information and it is, to a first approximation, self-calibrated.

Several signal processing techniques for the detection of the fluorescence lifetime, some of which are employed in this thesis coupled with *HP VEE* data acquisition software (*Hewlett-Packard*), have been used and categorized [1] according to the type of approach:

1) **pulse** measurements – the measurement is derived from an observation of the fluorescence decay after the removal of a high intensity ‘delta’ function pulse (e.g. a laser pulse or that from a flash lamp) or a rectangular pulse of excitation light. These include the

- *two-point time constant* method - compares the intensity levels at two points along the exponential decay curve after the excitation pulse has terminated
- *integration* method - based on the integration of the decaying fluorescence signal over different periods of time
- *digital curve fit* methods - a selected portion of each decay curve is digitized and the digital samples are then processed to provide the best exponential curve by means of a least squares curve fitting technique. The exponential is first converted to a straight line by

taking the natural logarithm of the digitized signal values. The slope of the best fit straight line resulting is then proportional to the decay time of the luminescence.

2) **phase and modulation** measurements - the intensity of the excitation light is sinusoidally modulated so that the fluorescence response from the sensor material is forced to follow the same sinusoidal law, but lagging behind the excitation light by a phase shift (ϕ) from which the fluorescence lifetime can be derived from a measurement of ϕ .

3) **phase-locked detection** of fluorescence lifetime (**PLD**) method - a simple, inexpensive and versatile electronic scheme developed by Grattan & Zhang [1] which converts the exponential fluorescence decay curve into a TTL compatible frequency signal whose period is directly proportional to the lifetime.

Fernicola *et al* [62] have recently analysed several different lifetime measurement approaches, both direct (i.e. involving actual optical signals as opposed to Monte Carlo simulations) and indirect (using a phase-locked A/D signal processor \rightarrow A-DSP), over the fluorescence lifetime range 0.2 – 2.3 ms. In that work, direct curve fitting methods (including Marquardt, log-fit and Prony) were used to estimate the fluorescence lifetime of a Cr^{3+} :YAG-based sensor system and the results were compared. They found an agreement to better than 0.5% between the Marquardt and the log-fit algorithms and an agreement of about 1.5% between the Marquardt and the Prony approaches, from which it was concluded temperature reproducibilities of 0.5°C and 1.2°C respectively. The A-DSP was found to

perform only slightly better than using direct curve fitting methods, except when it was directly calibrated against temperature and an improvement in the accuracy by at least a factor of 10 was seen.

The theory behind the lifetime approach has been well documented by Grattan and Zhang [1], who have proposed both a *2-level* model (including an additional *configurational coordinate* model which took into account the effects of non-radiative transitions at higher temperatures in that work) and a *3-level* model to explain the lifetime/temperature dependencies from previous works using Cr³⁺-doped crystalline alexandrite [64] and Yb³⁺-doped silica fibres [46] respectively. These models have successfully been used in the past to explain the lifetime dependencies upon temperature, depending upon the number of energy levels involved. The theory of the mechanism of the fluorescence lifetime has been paralleled with that of the fluorescence intensity ratio technique by Collins *et al* [51]. The underlying physical principle exploited in sensors using both techniques is that of a thermalisation which occurs between closely spaced energy levels in the ions when one or more are excited. Thus, according to the Boltzman distribution, the relative population of the levels will be temperature dependent, which in turn will affect the subsequent fluorescence decay from the levels. The excitation pulse from an LED or laser diode source causes a number of levels in the ions to be populated, and the subsequent fluorescence decay from these levels is monitored with a single detector. The determination of the temperature-related fluorescence lifetime is independent of possible variations in the source intensity.

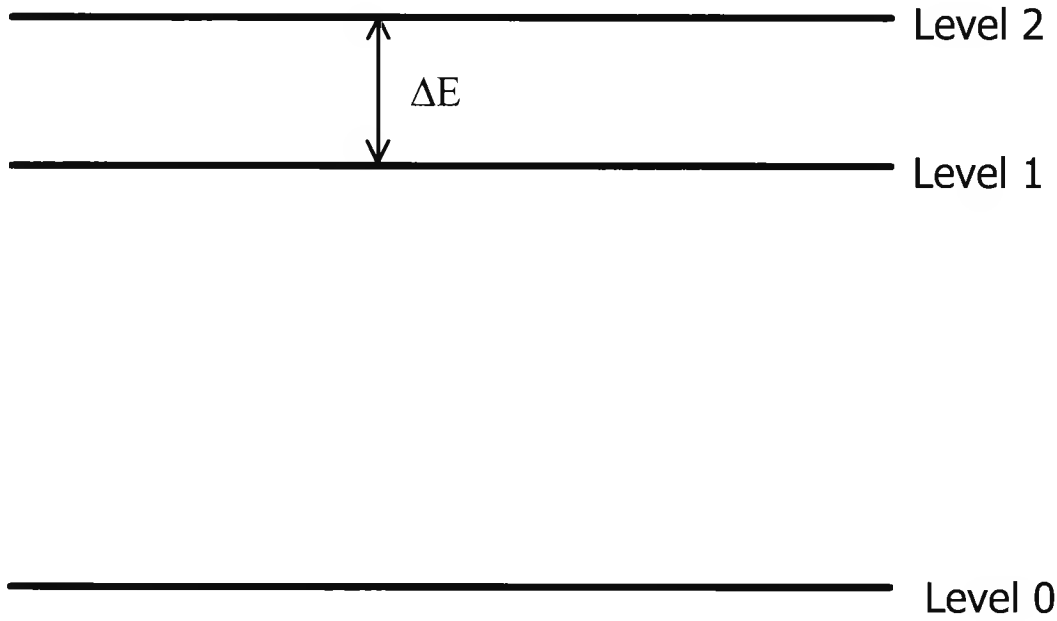


Fig.1.5 Simplified schematic energy level diagram [51].

Consider the generic energy level diagram depicted in Figure 1.5, typical for most rare earth materials. Levels 1 and 2 are closely spaced in energy (ΔE) and may decay radiatively to level 0. When levels 1 and 2 are excited through some pumping scheme there is a rapid thermalisation between the levels so that their relative populations, N_1 and N_2 respectively, are given by a Boltzmann distribution. Thus

$$N_2 = N_1 \frac{g_2}{g_1} \exp\left(\frac{-\Delta E}{kT}\right) \quad (1.3)$$

where g_1 and g_2 are the degeneracies of level 1 and 2 respectively, k is Boltzmann's constant and T is the temperature in Kelvin. For a total population $N = N_1 + N_2$ the partition functions are $z_1 = N_1/N$ and $z_2 = N_2/N$.

The radiative lifetime of an excited level k may be obtained by observing its decay to one or more levels i of lower energy. Assuming that at time $t = 0$, $N_k(0)$ atoms are excited into level k , the rate of decrease in the population of k is given by

$$-\frac{dN_k}{dt} = N_k \sum_{i < k} A_{ki} \quad (1.4)$$

where A_{ki} is the spontaneous transition rate from k to i . The excited state population decreases exponentially according to

$$N_k(t) = N_k(0) \exp(-t / \tau_k) \quad (1.5)$$

in which the radiative lifetime, τ_k , is given by

$$\tau_k = 1 / \sum_{i < k} A_{ki} \quad (1.6)$$

Irrespective of whether the light from the decaying atoms is measured at a single line (i.e. one value of i) or broadband (i.e. many or all possible values of i), the measured intensity will decrease exponentially at a rate governed by τ_k .

If the pumping scheme used excites a number of levels simultaneously then the measured decay will involve the summation of a number of decay curves. However, if the excited levels are in thermal equilibrium then the combined decay will follow a single decay curve. For the case of a number of thermalising levels, k , with partition function z_k and having individual lifetimes τ_k , the resultant decay rate is given by

$$\frac{1}{\tau} = \sum_k \frac{z_k}{\tau_k} \quad (1.7)$$

So for the case of the two thermalising levels, 1 and 2, depicted in Figure 1.5 having individual lifetimes τ_1 and τ_2 respectively, the resultant fluorescence lifetime (τ) will be given by

$$\tau = \frac{1 + \frac{g_2}{g_1} \exp\left(\frac{-\Delta E}{kT}\right)}{\frac{1}{\tau_1} + \frac{1}{\tau_2} \frac{g_2}{g_1} \exp\left(\frac{-\Delta E}{kT}\right)} \quad (1.8)$$

If the radiation at a particular wavelength is to be monitored, the intensity for the $k \rightarrow i$ transition exhibits the following proportionality:

$$I_{ki} \propto N_k w_{ki} A_{ki} \quad (1.9)$$

where w_{ki} is the angular frequency of the radiation. The intensity ratio for the transitions from levels 1 and 2 to level 0 is therefore given by

$$R = \frac{I_{20}}{I_{10}} = \frac{N_2 w_{20} A_{20}}{N_1 w_{10} A_{10}} = \frac{w_{20} A_{20}}{w_{10} A_{10}} \frac{g_2}{g_1} \exp\left(\frac{-\Delta E}{kT}\right) \quad (1.10)$$

Hence, the underlying physical principles of two fluorescence temperature sensors based on the fluorescent lifetime and intensity ratio techniques are given in equation 1.8 (this equation forms the basis of the models previously used [1] which can be modified if more than two energy levels are involved [46]) and equation 1.10 respectively. It is clear that both techniques will result in a quantity which is independent of the source intensity, and which is a non-linear function of temperature. The actual variation of this quantity with temperature has, however, been found to be very different for the two methods [51].

Despite the many advantages it can offer, there are a few inevitable drawbacks in using the fluorescence lifetime technique:

- the temperature *sensitivity* falls off at the lower temperatures ($< 20^\circ\text{C}$) [51] in some materials (not including erbium [17]), despite the large achievable temperature ranges, and this can adversely affect the accuracy in these zones.
- *annealing* effects - it is clearly important for a worthwhile sensor in any practical application that a stable and reproducible response is seen. Previous studies on

rare earth doped fibres [65] have shown that a significant and apparently irreversible change in the fluorescence characteristic occurs if the doped fibre has been exposed to high temperatures, above a certain point. In order to enable a probe to possess a consistent and stable thermal characteristic, an “annealing” process is recommended requiring pre-treatment of any potential fibre sensor at high temperatures. This effect is investigated further in some of the work done in this thesis using various materials.

- in recent work by Liu *et al* [66], and subsequently in work by Sun *et al* [67, 68], the fluorescence lifetime has been shown to be slightly *strain* sensitive. In that work, very small but similar lifetime strain sensitivities were observed and quantified for each of the doped fibre samples (Nd^{3+} and Yb^{3+}) tested, and these were also shown to be both independent of temperature. For most systems, the effect is too small to cause concern and therefore can be neglected in applications where a fibre temperature sensor is relatively unstrained. However, where higher levels of strain are applied, this potentially creates an alternative type of strain sensor which could possibly be exploited. These observed strain effects were also viewed as being complimentary to the known temperature sensitivities of the samples, and the possibility of a simultaneous temperature *and* strain measurement field using the lifetime approach opened up. This will be investigated further in this thesis, for a range of new materials, and also over greater temperature ranges.

Recent advances using the fluorescent lifetime technique to detect temperature include the work done in this thesis and the fabrication of a fire alarm system for aeroengine fire detection [69]. In that work, a short-range distributed sensor extensively using fluorescent materials was developed for fire sensing using hot-spot techniques.

1.5 Optical fibre strain sensing

1.5.1 Introduction and techniques of measurement

The measurement of strain forms an integral part of the sensing needs of certain sections of industry for large structures, aerospace, maritime etc. The previously discussed general advantages of optical fibre sensors (including light weight, corrosion resistance, EM immunity etc.) can sometimes make them more suited to a particular strain sensing application compared to the more conventional resistive foil strain gauges [70]. Two particular advantages for fibre strain sensing applications have been their small size capacity and geometric compatability - attributes which, for example, have enabled them to be embedded in composite materials for *in situ* real-time monitoring of strain. This was the original driving force behind the now ubiquitous fibre-optic sensors in “smart structures” for simultaneous strain and temperature recovery.

Strain has been measured by several optical fibre-based techniques - including using fibre *Bragg gratings* [3, 4, 21, 22, 30, 31], *Brillouin scattering* [3] and *polarimetry* [3] in birefringent materials, and by interferometric (usually white light) methods [71]. Of these techniques, based on recent papers at the 2002 International Optical Fiber Sensor Conference (*OFS 2002*), the FBG technology seems currently the one technique to be the most preferred.

As previously mentioned in this well known technique, a refractive index modulation grating is written into usually a single-mode germanium-doped silica fibre and strain is sensed by monitoring the reflected or transmitted wavelength from the grating, as it is subjected to elongation. The sensing mechanism is explained more fully in Chapter 4 where it is used. The strain can be sensed either individually from a basic grating [70] or from a multi-elemental array of perhaps specially constructed FBGs [72] in distributed sensing.

1.5.2 Recent advances in applications of fibre optic strain sensors

In recent years, there has been an increasing demand for a non-destructive method for inspecting and real-time monitoring of the structural integrity of civil and building structures. Distributed sensing of static strain, based on Brillouin scattering pulsed-based techniques, has shown promising results and techniques are currently being developed for civil engineering applications. In conventional techniques, a pulsed pump is used and spatial measurement is determined by the elapsed time between the launching of the pump and the receiving of the Brillouin scattered signal. As a consequence, localised strain access is sequential and interrupted, making pulse-based approaches inadequate in measuring dynamic strain at localised positions. Hotate and Leng [73] have recently overcome these conventional pulse-based problems in measuring dynamic strain at localised positions by using a correlation-based continuous-wave (CW) technique, which allows them to selectively and locally stimulate Brillouin scattering to allow random and uninterrupted access to strain information. They report results with an accuracy of $\pm 37.6 \mu\epsilon$ by achieving dynamic strain information from a 5 cm section along an optical fibre at a sampling rate of 8.8 Hz.

For strain sensing using FBGs - recent work James *et al* [34] revealed that the FBG temperature sensitivity drops to almost zero at temperatures less than 100 K, whereas the strain sensitivity remains unaffected. This paves the way for temperature-insensitive strain measurements in cryogenic environments. Also, Bragg gratings have recently been written into polymer optical fibres (POFs) [74] and have been subsequently shown to be better candidates for various strain applications, by tailoring the Young's modulus of the host polymer fibre to match particular applications, such as various liquid and elastic materials.

Plastic (polymer) optical fibres (POFs) are also being considered to detect strain in on-going work by Alexiou and colleagues [75]. Here, chemically tapered POFs were used and the transmission of light through both them and untapered POFs was measured as a function of applied stress. Preliminary results from using the tapered POFs showed a linear response to strain under tensile loading. POF - based research is beyond the scope of this work, but it is important to be aware of developments in the field, as they impact upon research into silica fibre sensors.

1.6 Summary and scope of the thesis

This thesis reports on work carried out by the author in order to make a contribution towards the development of optical fibre based sensor schemes, using the fluorescence obtained from various rare earth doped materials, for the purposes of strain and temperature measurement, either singularly or simultaneously.

1.6.1 Aims and objectives

The major aims and objectives of the work described in this thesis are:

- to review the “state-of-the-art” in the relevant field of fibre optic sensing and set the research done in that context
- to investigate developments in fluorescence-based fibre optic temperature sensors
- to determine the strain sensitivity of other (i.e. to compliment existing knowledge) important probes already used in temperature sensing, such as Er^{3+} , Nd^{3+} and Tm^{3+} silica fibre dopants (i.e. “spun off” from communications), in order to provide information for sensor compensation purposes if used in a potentially strained environment, i.e. address temperature-strain cross sensitivity issues.
- to test some of the more exotic fibres, now available from an increasingly wide range, for their sensor potential, e.g. $\text{Tm}^{3+} \text{Ho}^{3+}$, $\text{Er}^{3+} \text{Yb}^{3+}$ co-doped fibres
- to understand more about the strain effect on the measured fluorescent lifetime for the purposes of possible simultaneous temperature-strain sensing using deconvolution methods, e.g. in systems with two differently doped fibres

- to combine a lifetime sensor with another type of sensing element to achieve dual (and therefore inevitably simultaneous) temperature-strain sensing using deconvolution methods from effective, compact and intrinsic fibre probes
- to consider the role of FBG-based research in this field and carry out experiments where required.

1.6.2 Structure of thesis

An overview of current fibre sensor developments, with particular applications to temperature and strain measurement, is first presented as above. The work in Chapter 2 then goes on to explore relevant temperature-strain discrimination techniques. The recently discovered small strain sensitivity of fluorescent lifetime is also introduced in discussion as a theoretical candidate for application to simultaneous temperature-strain sensing techniques using two different doped fibres.

Chapters 3 and 4 contain the experimental results obtained by the author from using the fluorescent lifetime technique alone and the novel approach to the fluorescent lifetime, combined with the Fibre Bragg grating technique, respectively.

Finally, Chapter 5 contains a summary of the work presented in this thesis. The author's opinions on the achievements made from the work herein are given. Then, current trends in fluorescence lifetime-based sensing are discussed, both commercially and academically, together with projected work for the future.

1.7 References

- [1] K.T.V.Grattan and Z.Y.Zhang, *Fiber Optic Fluorescence Thermometry*, Chapman & Hall, London (1995)
- [2] K.T.V.Grattan and B.T.Meggitt, *Optical Fiber Sensor Technology*, Vols 1-5, Kluwer Academic Publishers (2000)
- [3] K.T.V.Grattan and B.T.Meggitt, *Optical Fiber Sensor Technology, Fundamentals*, Kluwer Academic Publishers (2000)
- [4] K.T.V.Grattan and B.T.Meggitt, *Optical Fiber Sensor Technology, Advanced Applications-Bragg Gratings and Distributed Sensors*, Kluwer Academic Publishers (2000)
- [5] S.A.Wade, *Temperature measurement using rare earth doped fibre fluorescence*, PhD thesis, Victoria University, Melbourne, Australia (1999)
- [6] M.Bellis, The Birth of fiber optics, *inventors.about.com* (2002)
- [7] Future Fibre Technologies Pty Ltd, Science of fibre optic sensors, *www.fft.com.au* (2001)
- [8] K.Kuriki, T.Kobayashi, N.Imia, T.Tamaru, S.Nishihara, A.Tagaya, Y.Koike and Y.Okamoto, Fabrication and properties of polymer optical fibers containing Nd-chelate, *IEEE Photonics Tech. Letters*, 12, 8, 989 (2000)
- [9] Q.Zhang, P.Wang, X.Sun, Y.Zhai, P.Dai, B.Yang, M.Hai and J.Xei, Amplified spontaneous emission of an Nd³⁺-doped poly (methyl methacrylate) optical fiber at ambient temperature, *Appl. Phys. Lett.*, 72, 4, 407 (1998)
- [10] K.Kuriki, T.Kobayashi, N.Imia, T.Tamaru, Y.Koike and Y.Okamoto, Organic dye – doped polymer optical fiber lasers, *Polymers for Advanced Technologies*, 11, 8-12, 612 (2000)

- [11] Y.M.Wong, P.J.Scully, R.Bartlett, V.Alexiou and H.J.Kadim, Automation and Characterisation of Chemical Tapering of Plastic Optical Fibres, in *Proceedings of Sensors and their Applications XI*, K. T. V. Grattan and S. H. Khan, eds. (IOP Publishing Ltd, London), pp. 203-208 (2001)
- [12] P.J.Scully, R.P.Chandy, Y.M.Wong, R.Bartlett, G.Grapin, G.Jonca, G.D'Ambrosio, F.Colin, N.McMillan, M.O.'Neill and P.Rouxhet, On-Line Measurement of Biofouling at Water Interfaces using Plastic Optical Fibre, in *Proceedings of Sensors and their Applications XI*, K. T. V. Grattan and S. H. Khan, eds. (IOP Publishing Ltd, London), pp. 221-227 (2001)
- [13] O.Suzuki, M.Miura, M.Morisawa and S.Muto, POF-Type Optic Humidity Sensor and its Application, in *Proceedings of 15th Optical Fiber Sensors Conference Technical Digest (published by IEEE), Portland, USA*, pp. 447 - 450 (2002)
- [14] K.T.V.Grattan, T.Sun, S.A.Wade and Z.Y.Zhang, Optical fiber sensors for high temperature measurement using fluorescence techniques, presented at the *4th International Conference on Applications of Photonics Technology (ICAPT), June 12th - 16th, Quebec City, Canada*, Applications of Photonic Technology 4 – closing the gap between theory, development, and application, pp. 1167 – 1174 (2000)
- [15] Summary of Japanese and US Optical Sensor Activities, *itri.loyola.edu* (1996)
- [16] A.Fellay, L.Thevenaz, J.Perez Garcia, M.Facchini, W.Scandale and P.Robert, Brillouin-based temperature sensing in optical fibres down to 1 K, in *Proceedings of 15th Optical Fiber Sensors Conference Technical Digest (published by IEEE), Portland, USA*, pp. 301 - 304 (2002)

Chapter 1 Optical fibre sensors

- [17] Z.Y.Zhang, T.Sun, K.T.V.Grattan and A.W.Palmer, Erbium-doped intrinsic fiber sensor for cryogenic temperature measurement, *Sensors and Actuators A – Physical* 71, 3, 183 (1998)
- [18] Data sheet from Orbis Technologies Ltd, www.orbitech.co.uk/lux10.html (2002)
- [19] J.V.Nicholas and D.R.White, *Traceable Temperatures: An Introduction to Temperature Measurement and Calibration*, 2nd edition, Chapter 9, pp343-392, John Wiley & Son (2001)
- [20] Z.Y.Zhang, K.T.V.Grattan and A.W.Palmer, Fiber optic temperature sensor based on the cross referencing between blackbody radiation and fluorescence lifetime, *Rev. Sci. Instrum.*, 63, 8, 3869 (1992)
- [21] T.Sun, *Fluorescence-based fibre optic sensor systems for temperature and strain measurement*, PhD thesis, City University, London, UK (1999)
- [22] K.T.V.Grattan and T.Sun, Fiber optic sensor technology: an overview, *Sensors and Actuators A - Physical*, 82, 40 (2000)
- [23] W.Ecke, Fibre optic interferometric sensors for measurement of physical quantities, Proc. SPIE Vol. 3483, pp. 4 - 4, European Workshop on Optical Fibre Sensors, eds. B.Culshaw and J.Jones (1998)
- [24] M.Szustakowski and W.Ciurapinski, Interferometric fiber sensors: technology and application, SPIE Vol. 4018, 80-95, Optoelectronic Metrology, eds. J.Owsick and T.Wiecek (1999)
- [25] J.Dakin and B.Culshaw, *Optical Fiber Sensors*, Artech House, Inc., Volumes 1-4 (1997)
- [26] R.M.Odic, R.I.Jones and R.P.Tatam, Distributed Temperature Sensor for Aeronautic Applications, in *Proceedings of 15th Optical Fiber Sensors Conference Technical Digest (published by IEEE), Portland, USA*, pp. 459 - 462 (2002)

- [27] Y.Shen, L.Tong, Z.Ding, Z.Y.Zhang, K.T.V.Grattan and T.Sun, Evaluation of sapphire-ruby single crystal fiber for thermometric use up to 1500°C, *Proc. of OFS 2000, Venice*, SPIE 4185, 632 (2000)
- [28] K.O.Hill, Y.Fujii, D.C.Johnson and B.S.Kawasaki, Photosensitivity in optical fiber waveguides: Application to reflection filter fabrication, *Applied Physics Letters*, 32, 647 (1978)
- [29] B.S.Kawasaki, K.O.Hill, D.C.Johnson and Y.Fujii, Narrow-band Bragg reflectors in optical fibers, *Optics Letters*, 3, 66-8 (1978)
- [30] Y.J.Rao, Review Article: In-fibre Bragg grating sensors, *Meas. Sci. Technol.* 8, 355-375 (1997)
- [31] A.Othonos, *Fiber Bragg gratings*, in *Optical Fiber Sensor Technology: Advanced Applications*, pp. 79 – 187, K.T.V.Grattan and B.T.Meggitt eds., Kluwer Academic Publishers, Dordrecht, Netherlands (2000)
- [32] A.Fernandez, B.Brichard, P.Borgermans, F.Berghmans, M.Decréton, P.Mégret, M.Blondel and A.Delchambre, Fibre Bragg grating temperature sensors for harsh nuclear environments, in *Proceedings of 15th Optical Fiber Sensors Conference Technical Digest (published by IEEE), Portland, USA*, pp. 63 - 66 (2002)
- [33] S.W.James, R.P.Tatam, A.Twin, M.Morgan and P.Noonan, Operation of Fibre Bragg Gratings At Cryogenic Temperatures, in Abstracts and Programme of *In-Fibre Bragg Gratings and Special Fibres*, meeting organised by the Institute of Physics (IOP) UK, 17 October 2001, Coventry, UK
- [34] S.W.James, R.P.Tatam, A.Twin, M.Morgan and P.Noonan, Strain response of fibre Bragg grating sensors at cryogenic temperatures, in *Proceedings of 15th Optical Fiber*

Chapter 1 Optical fibre sensors

Sensors Conference Technical Digest (published by IEEE), Portland, USA, pp. 87 - 90 (2002)

[35] M.Winz, K.Stump and T.K.Plant, High Temperature, Stable Fiber Bragg Gratings, in *Proceedings of 15th Optical Fiber Sensors Conference Technical Digest (published by IEEE), Portland, USA, pp. 195 - 198 (2002)*

[36] T.McCreadie, H.C.Seat and J.H.Sharp, Fabrication of Sapphire Fibre Long-Period Gratings, in Abstracts and Programme of *In-Fibre Bragg Gratings and Special Fibres*, meeting organised by the Institute of Physics (IOP) UK, 17 October 2001, Coventry, UK

[37] Y.L.Hu, Z.Y.Zhang, K.T.V.Grattan, A.W.Palmer and B.T.Meggitt, Ruby-based decay time thermometry: effect of probe size on extended measurement range (77-800K), *Sensors and Actuators A*, 63, 85 (1997)

[38] T.Sun, Z.Y.Zhang, K.T.V.Grattan and A.W.Palmer, Analysis of the double exponential behavior in alexandrite for optical temperature sensing applications, *Rev. Sci. Instrum.*, 68, 3442 (1997)

[39] G.W.Baxter, S.A.Wade, S.F.Collins, G.Monnom and E.Maurice, Rare-earth doped optical fibres for point temperature sensing, *SPIE Vol. 2841*, 249 (1996)

[40] T.Sun, Z.Y.Zhang, K.T.V.Grattan and A.W.Palmer, Temperature dependence of the fluorescence lifetime in Pr³⁺:ZBLAN glass for fiber optic thermometry, *Rev. Sci. Instrum.*, 68, 3447 (1997)

[41] Z.Y.Zhang, K.T.V.Grattan, A.W.Palmer and B.T.Meggitt, Potential for temperature sensor applications of highly neodymium-doped crystals and fiber at up to approximately 1000 °C, *Rev. Sci. Instrum.*, 68, 2759 (1997)

- [42] K.T.V.Grattan, J.D.Manwell, S.M.L.Sim and C.A.Willson, Lifetime investigation of fluorescence from neodymium-yttrium-aluminium garnet at elevated-temperature, *Opt. Commun.*, 62, 104 (1987)
- [43] Z.Y.Zhang, K.T.V.Grattan, A.W.Palmer and B.T.Meggitt, Spectral characteristics and effects of heat treatment on intrinsic Nd-doped fiber thermometer probes, *Rev. Sci. Instrum.*, 69, 139 (1998)
- [44] Z.Y.Zhang, T.Sun, K.T.V.Grattan and A.W.Palmer, Optical fiber temperature sensor scheme using Tm: doped yttrium oxide powder-based probe, *Proc. 13th Int. Conf. on Optical Fibre Sensors & Workshop on Device and System Technology toward Future Optical Fiber Communication and Sensing*, SPIE Vol. 3746, 422 (1999)
- [45] Z.Y.Zhang, K.T.V.Grattan, A.W.Palmer, B.T.Meggitt and T.Sun, Characterization of erbium-doped intrinsic optical fiber sensor probes at high temperatures, *Rev. Sci. Instrum.*, 69, 2924 (1998)
- [46] T.Sun, Z.Y.Zhang, K.T.V.Grattan and A.W.Palmer, Ytterbium-based fluorescence decay time fiber optic temperature sensor systems, *Rev. Sci. Instrum.*, 69, 4179 (1998)
- [47] Z.Y.Zhang, K.T.V.Grattan and B.T.Meggitt, Thulium-doped fiber optic decay-time temperature sensors - characterization of high temperature performance, *Rev. Sci. Instrum.*, 71, 1614 (2000)
- [48] T.Sun, Z.Y.Zhang, K.T.V.Grattan, Erbium/ytterbium fluorescence based fiber optic temperature sensor system, *Rev. Sci. Instrum.*, 71, 4017 (2000)
- [49] D.I.Forsyth, S.A.Wade, D.Perciante and K.T.V.Grattan, Temperature and Strain Characteristics of the 3F_4 and 3H_4 Energy levels of Tm:Ho Co-Doped Fibre, in *Proceedings of Sensors and their Applications XI*, K. T. V. Grattan and S. H. Khan, eds. (IOP Publishing Ltd, London), pp. 365-370 (2001)

- [50] S.A.Wade, S.F.Collins, G.W.Baxter, G.Monnom and E.Maurice, Rare-earth doped fibres for fluorescence-based temperature sensing, Proc. 24th Australian Conference on Optical Fibre Technology, Sydney, 195 (1999)
- [51] S.F.Collins, G.W.Baxter, S.A.Wade, T.Sun, Z.Y.Zhang and K.T.V.Grattan, Comparison of fluorescence-based temperature sensor schemes: theoretical analysis and experimental validation, *J. Appl. Phys.*, 84, 4649 (1998)
- [52] S.A.Wade, S.F.Collins, K.T.V.Grattan and G.W.Baxter, Strain-independent temperature measurement using a fluorescence intensity ratio technique in optical fiber, *Appl. Opt.*, 39, 3050 (2000)
- [53] S.A.Wade, G.W.Baxter, S.F.Collins, K.T.V.Grattan and T.Sun, Simultaneous strain-temperature measurement using fluorescence from Yb-doped silica fiber, *Rev. Sci. Instrum.*, 71, 2267 (2000)
- [54] S.A.Wade, G.W.Baxter, S.F.Collins, T.Sun, Z.Y.Zhang and K.T.V.Grattan, Strain effects in fluorescence based optical fibre temperature sensors, presented at *14th Optical Fiber Sensors Conf., Venice*, 576 (2000)
- [55] S.A.Wade, S.F.Collins, G.W.Baxter, K.T.V.Grattan, Strain-independence of the fluorescence intensity ratio temperature sensing technique in neodymium-doped optical fibre, presented at *Applied Photonics - Applications of Optical Fiber Sensors, Glasgow*, SPIE Vol. 4074, pp. 222 - 228 (2000)
- [56] S.A.Wade, S.F.Collins, G.W.Baxter and G.Monnom, Effect of strain on temperature measurements using the fluorescence intensity ratio technique (with Nd³⁺- and Yb³⁺-doped silica fibers), *Rev. Sci. Instrum.*, 72, 3180 (2001)

- [57] S.Trpkovski, S.A.Wade, S.F.Collins, G.W.Baxter and P.M.Farrel, Temperature and Strain Measurement using a Combined Fiber Bragg Grating and Fluorescence Intensity Ratio Technique in Er^{3+} -doped Fiber, in *Proceedings of 15th Optical Fiber Sensors Conference Technical Digest (published by IEEE), Portland, USA*, pp. 107 - 110 (2002)
- [58] M.Cates, D.Beshears, S.Allison and C.Simmons, Phosphor thermometry at cryogenic temperatures, *Rev. Sci. Instrum.*, 68, 2412 (1997)
- [59] S.W.Allison and G.T.Gillies, Remote thermometry with thermographic phosphors: Instrumentation and applications, *Rev. Sci. Instrum.*, 68, 2615 (1997)
- [60] S.Nagel, J.B.MacChesney and K.Walker, An Overview of the Modified Chemical Vapor Deposition (MCDV) Process and Performance, *IEEE Journal of Quantum Electronics*, QE - 18, 4, 459 (1982)
- [61] M.J.F.Digonnet, *Rare Earth Doped Fiber Lasers and Amplifiers*, 2nd edition, Marcel Dekker, Inc (2001)
- [62] V.C.Fernicola, L.Rosso, R.Galleano, T.Sun, Z.Y.Zhang and K.T.V.Grattan, Investigations on exponential lifetime measurements for fluorescence thermometry, *Rev. Sci. Instrum.*, 71, 2938 (2000)
- [63] V.C.Fernicola, Z.Y.Zhang and K.T.V.Grattan, Fiber optic thermometry based on Cr-fluorescence in olivine crystals, *Rev. Sci. Instrum.*, 68, 2418 (1997)
- [64] Z Y Zhang, K T V Grattan and A W Palmer. Thermal characteristics of alexandrite fluorescence decay at high temperatures, induced by a visible laser diode emission, *Journal of Applied Physics*, 73, 3493 (1993)
- [65] T.Sun, K.T.V.Grattan, S.A.Wade, D.I.Forsyth, Silica optical fiber based rare-earth doped sensors, in Proceedings of SPIE Vol 4596, *Advanced Photonic Sensors and Applications II*, 27-30 November, Singapore pp. 219 - 229 (2001)

- [66] T.Liu, G.F.Fernando, Z.Y.Zhang and K.T.V.Grattan, Simultaneous strain and temperature measurements in composites using extrinsic Fabry-Perot interferometric and intrinsic rare-earth doped fibre sensors, in *SPIE Conference on Sensory Phenomena and Measurement Instrumentation for Smart Structures and Materials*, San Diego, SPIE Vol. 3330, 332 (1998)
- [67] T.Sun, Z.Y.Zhang, K.T.V. Grattan and A.W.Palmer, Intrinsic doped fluorescence decay-time based measurements – strain and temperature characteristics for sensor purposes *Rev. Sci. Instrum.*, 69, 4186 (1998)
- [68] T.Sun, Z.Y.Zhang, K.T.V.Grattan and A.W.Palmer, Intrinsic strain and temperature characteristics of Yb-doped silica-based optical fibers, *Rev. Sci. Instrum.*, 70, 1447 (1999)
- [69] T.Sun, K.T.V.Grattan and W.M.Sun, Fluorescence based optical fibre fire alarm system, in *Proceedings of 15th Optical Fiber Sensors Conference Technical Digest (published by IEEE), Portland, USA*, pp. 471 - 474 (2002)
- [70] S.Melle, K.Liu and R.Measures, Practical fiber-optic Bragg grating strain gauge system, *Applied Optics*, 32, 19 (1993)
- [71] L.Yuan and L.Zhou, Temperature-compensated fibre optic strain sensor using the differential white-light interferometric technique, *Meas. Sci. Technol.*, 9, 1174 (1998)
- [72] G.Miller, C.Askins, P.Skeath, C.Wang and E.Friebele, Fabricating fiber Bragg gratings with tailored spectral properties for strain sensor arrays using a post-exposure rescan technique, in *Proceedings of 15th Optical Fiber Sensors Conference Technical Digest (published by IEEE), Portland, USA*, postdeadline paper (2002)
- [73] K.Hotate and S.Leng, A correlation-based continuous-wave technique for measurement of dynamic strain along an optical fiber using Brillouin scattering with fully distributed

Chapter 1 Optical fibre sensors

ability, in *Proceedings of 15th Optical Fiber Sensors Conference Technical Digest* (published by IEEE), Portland, USA, postdeadline paper (2002)

[74] G.Peng, Prospects of Polymer Optical Fibres and Gratings in Sensing, presented at *OFS 2002, Portland, USA*

[75] V.Alexiou, R.Bartlett, P.J.Scully and Y.M.Wong, Strain sensors using tapered plastic optical fibre, in Abstracts and Programme of *In-Fibre Bragg Gratings and Special Fibres*, meeting organised by the Institute of Physics (IOP) UK, 17 October 2001, Coventry, UK

Chapter 2

Temperature-Strain discrimination

2.1 Abstract

The work in this chapter reviews the theory and techniques for fibre temperature-strain discrimination. The recently discovered small strain sensitivity of fluorescent lifetime is put forward as a possible candidate for application to simultaneous temperature-strain sensing, using two different doped fibres in a single sensing element.

2.2 Introduction

An important goal of much current research remains the design of simple, inexpensive and easily configured sensors for monitoring temperature and strain simultaneously [1]. The many advantages on offer from the use of optical fibre sensors were explored in detail in Chapter 1, particularly for application to these more popular measurands (i.e. temperature and strain), but the last advantage of an optical fibre sensor should surely be its potential to achieve true, accurate and reliable temperature and strain data simultaneously from a single fibre sensing element [2].

The simultaneous measurement of temperature and strain is required in a large number of applications [3 - 5]. Temperature compensation is still a common problem in many instrument designs, including the measurement of slowly varying strain fields in the presence of significant temperature changes using fibre optical methods (e.g. structural monitoring with embedded sensors), and this continues to present considerable challenges to designers [6, 7]. Typically a temperature change of 1°C will have the same influence as an applied strain change of 10 $\mu\epsilon$. Of course, the simplest way to measure temperature and strain in such circumstances is to use two physically separate sensors with one isolated from strain. However, this is not practical in cases where sensors need to be embedded with minimal intrusion and where the simultaneous measurement of temperature and strain is desired from one common sensor.

2.3 Theory

The theory has been explained in some detail by Jones [6], with a good treatise on associated error propagation analyses given by Jin *et al* [7]. The temperature/strain recovery process from a single length of optical fibre is usually described using an ideal 2D matrix that maps the temperature and strain changes to the outputs of the observable measurands. In Bragg grating sensor systems and to a lesser, but noticeable, extent in doped fibre schemes, the measurement parameters are influenced by both strain and temperature. Optical fibre sensors could offer significant advantages over conventional gauges if these thermal effects and the physical strain could be separated.

The recovery of the individual values of temperature and strain in such a situation has previously been discussed in some detail by Jones [6]. In the case where the two measurand-dependent observables, such as τ (a fluorescent lifetime) and λ (an FBG wavelength), are obtained at a certain temperature T and a specific strain ε this can be represented using the following matrix equation:

$$\begin{bmatrix} \Delta\tau \\ \Delta\lambda \end{bmatrix} = \begin{bmatrix} K_{1T} & K_{1\varepsilon} \\ K_{2T} & K_{2\varepsilon} \end{bmatrix} \begin{bmatrix} T \\ \varepsilon \end{bmatrix} \quad (2.1)$$

such that,

$$\begin{bmatrix} T \\ \varepsilon \end{bmatrix} = \frac{1}{K_{1T}K_{2\varepsilon} - K_{2T}K_{1\varepsilon}} \begin{bmatrix} K_{2\varepsilon} & -K_{1\varepsilon} \\ -K_{2T} & K_{1T} \end{bmatrix} \begin{bmatrix} \Delta\tau \\ \Delta\lambda \end{bmatrix} \quad (2.2)$$

where K_{nT} and $K_{n\varepsilon}$ are the temperature and strain coefficients corresponding to the change in fluorescence lifetime $\Delta\tau$ ($n = 1$) and the change of the FBG wavelength $\Delta\lambda$ ($n = 2$).

Chapter 2 Temperature-Strain discrimination

Experimental systems can be created to exploit the above relationship, to ideally enable the simultaneous measurements of temperature and strain to be achieved, using calibration data.

The same theory could be applied to two differently doped fibres. Therefore, consider another set of measurand-dependent observables, for example τ_1 and τ_2 (the fluorescence lifetimes produced by two different rare earth doped fibres) at a certain temperature T and strain ε where each shows some sensitivity to both measurands so that

$$\begin{bmatrix} \Delta\tau_1 \\ \Delta\tau_2 \end{bmatrix} = \begin{bmatrix} K_{1T} & K_{1\varepsilon} \\ K_{2T} & K_{2\varepsilon} \end{bmatrix} \begin{bmatrix} T \\ \varepsilon \end{bmatrix} \quad (2.3)$$

such that

$$\begin{bmatrix} T \\ \varepsilon \end{bmatrix} = \frac{1}{K_{1T}K_{2\varepsilon} - K_{2T}K_{1\varepsilon}} \begin{bmatrix} K_{2\varepsilon} & -K_{1\varepsilon} \\ -K_{2T} & K_{1T} \end{bmatrix} \begin{bmatrix} \Delta\tau_1 \\ \Delta\tau_2 \end{bmatrix} \quad (2.4)$$

where $\Delta\tau_1$ and $\Delta\tau_2$ are the induced lifetime changes of sensors 1 and 2 respectively and K_{nT} and $K_{n\varepsilon}$ are the coefficients of temperature and strain respectively, for $n = 1$ or 2 in this case.

Thus the simultaneous measurement of strain and temperature by using two sensing elements is possible with knowledge of the calibration parameters of the system, assuming linear relationships and constant coefficient values [7]. From this, temperature and strain errors arising from the above system may be estimated respectively below as:

$$|\delta T| = \frac{|K_{2\varepsilon}||\delta\tau_1| + |K_{1\varepsilon}||\delta\tau_2|}{|K_{1T}K_{2\varepsilon} - K_{2T}K_{1\varepsilon}|} \quad (2.5)$$

$$|\delta\varepsilon| = \frac{|K_{2T}||\delta\tau_1| + |K_{1T}||\delta\tau_2|}{|K_{1T}K_{2\varepsilon} - K_{2T}K_{1\varepsilon}|} \quad (2.6)$$

where $\delta\tau_n$ is the error in the lifetime, and $n=1$ or 2 in this instance.

Chapter 2 Temperature-Strain discrimination

A particular description of the simultaneous discrimination of temperature and strain based on the use of dual elements involving for example two different doped fibres, or one doped fibre combined with an in-fibre grating or Fabry-Perot interferometer, is possible in terms of equations 2.3 and 2.4 for the latter, or equations 2.1 and 2.2 for the former, with the error tolerance being estimated from equations 2.5 and 2.6.

A particularly important use of the results obtained would be to form the basis of a dual element sensor [8] which could obtain temperature and strain information independently. A possible configuration for such a sensor would be to have two elements, say Nd^{3+} and Yb^{3+} , or Yb^{3+} and Er^{3+} in close proximity along one arm of a sensor network. An advantage of the use of the latter combination is the ability to pump both elements at 980 nm - the two resulting decay times could be deconvolved mathematically from the matrix and they differ quite considerably. The alternative configuration of a Bragg grating combined with a fluorescence decay time element, therefore exploiting the greater sensitivity of the grating but also recognizing its need for temperature compensation, may be the more effective dual element combination.

2.4 Temperature-strain discrimination techniques

2.4.1 Previous work

2.4.1.1 General approaches

Numerous dual parameter techniques (see Table 2.1) have previously been used by many groups [6] over the years for decoupling the influence of temperature from strain (T, ϵ) in fibre systems including:

- *interferometers* and *polarimeters* incorporating air cavities [9], using birefringent Fabry-Perot devices, two mode fibres (e.g. Vengsarkar *et al*, 1994), a Brillouin scattering scheme [10] and Dispersive Fourier transform spectroscopy (DFTS) methods (e.g. Flavin *et al*, 1994). Various resolutions have been reported (see Table 2.1). These complex extrinsic methods have posed difficulties in defining the sensing element, with similar problems reported for grating techniques that have required modification of the fibre cladding diameter.
- *FBG* techniques - usually involving intricate schemes with reference Bragg gratings (e.g. Liu *et al*, 1997 and 1998), different Bragg gratings (e.g. Patrick *et al*, 1996), dual wavelength FBGs (e.g. Xu *et al*, 1994 and Brady *et al* 1996), polarisation-rocking filters [11] or long period gratings (e.g. Bhatia *et al*, 1997 and more recently Younggeun *et al*, 2000). These techniques typically offer resolutions in the 1°C and $10 \mu\epsilon$ range, as shown in Table 2.1, and are probably the best known methods of dual temperature and strain measurement. However, such “exotic” FBG systems tend to be quite expensive when compared to the use of “stand-alone” gratings at common wavelengths [8], for example those written for communication applications, and therefore this adds considerably to the cost and complexity of use. Techniques requiring more than one type of grating to form

Chapter 2 Temperature-Strain discrimination

the sensing element have also complicated fabrication, and Bragg gratings have also been reported to have had the poorest performance in terms of temperature and strain recovery [7]. Other disadvantages may be that Long-period gratings and polarisation rocking filters are much longer than Bragg gratings (they can be a few cm in length), thus the spatial resolution will be degraded.

Often the choice of technique will be determined by multiplexing requirements, in which case FBGs are attractive because of their ease of WDM. Excellent reviews on all aspects of FBGs, including their relevant capabilities applicable to dual temperature/strain sensing, have been given by Kersey *et al* [12] and Rao [13].

Distributed systems have also featured for simultaneous temperature and strain measurement. The first fully distributed measurement system to achieve this was created by Parker and co-workers [14] using spontaneous Brillouin backscatter. However, this technique required long averaging times because of the weak scattered signals and accuracies of only 4°C and 100 µε were reported, over a 1200 m sensing length, using ranges of 22 - 70°C and 0 – 5350 µε. The technique is less well suited to point sensing due to the sophistication of the equipment required and the limited resolution achievable. It does, however, present a useful alternative to the multiplexing of a large number of FBGs to achieve an optical sensor network. Since the completion of this work, other groups started similar work in distributed sensing [15] and many groups now utilise Brillouin techniques in more sophisticated distributed fibre temperature and strain sensing work [16 - 18].

Alternatively, using fluorescence-based techniques, Jung and co-workers have demonstrated simultaneous strain and temperature measurement using the amplified spontaneous emission

Chapter 2 Temperature-Strain discrimination

(ASE) power of Er^{3+} [19] and $\text{Er}^{3+}:\text{Yb}^{3+}$ -doped fibre [20] combined with a FBG. While reasonable accuracies were obtained, the relatively long length of doped fibre required to achieve the desired level of signal amplification (7 m for Er^{3+} and 25 cm for $\text{Er}^{3+}:\text{Yb}^{3+}$) and the dependence of the amplified spontaneous emission power on the excitation power may limit the potential use of this technique for point measurements. Zhang and co-workers [21] at the *Photonics Research Group at Aston University, Birmingham, UK* have managed to overcome these sensor size and pump power-dependency problems in currently-developing work based on the same technique. Also, more recently (and after some of the initial work on Er^{3+} was completed in this thesis) fluorescence-based techniques have been discussed for temperature-strain measurement by Wade *et al* [22] using the combination of the fluorescence lifetime and the fluorescence intensity ratio, where the later approach has been shown to be essentially strain insensitive [23].

From all the general approaches to temperature-strain discrimination techniques highlighted in Table 2.1, it becomes clear that much simpler and more compact optical fibre sensor configurations for dual strain and temperature determination still need to be investigated.

2.4.1.2 With relevance to the strain sensitivity of fluorescence lifetime

Previous work on *pressure* effects (and therefore implicitly stress or *strain* [8]) in rare earth ion doped crystals and garnets have been reported by Troster *et al* [24] and more recently by Shen and Bray [25]. In [24], high pressure effects on the energy levels of Nd^{3+} and Pr^{3+} in RCl_3 have been reported, and measured fluorescent lifetimes were observed to decrease from certain energy levels when subjected to these high pressures which caused material structural changes. In [25], it was indicated that both pressure (and thus strain) and temperature have a

Chapter 2 Temperature-Strain discrimination

significant effect on the measured fluorescence lifetime of chromium doped into yttrium aluminum garnet ($\text{Cr}^{3+}:\text{YAG}$). In that work [25], the main effect of applied high pressures was to increase the ${}^4T_2 - {}^2E$ state energy separation, where pressure resulted in a reduction of the ${}^4T_2 - {}^2E$ admixture and, as a consequence, this increased the lifetime. The pressure effects on the lifetimes of other Cr^{3+} -doped crystals such as ruby [26], $\text{Cr}^{3+}:\text{Gd}_3\text{Sc}_2\text{Ga}_3\text{O}_{12}$ and $\text{Cr}^{3+}:\text{Gd}_3\text{Ga}_5\text{O}_{12}$ [27] have also been reported, and similar results published. Measurements of the pressure dependence of the lifetime of rare earth ion doped crystals, such as $\text{Gd}_2\text{O}_3:\text{Tb}$ and $\text{La}_2\text{O}_3:\text{Eu}$ have also been made [28], and these two phosphors exhibited the strongest pressure dependence of all the materials surveyed by these authors. This therefore prompted a new investigation into the effect of strain upon rare earth doped fibres, which are relatively more convenient to configure as sensing materials than bulk crystals, for the purposes of possible application simultaneous temperature-strain measurement. Strains of up to 2000 $\mu\epsilon$ can routinely be tolerated in such standard fibres of diameters in the 100–200 μm region [8].

A catalyst in this new investigation was that in work by Liu *et al* [29], it was discovered that a small strain effect occurred on the measured fluorescence lifetime of neodymium (Nd^{3+})-doped fibre. In that configuration, an optical fibre network comprising an in-fibre Fabry-Perot etalon strain sensor was coupled to an Nd^{3+} -doped fibre for the purpose of dual strain and temperature measurements, with results on tests carried out showing standard deviations of 32 $\mu\epsilon$ and 0.9°C, obtained for ranges of 0 to 1800 $\mu\epsilon$ and 20 to 90°C respectively. A further investigation of this small strain effect was subsequently taken up by Sun *et al* on Nd^{3+} [30] and Yb^{3+} [31]-doped fibres and this has confirmed the existence of the strain effect

Chapter 2 Temperature-Strain discrimination

on the fluorescence signal for potential applications to simultaneous temperature and strain measurement.

The theoretical background which can be applied to generalised two-element sensors has been discussed previously in section 2.3. Hence, the performances of different fibre materials under various strain and/or temperature excursions need to be considered, results reported, and a full discussion of their characteristics for potential use with such an in-fibre sensor system should follow. More recently, after some of the initial work on Er^{3+} was completed in this thesis, Sharp & Seat [32] also found the fluorescence lifetime to be slightly strain sensitive in work using single-crystal ruby fibre.

2.4.2 Other recent work

Recent work on fibre temperature-strain discrimination has mainly involved the use of ubiquitous Fibre Bragg gratings (FBGs), which are seemingly now also dominating temperature-strain discrimination techniques (i.e. as well as presently the measurement of those quantities individually, as explained in Chapter 1). For example:

- Rao *et al* [2] have recently used a chirped in-fibre Bragg grating (CFBG)/extrinsic Fabry-Perot (EFPI) sensor system to achieve fast and novel absolute temperature and strain data simultaneously by effectively separating the output of the EFPI from that of the CFBG by wavelength division multiplexing (WDM) methods, allowing strain to be measured without cross-talk from the temperature measurement. Experimental results show uncertainties of 2°C and $20\ \mu\epsilon$ over the ranges $30 - 95^\circ\text{C}$ and $0 - 800\ \mu\epsilon$ respectively.

Chapter 2 Temperature-Strain discrimination

- Shu *et al* [33] have reported results of a systematic investigation into the dependence of both temperature and strain sensitivities on the grating type (I, IIA and their new type IA). Having identified the distinct sensitivity characteristics for each, they have implemented a novel, dual grating, dual parameter sensor device which is reported to be accurate to $0.54^{\circ}\text{C}/\mu\text{m}$ and $4.4 \mu\epsilon/\mu\text{m}$ over the ranges $0 - 80^{\circ}\text{C}$ and $0 - 2000 \mu\epsilon$ respectively.
- Valdivielso *et al* [34] have used a FBG and a thermochromic material attached to the end of the same fibre pigtail; the first one to measure strain and the second one to measure temperature and correct the information of the FBG. They do not mention specific resolutions in the work, but report successful testing over the $20 - 80^{\circ}\text{C}$ and $0 - 7000 \mu\epsilon$ range.
- Wade *et al* [35] have recently combined the fluorescent intensity ratio technique of temperature sensing [36] with a FBG for the first time to achieve dual temperature-strain sensing in on-going work. Preliminary reports suggest that forthcoming resolutions will be satisfactory, over the ranges $19 - 140^{\circ}\text{C}$ and $0 - 3000 \mu\epsilon$ respectively, since this particular thermometric technique is known to have a very low cross sensitivity to strain.

2.5 Summary

Along with the theory, a plethora of methods from the last 8 years or so aimed at achieving accurate and reliable temperature and strain data from a single length of fibre sensor have been described in detail in this chapter, and these have been mostly summarised in Table 2.1. Reports of accuracies in most of the published work tend to talk in terms of resolutions given as root-mean-square (rms) values (i.e. equal to a standard deviation (σ) of 1σ), and these are shown as temperature T ($^{\circ}\text{C}$) and strain ϵ ($\mu\epsilon$) errors in Table 2.1. In common with all these techniques, as can easily be seen from Table 2.1, is that a clear and effective practical solution has yet to be put forward and all approaches suffer to some degree from errors associated with the measurement process. We will now investigate our own sensor schemes for determining these (T, ϵ) parameters, and the associated errors, and compare the results we achieve with those described here.

Chapter 2 Temperature-Strain discrimination

T (°C)	ε ($\mu\varepsilon$)	technique	source and range
0.2	3	Demultiplexing gratings	Brady <i>et al</i> Optics Communications 111 1994 51 (23-50°C, to 1000 $\mu\varepsilon$)
0.4	12	Dispersive Fourier transform spectroscopy (DFTS)	Flavin <i>et al</i> Opt Letters 19 1994 2167 (over 25°C, over 1500 $\mu\varepsilon$)
5	10	Dual wavelength gratings	Xu <i>et al</i> Electronic Letters 30 1994 1085 (10 - 60°C, 0 - 600 $\mu\varepsilon$)
5	10	Two-mode fibres	Vengsarkar <i>et al</i> J Light Tech. 12 1994 170 (over 90°C, over 500 $\mu\varepsilon$)
1.7/pm	17/pm	Dual wavelength gratings	Brady <i>et al</i> Proc SPIE 2839 1996 8 (32 - 57°C, 400 - 3200 $\mu\varepsilon$)
1.5	9	Different gratings	Patrick <i>et al</i> IEEE Phot Tech. Letts 8 1996 1223 (25 - 50°C, 290 - 1270 $\mu\varepsilon$)
1	17	Two Bragg Gratings	James <i>et al</i> Electronic Letters 32 1996 12 (25 - 150°C, 0 - 2500 $\mu\varepsilon$)
4	100	Spontaneous Brillouin Backscatter	Parker <i>et al</i> IEEE Phot Tech. Letts 9 1997 7 (22 - 70°C, 0 - 5350 $\mu\varepsilon$)
1	58	Long period grating	Bhatia <i>et al</i> Opt Letters 22 1997 648 (over 125°C, over 2100 $\mu\varepsilon$)
1.7/pm	17/pm	Dual wavelength gratings	Brady <i>et al</i> IEE Proc. Optoelectronics, 144, 3, 1997 (37 - 57°C, 1800 $\mu\varepsilon$)
2.4	31.8	Combined FBG/Extrinsic Fabry-Perot interferometric (EFPI)	Liu <i>et al</i> Proc. 12th International Conference on Optical Fiber Sensors, 1997 (30 - 60°C, 0 - 1200 $\mu\varepsilon$)
0.9	32	Combined fluorescence/Extrinsic Fabry-Perot interferometric (EFPI)	Liu <i>et al</i> Proc SPIE 3330 1998 p332-341 (20 - 90°C, 0 - 1800 $\mu\varepsilon$)
0.7	40	Two-mode fibre scanning interferometer	Sinha <i>et al</i> Proc SPIE 3541 1999 p82 (20 - 60°C, over 1600 $\mu\varepsilon$)
1.9	22	Bragg gratings + Brillouin OTDA	Posey <i>et al</i> Proc SPIE 3746 1999 p341-4 (0 - 60°C, 200 - 2400 $\mu\varepsilon$)
0.7	18.2	ASE	Jung <i>et al</i> Applied Optics 38 1999 13 (45 - 150°C, 0 - 1200 $\mu\varepsilon$)
4	35	Two Bragg Gratings	Frank <i>et al</i> Proc SPIE 3860 1999 p89-97 (2 - 95°C, 0 - 3500 $\mu\varepsilon$)
1.6	8.5	Single Bragg Grating	Guan <i>et al</i> Electronic Letters 36 2000 12 (40 - 100°C, 0 - 500 $\mu\varepsilon$)
1.2	20	Superstructure Bragg Grating	Guan <i>et al</i> IEEE Phot Tech. Letts 12 2000 6 (20 - 120°C, 0 - 1200 $\mu\varepsilon$)
3	54.8	ASE	Jung <i>et al</i> Applied Optics 39 2000 7 (50 - 180°C, 0 - 1100 $\mu\varepsilon$)
2.5	26	Interferometric interrogated FBG	Ferreira <i>et al</i> Optical Eng. 39 2000 8 (20 - 140°C, 0 - 1000 $\mu\varepsilon$)
4	290	Spontaneous Brillouin Backscatter	Kee <i>et al</i> Opt Letters 25 2000 10 (23 - 53°C, 0 - 6500 $\mu\varepsilon$)
1.6	32	Stimulated Brillouin scattering	Posey <i>et al</i> IEICE T-on-E E83-C 3 2000 p413-17 (10 - 60°C, 178 - 1245 $\mu\varepsilon$)
1.3	23	Long period Gratings	Younggeun <i>et al</i> IEICE T-on-E E83-C 3 2000 p282-6 (20 - 70°C, 0 - 3000 $\mu\varepsilon$)
4	100	Microwave spontaneous Brillouin backscatter	Maughan <i>et al</i> Meas. Science & Tech. 12 2001 7 (22 - 65°C, 730 - 4600 $\mu\varepsilon$)
0.54/pm	4.4/pm	Dual grating, dual parameter sensor	Shu <i>et al</i> Proc OFS 2002 p83 (0 - 80°C, 0 - 2000 $\mu\varepsilon$)
2	20	WDM chirped intrinsic FBG + extrinsic Fabry - Perot	Rao <i>et al</i> Proc OFS 2002 p207 (30 - 95°C, 0 - 800 $\mu\varepsilon$)

Table 2.1 Summary of techniques and reported errors (rms) from various dual temperature/strain (T, ε) fibre-based sensor schemes (ranges used in brackets).

2.6 References

- [1] S.A.Wade, G.W.Baxter, S.F.Collins, K.T.V. Grattan and T.Sun, Simultaneous strain-temperature measurement using fluorescence from Yb-doped silica fiber, *Rev. Sci. Instrum.* 71, 2267 (2000)
- [2] Y.J.Rao, X.K.Zeng, Y.P.Wang, T.Zhu and Z.L.Ran, Temperature-Strain Discrimination Using a Wavelength-Division-Multiplexed Chirped in-Fibre-Bragg-Grating/Extrinsic Fabry-Perot Sensor System, in *Proceedings of 15th Optical Fiber Sensors Conference Technical Digest (published by IEEE), Portland, USA*, pp. 207 - 210 (2002)
- [3] C.I.Merzbacher, A.D.Kersey and E.J.Friebele, Fiber optic sensors in concrete structures: a review, *Smart Mater. Struct.* 5, 196 (1996)
- [4] E.J.Friebele, C.G.Askins, A.B.Bosse, A.D.Kersey, H.J.Patrick, W.R.Pogue, M.A.Putnam, W.R.Simon, F.A.Tasker, W.S.Vincent and S.T.Vohra, Optical fiber sensors for spacecraft applications, *Smart Mater. Struct.* 8, 813 (1999)
- [5] E.Udd, Fiber optic smart structures, *Proc. IEEE* 84, 6, 884 (1996)
- [6] J.D.C.Jones, Review of fibre sensor techniques for temperature-strain discrimination, *12th International Conf. on Optical Fibre Sensors*, Williamsburg, VA, USA, OSA Tech. Digest Series 16, 36 (1997)
- [7] W.Jin, W.C.Michie, G.Thursby, M.Konstantaki and B.Culshaw, Simultaneous measurement of strain and temperature: error analysis, *Opt. Eng.* 36, 2, 598 (1997)
- [8] T.Sun, Z.Y.Zhang, K.T.V.Grattan and A.W.Palmer, Intrinsic strain and temperature characteristics of Yb-doped silica-based optical fibers, *Rev. Sci. Instrum.*, 70, 1447 (1999)
- [9] E.J.Friebele, M.A.Putnam, H.J.Patrick, A.D.Kersey and A.S.Greenblatt, Ultrahigh-sensitivity fibre-optic strain and temperature sensor, *Optics Letters*, 23, 222 (1998)

Chapter 2 Temperature-Strain discrimination

- [10] T.R.Parker, M.Farhadiroushan, R.Feced, V.A.Handerek and A.J.Rogers, Simultaneous distributed measurement of strain and temperature from noise-initiated Brillouin Scattering in optical fibres, *IEEE Journal of Quantum Electronics*, 34, 645 (1998)
- [11] S.E.Kanellopoulos, V.A.Handerek and A.J.Rogers, Simultaneous strain and temperature sensing with photogenerated in-fiber gratings, *Opt. Lett.*, 20, 333 (1995)
- [12] A.D.Kersey, M.A.Davis, H.J.Patrick, M.LeBlanc, K.P.Koo, C.G.Askins, M.A.Putnam and E.J.Friebele, Fiber Grating Sensors, *J. Lightwave Tech.* 15, 8, 1442 (1997)
- [13] Y.J.Rao, Review Article: In-fibre Bragg grating sensors, *Meas. Sci. Technol.* 8, 355 (1997)
- [14] T.R.Parker, M.Farhadiroushan, V.A.Handerek and A.J.Rogers, A Fully Distributed Simultaneous Strain and Temperature Sensor using Spontaneous Brillouin Backscatter, *IEEE Photon. Technol. Lett.* 9, 979 (1997)
- [15] K.De Souza, P.C.Wait and T.P.Newson, Characterisation of strain dependence of the Landau-Placzek ratio for distributed sensing, *Electron. Lett.* 33, 7, 615 (1997)
- [16] H.H.Kee, G.P.Lees and T.P.Newson, All-fiber system for simultaneous interrogation of distributed strain and temperature sensing by spontaneous Brillouin scattering, *Optics Letters*, 25, 695 (2000)
- [17] R.Posey Jr., S.T.Vohra and A.B.Tveten, Simultaneous measurements of temperature and strain using stimulated Brillouin scattering in GeO₂ –doped core and dispersion shifted fiber, *IEICE-Transactions-on-Electronics*, E83-C, 3, 413 (2000)
- [18] S.M.Maughan, H.H.Kee and T.P.Newson, Simultaneous distributed fibre temperature and strain sensor using microwave coherent spontaneous Brillouin backscatter, *Meas. Sci. Technol.* 12, 834 (2001)

Chapter 2 Temperature-Strain discrimination

- [19] J.Jung, H.Nam, J.H.Lee, N.Park and B.Lee, Simultaneous measurement of strain and temperature by use of a single-fiber Bragg grating and an erbium-doped fiber amplifier, *Appl. Opt.* 38, 2749-51 (1999)
- [20] J.Jung, N.Park and B.Lee, Simultaneous measurement of strain and temperature by use of a single fiber Bragg grating written in an erbium: ytterbium-doped fiber, *Appl. Opt.* 39, 1118-20 (2000)
- [21] Y.C.Lai, G.F.Qiu, W.Zhang, L.Zhang, I.Bennion and K.T.V.Grattan, Simultaneous Measurement of Temperature and Strain by Combining Active fibre with Fibre Gratings, in *Proceedings of Sensors and their Applications XI*, K. T. V. Grattan and S. H. Khan, eds. (IOP Publishing Ltd, London), pp. 135-139 (2001)
- [22] S.A.Wade, G.W.Baxter, S.F.Collins, K.T.V. Grattan and T.Sun, Simultaneous strain-temperature measurement using fluorescence from Yb-doped silica fiber, *Rev. Sci. Instrum.* 71, 2267 (2000)
- [23] S.A.Wade, S.F.Collins, K.T.V.Grattan and G.W.Baxter, Strain-independent temperature measurement using a fluorescence intensity ratio technique in optical fiber, *Appl. Opt.*, 39, 3050 (2000)
- [24] Th.Troster, T.Gregorian and W.B.Holzapfel, Energy levels of Nd^{3+} and Pr^{3+} in RCL_3 under pressure, *Physical Review B*, Vol. 48, 5 (1993)
- [25] Y.R.Shen and K.L.Bray, Effect of pressure and temperature on the lifetime of Cr^{3+} in yttrium aluminum garnet, *Physical Review B*, 56, 10882 (1997)
- [26] J.H.Eggert, K.A.Goettel and I.F.Silvera, Ruby at high pressure. II. Fluorescence lifetime of the R line to 130gpa, *Physical Review B*, 40, 5733 (1989)
- [27] U.Hommerich and K.L.Bray, High-pressure laser spectroscopy of $\text{Cr}^{3+}:\text{Gd}_3\text{Sc}_2\text{Ga}_3\text{O}_{12}$ and $\text{Cr}^{3+}:\text{Gd}_3\text{Ga}_5\text{O}_{12}$, *Physical Review B*, 51, 12133 (1995)

Chapter 2 Temperature-Strain discrimination

- [28] S.W.Allison and G.T.Gillies, Remote thermometry with thermographic phosphors: Instrumentation and applications, *Rev. Sci. Instrum.*, 68, 2615 (1997)
- [29] T.Liu, G.F.Fernando, Z.Y.Zhang and K.T.V.Grattan, Simultaneous strain and temperature measurements in composites using extrinsic Fabry-Perot interferometric and intrinsic rare-earth doped fibre sensors, in SPIE Conference on *Sensory Phenomena and Measurement Instrumentation for Smart Structures and Materials*, San Diego, SPIE Vol. 3330, 332 (1998)
- [30] T.Sun, Z.Y.Zhang, K.T.V. Grattan and A.W.Palmer, Intrinsic doped fluorescence decay-time based measurements – strain and temperature characteristics for sensor purposes *Rev. Sci. Instrum.*, 69, 4186 (1998)
- [31] T.Sun, Z.Y.Zhang, K.T.V.Grattan and A.W.Palmer, Intrinsic strain and temperature characteristics of Yb-doped silica-based optical fibers, *Rev. Sci. Instrum.*, 70, 1447 (1999)
- [32] J.H.Sharp and H.C.Seat, Temperature and Strain Characteristics of Ruby Fibre Fluorescence Emission, in *14th International Conference on Optical Fiber Sensors*, A.G.Mignani and H.C.Lefèvre, eds., Proc. SPIE 4185, 54 (2000)
- [33] X.Shu, Y.Liu, D.Zhao, B.Gwandu, F.Floreani, L.Zhang and I.Bennion, Fiber grating type dependence of temperature and strain coefficients and application to simultaneous temperature and strain measurement, in *Proceedings of 15th Optical Fiber Sensors Conference Technical Digest (published by IEEE), Portland, USA*, pp. 83 - 86 (2002)
- [34] C.Fernandez-Valdivielso, I.R.Matias and F.J.Arregui, Simultaneous Measurement of Strain and Temperature using a Fiber Bragg Grating and a Thermochromic Material, in *Proceedings of 15th Optical Fiber Sensors Conference Technical Digest (published by IEEE), Portland, USA*, pp. 203 - 206 (2002)

Chapter 2 Temperature-Strain discrimination

- [35] S.Trpkovski, S.A.Wade, S.F.Collins, G.W.Baxter and P.M.Farrel, Temperature and Strain Measurement using a Combined Fiber Bragg Grating and Fluorescence Intensity Ratio Technique in Er^{3+} -doped Fiber, in *Proceedings of 15th Optical Fiber Sensors Conference Technical Digest (published by IEEE), Portland, USA*, pp. 107 - 110 (2002)
- [36] S.A.Wade, S.F.Collins, G.W.Baxter, K.T.V.Grattan, Strain-independence of the fluorescence intensity ratio temperature sensing technique in neodymium-doped optical fibre, presented at *Applied Photonics - Applications of Optical Fiber Sensors, Glasgow*, SPIE Vol. 4074, pp. 222 - 228 (2000)

Chapter 3

Optical fibre temperature and strain sensors based on fluorescence lifetime monitoring

3.1 Abstract

The work in this chapter reports on, compares and models results obtained from various experimental schemes containing a range of different rare-earth doped sensing materials using fluorescent lifetime techniques for potential application to the measurement of both temperature and strain. In addition to the better known temperature effect on the fluorescent lifetime used extensively before for temperature sensing, the observed small strain sensitivity of rare-earth doped fibres is studied and quantified extensively for various doped fibres, to consider its potential for application to dual temperature/strain sensing. Furthermore, other parameters, such as sensor length, pump power and high temperature annealing effects, which may affect the fluorescence signal, have been considered and the results of these tests are discussed here.

3.2 Introduction

Optical fibre sensor schemes for the measurement of a range of parameters have been developed and considered in some detail over several decades [1]. Fibre optic thermometry, based upon the use of rare-earth doped silica fibre as the sensor element, has been discussed in detail in the last two chapters and has proved to be a cheap, intrinsic and simple sensor scheme to implement [2]. A range of doped fibre is now available, usually arising from telecommunications applications, and this has been exploited in several systems, even though the small diameter core single mode fibre most readily available is less than optimum for sensor use in this way. In most previous work, the effects of strain upon the fibre used for temperature sensing, such as may occur when simultaneous strain and temperature measurements are made with a single optical network, had been ignored. In this work, the proven small strain sensitivity of the fluorescence lifetime in rare-earth doped fibres is studied and quantified extensively for various dopants, to consider their potential for application to dual temperature/strain sensing. A $Y_2O_3:Tm^{3+}$ powder probe will also be investigated for high temperature thermometry applications.

3.3 Erbium doped fibre based sensors

Er^{3+} doped fibre has been widely used for optical fibre communications due to its low loss at a band around 1550 nm wavelength. It also has proven its importance in high-temperature thermometry by researchers in the development of a range of temperature sensors [3]. In this work, a study has been carried out on the effect of longitudinal strain (up to the level of fibre fracture) upon fluorescence decay-time based temperature sensor schemes, using various doping levels of Er^{3+} , and the resulting potential errors in uncorrected systems have been

Chapter 3 Optical fibre temperature and strain sensors based on fluorescence lifetime monitoring

evaluated and quantified. Results obtained are compared with those from other similar systems and recommendations for intrinsic optical fibre-based, simultaneous strain-temperature sensors are made.

3.3.1 200 ppm and 960 ppm doped fibres

3.3.1.1 Experimental arrangement

The experimental arrangement used was similar to that of previous work [4, 5], and is shown schematically in Fig.3.1:

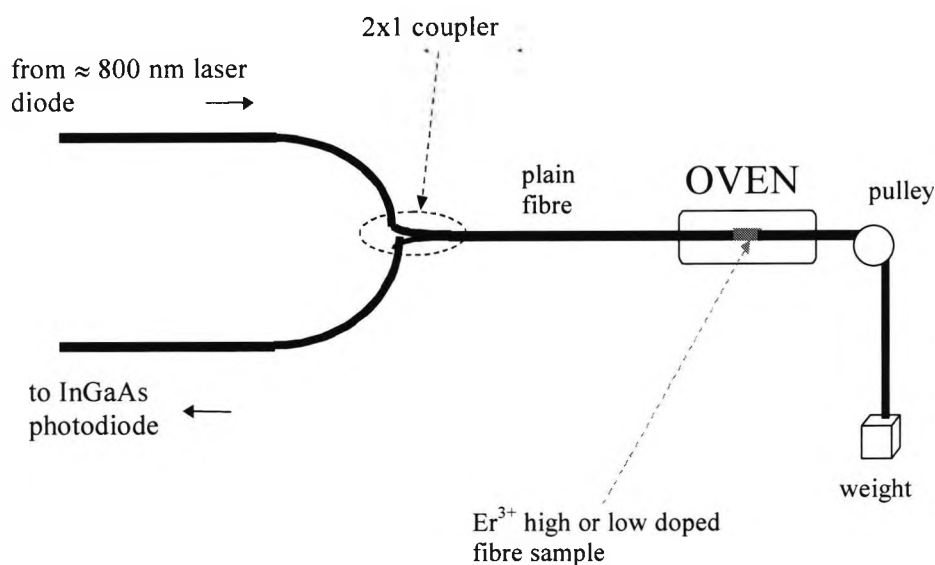


Fig.3.1 Simplified schematic of experimental arrangement used in Er³⁺ doped fibre strain and temperature tests.

It consisted of a laser diode pump (centre wavelength $\lambda = 813$ nm and maximum power $P_0 = 40$ mW) which was modulated via an external electronic source. The 813 nm wavelength of the laser was selected to fall within the absorption band of the Er³⁺-doped material used [6],

Chapter 3 Optical fibre temperature and strain sensors based on fluorescence lifetime monitoring

and the laser output was coupled by fusion splicing the fibre output of the laser diode to one fibre input of a 2x1 coupler. The output of the coupler was connected to a conventional communications fibre leading to a stable tube oven (STANTON REDCROFT), into which was fusion-spliced the ~5 cm long test piece of single-mode (3 μm /125 μm core/cladding diameter) Er^{3+} fibre, using both 960 ppm and 200 ppm levels of doping, in two separate experiments. This length of fibre used was chosen to ensure an adequate absorption and fluorescence signal yield. The other end of the sample was fused to a similar piece of communications fibre. The outer plastic coating of both fibre types, within the oven confines, were removed as plastic cannot survive at these very high temperatures. Strain was applied by using a pulley system with weights added, progressively, controlling the overall strain exerted on the test fibre. Care was taken to prevent the fibre from touching the tube oven glass and to lubricate the pulley in order to minimize friction. The detector used, an InGaAs photodiode, was chosen to cover the spectral fluorescence emission range at wavelengths greater than the laser wavelength and was connected to the other input of the coupler [6]. Thus with the above system the temperature and strain applied to the fibre sensor could be carefully controlled and monitored.

It was necessary to measure the fluorescence lifetime change arising from the doped fibre, due to the applied strain or the temperature variation, and for this task an analogue-to-digital card connected to a PC was used to process the signal electronically. The time evolution of the exponential decay in the fluorescence was obtained by the photodiode when the laser diode was modulated to switch off, with a sampling frequency of 10 kHz being employed. A test was first performed to estimate the range of strains which could be applied to the

Chapter 3 Optical fibre temperature and strain sensors based on fluorescence lifetime monitoring

completed fibre system without damage. From a knowledge of the dimensions and mechanical properties of a fibre, any applied longitudinal strain (ϵ) arising due to a weight (mg) applied to the fibre via a pulley can be easily calculated from:

$$\epsilon = \frac{mg/A}{Y} \quad (3.1)$$

where A is the cross-sectional area of the fibre (m^2), Y is Young's Modulus (= stress/strain) = $7.31 \times 10^{10} \text{ Nm}^{-2}$ (for fused quartz at room temperature), and m is the mass of the weight stretching the fibre (kg). This fibre was found to break for a total load of approximately 236 g which corresponded to a strain of about $2500 \mu\epsilon$ (calculated from equation 3.1 for the $125 \mu\text{m}$ diameter used in this case). Therefore strain levels well below this were routinely used to prevent fibre fracture.

3.3.1.2 Results

It is found that following the termination of the excitation light pulse, the fluorescence decay signal can be written as an exponential as a function of time, t , by:

$$f(t) = A \exp(-t/\tau) + B \quad (3.2)$$

where A corresponds to the initial fluorescence amplitude; τ is the corresponding fluorescence lifetime, which is temperature-dependent; and B is the signal baseline offset.

A series of results was taken, from which an exponential relationship was found to fit very closely to the data, without having a substantial mismatch. All the plots were obtained by processing a 512 point time series, with an integration run-time of 100 mins in each case. This integration time is much longer than would be expected for an actual sensor system, but

Chapter 3 Optical fibre temperature and strain sensors based on fluorescence lifetime monitoring

it was useful to undertake, in this laboratory test, an analysis which would ensure an accurate determination of the magnitude of the very small strain effect present and examine the viability of a sensor based on this. The method of signal analysis was quite different from the previously employed phase-locked detection (PLD) method [4, 5, 7] or the non-iterative method reported [8]; but an acceptable level of error was obtained. Although the signal-to-noise ratio of the system is relatively small, it is satisfactory in that the effects of temperature and strain on the lifetime can still be clearly identified and measured. The processing scheme employed a Marquardt-Levenberg algorithm for parameter estimation - an accurate tool but slow for on-line operation.

Fig.3.2 shows a plot of the lifetime as a function of strain for one of the fibres (960 ppm) at one of the typical stabilised oven temperatures (125°C), whereas the lifetime observed over a range of temperatures is shown in Fig.3.3. The slopes of all the graphs are obtained by assuming a linear fit to the data, using a straightforward least squares regression, which seems satisfactory given the measurement errors.

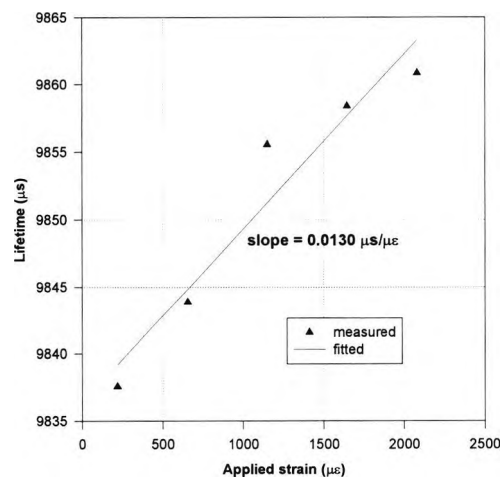


Fig.3.2 Lifetime as a function of strain for 960 ppm Er^{3+} doped fibre at 125°C.

Chapter 3 Optical fibre temperature and strain sensors based on fluorescence lifetime monitoring

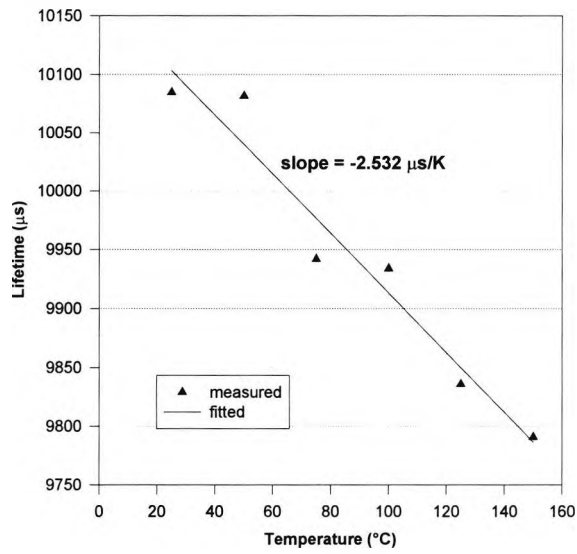


Fig.3.3 Lifetime vs. temperature (without strain) for 960 ppm Er³⁺ doped fibre.

Similar calibration graphs were obtained for the 200 ppm fibre. Fig.3.4 shows the lifetime as a function of strain at 50°C for the 200 ppm Er³⁺ doped fibre and Fig.3.5 shows the lifetime versus temperature plot for this same fibre.

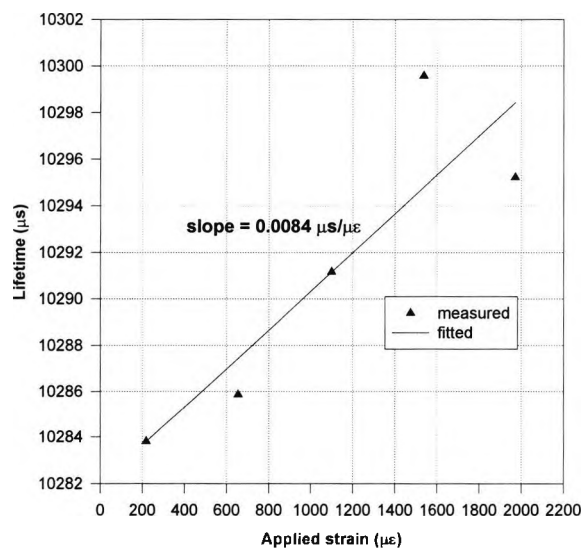


Fig.3.4 Lifetime as a function of strain at 50°C for 200 ppm Er³⁺ doped fibre.

Chapter 3 Optical fibre temperature and strain sensors based on fluorescence lifetime monitoring

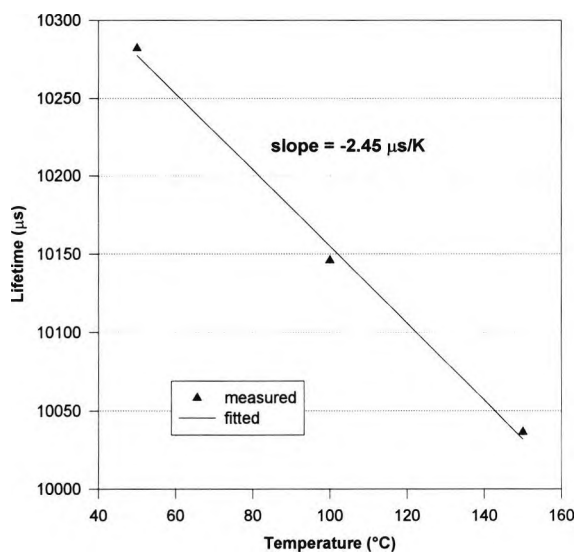


Fig.3.5 Lifetime vs. temperature (without strain) plot for 200 ppm Er³⁺ doped fibre.

In Fig.3.6, the strain sensitivity of the lifetime to temperature for both fibres is shown with standard deviation error bars, to show explicitly the high level of uncertainty in these results.

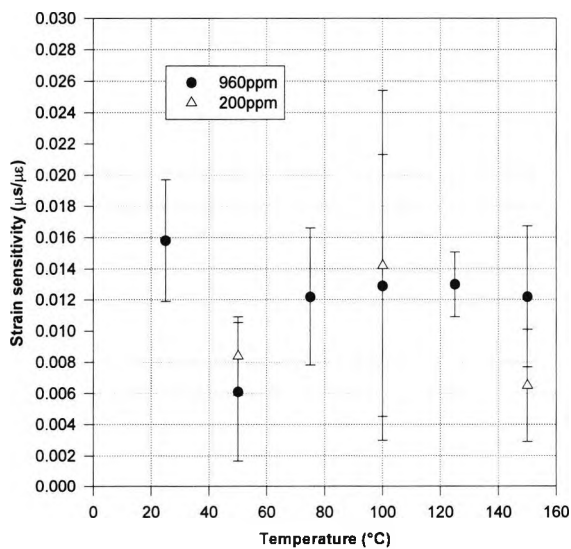


Fig.3.6 Strain sensitivity of fluorescent lifetime to temperature for both fibres.

Chapter 3 Optical fibre temperature and strain sensors based on fluorescence lifetime monitoring

Results were obtained for both fibres over a range of stable temperatures between 20 and 150°C. They each show quite a high degree of error, in spite of the long integration time, due to the comparatively small nature of the strain effect, when compared to the temperature sensitivity. However, and very important for potential sensor applications, there appears to be no *additional* temperature effect in that the change in sensitivity plotted as a function of temperature shows a zero slope for both the 960 ppm and 200 ppm doped fibres, at an average value of $\approx 1 \times 10^{-2} \mu\text{s}/\mu\epsilon$. This observation is consistent with results from previous work studying Nd^{3+} and Yb^{3+} doped fibre characteristics [4, 5].

The performance of the three different thermometer schemes using different doped fibres, in terms of the effect of strain on temperature measurement, is compared in order to assess the most suitable for sensor applications. The other fibres considered are Nd^{3+} (7.5%wt)* and Yb^{3+} (2.5%wt) doped fibres, and the results shown in Table 3.1 were obtained from previously reported work in this field [4, 5]. As an index of sensitivity against strain for these temperature-based sensors, the following can be used:

$$\frac{\partial T}{\partial \epsilon} = \frac{\partial T}{\partial L} \cdot \frac{\partial L}{\partial \epsilon} \quad (3.3)$$

where T represents temperature, L lifetime and ϵ strain showing the degree to which the apparent temperature response of the thermometer changes due to the applied strain. Values

of $\frac{\partial L}{\partial T}$ in units of $\mu\text{s K}^{-1}$ are obtained from the temperature calibrations and values of $\frac{\partial L}{\partial \epsilon}$ in

units of $\mu\text{s } \mu\epsilon^{-1}$ (sensitivity) are estimated from the slopes of the graphs of the type of Fig.3.2.

(* Nd^{3+} 300 ppm was an error in the published paper *Rev. Sci. Instrum.*, 71, 104 (2000))

Chapter 3 Optical fibre temperature and strain sensors based on fluorescence lifetime monitoring

The gradients were assumed constant (this was consistent with previously reported work) for this estimation and so they are not expressed for a given temperature or strain. Table 3.1 shows the estimations of the slopes in four cases (200 ppm and 960 ppm doping levels of Er^{3+} , and the samples of Yb^{3+} and Nd^{3+}) with an index of sensor performance for the equivalent variation, ΔT (in K), in the sensor output temperature for a case of 1000 $\mu\epsilon$ applied to the fibre.

3.3.1.3 Discussion

From these results in Table 3.1, it can be observed that the Er^{3+} -doped fibre lifetime is much longer in comparison to those of the Nd^{3+} and Yb^{3+} doped fibres at room temperature, and that the lifetime change and resulting temperature dependencies are essentially similar for both the 960 ppm and the 200 ppm doped Er^{3+} fibres. However, the absolute sensitivity of lifetime against strain is very different to the previous values reported for Nd^{3+} and Yb^{3+} (both of which are very similar to each other).

For the optimisation of temperature measurement, Nd^{3+} -doped appears to be still the most suitable fibre since it has the highest *relative* sensitivity ($\frac{\partial L}{\partial T}/L$), allowing more precise temperature measurement, as well as the lowest sensitivity to strain (for example, an error in the temperature measurement of 1.8°C arises due to a 1000 $\mu\epsilon$ variation).

This property of strain sensitivity and consequent lifetime variation could be employed for strain-temperature measurements in composite sensors [4, 5]. From this point of view, Er^{3+} -

Chapter 3 Optical fibre temperature and strain sensors based on fluorescence lifetime monitoring

doped fibres seem to be in the middle range of sensitivity of the other two samples considered, with a *relative* sensitivity ($\frac{\partial L}{\partial \epsilon}/L$) also lying between that of the Nd³⁺ and the Yb³⁺-doped fibres. The results also show that there seems to be little difference in the strain dependence of the fluorescence lifetime between the use of the different dopant Er³⁺ fibres, which will be further confirmed below, but only between the doping ions, i.e Er³⁺, Yb³⁺ and Nd³⁺.

	Er ³⁺ 200 ppm	Er ³⁺ 960 ppm	Yb ³⁺ 2.5%wt [5]	Nd ³⁺ 7.5%wt [4]
typical lifetime at 25°C (μs)	10350	10100	875	365
$\frac{\partial L}{\partial \epsilon} \left(\frac{\mu s}{\mu \epsilon} \right)$	$(1.0 \pm 0.2) \times 10^{-2}$	$(1.2 \pm 0.3) \times 10^{-2}$	$(4.3 \pm 0.8) \times 10^{-4}$	$(5.0 \pm 0.5) \times 10^{-4}$
$\frac{\partial L}{\partial T} \left(\frac{\mu s}{K} \right)$	$-2.45 \pm (0.2)$	$-2.53 \pm (0.3)$	$-0.07 \pm (0.01)$	$-0.28 \pm (0.03)$
$\frac{\partial T}{\partial \epsilon} \left(\frac{K}{\mu \epsilon} \right)$	0.0040	0.0047	0.0061	0.0018
$\Delta T @ 1000 \mu \epsilon$ (K)	4.0	4.7	6.1	1.8

Table 3.1 Comparison of performance of doped fibres for sensor use.

(* Nd³⁺ 300 ppm was an error in the published paper *Rev. Sci. Instrum.*, 71, 104 (2000))

3.3.2 1050 ppm doped fibre

3.3.2.1 Experimental arrangement

The set-up for the calibration measurements of temperature and strain for this fibre was as shown in Fig. 3.7. The experimental arrangement consisted of a laser diode pump (centre

Chapter 3 Optical fibre temperature and strain sensors based on fluorescence lifetime monitoring

wavelength, $\lambda = 980 \text{ nm}$ and maximum power, $P_0 = 2 \text{ mW}$) which was modulated via an external electronic source.

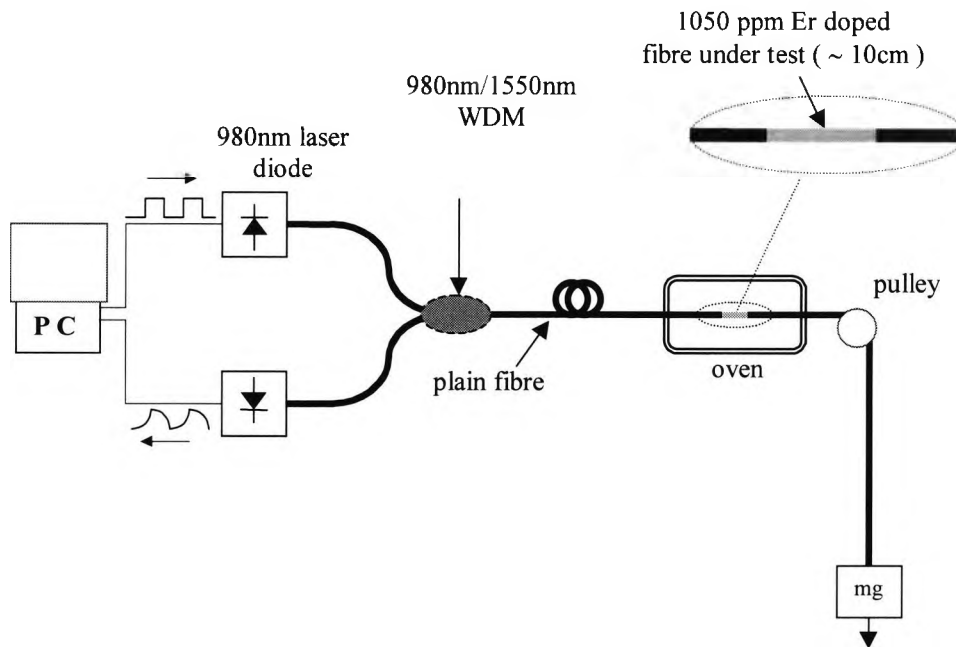


Fig.3.7 Experimental arrangement used for temperature and strain calibration of 1050 ppm Er^{3+} doped fibre.

The 980 nm wavelength at which it operated was again selected to fall within an appropriate absorption band of the Er^{3+} doped material used [6]. During tests, the sensing element was centered within the controlled zone of a temperature stabilized oven (Carbolite, type: MTF 12/38/400). This experimental arrangement used again allowed a range of strains to be applied to the sensor at various temperatures, from ambient to a maximum of 700°C during the calibration tests. Excitation of the 10 cm sample of single mode ($5/125 \mu\text{m}$ core/cladding diameter) Er^{3+} -doped fibre was achieved by coupling the output of the laser diode to the 980 nm port of a 2×1 980 nm/1550 nm WDM coupler arrangement, with all

Chapter 3 Optical fibre temperature and strain sensors based on fluorescence lifetime monitoring

fibres within the oven being stripped of their coating. A pulley system was again used to apply strain to the fibre sensor, where the mass, m , that was added determined the overall strain exerted on the test fibre, and equation 3.1 was used for this. An InGaAs photodiode was used to measure the well-known 1.55 μm fluorescence emission from the Er^{3+} doped fibre which was connected to the other input port of the WDM coupler. The lifetime of the Er^{3+} doped fibre was measured using an analogue-to-digital card connected to a PC, which sampled the output of the photodiode, this being triggered by the falling edge of the excitation pulse. The value of the fluorescence lifetime was subsequently obtained using Prony's method [8].

3.3.2.2 Results

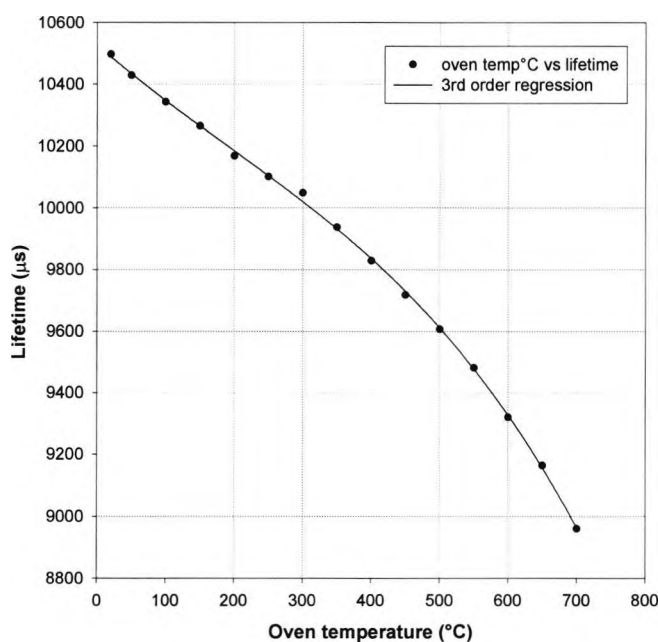


Fig.3.8 Er^{3+} 1050 ppm temperature calibration (without strain).

Chapter 3 Optical fibre temperature and strain sensors based on fluorescence lifetime monitoring

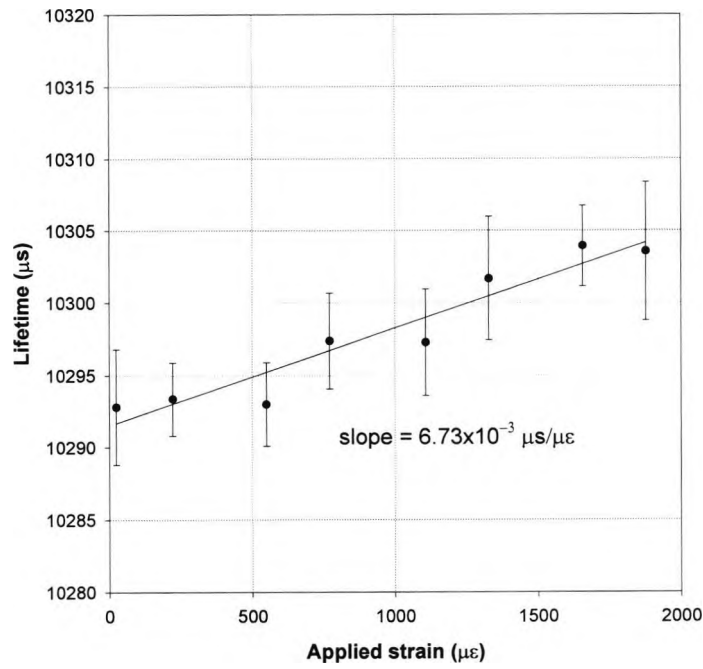


Fig.3.9 Er^{3+} 1050 ppm strain sensitivity of the fluorescent lifetime at 100°C.

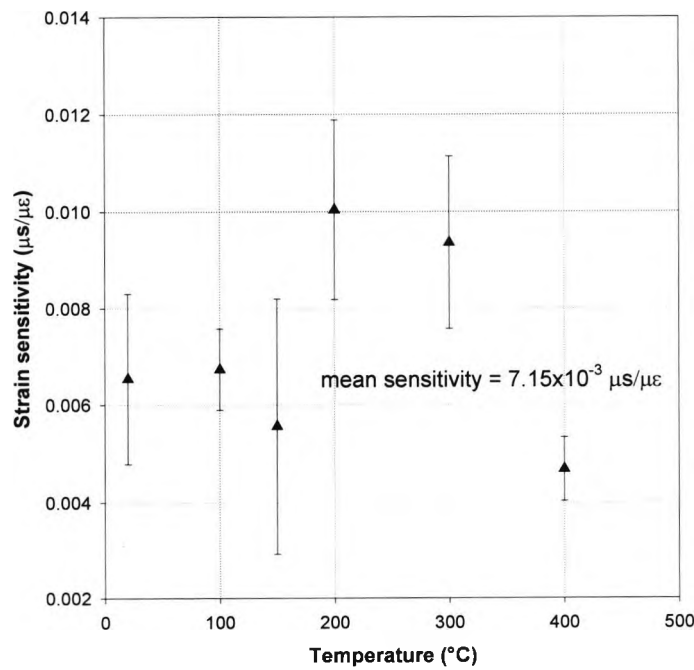


Fig.3.10 Er^{3+} 1050 ppm strain sensitivity of the fluorescent lifetime as a function of temperature.

Chapter 3 Optical fibre temperature and strain sensors based on fluorescence lifetime monitoring

Results of the investigation into the strain sensitivity of the fluorescent lifetime to temperature for this particular material is shown in Fig.3.10, with standard error bars. The individual data points show quite a high level of uncertainty (due to the small effect being observed). However, the mean value of this strain sensitivity is $\sim 0.007 \mu\text{s}/\mu\epsilon$, up to 400°C .

3.3.2.3 Discussion

The temperature calibration of this fibre from Fig.3.8 shows the familiar trend for erbium-doped fibre, in line with the results of previous work [3, 9], with a 3rd order polynomial fit to the data seeming best suited, as illustrated. The strain effect on the lifetime at 100°C is clearly evident from Fig.3.9, which is shown with standard error bars and given a linear 1st order fit, with the gradient at this particular temperature also shown. The strain sensitivity of the fibre from Fig.3.10 is consistent with the previous results on the 200 ppm and 960 ppm Er-doped fibre, with the average found to be $\sim 0.007 \mu\text{s}/\mu\epsilon$, taken over a much wider temperature range than before and again taken as constant. Thus, again by assuming linearity for the lifetime/temperature sensitivity over a short temperature range (i.e. up to 200°C), it was possible to estimate the temperature correction under a strained fibre environment for this material in the same way as before, the results of which are shown in Table 3.2.

3.3.3 4370 ppm doped fibre

3.3.3.1 Experimental arrangement

This was essentially similar to the apparatus used for the 1050 ppm erbium doped fibre previously reported, except that the sensor length was chosen to be 5 cm this time, and the

Chapter 3 Optical fibre temperature and strain sensors based on fluorescence lifetime monitoring

schematic set-up is shown in Fig.3.11. The much higher doping concentration of the single mode 3.6 μm /125 μm (core/cladding) diameter 4370 ppm Er^{3+} doped fibre used here ensured a greater signal yield, therefore the sensor size could be minimised, thus reducing material costs and creating potentially a more compact sensor. There was also the addition of an OSA (optical spectrum analyser), used here to take some additional spectral data from the measurements. As before, all fibre within the oven zone was again stripped of the plastic coating. The same procedure was again used to calibrate the sensor, at two temperatures (40°C and 100°C) with strain (calculated again using equation 3.1), and up to 200°C with temperature. A fuller analysis of this particular fibre is reported in Chapter 4, when it is combined with a fibre Bragg grating (FBG) in another dual sensor experiment.

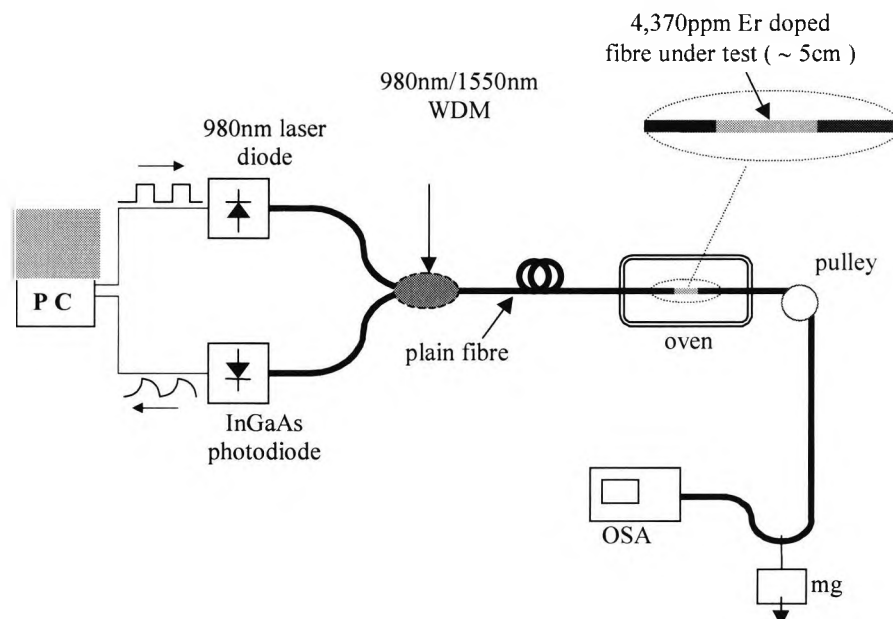


Fig.3.11 Experimental arrangement used for temperature and strain calibration of 4370 ppm Er^{3+} doped fibre.

Chapter 3 Optical fibre temperature and strain sensors based on fluorescence lifetime monitoring

3.3.3.2 Results

Initial tests were performed, using the optical spectrum analyser (OSA), in order to provisionally ensure that the nature and quality of the fluorescence from the erbium doped fibre sample was good enough, i.e for the signal to be measurable. The fluorescence obtained is shown normalised at three of the temperatures used in Fig.3.12.

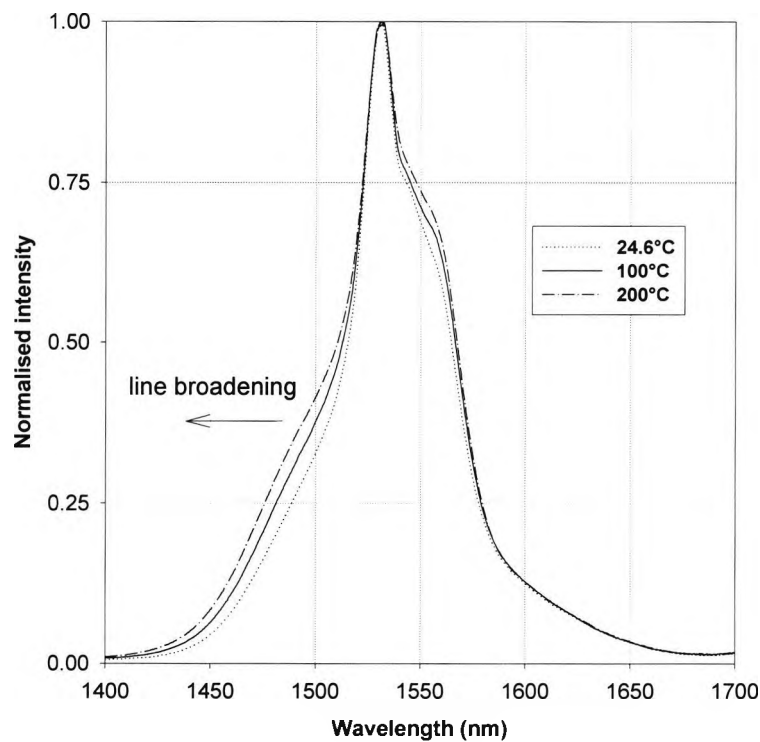


Fig.3.12 Er³⁺ 4370 ppm fluorescence spectra recorded from OSA.

These plots show the characteristic shape of Er³⁺ fluorescence spectra, with peaks being around 1.53 μm at each temperature for this particular fibre, familiar from much previous work [3, 9]. They also show the fluorescence spectral line broadening effect with increasing temperatures, shown by the arrow in Fig.3.12. Fig.3.13 shows the Er³⁺ 4370 ppm fluorescence spectra line broadening more clearly, normalised from 24.6°C with

Chapter 3 Optical fibre temperature and strain sensors based on fluorescence lifetime monitoring

temperature, calculated from the data obtained and is shown at three temperatures. The units are arbitrary and are simply to show the effect of temperature on the fluorescence.

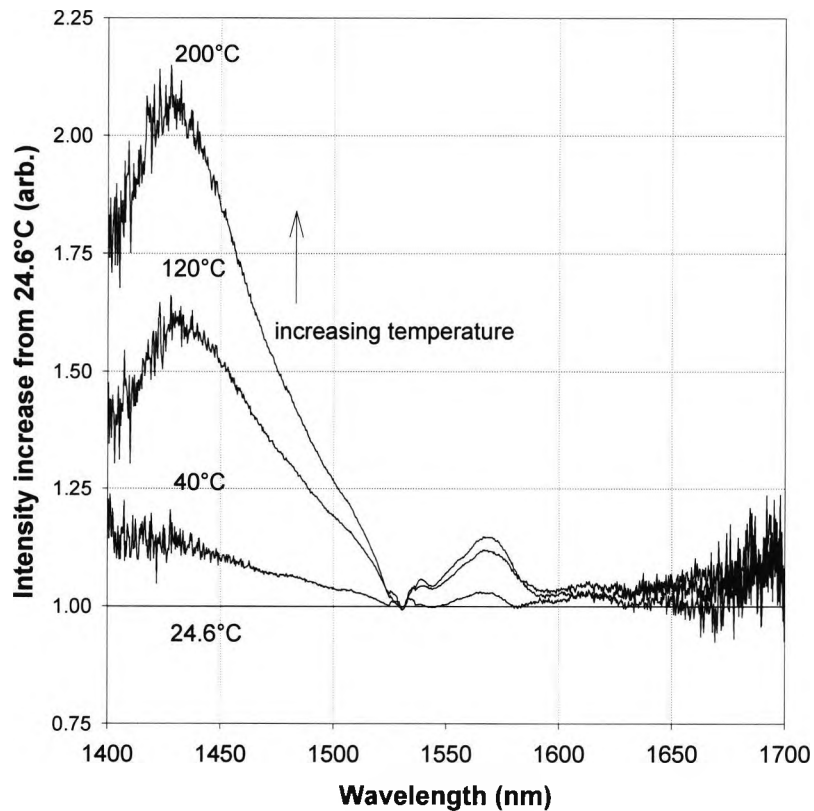


Fig.3.13 Er^{3+} 4370 ppm fluorescence spectral line broadening with temperature.

Fig.3.14 shows the Er^{3+} 4370 ppm fluorescent lifetime vs. temperature calibration with a 3rd order polynomial fit to the data from temperature two cycles (i.e up and down), displayed with 99% confidence error bars for each plot (they are very small). The fluorescent lifetime temperature sensitivity (again assumed to be linear over the short range 20°C – 200°C) from this data was estimated to be $\sim -1.48 \mu\text{s}/\text{K}$, an important figure for comparison.

Chapter 3 Optical fibre temperature and strain sensors based on fluorescence lifetime monitoring

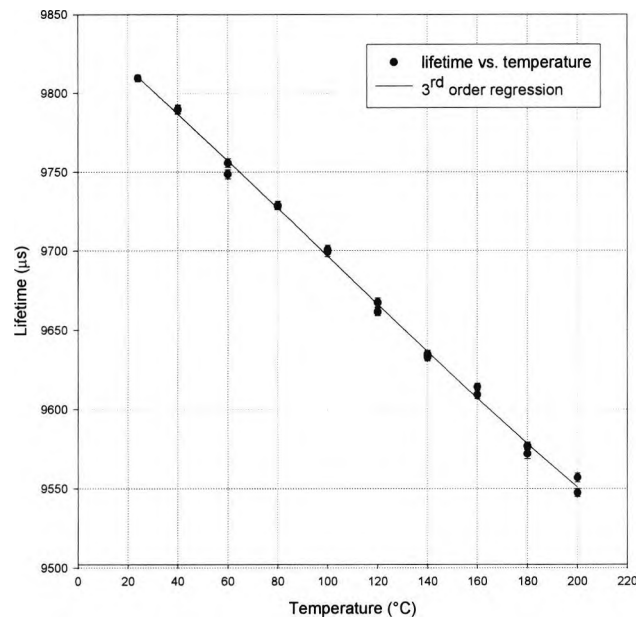


Fig.3.14 Er³⁺ 4370 ppm fluorescent lifetime versus temperature.

Figs 3.15 and 3.16 both show linear fits to the lifetime/strain sensitivities. These were recorded at 40°C and 100°C respectively, both displayed with standard error bars.

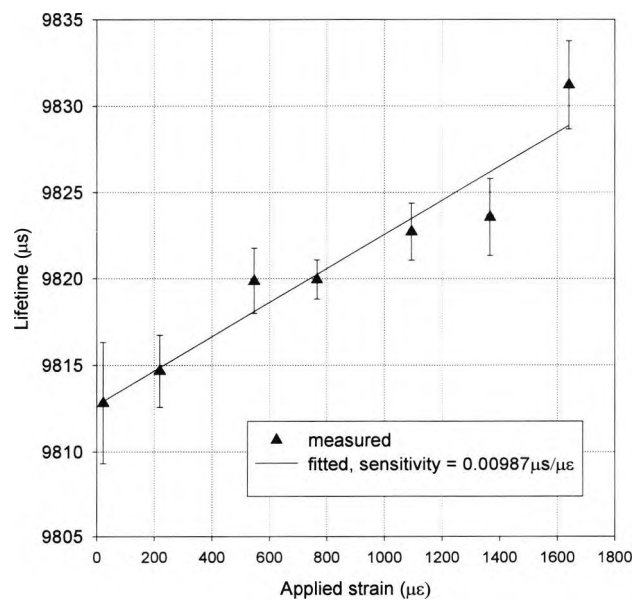


Fig.3.15 Er³⁺ 4370 ppm fluorescent lifetime strain effect at 40°C.

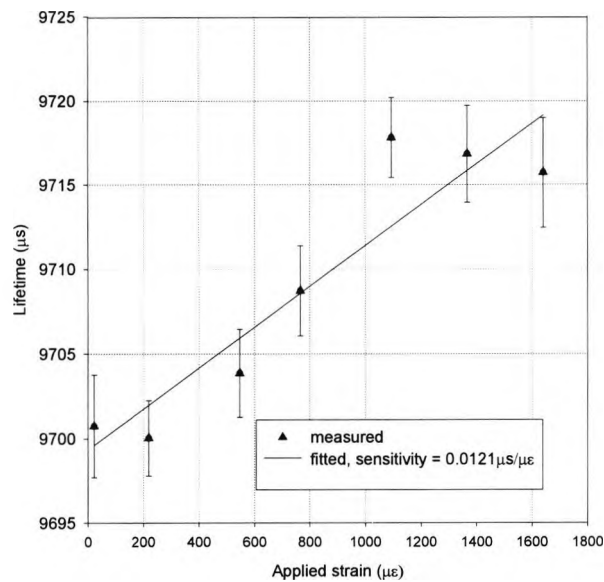


Fig.3.16 Er^{3+} 4370 ppm fluorescent lifetime strain effect at 100°C.

3.3.3.3 Discussion

Again, by making the assumption of linearity over the short temperature range (i.e up to 200°C), the temperature correction was estimated under a strained environment for this material using the available data, and the result is shown below in Table 3.2. It can be seen then that, in uncorrected systems, a fluorescent lifetime-based thermometer would suffer a certain measurement error in the temperature data, based on this material. The temperature equivalence of the error due to 1000 $\mu\epsilon$ is estimated as 7.7°C, as shown in Table 3.2, for the unlikely but interesting case of this comparatively high strain (1% extension). This is quite high, but the strain sensitivity for this particular fibre was estimated from data at only two temperatures. A further characterisation of this Er^{3+} 4370 ppm doped fibre, and its associated temperature error in strain monitoring, is reported later in the thesis when it is combined with a FBG, and calibrated in that system.

Chapter 3 Optical fibre temperature and strain sensors based on fluorescence lifetime monitoring

3.3.4 Erbium doped fibre based sensors – summary

It has been estimated from the data collected from various Er^{3+} doped fibres that erbium has a small but consistent strain sensitivity in the measured fluorescent lifetime, summarised and quantified for the various levels of dopant tested, below in Table 3.2. From this, there seems to be no clear relationship between the level of dopant (i.e concentration) and the fluorescent lifetime strain sensitivity, which is generally around $0.01 \mu\text{s}/\mu\epsilon$ and appears to be constant with temperature. However, with strain compensation, an accurate measurement of temperature can be achieved from erbium fibre, making it well suited to practical fibre optic sensors.

	Er^{3+} 200ppm	Er^{3+} 960ppm	Er^{3+} 1050ppm	Er^{3+} 4370ppm
s/p method	A/D	A/D	A/D	A/D
LD pump (nm)	813	813	980	980
typical lifetime @25°C (μs)	10350	10100	10480	9800
strain sensitivity ($\mu\text{s}/\mu\epsilon$)	$(1.0 \pm 0.2) \times 10^{-2}$	$(1.2 \pm 0.3) \times 10^{-2}$	$(7.15 \pm 2.1) \times 10^{-3}$	$(1.14 \pm 0.14) \times 10^{-2}$
temperature sensitivity ($\mu\text{s}/\text{K}$)	$-2.45 \pm (0.2)$	$-2.53 \pm (0.3)$	$-1.67 \pm (0.04)$	$-1.48 \pm (0.02)$
K/ $\mu\epsilon$	0.0040	0.0047	0.0043	0.0077
ΔT @1000 $\mu\epsilon$	4.0	4.7	4.3	7.7

Table 3.2 Comparison of performance from all dopant levels of Er^{3+} tested.

3.4 Erbium/Ytterbium co-doped fibre based sensors

3.4.1 Introduction

The ever increasing availability of doped fibres, of different sizes, modal properties and especially dopants has increased the potential to tailor sensors based on these fibres to specific applications, dependent upon the most favorable aspects of the active sensor ingredient [10]. To that end, there has been a number of studies to examine the characteristics of newly available fibres, to determine if better sensor schemes can be produced or deleterious effects eliminated. Co-doped rare earth fibres have been used extensively in communications applications, especially for fibre amplifiers as the co-dopant is usually introduced to enhance the ‘pumping’ of the fibre, and thus make better use of the excitation photons from the source. This is also potentially advantageous in sensors based upon such fibres, but the presence of the second dopant may cause interactions which change the temperature characteristics of the material. This may enhance (or indeed otherwise) the sensitivity of the sensor, or reduce the cross-sensitivity to another parameter e.g. strain.

3.4.1.1 Theory

The active material of an $\text{Er}^{3+} \text{Yb}^{3+}$ co-doped fibre sensor scheme is essentially erbium (Er^{3+}), which has been shown, when used as a single dopant in a fibre in previous work, to be a very effective material for thermometric sensors [3, 9]. The energy levels involved are shown schematically in Fig.3.17, illustrating the transitions which govern the performance of the sensor scheme [11]. The mechanism by which the Yb^{3+} ions improve the excitation of the upper state involved in the thermally-sensitive decay process is evident here. Absorption of a pump photon by a Yb^{3+} ion promotes an electron from the $^2F_{7/2}$ ground state level to the

Chapter 3 Optical fibre temperature and strain sensors based on fluorescence lifetime monitoring

$^2F_{5/2}$ manifold, which is followed by efficient energy transfer from this level to the $^4I_{11/2}$ level of erbium (dashed arrows A and B in Fig.3.17) and a non-radiative decay to the upper laser level $^4I_{13/2}$ (wavy arrow C).

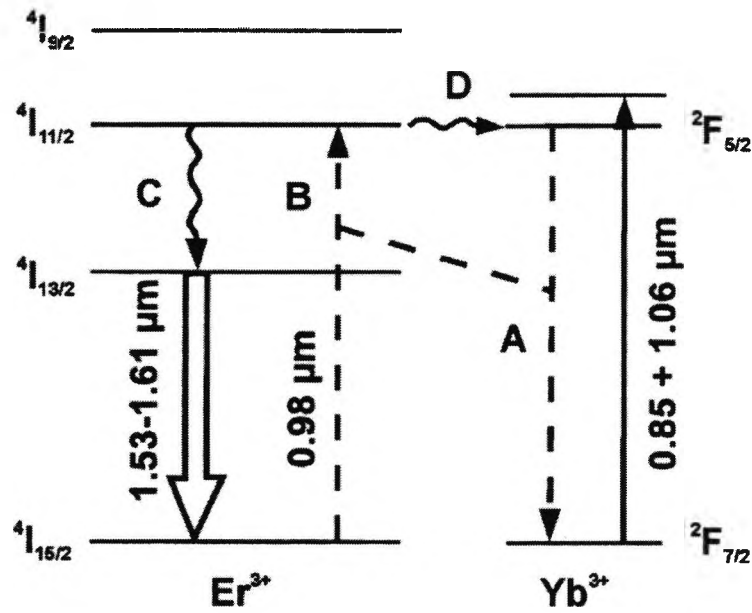


Fig.3.17 Energy levels involved in $Er^{3+} Yb^{3+}$ energy transfer [11].

This process is efficient, provided the transferred energy remains in the Er^{3+} ion: that is, provided the electron relaxes preferentially to the Er^{3+} upper laser state rather than back to the $^2F_{5/2}$ level of the Yb^{3+} ion (wavy arrow D). Previous work with phosphate glasses has indicated that high energy transfer efficiencies are possible, and thus the excitation photons may be used more efficiently in the sensor system.

The sensitization of erbium-doped silica fibers by Yb^{3+} presents several advantages. First, it allows for a high concentration species strongly to absorb the pump power. Since the sensitizer does not introduce absorption bands at longer wavelengths, it should not affect the

Chapter 3 Optical fibre temperature and strain sensors based on fluorescence lifetime monitoring

fiber loss at the emission wavelength. A second advantage is that the significant inhomogeneous broadening of the ${}^2F_{5/2}$ level of the Yb^{3+} ions results in a broad absorption band, which in turn permits a wider range of pump wavelengths to be used, the band being typically about ± 200 nm around 930 nm, and this eases the requirements on the wavelength stability of the pump source.

3.4.1.2 Previous work

Much work has been previously reported on the addition of Yb^{3+} as a sensitizer to Er^{3+} in many fibre laser, amplifier and crystal applications - some of the many examples include the work of Winick and Vossler [12], Karasek [13] or Pacheco and Di-Bartolo [14], with respect to each of these types of application. However, apparently no work had been done on the thermal characterisation of the commonly available silica $\text{Er}^{3+} \text{Yb}^{3+}$ co-doped fibre (and hence its suitability for fluorescence-based high temperature thermometry) until that by Sun *et al* [15]. Here, several samples of single mode co-doped $\text{Er}^{3+} \text{Yb}^{3+}$ fibre were tested for their high temperature performance characteristics. The results obtained from an annealing test were less pronounced than from previously tested rare-earth ions, such as Er^{3+} [3, 9] or Nd^{3+} [2]: therefore some promise for high temperature thermometry was evident from this type of fibre. It was therefore decided to test the potential of this material further to build on the results already achieved, but only this time using a more sensitive fibre which had been specially constructed, and was obtained from *Nanyang Technological University, Singapore* as part of a cooperative agreement.

3.4.2 Photosensitively enhanced $\text{Er}^{3+} \text{Yb}^{3+}$ co-doped fibre

The fibre under test had a cladding diameter of 125 μm , a numerical aperture of 0.2 and core dopants of Er^{3+} , Yb^{3+} and aluminium. It was of unique construction in that it had been

Chapter 3 Optical fibre temperature and strain sensors based on fluorescence lifetime monitoring

designed with a photosensitive ring (during the manufacturing process). Results obtained from this fibre are compared with those previously obtained from “normal” single mode Er^{3+} Yb^{3+} co-doped silica fibre [15] and conclusions are drawn. Also, later in the thesis (section 4.4.4), the results obtained here are compared with results from a chosen-to-be equal length of similar fibre, but this time with a FBG written in, where strain is also applied to the fibre.

3.4.2.1 Experimental arrangement

The experimental arrangement used for the temperature calibrations is shown in Fig.3.18.

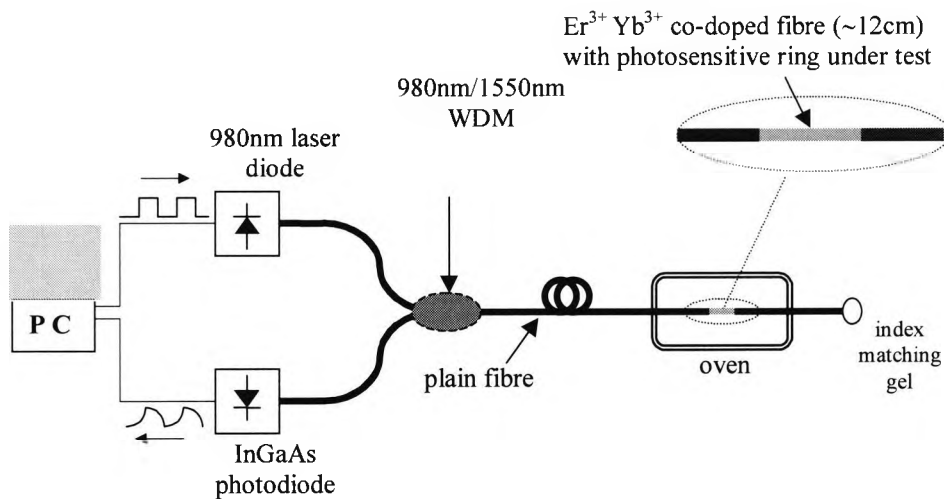


Fig.3.18 Er^{3+} Yb^{3+} co-doped fibre experimental set-up for temperature measurement.

A 12 cm sample of the fibre was specifically chosen to be the sensor length, in order to ensure good absorption and achieve a strong signal yield. The 980 nm laser diode employed here (maximum power $P_0 = 2$ mW), previously used for many other applications, is conveniently well suited to the broadened absorption band of this co-doped material, and it was modulated via an external electronic source. Excitation of the single mode co-doped fibre was achieved by coupling the output of the laser diode to the 980 nm port of a 2×1 980

Chapter 3 Optical fibre temperature and strain sensors based on fluorescence lifetime monitoring

nm/1550 nm WDM coupler arrangement. Also, as had been done before, all fibres within the oven confines were completely stripped of their coatings to eliminate the effects of the very high temperatures on plastic. As a precaution, the end of the fibre system closest to the sensor was dipped in index matching gel to minimise the back reflection. An InGaAs photodiode was used to measure the fluorescence emission from Er^{3+} ions, after undergoing the direct energy transfer mechanism explained earlier, and this was connected to the other input port of the WDM coupler. The lifetime of the co-doped fibre was measured using an analogue-to-digital card connected to a PC, which sampled the output of the photodiode, this being triggered by the falling edge of the excitation pulse. The value of the fluorescence lifetime was subsequently obtained using Prony's method [8].

3.4.2.2 Results

A) Temperature characteristics

The initial $\text{Er}^{3+} \text{Yb}^{3+}$ temperature calibration, before annealing, was performed up to 600°C and the recorded data shown in Fig.3.19. This is displayed with a 3rd order polynomial fit for convenience, and with standard deviation error bars. The result is very similar to the profile of the data obtained from the previous work on conventional co-doped $\text{Er}^{3+} \text{Yb}^{3+}$ fibre [15], except that the lifetime obtained here is longer. The latter could be due to a number of factors, such as the core composition or the ratios of the two dopants used, i.e Er^{3+} and Yb^{3+} , differing from that in the previous work. Detailed data on the composition of the fibre were not available. The lifetime/temperature sensitivity shows a similar trend to that of previous work with erbium [3, 9], and increases noticeably at higher temperatures.

Chapter 3 Optical fibre temperature and strain sensors based on fluorescence lifetime monitoring

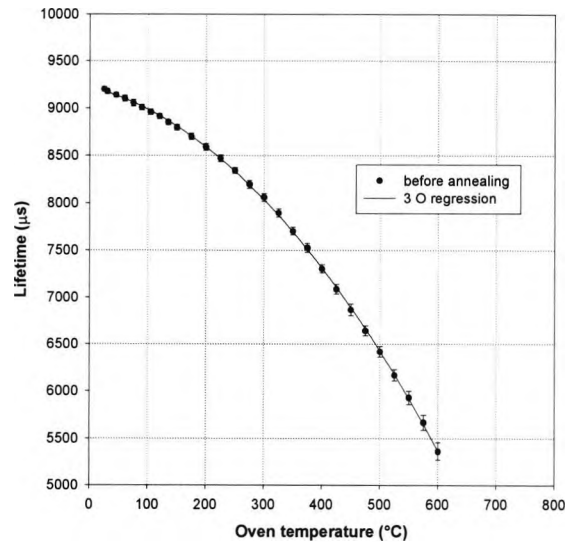


Fig.3.19 Er³⁺ Yb³⁺ co-doped fibre initial temperature calibration.

B) Annealing

Previous work has shown the annealing of the fibre to be essential for a reproducible output characteristic [15]. The results obtained during this process are shown in Fig.3.20. The same sample was heated to 800°C, and left for 24 hrs, by which time the measured fluorescent lifetime had appeared to stabilise. This occurs after the lifetime was seen to be initially increasing at what appeared to be an exponential rate, and therefore a time constant (τ), as shown on the graph by the white line, could be estimated from the data to give an indication of the rate of lifetime increase. The temperature was chosen from the previous work, where the annealing temperature was reported to be around 870°C.

Chapter 3 Optical fibre temperature and strain sensors based on fluorescence lifetime monitoring

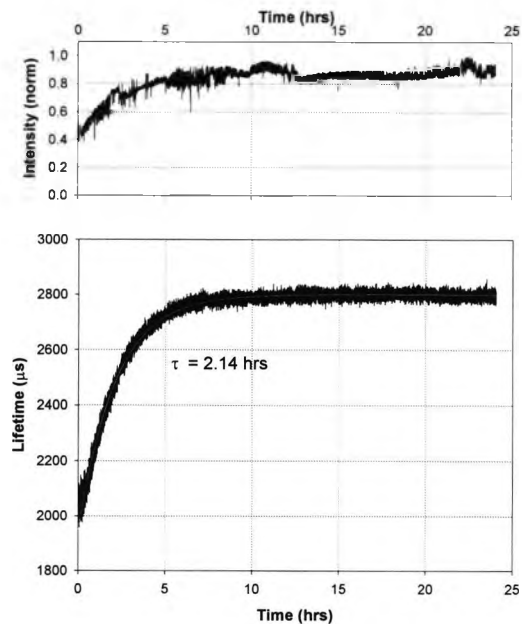


Fig.3.20 Er^{3+} Yb^{3+} co-doped fibre annealing at 800°C for 24 hrs.

The results from before and after annealing are compared in Fig.3.21, both shown with standard deviation error bars. For comparison, the results from the previous work [15] are also shown in Fig. 3.22.

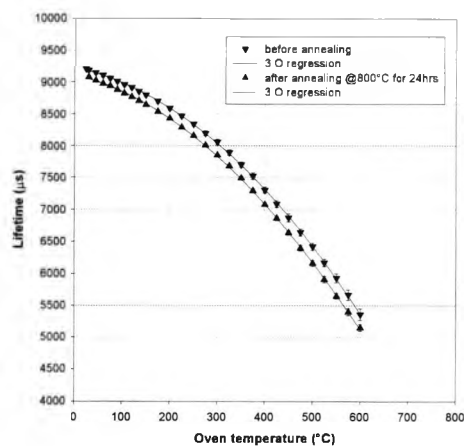


Fig.3.21 Er^{3+} Yb^{3+} co-doped fibre annealing effects.

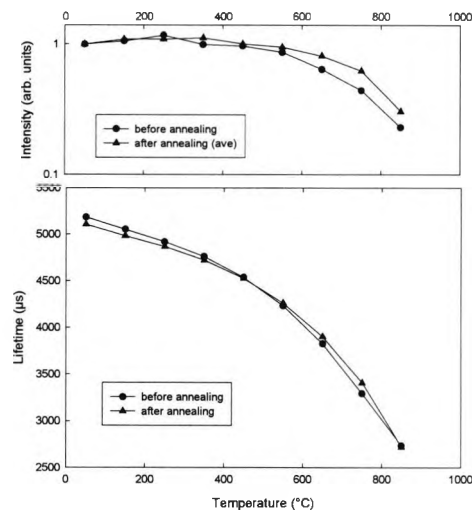


Fig.3.22 Results from previous work on $\text{Er}^{3+} \text{Yb}^{3+}$ co-doped fibre [15].

3.4.2.3 Discussion

It can be seen from Fig.3.21 that after the completion of the full annealing process the measured fluorescent lifetime has decreased slightly after experiencing the temperature regime to which it was subjected, even though it was previously observed to increase whilst apparently undergoing the annealing process, as shown in Fig.3.20 at 800°C. The reason for the lifetime to decrease is that the “true” annealing temperature of this fibre was not reached in this work. It was heated at 800°C for 24 hrs, and the data obtained after this only tests to 600°C. This has been confirmed by the previous work [15] and further work which will be discussed in Chapter 4 (in section 4.4.4) using this same fibre, i.e that some “cross-over” point appears at a higher temperature (i.e closer to 800°C) from which temperature the lifetime can be seen to increase. Furthermore, the actual lifetime change and drift is very small, in line with previous results as shown in Fig.3.22, and also the sensor still retains more or less the same temperature sensitivity it had before the process applied.

3.5 Neodymium doped fibre based sensors

3.5.1 Previous work

Neodymium has been widely used in temperature sensing, based on employing lifetime techniques in much previous work in this field [2]. Some work on the strain effect on the fluorescent lifetime of this dopant has also been done by Sun *et al*, mainly using multimode Nd³⁺ doped fibre [4], and the new results obtained from the work done here using single mode Nd³⁺ doped fibre are compared with those obtained previously.

3.5.2 1460 ppm Nd³⁺ doped fibre

3.5.2.1 Experimental arrangement

The fibre under test was single mode, 7/125 µm (core/cladding) diameter, 1460 ppm Nd³⁺ doped silica fibre (INO 514 - 5382), NA = 0.1. Three similar sensors were constructed in this work: sensor 1 (11 cm), sensor 2 (10 cm) and sensor 3 (10 cm) and these could be switched using a 2x1 optical switch. The practical arrangement, as shown in Fig.3.23, consisted of a 785 nm laser diode pump and an InGaAs photodetector. Strain was carefully applied in the same way as before, using a simple pulley system, and the measurement

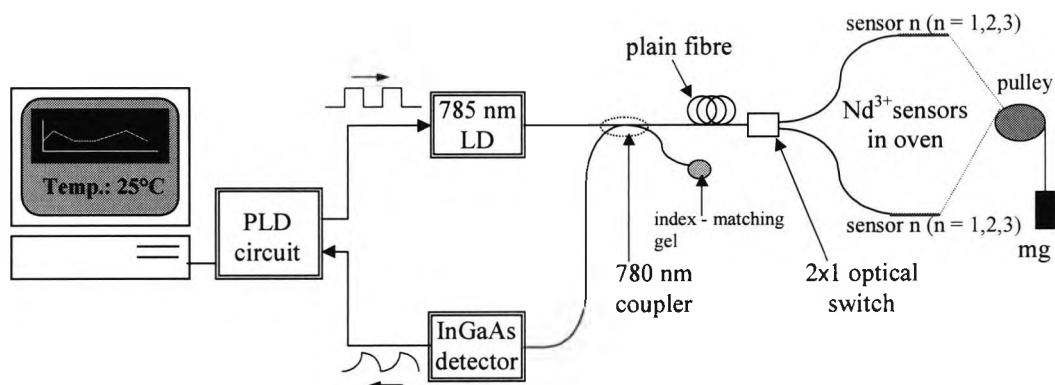


Fig.3.23 Experimental set-up for Nd³⁺ fibre temperature/strain calibration.

Chapter 3 Optical fibre temperature and strain sensors based on fluorescence lifetime monitoring

system employed is the PLD method of signal processing [7].

3.5.2.2 Results

A) sensor 1

Sensor 1 was heated from 30°C to 150°C, in steps of 10°C, and the lifetime results are shown in Fig.3.24 with a 3rd order polynomial fit to the data.

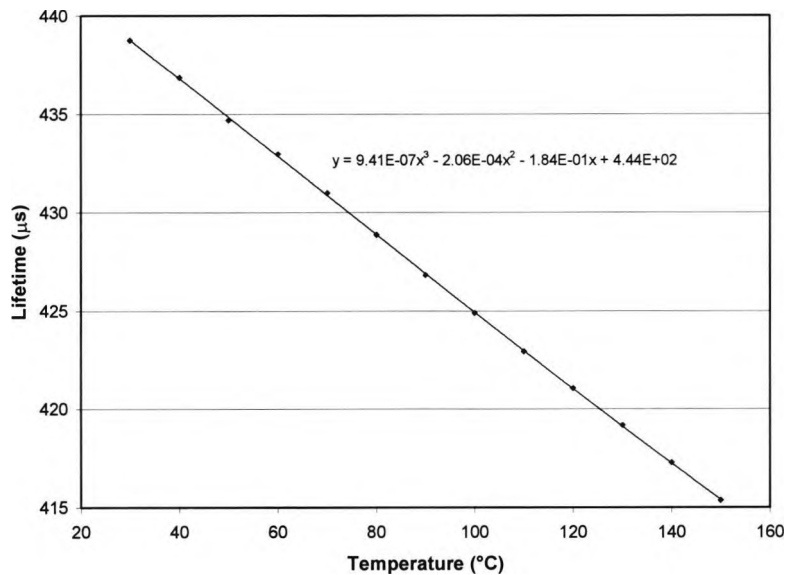


Fig.3.24 Nd³⁺ temperature calibration data for sensor 1.

The temperature sensitivities are estimated from the 3rd order polynomial fit displayed on the graph and these are shown in Fig.3.25, where the change in absolute lifetime temperature sensitivity is illustrated alongside the percentage (%) change in lifetime temperature sensitivity as the sensor is heated. The effect of applied strain on the Nd³⁺ fibre sensor at 100°C is shown in Fig.3.26, where a 100g mass was carefully placed onto the pulley system and the lifetime recorded in real-time, using the PLD system set on an averaging time of 10s. Fig.3.27 shows the recorded lifetime vs. strain data at one temperature chosen to be 35°C,

Chapter 3 Optical fibre temperature and strain sensors based on fluorescence lifetime monitoring

shown with a 3rd order polynomial fit to the non-linear data and with standard deviation error bars.

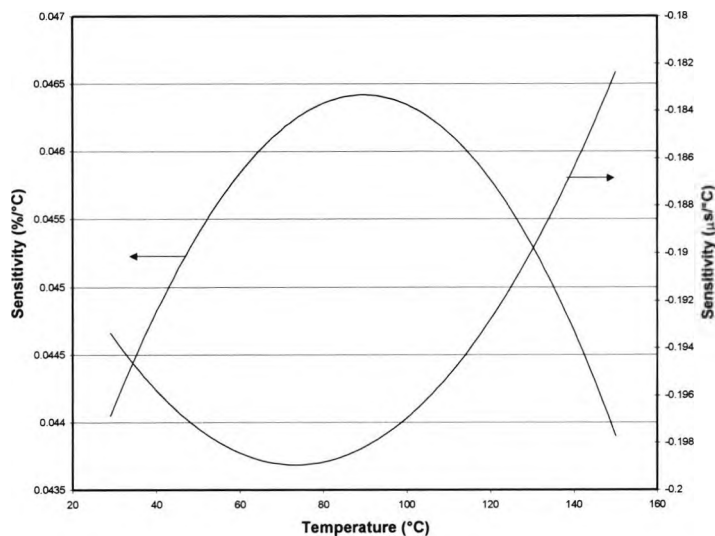


Fig.3.25 Nd³⁺ temperature sensitivities of sensor 1.

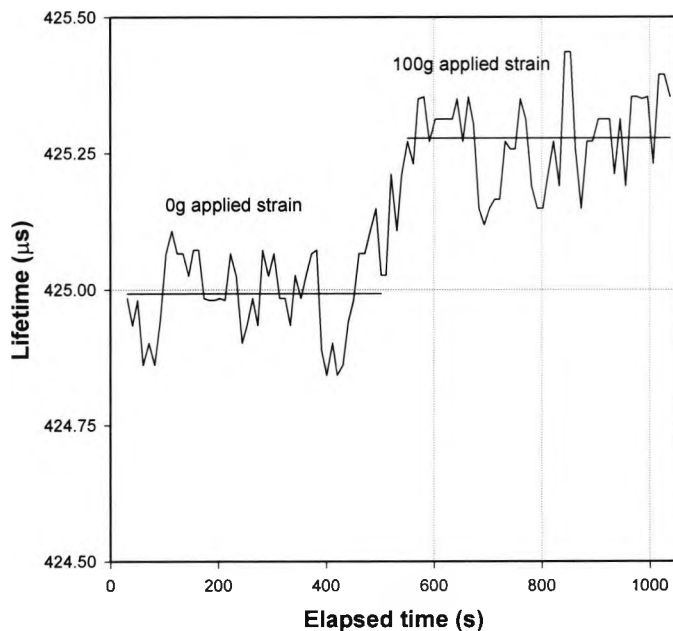


Fig.3.26 Nd³⁺ sensor 1 – effect of strain at 100°C.

Chapter 3 Optical fibre temperature and strain sensors based on fluorescence lifetime monitoring

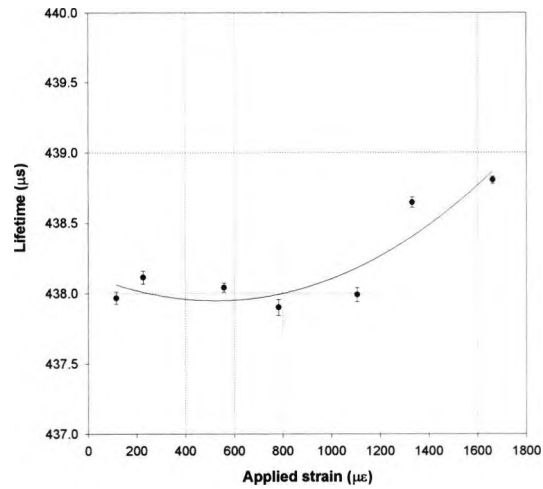


Fig.3.27 Nd^{3+} sensor 1: strain effect on lifetime at 35°C.

B) sensor 2

Sensor 2 was heated from 35°C to 150°C, in 5 discrete steps, and strain was applied at each

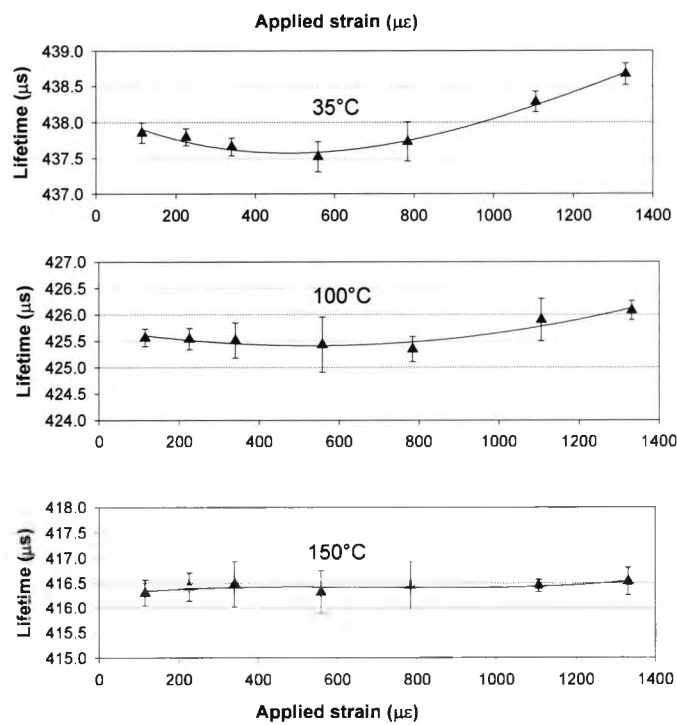


Fig.3.28 Nd^{3+} sensor 2: lifetime versus strain for the minimum, middle and maximum temperatures.

Chapter 3 Optical fibre temperature and strain sensors based on fluorescence lifetime monitoring

stabilised temperature. The lifetime/strain results from extensive cycling (15 cycles) are shown in Fig.3.28, for three discrete (minimum, middle and maximum respectively) temperatures only, with a 3rd order polynomial fit to each set of data and with standard deviation error bars.

C) sensor 3

Sensor 3 was heated from 30°C to 150°C, in steps of 10°C, and the results are shown in Fig.3.29 together with a 1st order linear fit to the data and standard deviation error bars (very small).

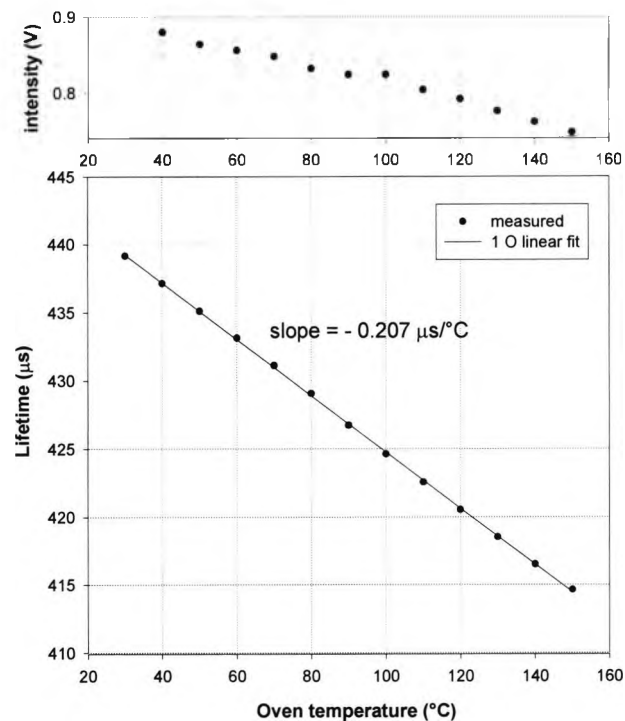


Fig.3.29 Nd³⁺ sensor 3: lifetime versus temperature calibration.

From this fit, the Nd³⁺ temperature sensitivity of the fluorescence lifetime over this temperature range was estimated to be $\sim -0.2 \mu\text{s}/^\circ\text{C}$. The same linear fit to data for sensor 1

Chapter 3 Optical fibre temperature and strain sensors based on fluorescence lifetime monitoring

gives a temperature sensitivity of $\sim -0.196 \mu\text{s}/^\circ\text{C}$ over the same temperature range. Also, the intensities are displayed here and are generally seen to decrease with increasing temperature, in line with previous work [2]. The sensor was then subjected to strain and the lifetime/strain results from extensive cycling (15 cycles) are shown in Fig.3.30 for 30°C and 60°C temperatures, with a 3rd order polynomial fit to each set of data and with standard deviation error bars.

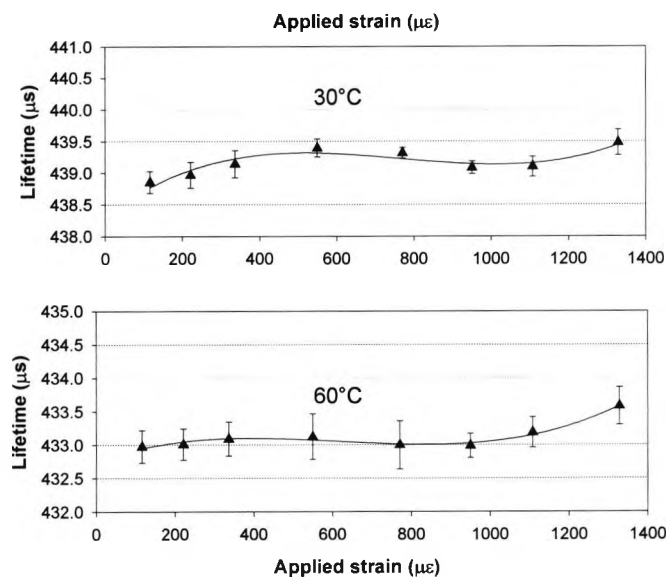


Fig.3.30 Nd^{3+} sensor 3: lifetime versus strain at 30°C and 60°C .

3.5.2.3 Discussion

It can be seen from the experimental data obtained that the measured fluorescent lifetime of single mode Nd^{3+} doped fibres is less sensitive to the influence of strain ($\sim 10^{-4} \mu\text{s}/\mu\epsilon$) compared to that of multimode Nd^{3+} fibres ($\sim 10^{-5} \mu\text{s}/\mu\epsilon$) from previous results reported [4]. In these previous results from 300 ppm Nd^{3+} doped single mode fibre, there is a degree of

Chapter 3 Optical fibre temperature and strain sensors based on fluorescence lifetime monitoring

consistency here in that the error then was also large due to poor coupling, and therefore a linear fit may not have been optimum when attempting to measure the very small strain effect present. A thermometer based on the use of the multimode fibre used in that previous work would be in a temperature measurement error of only 1.9°C for an applied strain of 1000 $\mu\epsilon$, suggesting a preferential use for this type of fibre in dual temperature/strain sensing as opposed to single mode Nd³⁺ fibre.

The strain sensitivity of the fluorescent lifetime (and therefore the thermometer correction) at a particular temperature and strain can be estimated from the data by mathematical means, e.g for sensor 1 @35°C, 1000 $\mu\epsilon$:

lifetime *temperature* sensitivity @35°C from 3rd order polynomial fit $\sim -0.196 \mu\text{s}/^\circ\text{C}$

lifetime *strain* sensitivity @35°C & 1000 $\mu\epsilon$ from 3rd order polynomial fit $\sim 6.64 \times 10^{-4} \mu\text{s}/\mu\epsilon$

\therefore the temperature correction factor (K/ $\mu\epsilon$) = $3.40 \times 10^{-3} \text{ K}/\mu\epsilon$

so for an applied strain of 1000 $\mu\epsilon \equiv 3.4^\circ\text{C}$ temperature error.

3.6 Thulium/Holmium co-doped fibre based sensors

3.6.1 Introduction

As the range of commercial fibres expands, it is valuable to investigate the characteristics of sensors configured using newly available fibres [16], especially those developed for the telecommunications industry. Clear strain effects have previously been seen on a range of doped fibres, and the issue of using this technique as a means to compensate for thermal effects in, for example, Bragg grating-based sensor systems or in combination with a second fluorescent fibre in strain and temperature recording was important to investigate.

Co-doped rare earth fibres have been used in communications applications, especially for fibre amplifiers as the co-dopant is usually introduced to enhance the ‘pumping’ of the fibre, and thus make better use of the excitation photons from the source [10]. This is also potentially advantageous in sensors based upon such fibres, but the presence of the second dopant may cause interactions which change the temperature characteristics of the material [15]. This may enhance (or indeed otherwise) the sensitivity of the sensor, or reduce the cross-sensitivity to another parameter e.g. strain. The potential does exist to make better sensors, and this is the *raison d’etre* for this particular study [10].

The co-doped fibre material used here is thulium/holmium ($\text{Tm}^{3+}/\text{Ho}^{3+}$), which has in the past been used extensively in the communications field to produce fibre lasers with an output at a wavelength of approximately $2\ \mu\text{m}$ [17] using Tm^{3+} as the sensitizer, the mechanism of which is shown in Fig.3.31 with approximate lifetimes obtained from the relevant energy

Chapter 3 Optical fibre temperature and strain sensors based on fluorescence lifetime monitoring

levels added. Energy transfer occurred from the Tm^{3+} to the Ho^{3+} ions, as shown by the dashed arrow in Fig.3.31. The active material of this sensor scheme is thulium (Tm^{3+}), which has been shown when used as a single dopant in a fibre, in previous work, to be a very effective material for thermometric sensors [18]. The energy levels involved are shown below schematically in Fig.3.32, illustrating the infrared transitions which govern the performance of this sensor scheme.

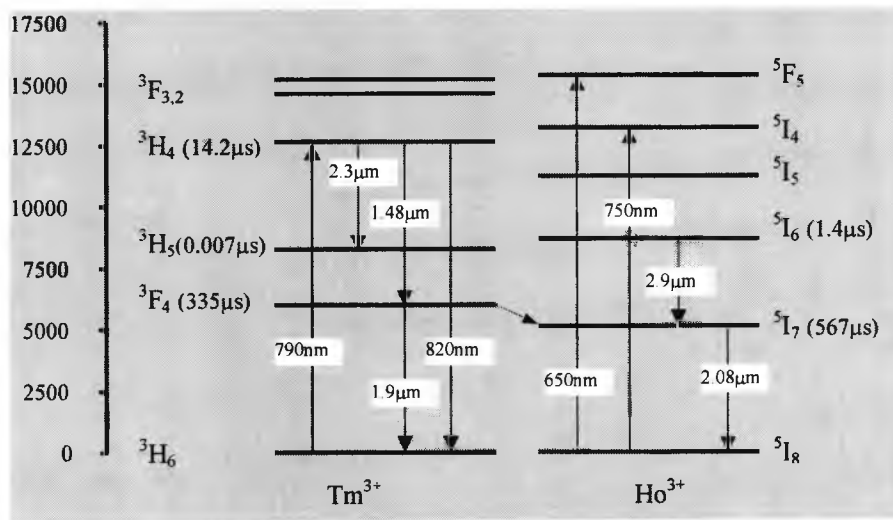


Fig.3.31 Energy level diagram of the Tm^{3+} and Ho^{3+} rare earth ions, showing the transitions previously used and lifetimes obtained in brackets from the relevant energy levels [10].

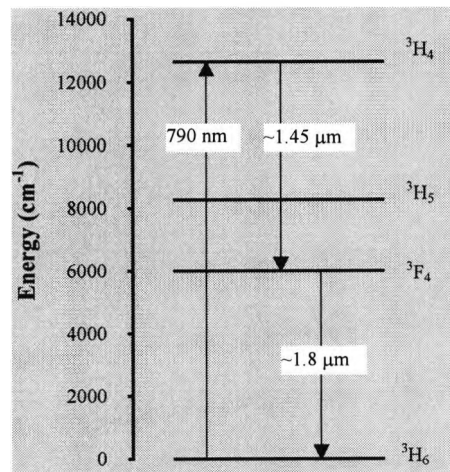


Fig.3.32 Energy level diagram of the Tm^{3+} ion, showing transitions of interest [11].

Chapter 3 Optical fibre temperature and strain sensors based on fluorescence lifetime monitoring

In this work, a silica $\text{Tm}^{3+}/\text{Ho}^{3+}$ co-doped single mode optical fibre has been extensively tested for the first time to determine the magnitude of the strain effects upon its thermal performance. The goal is the design of a comparatively strain-insensitive fibre thermometer that could readily be used with multiplexed Bragg grating strain measurement systems. Also, $\text{Tm}^{3+}/\text{Ho}^{3+}$ co-doped optical fibre high temperature and annealing effects are examined in this work.

3.6.2 4600 ppm/1100 ppm co-doped $\text{Tm}^{3+}/\text{Ho}^{3+}$ fibre

The fibre used was single mode, silica $\text{Tm}^{3+}/\text{Ho}^{3+}$ co-doped fibre (528-6671, INO, Canada) and absorption data, as supplied by the manufacturer, is shown below in Fig.3.33.

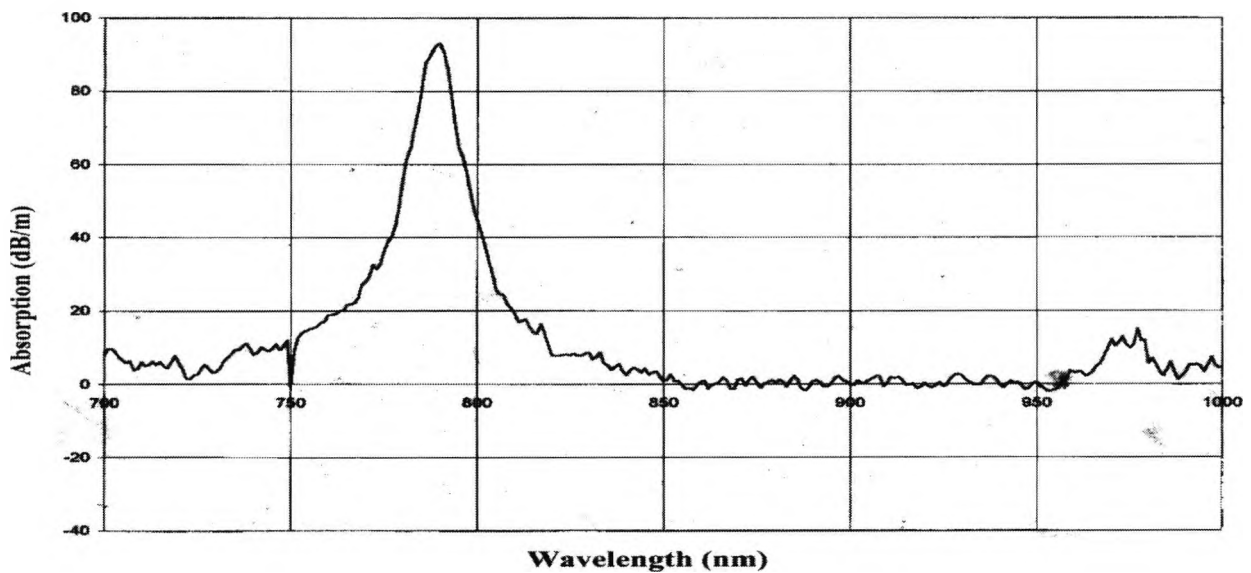


Fig.3.33 $\text{Tm}^{3+}/\text{Ho}^{3+}$ fibre absorption in the region of 780 nm wavelength (source: INO).

This co-doped fibre had a core size of $11.5 \mu\text{m}$ and doping concentrations of Tm_2O_3 : 4600ppm-wt, Ho_2O_3 : 1100ppm-wt and Al_2O_3 : 9.43wt%. As can be seen from the given fibre

Chapter 3 Optical fibre temperature and strain sensors based on fluorescence lifetime monitoring

data specification in Fig.3.33, there was strong absorption around the 780 nm wavelength region which could be attributed to the high level of the Tm^{3+} dopant within the fibre, and this was useful detail which could be conveniently exploited for sensor purposes.

3.6.2.1 Experimental arrangements

Two experimental arrangements were used in this work. The initial (arrangement A) set-up utilised [16] a phase-locked detection (PLD) scheme in the same way as used in much previous work [4, 5, 7]; the second (arrangement B) arrangement contained a signal processing system which used an A/D card [10]. After using method (A), it became clear that this type of signal processing was ineffective for the type of fibre under test here, and therefore could not be employed to measure the two lifetimes shown below in the way of method (B). As can be seen from the results below, the A/D card method was found to be a much more suitable measurement system for this type of fibre yielding more signal information, greater resolution and therefore potentially higher accuracy.

A) PLD system method

The experimental set-up was as shown schematically in Fig.3.33. The laser diode pump (780 nm centre wavelength, and maximum power $P_0 = 20$ mW) was selected as its output fell conveniently within the absorption band of the $\text{Tm}^{3+}/\text{Ho}^{3+}$ co-doped material used (Fig.3.33), and the laser was coupled to one fibre input of a 2x1 coupler arrangement. The output of the coupler was connected to a conventional communications fibre leading to a stable tube oven (type Carbolite, $\pm 5^\circ\text{C}$ within 10 cm in the centre of the tube), into which was fusion-spliced the sensor element, about a 10 cm single-mode $\text{Tm}^{3+}/\text{Ho}^{3+}$ co-doped fibre. The length of fibre used (a few centimetres) ensured an adequate absorption and fluorescence signal yield.

Chapter 3 Optical fibre temperature and strain sensors based on fluorescence lifetime monitoring

The other end of the sample was fused to a similar piece of communications fibre to enable the tests to be carried out, as discussed. Strain was applied in the usual way by using the pulley system with weights added, progressively controlling the overall strain exerted on the test fibre. Care was taken to prevent the fibre from touching the tube oven glass and to lubricate the pulley in order to minimize friction. The detector used, an InGaAs photodiode, was chosen to cover the spectral fluorescence emission range at wavelengths greater than the laser wavelength and was connected to the other input of the coupler.

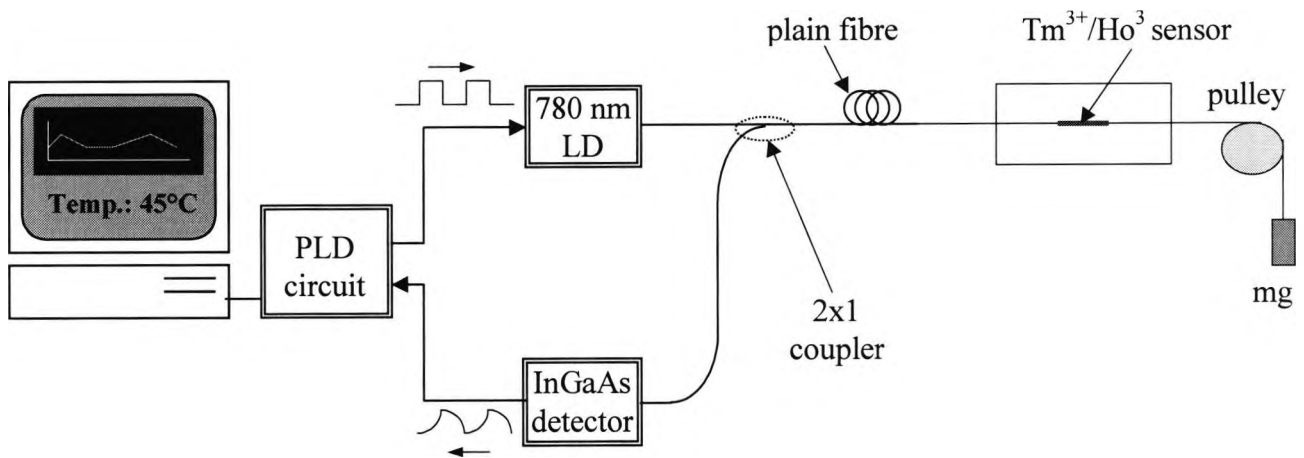


Fig.3.34 Schematic of PLD method (A).

B) A/D card method

The experimental arrangement used is shown schematically in Fig.3.35. The laser diode pump ($\lambda_c \sim 785$ nm, $P_0 = 24$ mW max.) was selected as its output fell conveniently within the absorption band of the 3H_4 energy level of the Tm^{3+} ion in the co-doped material used. Excitation of the doped fibre was achieved by splicing the fibre optic pigtail of the laser to one of the fibre inputs of a 2x2 optical fibre coupler arrangement. One of the output arms of

Chapter 3 Optical fibre temperature and strain sensors based on fluorescence lifetime monitoring

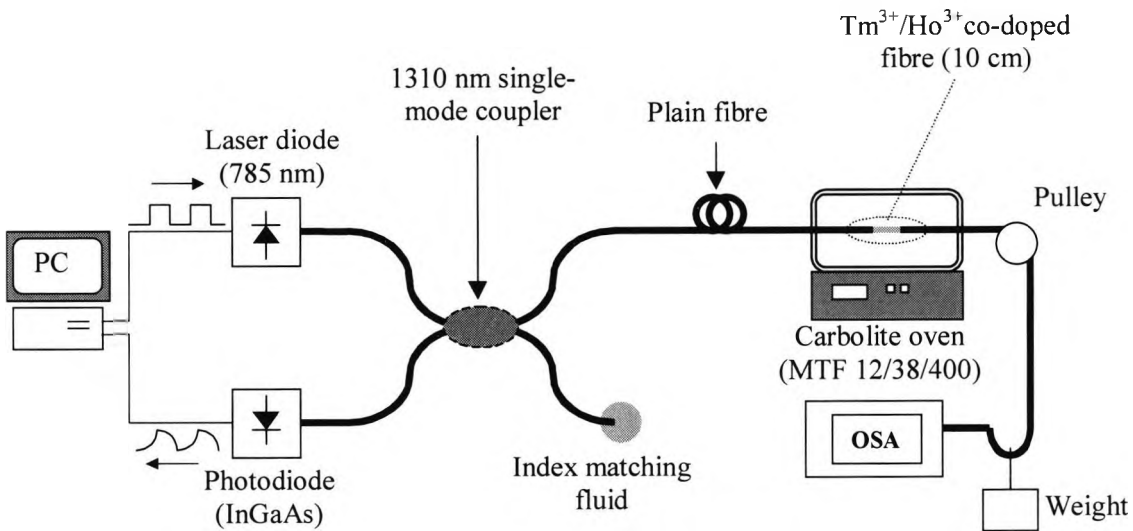


Fig.3.35 Experimental arrangement (B) used to measure the temperature and strain dependence of Tm^{3+}/Ho^{3+} co-doped fibre.

the coupler (1310 nm SM, 50:50) was chosen so as to maximise the pump power delivered to any Tm^{3+}/Ho^{3+} co-doped fibre sensor and was therefore fusion spliced to a length of conventional communications fibre, on to which a 10 cm section of the test fibre was attached. This length of the Tm^{3+}/Ho^{3+} co-doped fibre sensor was chosen to achieve both adequate absorption and fluorescence signal yield [6]. The end of the doped fibre was in turn spliced to another length of conventional communications fibre, to which weights could be attached for strain tests, in a similar way as has been done in previous strain work with other fibres. As before, all fibres within the confines of the oven were stripped of plastic coatings. An Optical Spectrum Analyser (OSA) was added to the system to provide some additional information on the nature of the fluorescence obtained, and the record obtained at room temperature using a resolution bandwidth (RBW) of 10 nm is shown in Fig.3.36. This

Chapter 3 Optical fibre temperature and strain sensors based on fluorescence lifetime monitoring

shows a peak around 1.46 μm and increasingly stronger fluorescence from longer wavelengths (upper wavelength limit of OSA was however 1700 nm).

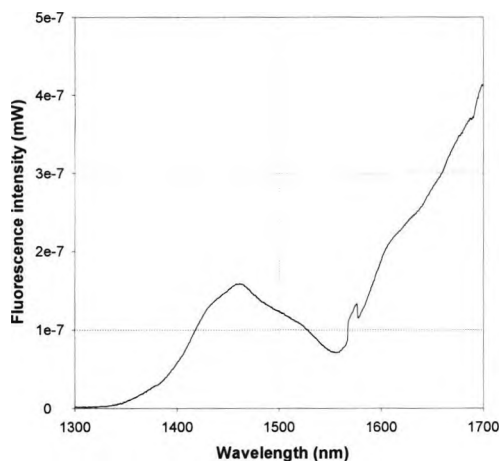


Fig.3.36 Optical Spectrum Analyzer (OSA) plot recorded at room temperature of 20.5°C
(Resolution bandwidth, RBW of 10 nm).

The temporal characteristics of the $\text{Tm}^{3+}/\text{Ho}^{3+}$ co-doped fibre fluorescence were measured using an InGaAs photodiode connected to the remaining input port of the coupler. The normal wavelength response range of InGaAs photodiodes covers the wavelength range from approximately 800 nm to about 1800 nm and as such fluorescence from both the $^3\text{F}_4$ (at $\sim 1.8 \mu\text{m}$) and $^3\text{H}_4$ (at $\sim 1.45 \mu\text{m}$) energy levels of the Tm^{3+} ion was detected. Measurements were transferred to a PC for analysis using an analogue-to-digital card connecting the photodiode output to the PC, this being triggered by the falling edge of the excitation pulse. It can be seen from Fig.3.31 that fluorescence from the Ho^{3+} ion occurs predominately at wavelengths near 2000 nm [17]. This is unfortunately outside the range of the InGaAs detector and, as such, it has been (reasonably) assumed that the fluorescence in this case is

Chapter 3 Optical fibre temperature and strain sensors based on fluorescence lifetime monitoring

measured only from the Tm^{3+} ion, even though some energy transfer from the 3F_4 energy level to the 5I_7 level in Ho^{3+} would have most probably been occurring within the fibre. This may well have been confirmed by Fig.3.36 had the upper λ limit of the OSA been higher.

The multi-exponential form of the fluorescence decay is illustrated in Fig.3.37. Similar fluorescence decay curves have been observed for 2000 ppm Tm^{3+} -doped aluminosilicate fibre [19], which were fitted with two lifetimes $\tau_1 = 13 \mu s$ and $\tau_2 = 406 \mu s$, attributed to fluorescence from the 3H_4 and 3F_4 energy levels respectively. In this work estimates of the fluorescence lifetimes of the 3F_4 and 3H_4 levels were obtained using a Levenberg-Marquard approximation (see Istratov and Vyvenko [20] for a more detailed description). In many instances the fluorescence lifetime data are estimated using a single exponential and so for comparison the data were also analysed using a single exponential Prony's algorithm [8].

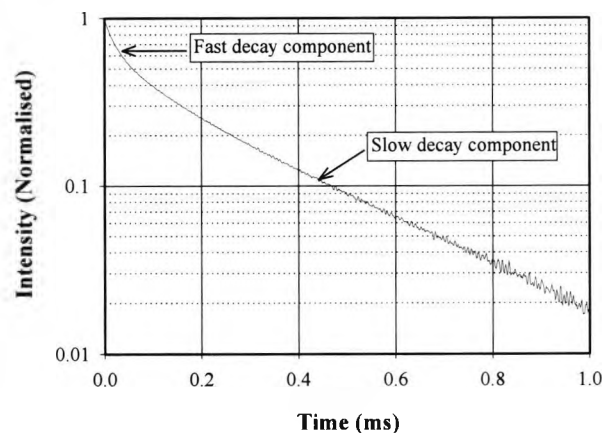


Fig.3.37 Multi-exponential form of Tm^{3+}/Ho^{3+} co-doped fibre fluorescence, measured at $22^\circ C$.

Chapter 3 Optical fibre temperature and strain sensors based on fluorescence lifetime monitoring

The temperature of the doped fibre was controlled by placing it in the centre of a temperature stabilized oven (Carbolite, type: MTF 12/38/400). Strain was applied to the fibre sensor using the pulley system where weights were added, thus progressively increasing or decreasing, in a controlled and reproducible way, the overall strain exerted on the test fibre. Care was taken to prevent the fibre from touching the tube oven glass and to lubricate the pulley in order to minimize friction, for better repeatability of the test measurements. The applied strain, ϵ , due to a mass, m , was calculated using Equation 3.1 shown before.

Several $\text{Tm}^{3+}/\text{Ho}^{3+}$ co-doped fibre sensors (~10 cm) were constructed for high temperature work, as shown in Fig.3.38 using a similar arrangement to that shown in Fig.3.35, but

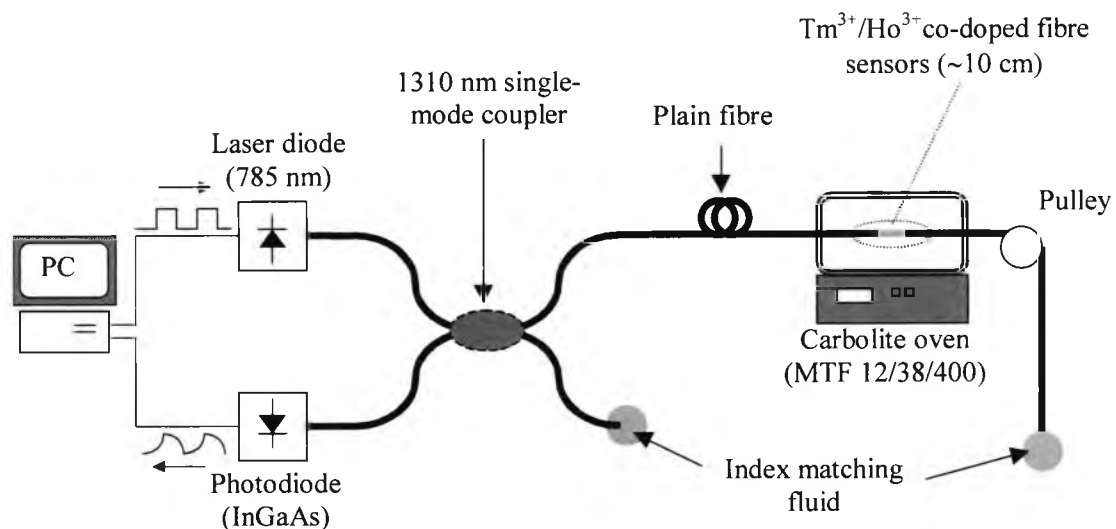


Fig.3.38 Set up for high temperature analysis of $\text{Tm}^{3+}/\text{Ho}^{3+}$ co-doped fibre.

without the need to apply strain. The use of index matching gel again minimised any back reflection from the source, and also all fibres placed within the oven were stripped of plastic coatings as before.

Chapter 3 Optical fibre temperature and strain sensors based on fluorescence lifetime monitoring

3.6.2.2 Results

A) PLD system

i) Temperature calibration

Fig.3.39 shows a 4th order polynomial fit to the measured data from 40 - 800°C, when monitoring the fluorescence lifetime, with standard deviation error bars (very small).

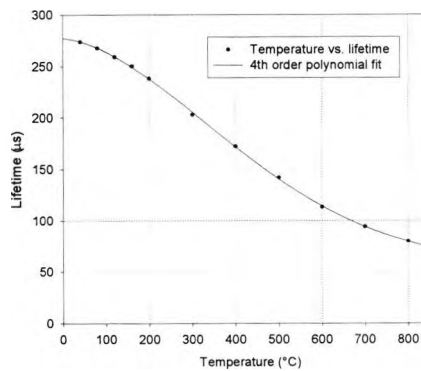


Fig.3.39 Temperature characteristics of Tm^{3+}/Ho^{3+} .

These results can be compared to the lifetime versus temperature calibration graph (Fig.3.40) obtained for 280 ppm Tm^{3+} -doped fibre from previous work [21]. It can be seen that

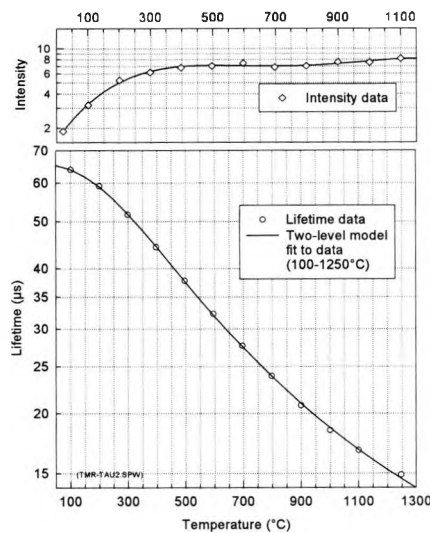


Fig.3.40 Thermal characteristics of the fluorescence of 280 ppm Tm^{3+} -doped fibre [21].

Chapter 3 Optical fibre temperature and strain sensors based on fluorescence lifetime monitoring

although the trend in reducing lifetime with temperature is the same, the 3F_4 lifetime measured in this work is approximately 4 times longer. Both results were obtained by using PLD, although the fibre dopant concentrations, core compositions, sensor lengths etc. are quite different under the two circumstances.

ii) Strain calibration

The requirement of the PLD method is a single exponential decay and it has been shown in the subsequent work on Tm^{3+}/Ho^{3+} co-doped fibre that the fluorescence decay is, in fact, multi-exponential in nature, and can be attributed to fluorescence originating from specific energy levels of the Tm^{3+} ion, therefore the A/D method is seen as the more reliable method of signal processing in this case. In the previous measurements obtained using the PLD lifetime approach for Tm^{3+}/Ho^{3+} the lifetime was found to decrease with increasing strain [16], rather than increasing as was found in the A/D case [10]. The negative strain gradients observed in this preliminary work on the fibre are believed to be a result of either drift in the lifetime reading during the course of strain calibrations at individual temperatures, or small fluctuations in the oven temperature during this time (as the variations in lifetime with strain recorded were extremely small), and in the light of the results from further investigations into this fibre they are not reported on here.

B) A/D card

i) Temperature calibration

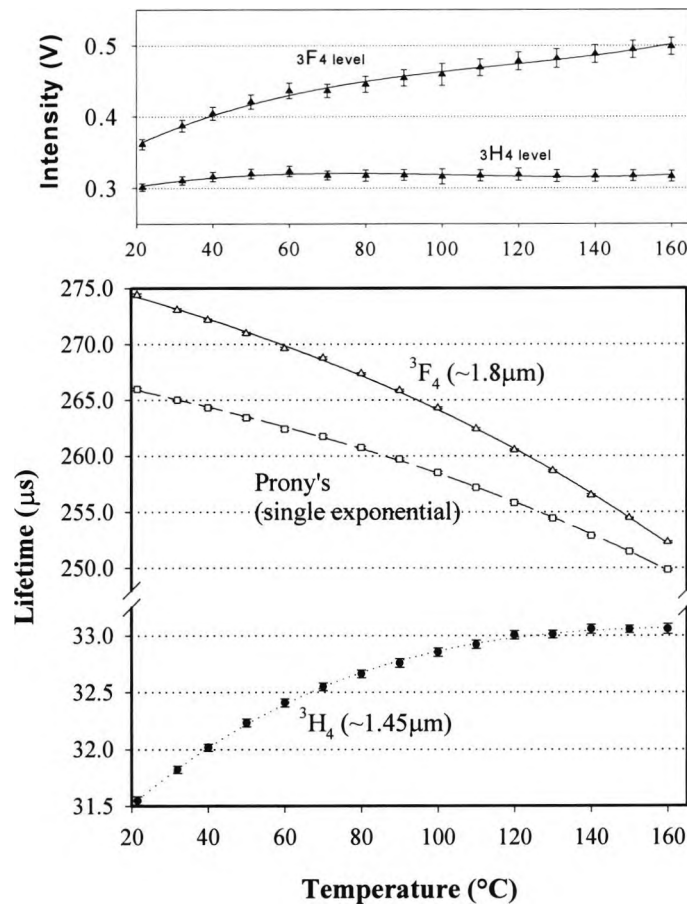


Fig.3.41 Temperature dependence of the intensities and fluorescent lifetimes of the 3F_4 and 3H_4 energy levels of Tm^{3+}/Ho^{3+} co-doped fibre together with the single exponential Prony fit to the fluorescence decay. Solid lines are 3rd order polynomial fits.

A series of calibration tests was performed, to assess the temperature and strain dependence of the fluorescence decay from the Tm^{3+}/Ho^{3+} co-doped fibre. In the first test the fluorescence decay was recorded over the range from 20–160°C, with no weights applied to the pulley system (i.e. effectively zero applied strain). Fig.3.41 shows the dependence of the

Chapter 3 Optical fibre temperature and strain sensors based on fluorescence lifetime monitoring

fluorescence lifetimes and intensities attributed to the 3F_4 and 3H_4 energy levels of Tm^{3+} , estimated using the aforementioned method [20], as well as data obtained using Prony's technique assuming the signal is single exponential. The lifetime attributed to the 3H_4 energy level increases with temperature in a manner similar to the lifetime versus temperature results obtained with Pr^{3+} :ZBLAN [22]. Fig.3.42 shows the changes in temperature sensitivities of the various lifetimes with temperature inferred from the data in Fig.3.41. Fig.3.43 shows the OSA recorded changes in fluorescence intensities of the lifetimes with temperature. These spectra confirm the intensity data of Fig.3.41, showing the greater increase in the long lifetime (3F_4) intensities from room temperature to $100^\circ C$. The second harmonic of the pump (occurring ~ 1570 nm) should be ignored here.

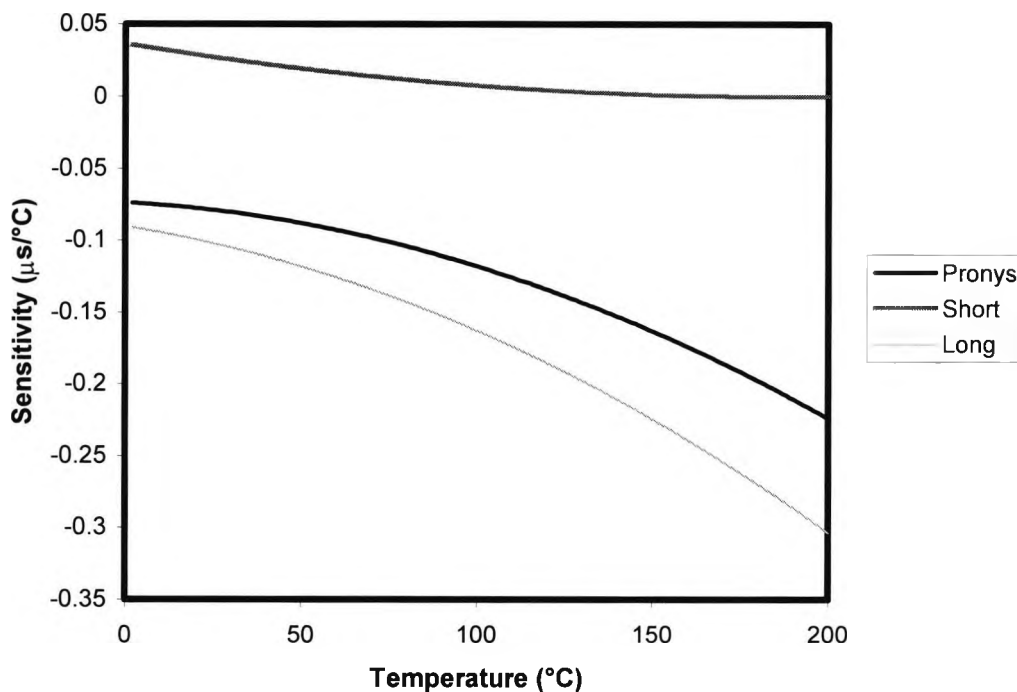


Fig.3.42 Tm^{3+}/Ho^{3+} co-doped fibre temperature sensitivities.

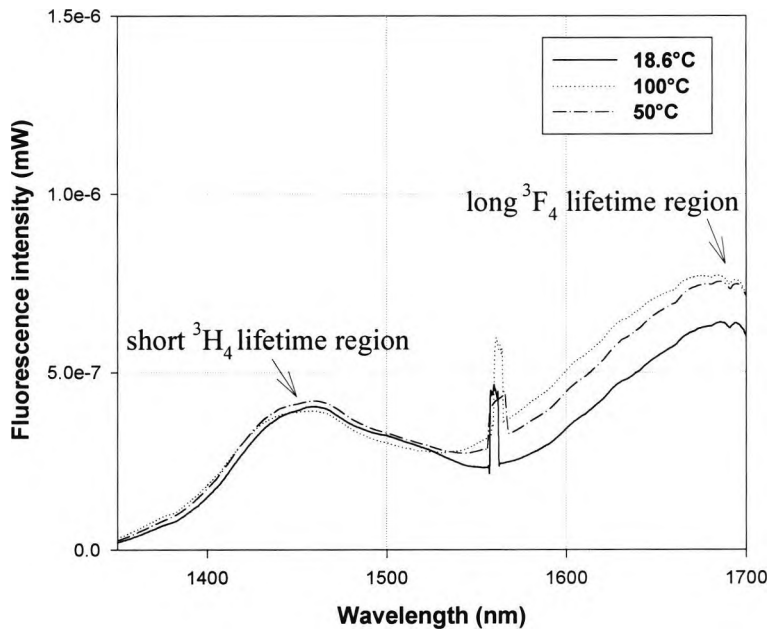


Fig.3.43 Tm^{3+}/Ho^{3+} co-doped fibre temperature dependent fluorescent intensities.

ii) Strain calibration

The effect of strain on the fluorescence lifetimes was measured for values of applied strain between 220 and 1330 $\mu\epsilon$, an example of which is given in Fig.3.44 for the decay component ascribed to the 3F_4 energy level lifetime. Data were also obtained for the 3H_4 energy level fluorescence lifetime and using Prony's algorithm. The strain sensitivity for the lifetime versus strain data was obtained by fitting a straight line to the data. Measurements of the strain sensitivities of the fluorescence lifetimes were carried out at temperatures of 30°C, 40°C, 100°C, 150°C and 200°C, the results of which are plotted in Fig.3.45. In this work, to avoid any ambiguity due to drift or small temperature fluctuations, multiple strain cycles were recorded at each temperature with the average of the cycles being used for the final reading.

Chapter 3 Optical fibre temperature and strain sensors based on fluorescence lifetime monitoring

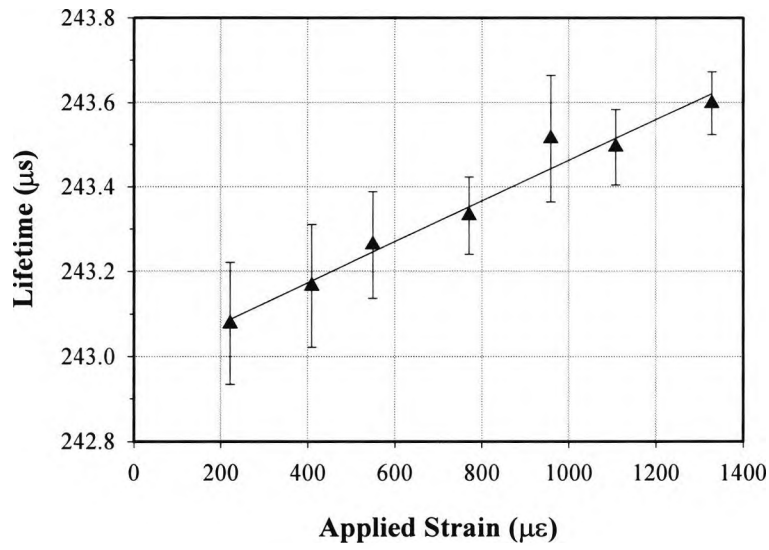


Fig.3.44 Effect of applied strain on the 3F_4 fluorescence lifetime, measured at 200°C.

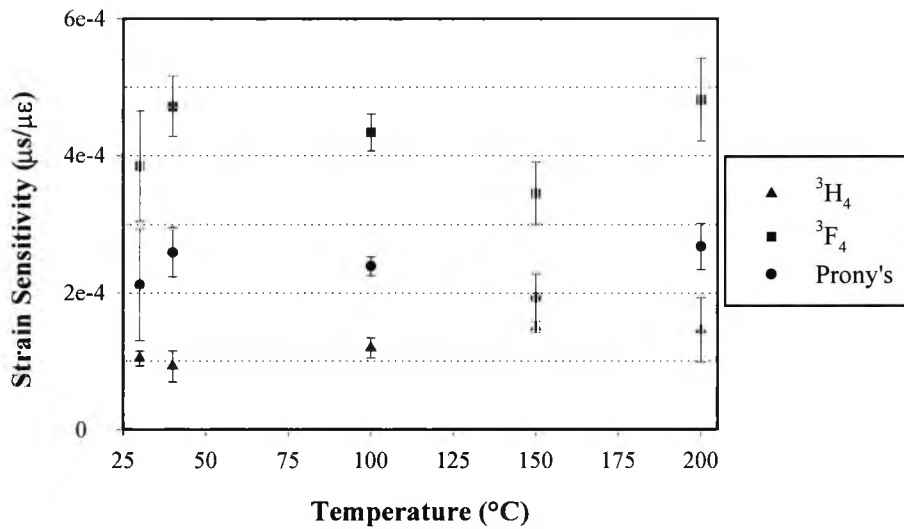


Fig.3.45 Strain sensitivity of the 3F_4 and 3H_4 energy level lifetimes of Tm^{3+}/Ho^{3+} co-doped fibre together with the single exponential Prony fit to the fluorescence decay at various temperatures.

Chapter 3 Optical fibre temperature and strain sensors based on fluorescence lifetime monitoring

A summary of the strain and temperature sensitivity results obtained is presented in Table 3.3, together with results obtained previously for Nd³⁺ and Yb³⁺-doped fibres.

Dopant	Tm ³⁺ /Ho ³⁺ (this work)			Yb ³⁺	Nd ³⁺
	³ H ₄	³ F ₄	Prony's	[5]	[4]
$\delta\tau/\delta\varepsilon$ ($\mu\text{s}/\mu\text{e}$)	1.2×10^{-4}	3.2×10^{-4}	2.3×10^{-4}	3.3×10^{-4}	5.0×10^{-4}
$\delta\tau/\delta T$ ($\mu\text{s}/^\circ\text{C}$)*	0.03	-0.1	-0.08	-0.07	-0.28
$\delta T/\delta\varepsilon$ ($^\circ\text{C}/\mu\text{e}$)	3.0×10^{-3}	3.2×10^{-3}	2.9×10^{-3}	6.1×10^{-3}	1.8×10^{-3}
$\Delta T @ 1000\mu\text{e}$ ($^\circ\text{C}$)	3.0	3.2	2.9	6.1	1.8

Table 3.3 Strain and temperature sensitivity of fluorescence lifetimes (*Tm³⁺/Ho³⁺ temperature sensitivity data at 20°C calculated from data).

iii) High temperature calibrations and annealing effects

a) High temperature calibration

Using the experimental arrangement in Fig.3.38, but with a new Tm³⁺/Ho³⁺ co-doped fibre sample (9 cm), measurements were made to determine the high temperature characteristics (up to 900°C) of the energy levels involved (i.e without any prior thermal annealing), and the results obtained are shown in Fig.3.46 with 4th order polynomial fits to the data and with standard deviation error bars (very small).

Similarities in Fig.3.46 can be drawn with Fig.3.41 in that there is an initial slight increase in lifetime from the ³H₄ level at the lower temperatures with equal trends in the Prony's and the ³F₄ energy level, despite the small differences in recorded lifetimes due to using a shorter sample length here (9 cm).

Chapter 3 Optical fibre temperature and strain sensors based on fluorescence lifetime monitoring

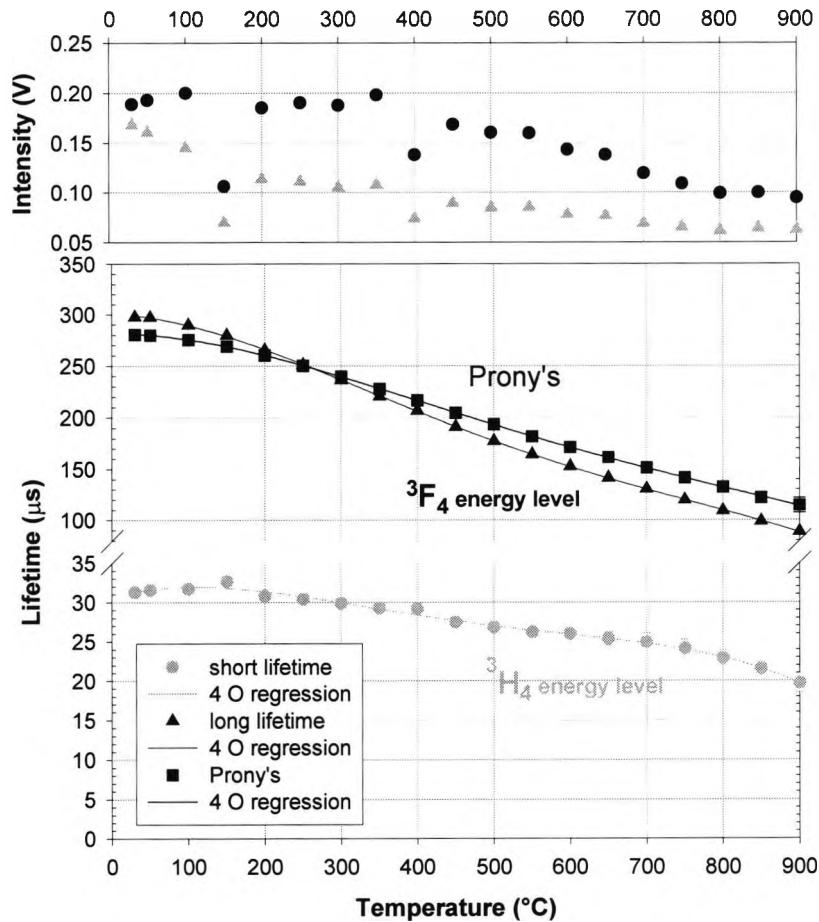


Fig.3.46 Tm^{3+}/Ho^{3+} co-doped fibre high temperature characteristics (up to $900^{\circ}C$) of the energy levels involved (without any thermal annealing).

b) Annealing effects

Using the same experimental arrangement as shown in Fig.3.38, measurements were obtained to determine the repeatability of the lifetime versus temperature dependence before and after an annealing process where doped fibre samples were heated to a set temperature and held there for a specific time [23]. Fig.3.47 shows the lifetime and fluorescence intensity versus temperature dependence for two different samples (both ~ 10 cm in length)

Chapter 3 Optical fibre temperature and strain sensors based on fluorescence lifetime monitoring

of Tm^{3+}/Ho^{3+} before and after undergoing an annealing process, using Prony's method only. The first sample (sample A) was annealed at $800^{\circ}C$ for 28 hrs (Fig.3.48) and then at $850^{\circ}C$ for 83 hrs, while the second sample (sample B) was annealed at $900^{\circ}C$ for 70 hrs (Fig.3.49). The data shown in Fig.3.47 was obtained during 5 thermal cycles prior to and following the annealing process. Analysis of the data obtained from the first sample indicated that during the cycling prior to the annealing process a small incremental and irreversible change in the lifetime characteristics occurred. This would indicate that even though the maximum temperature of the cycling ($600^{\circ}C$) was significantly lower than the annealing temperatures used ($800^{\circ}C$ and $850^{\circ}C$) a small annealing process may have occurred during the measurements (~ 10 mins each). The maximum temperature in the cycling prior to annealing of the sample B was kept to $500^{\circ}C$ for the measurements, and no drift was observed for this temperature range.

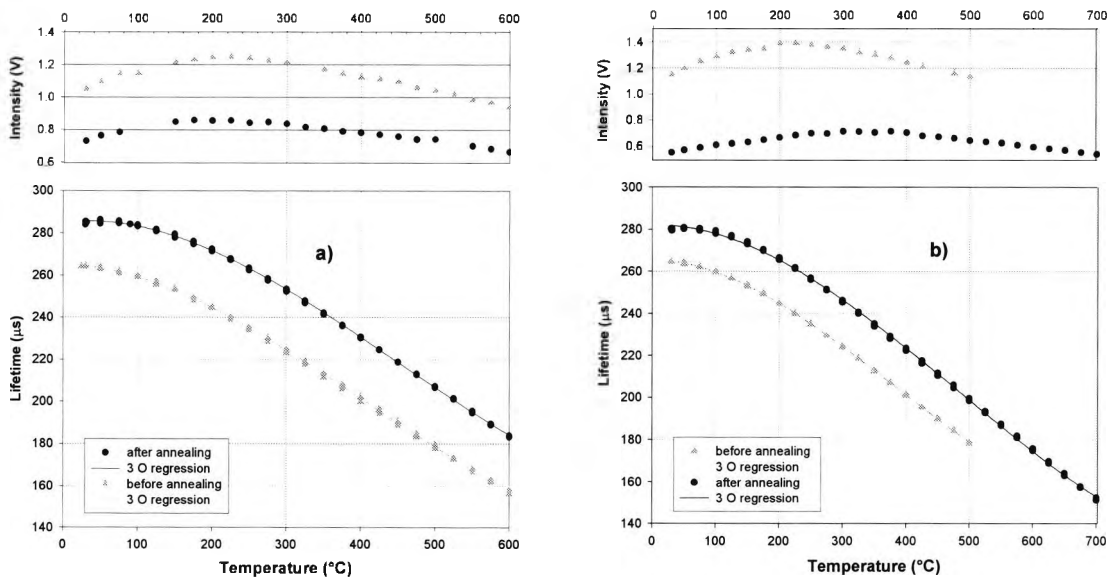


Fig.3.47 Tm^{3+}/Ho^{3+} co-doped fibre samples before and after annealing process (a) sample A and (b) sample B.

Chapter 3 Optical fibre temperature and strain sensors based on fluorescence lifetime monitoring

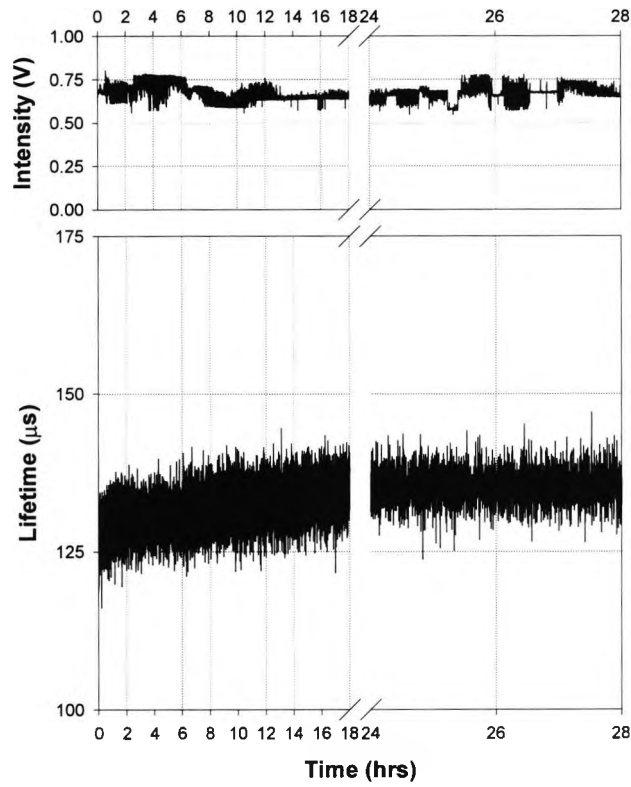


Fig.3.48 Sample (a) annealing at 800°C for 28 hours.

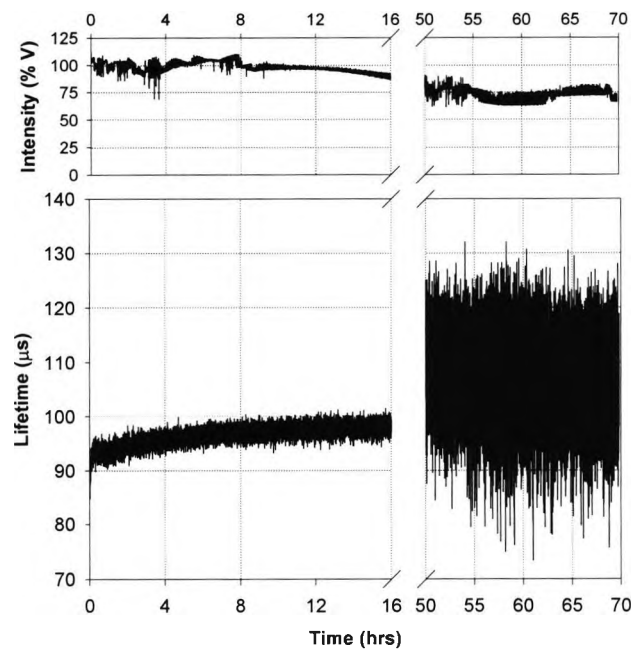


Fig.3.49 Sample (b) annealing at 900°C for 70 hours.

Chapter 3 Optical fibre temperature and strain sensors based on fluorescence lifetime monitoring

Fig.3.48 and Fig.3.49 show some of the data taken during the annealing processes, from which the lifetime increases can be seen as an exponential rise until stability occurs around 24 hrs and 50 hrs respectively. The more noisy signal in Fig.3.49 after the fibre was annealed at 900°C for much longer than 28 hrs shows that 900°C is the maximum temperature at which the fibre can survive. This contrasts with previous work using singly doped Tm^{3+} fibre [21] where the maximum working temperature (1250°C) was much higher than the co-doped Tm^{3+}/Ho^{3+} material used here, where the presence of the additional dopant (Ho^{3+}) has lowered the threshold of usefulness. Further analyses of these results are shown in Tables 3.4, 3.5, 3.6 and 3.7. They show the lifetime and subsequent temperature accuracies (using rms (σ) values) obtained from these sensor schemes from fitting both 3rd and 4th order polynomial regressions to the measured data over certain temperature ranges.

temperature range °C	sample (a)		sample (b)	
	before annealing	after annealing	before annealing	after annealing
30°C - T_{max}	0.694	0.497	0.290	0.857
100°C - T_{max}	0.687	0.421	0.277	0.614
150°C - T_{max}	0.682	0.395	0.272	0.493
200°C - T_{max}	0.692	0.322	0.266	0.425

Table 3.4 Lifetime (μs) rms errors arising from fitting 3rd order polynomial fits to the Tm^{3+}/Ho^{3+} annealing data over each of the above ranges.

Chapter 3 Optical fibre temperature and strain sensors based on fluorescence lifetime monitoring

temperature range °C	sample (a)		sample (b)	
	before annealing	after annealing	before annealing	after annealing
30°C – T _{max}	3.45	-	2.71	-
100°C – T _{max}	3.42	3.74	1.49	3.38
150°C – T _{max}	3.18	2.27	1.31	2.33
200°C – T _{max}	3.16	1.54	1.20	1.86

Table 3.5 Temperature (°C) rms errors arising from fitting 3rd order polynomial fits to the Tm³⁺/Ho³⁺ annealing data over each of the above ranges.

temperature range °C	sample (a)		sample (b)	
	before annealing	after annealing	before annealing	after annealing
30°C – T _{max}	0.648	0.406	0.267	0.386
100°C – T _{max}	0.673	0.373	0.265	0.395
150°C – T _{max}	0.679	0.373	0.266	0.393
200°C – T _{max}	0.692	0.315	0.262	0.392

Table 3.6 Lifetime (µs) rms errors arising from fitting 4th order polynomial fits to the Tm³⁺/Ho³⁺ annealing data over each of the above ranges.

Chapter 3 Optical fibre temperature and strain sensors based on fluorescence lifetime monitoring

	sample (a)		sample (b)	
temperature range °C	before annealing	after annealing	before annealing	after annealing
30°C - T_{max}	3.47	-	2.68	-
100°C - T _{max}	3.34	2.52	1.43	2.14
150°C - T_{max}	3.16	2.24	1.28	1.93
200°C - T _{max}	3.16	1.52	1.18	1.71

Table 3.7 Temperature (°C) rms errors arising from fitting 4th order polynomial fits to the Tm³⁺/Ho³⁺ annealing data over each of the above ranges.

These tables show that errors in the temperature measurement are quite reasonable over a number of ranges. For sample (a), the errors generally lessen after annealing, whereas for sample (b) they generally increase. The reason why sample (a) is more accurate after annealing is that sample (b) has been exposed to its maximum temperature for too long (70 hrs), and the signal has become noisy (Fig.3.49). The calculated errors for the temperature range (i.e 30°C - T_{max}) after annealing for both sensors was found to be unreliable, as the temperature sensitivities became too low ($\rightarrow 0$) at these lowest temperatures ($\sim 35^\circ\text{C}$) with the sensors “turning down” at the ends after annealing, and are therefore omitted.

3.6.3 Tm³⁺/Ho³⁺ co-doped fibre – conclusions

The performance of a sensor system, in terms of both strain and temperature sensitivity, using Tm³⁺/Ho³⁺ co-doped fibre has been reported. For one of the arrangements used, the sensor scheme shows a two component decay with both components providing interesting data for temperature sensor systems. Analysis of the fluorescence decay shows how, by selecting appropriate components of the decay curve, the temperature and strain sensitivity can be maximised or minimised depending upon the requirements of the application. Results for both the PLD system (Fig.3.34) and the A/D card system (Fig.3.38) show high temperature sensitivities between 200°C and 700°C, similar to other doped fibres (Fig.3.40) [21]. It is also interesting to note that the lifetime of the ³F₄ energy level decreases (Fig.3.41) with temperature in a manner similar to that observed with both the Prony's and the PLD technique, and it is comparable in magnitude.

3.7 Tm³⁺ in Y₂O₃ powder probe sensor

3.7.1 Introduction

The need to develop robust, sensitive and effective optical fibre sensor probes to measure at the higher (>1000°C) temperatures remains an integral goal of sensor research. Fluorescence-based methods have previously offered some very effective sensor probes. Using optical glasses doped with appropriate luminescent ions (Nd³⁺) and conventional cements, in a tailored mechanical probe, temperatures as high as approximately 400°C were reached in early research [24]. This range was extended (with the use of gold coated fibres) to approximately 600-700°C in further work [25] and the use of intrinsic fibre optic probes

Chapter 3 Optical fibre temperature and strain sensors based on fluorescence lifetime monitoring

with Nd^{3+} and Er^{3+} doped into optical fibre and fused to conventional silica fibre has enabled the extension of the upper temperature to approximately 780°C (with Nd^{3+}) and 1100°C (with Er^{3+}) [2, 3, 9]. This type of probe is compact, relatively inexpensive to fabricate and operates over a wide temperature range. Their intrinsic nature offers many advantages, but for a number of applications in testing and evaluation there is a need for even higher maximum temperatures, offering a stable response without the problems for irreversible material changes.

One approach to the solution of the problem of the creation of a reliable and inexpensive probe is the use of *powdered* fluorescent materials. A wide range of dyes and scintillators are available in this form but their decay times are usually rapid and they are best excited in the short wavelength spectral regions of the blue and ultra violet. The goal of this work has been the identification of a suitable powdered material which could easily be coupled to an optical fibre probe, respond to the longer wavelength radiation from cheaper and more readily available laser diodes and LEDs and have a fluorescence decay time $>1\mu\text{s}$, for greater ease of measurement. These rare earth materials are familiar in crystals, garnets and more recently in doped fibres for laser and sensor applications, but have not been used in this way in sensor studies. One such useful type of powder probe is thulium in yttrium oxide powder, i.e. Tm^{3+} in Y_2O_3 .

3.7.2 Previous work

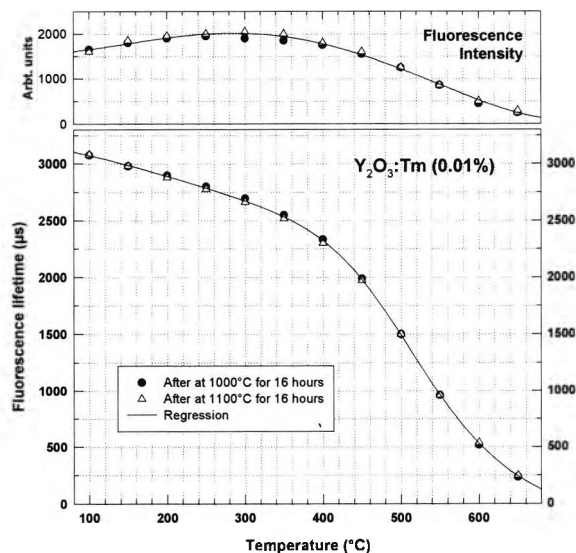


Fig.3.50 Results from the previous work with Tm^{3+} in Y_2O_3 [26].

The principal results achieved from previous work with this powder sensor by Zhang *et al* [26] are shown in Fig.3.50, which describes the lifetime of the Tm^{3+} fluorescence emission at wavelengths of 1.45 μm and 1.7 μm as a monotonic function of temperatures up to 650°C. The work excited the 3F_4 (12802 cm^{-1}) energy level (Fig.3.51) of Tm^{3+} in Y_2O_3 using an 800 nm wavelength laser diode source to measure fluorescence at wavelengths greater than 1 μm only, with a long-pass (i.e $\lambda > 1 \mu m$) filter to aid the fluorescent detection.

Heat treatments at 1000°C and 1100°C revealed the potential for high temperature applications of this material. These called for further investigations on this material which are reported herein [27]. The same batch of $Tm^{3+}:Y_2O_3$ was used during these further tests (having been supplied by Phosphor Technology, UK). It is in the form of fine powders,

Chapter 3 Optical fibre temperature and strain sensors based on fluorescence lifetime monitoring

having a particle size distribution measured by a Coulter Counter (100 μm aperture) of: 1.7 μm — 5 vol%, 2.3 μm — 25 vol%, 2.9 μm — 50 vol%, 3.6 μm — 75 vol% and 3.9 μm — 95 vol%. The concentration of the Tm^{3+} dopant is about 0.01 mole %.

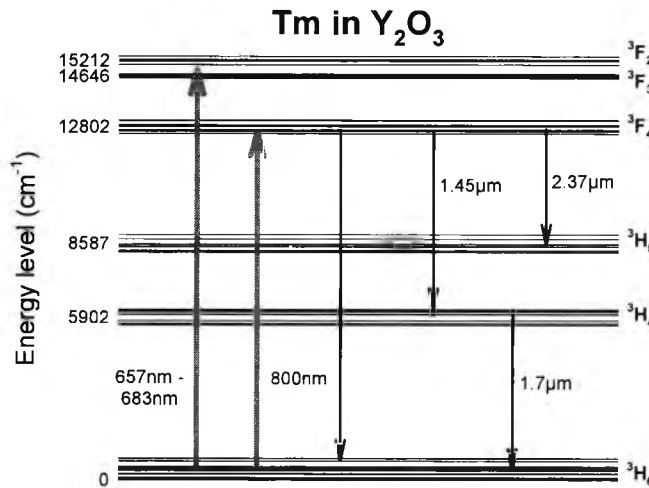


Fig.3.51 Tm^{3+} in Y_2O_3 energy level diagram showing the relevant electronic energy levels of Tm^{3+} in Y_2O_3 (data from RSTB's database of laser materials, MS474, NASA-LaRC, Hampton, VA23681-2199, USA).

The electronic energy levels of Tm^{3+} ions in Y_2O_3 are illustrated in Fig.3.51. This shows how Tm^{3+} in Y_2O_3 was excited with radiation at ~ 800 nm and to give fluorescence emission at 1.45 μm , 1.7 μm and 2.37 μm in the previous work [26]. Apart from the radiative $^3\text{H}_4 \rightarrow ^3\text{H}_6$ transition at ~ 1.7 μm , the energies involved in these transitions are quite close to those observed from emission associated with the $^3\text{H}_4 \rightarrow ^3\text{H}_6$ transitions around ~ 1.9 μm in much previous work [18, 21] on the sensing applications of Tm^{3+} doped silica fibres.

The further work done here also excites the higher energy levels of the 14646 cm^{-1} ($^3\text{F}_3$) to 15212 cm^{-1} ($^3\text{F}_2$) region (i.e that between 682 nm and 657 nm respectively) of the Tm^{3+} in Y_2O_3 energy levels, using a 678 nm source [27] to achieve fluorescence at both 1 $\mu\text{m}+$ and at

Chapter 3 Optical fibre temperature and strain sensors based on fluorescence lifetime monitoring

800 nm. The mechanism can be seen more clearly from Fig.3.51 which shows the Tm^{3+} in Y_2O_3 energy level diagram (source: RSTB's database of laser materials). In addition to the long-wavelength emission at 1.45 μm and 1.7 μm tested previously, the emission at the 800 nm band can be induced by light from a widely available red laser diode at a wavelength band of 660 nm – 680 nm and this has been more closely examined in this work. Its lifetime is one magnitude less than that of its long-wavelength counterpart, and that enables the potential thermometer system to have a much shorter response time. Low-cost visible laser diodes and silicon photodetectors can be used in the measurement of the fluorescence. These features are favourable for the sort of applications in mind for the sensor system.

3.7.3 Experimental method and results

The schematic of the experimental arrangement used is depicted in Fig.3.52. It was designed to couple to the optical spectral features of $\text{Y}_2\text{O}_3:\text{Tm}^{3+}$ highlighted in the energy level scheme shown in Fig.3.51, and shares a certain degree of similarity with that used in previous Tm^{3+} doped silica fibre work [18, 21]. An 800 nm laser diode was used to provide efficient excitation of fluorescence emission in one scheme. Though an InGaAs photodiode with a standard spectral response 0.9-1.7 μm can be used to monitor the fluorescence emissions at 1.45 μm and 1.7 μm , a wavelength extended (0.9 - 2.1 μm) InGaAs photodiode was employed as it had a much higher spectral sensitivity at 1.7 μm (the corresponding emission at 1.9 μm in Tm^{3+} doped silica fibre is the strongest among the three radiative transitions depicted in Fig.3.51).

Chapter 3 Optical fibre temperature and strain sensors based on fluorescence lifetime monitoring

The inset of Fig.3.52 illustrates the original structure of the sensing element [26]. Initially for the previous work it was fabricated by inserting the cleaved end of a transmission fibre into silica glass tubing and joining them by electric arc fusion. $Y_2O_3:Tm^{3+}$ powder was then filled into the tubing through the extended open end, which was sealed by again using electric arc. The silica glass capsule formed hermetically sealed the sensing material - the $Y_2O_3:Tm^{3+}$ powder - and held it firmly against the transmission fibre. Here, 50/125 μm multimode silica glass fibres were used for the transmission of the excitation and the return fluorescence light, which eased the task of launching excitation radiation into the optical fibre and maximised the collection of the incoherent fluorescence emission.

Some changes in the experimental arrangement compared to that used previously were made following various tests that were carried out [27]. Apart from using a 678 nm laser diode to induce the 800 nm fluorescence emission and a silicon PIN diode to detect the emission, the $Tm^{3+}:Y_2O_3$ powder sample under test had to be held in an alumina tube instead of a silica capsule as was used in preliminary tests, so that heat treatment tests at temperatures above 1100°C could be carried out. Fig.3.52 shows the set-up schematically.

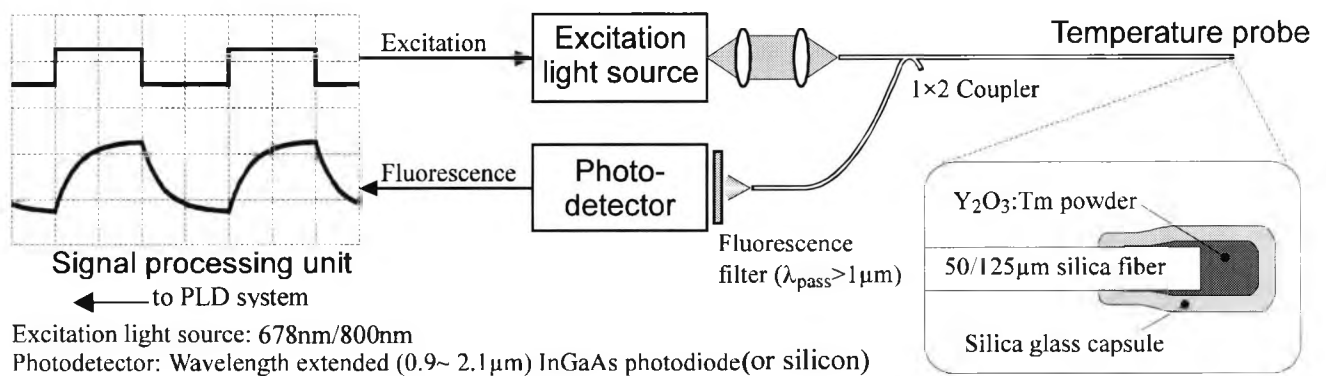


Fig.3.52 Experimental set-up used for Tm^{3+} in Y_2O_3 [27].

Chapter 3 Optical fibre temperature and strain sensors based on fluorescence lifetime monitoring

Due to severe thermal quenching, the Tm^{3+} fluorescence in Y_2O_3 was too weak to be detected at temperatures above $750^{\circ}C$, as shown below in Fig.3.53.

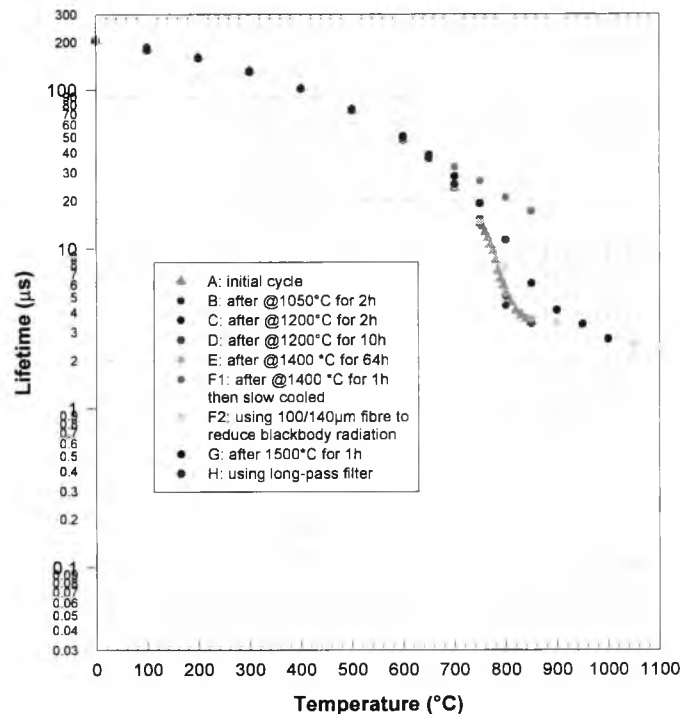


Fig.3.53 Fluorescence @800 nm band - all results.

Thus, the fluorescence approach could only be used in the temperature range below that temperature. Here, again as used previously, multimode silica optical fibres were used for the transmission of the excitation light and the subsequent fluorescence emission. However, the silica transmission fibre had to be detached from the sample when it was under heat treatment at temperatures above $1100^{\circ}C$ and re-attached to the sample afterwards to carry out the fluorescence measurements.

Chapter 3 Optical fibre temperature and strain sensors based on fluorescence lifetime monitoring

3.7.3.1 Heat treatment

The purpose of the heat treatment tests was to assess the high temperature stability of the candidate sensor material and to establish the maximum exposure temperature for the materials from the observation of the annealing effect on its fluorescence characteristics. The $\text{Tm}^{3+}:\text{Y}_2\text{O}_3$ powder sample under test was subjected to the five heat treatment regimes as shown in Table 3.8, following an initial cycle (A).

annealing temperature	duration	measurement cycle afterwards
N/A	N/A	A: initial cycle
1050°C	2 hours	B
1200°C	2 hours	C
1200°C	10 hours	D
1400°C	64 hours	E
1400°C	1 hour	F

Table 3.8 Heat treatments for $\text{Tm}^{3+}:\text{Y}_2\text{O}_3$.

Fluorescence lifetime measurements were made prior to and after each cycle, over the 0 - 700°C region. The annealing temperature and duration of each treatment as well as the designation of the following measurement cycles are listed in Table 3.8. Results from these measurement cycles are presented in the following sections.

Chapter 3 Optical fibre temperature and strain sensors based on fluorescence lifetime monitoring

3.7.3.2 Fluorescence at 800 nm band

The fluorescence lifetime data taken during the measurement cycles prior to and after each annealing process are depicted in Fig.3.54 up to 700°C. The lifetime of $Tm^{3+}:Y_2O_3$ fluorescence at 800 nm band is approximately one magnitude less than its counterpart at the longer wavelength bands, shown in Fig.3.50. It can be seen that these cycles vary widely in length from 1 hour (F) to 64 hours (E).

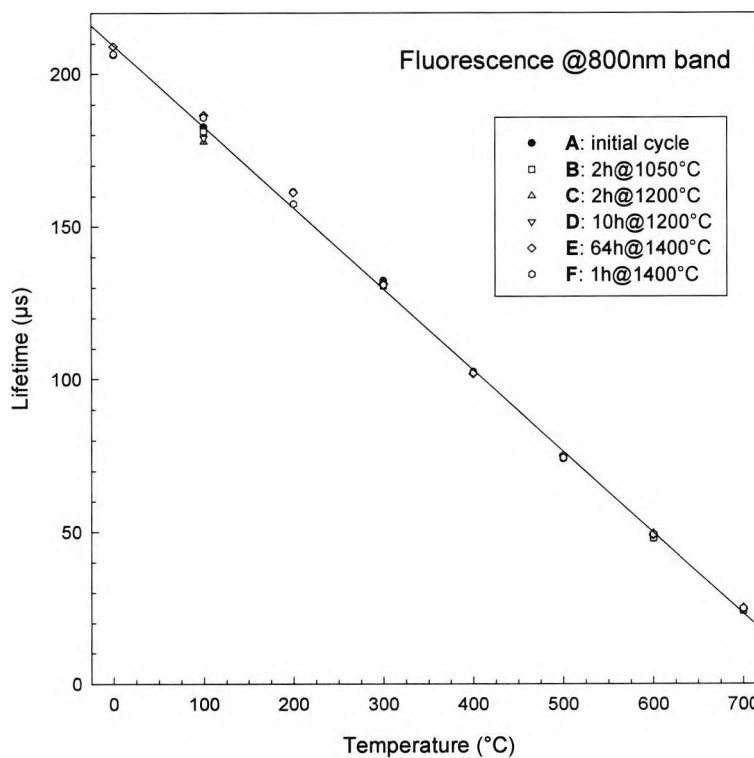


Fig.3.54 Lifetime of $Tm^{3+}:Y_2O_3$ fluorescence at 800 nm.

The linear regression line plotted in Fig.3.54, which fits to all the data presented in the graph, reveals that the lifetime of the fluorescence at 800 nm shows essentially a linear response to the temperature over this range. The rate of lifetime change with temperature is about $-0.27 \mu s / ^\circ C$.

Chapter 3 Optical fibre temperature and strain sensors based on fluorescence lifetime monitoring

Errors from a third order polynomial regression of data from all the measurement cycles are illustrated in Fig.3.55. The regression errors at each temperature are randomly distributed across the series of measurement cycles. No annealing effect is apparent from these heat treatment tests. This result contrasts very positively with the results of tests on some rare earth doped fibres, which show a strong annealing effect at these temperatures, and makes for better use in thermometer systems.

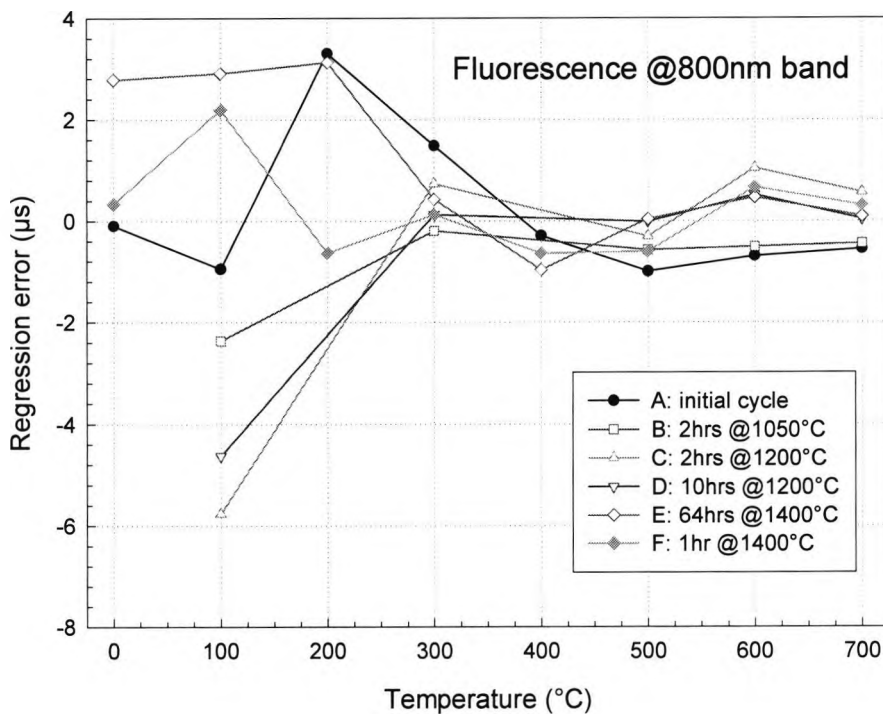


Fig.3.55 Regression errors of lifetime data of $Tm^{3+}:Y_2O_3$ fluorescence at 800 nm.

3.7.3.3 Fluorescence at 1.45 µm and 1.7 µm

The lifetime data for the fluorescence at 1.45 µm and 1.7 µm, taken at each of the measurement cycles, also show no annealing effect. They are essentially the same as those taken during the preliminary tests, confirming the usefulness of this medium.

Chapter 3 Optical fibre temperature and strain sensors based on fluorescence lifetime monitoring

Both the 800 nm and 678 nm light sources can be used to induce fluorescence at 1.45 μm and 1.7 μm . They pump into the 3F_4 and $^3F_{2,3}$ energy levels shown in Fig.3.51 respectively. The fluorescence lifetime measurements taken with the use of different wavelength light sources are presented in Fig.3.56. It can be seen that the choice of excitation band has little effect on the lifetime measurement and that there is close agreement between the experimental results and the theoretical expectation.

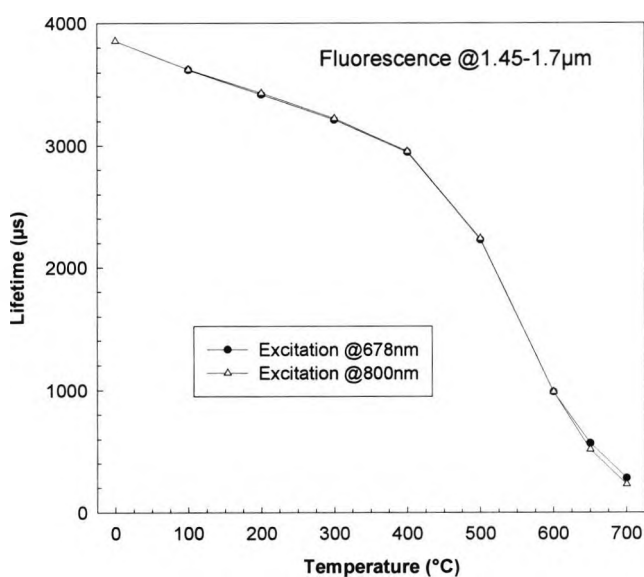


Fig.3.56 Lifetime data of $\text{Tm}^{3+}:\text{Y}_2\text{O}_3$ fluorescence at 1.45 μm and 1.7 μm induced by different wavelength sources.

3.7.4 Modelling of results

The temperature dependence of fluorescence intensity at 1.45 μm and 1.7 μm , illustrated in Fig.3.57, shows that there are at least two competing transition processes involved which cause the fluorescence intensity to increase with temperature up to $\sim 500^{\circ}\text{C}$ and decrease above that point. These competing processes also determine the characteristics of the

Chapter 3 Optical fibre temperature and strain sensors based on fluorescence lifetime monitoring

lifetime. With the (reasonable) assumption that only two competing transitions are involved, a 3-level model [21], expressed as

$$\tau = \frac{\tau_s}{1 + \alpha \exp(-\Delta E_1/kT) + \beta \exp(-\Delta E_2/kT)} \quad (3.4)$$

is used here in fitting to the lifetime measurement data, where T is the absolute temperature; k the Boltzmann constant; and ΔE_1 and ΔE_2 , the energy gaps of two competing transitions. Equation 3.4 is a modification of equation 1.8 given previously in Chapter 1, which was then used to explain the theory of the fluorescence lifetime temperature dependence using the basic two-level model. The adapted 3-level model used here closely fits the long-wavelength lifetime data, as is depicted in Fig.3.57. The fitted values for ΔE_1 and ΔE_2 , are 731 cm^{-1} and 9014 cm^{-1} , respectively. However, it is more difficult to relate these values to any transition between energy levels shown in Fig.3.51. Though $\Delta E_2 = 9014 \text{ cm}^{-1}$ can be regarded as the thermal agitation energy for thermal quenching, the 3-level model is thus of an empirical nature.

A simple polynomial function provides a satisfactory empirical model for the temperature dependence of fluorescence at 800 nm. However, the mechanism for such dependence is more complicated than that in the former case. At this stage it is not of particular value to study this further.

Chapter 3 Optical fibre temperature and strain sensors based on fluorescence lifetime monitoring

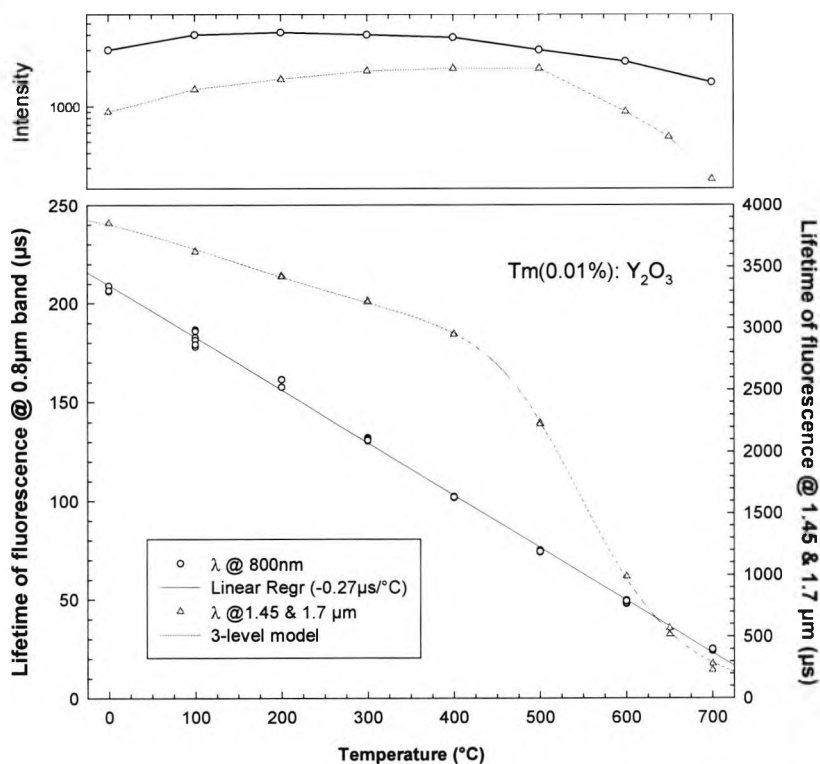


Fig.3.57 Thermal characteristics of Tm^{3+} fluorescence in Y_2O_3 .

3.7.5 Discussion

An important goal of the work was to establish a medium well suited to allowing a fibre optic probe to be cycled to very high temperature, and yet retain its calibration. In previous work with some rare earth doped optical fibres such annealing effects and similar problems caused severe mis-calibrations and could only partially be eliminated by a careful regime of heating, using relatively low doped levels of rare earth in these fibres. The work done here appears to show the value of the powder approach for the active sensor element to overcome these difficulties.

Chapter 3 Optical fibre temperature and strain sensors based on fluorescence lifetime monitoring

The experimental results obtained revealed that the thermal characteristics of Tm^{3+} fluorescence in yttrium oxide are highly stable at least up to 1100°C. Though in this work, with the present sensitivity of the detection system, the thermometric use of the fluorescence is limited to below 700°C, the material has the real potential for use in a fluorescence-radiation pyrometry cross-referencing scheme to cover temperatures up to 1100°C or higher (with the use of sapphire fibres).

Such sapphire fibres are needed to evaluate the material at temperatures higher than 1100°C. At the moment, the high transmission attenuation at wavelengths shorter than 1 μm of commercially available sapphire fiber is the main technical obstacle to implement the sensor scheme (the loss of excitation light at 800 nm in sapphire fibre will be too high). Work is continuing to investigate the characteristics of a range of materials for this purpose, and to extend the sensitivity range of the detection system used, to aim for a calibration valid over a wide range.

3.7.6 Further probe analyses

Another identical probe (probe B), i.e. configured to be exactly the same as the original probe (probe A) shown in Fig.3.52, was constructed for this work in order to further investigate the sensor performance in terms of reproducibility, and the results obtained from cycles of the new sensor for fluorescence at the 800 nm band are shown in Fig.3.58. Comparisons of probe A and probe B results for fluorescence from both bands are shown in Fig.3.59 and Fig.3.60.

Chapter 3 Optical fibre temperature and strain sensors based on fluorescence lifetime monitoring

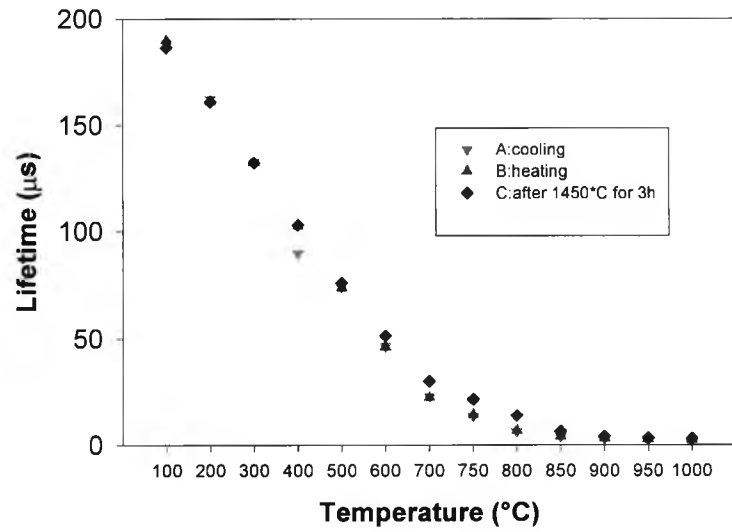


Fig.3.58 Fluorescence at the 800 nm band probe B calibration results.

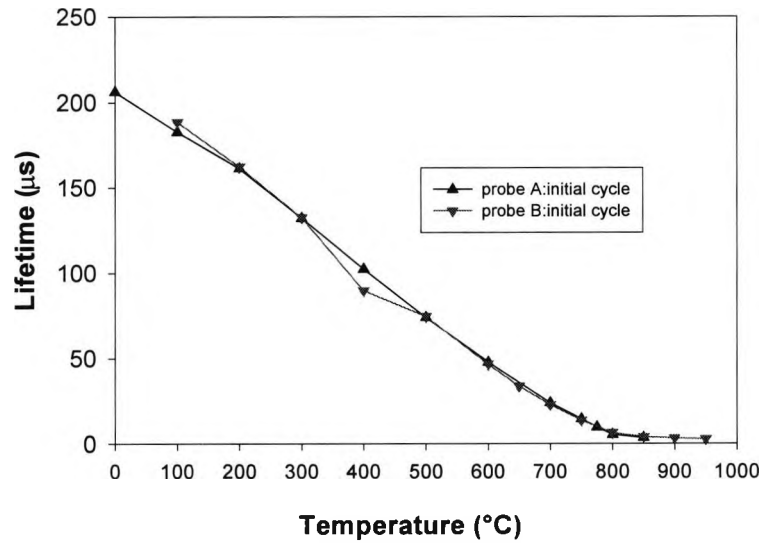


Fig.3.59 Comparison of probe A and probe B results for fluorescence at the 800 nm band.

Chapter 3 Optical fibre temperature and strain sensors based on fluorescence lifetime monitoring

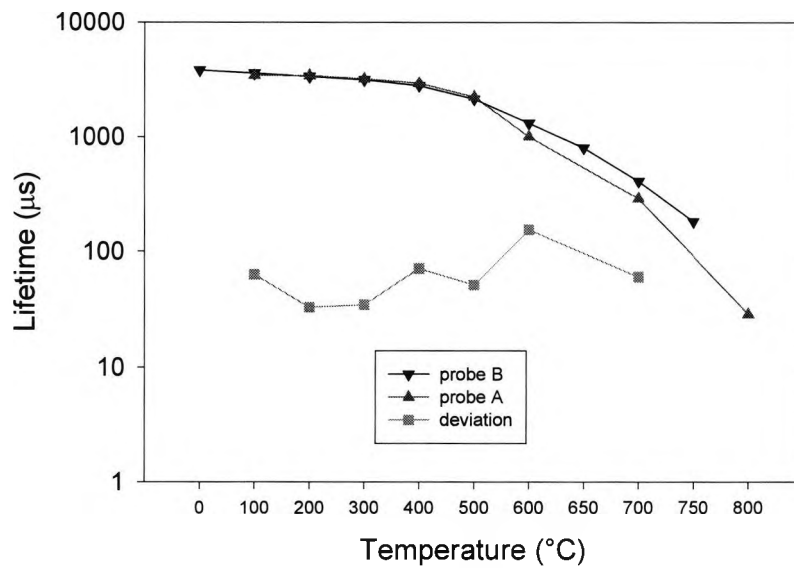


Fig.3.60 Probe A and probe B comparisons and exchangeability for fluorescence at the 1 $\mu\text{m}+$ band.

For the purposes of probe exchangeability, it can be calculated from the data that 309.1 μs is the maximum difference between the probe A and probe B lifetimes for fluorescence at the 1 $\mu\text{m}+$ band, and 12.7 μs the maximum difference for fluorescence at the 800 nm band. This means a maximum peak to peak deviation of $\pm 154.6 \mu\text{s}$ for fluorescence at the 1 $\mu\text{m}+$ band and $\pm 6.4 \mu\text{s}$ for fluorescence from the 800 nm band.

3.8 Effects of sensor lengths and other parameters of interest

3.8.1 Introduction

There are numerous other parameters (i.e apart from thermal annealing, temperature and strain) that have been found, or inferred, to influence the measured fluorescence lifetime obtained. The magnitude by which each of the following will affect the lifetime of a given fibre is highly dependent upon a large number of factors, e.g in a particular material the measured lifetime may be highly dependent upon the doping concentration but be found to have only a minimal dependence on the pump power. The most important of these factors are:

1) doping concentration - the doping concentration for a particular fibre has been shown to affect the measured fluorescent lifetime, as seen from section 3.4 of this thesis (different levels of Er^{3+} doped fibre) and from previous work [3]. If it is too high, an effect known as clustering can occur which will alter the lifetime. The amount of excitation light absorbed will also depend upon the doping concentration, e.g if too high fluorescence will mainly occur from a localised position in the rare earth doped material which may have a different lifetime from other sections of the doped material.

2) host material – the lifetime of a particular energy level of a given rare earth ion has a strong dependence on the composition of the material in which the rare earth ion is doped. Even the addition of aluminium to the silica based host normally used in rare earth doped optical fibres (which can be quite common) for example will affect the lifetime [11]. The host material will also affect the absorption and fluorescence spectra of the rare earth

Chapter 3 Optical fibre temperature and strain sensors based on fluorescence lifetime monitoring

ion. A good example of this can be seen in section 3.5 of this thesis (i.e. $\text{Er}^{3+} \text{Yb}^{3+}$ co-doped specially produced fibre) where the measured lifetime was much longer than that obtained in the previous work [15] using “normal” $\text{Er}^{3+} \text{Yb}^{3+}$ co-doped fibre.

3) pump wavelength – the wavelength of light used to excite the rare earth doped material will largely determine which energy level of the rare earth ion will absorb the light. As different energy levels have different lifetimes changes in the pump wavelength will affect the lifetime (see section 3.8). In materials such as silica, the rare earth ions can be located in different positions in the host material, and the lifetime of the rare earth ions can depend upon which location they are in. The study of the latter effect is often known as site selective spectroscopy. Also, if the laser diode source used is not temperature stabilised, then fluctuations in its operating temperature will occur causing its output centre wavelength to vary slightly, and this could possibly affect the measured lifetime.

4) pump power – there are several interactions that can occur in rare earth doped materials that can potentially cause the lifetime to be affected by the pump/excitation power. This can include processes such as energy transfer, cross relaxation and up-conversion [11]. The majority of pump power related effects on the lifetime will mainly occur for rare earth doped materials with high doping concentrations. The effect of pump power will be investigated further here using $\text{Tm}^{3+} \text{Ho}^{3+}$ co-doped fibre as shown below.

5) sample size - previous work [9] has shown that sensor length can affect the fluorescent signal, i.e. lifetime and intensity. The effects of sensor length will be investigated further here for various other materials as shown below.

6) measurement technique employed – as with all measurements the method by which the lifetime is obtained will have an influence on the recorded value, e.g. Prony's

Chapter 3 Optical fibre temperature and strain sensors based on fluorescence lifetime monitoring

method depends upon the number of data points in the decay curve, the length of the decay curve sampled and the intensity of any background light. The work in this thesis in section 3.7 contrasts two different techniques.

7) *detection wavelength used* – the detector and (if used) filter will determine the wavelength range of light measured by the detector (see section 3.8). As light of different wavelengths may be from different energy levels, or from rare earth ions in different locations in the host material, the lifetime will depend upon the wavelength range of light measured by the detector.

The work in this section compliments the information already gained on the above influencing factors, both from previous work and from some results in this thesis, by investigating further the effects of fibre lengths and also the effects of pump power on various fibres for their application to fluorescent lifetime based fibre-optical based sensors.

3.8.2 Sample size

3.8.2.1 Erbium doped fibres

A) Experimental arrangement used

This is shown below in Fig.3.61 and was essentially similar to previous work, but without the need for an oven, as all the tests were conducted at room temperature (measured to be constant at 26.2°C). Three different Er^{3+} doped fibre sensors (192 ppm, 1000 ppm and 4500 ppm) could be conveniently pumped using this same experimental set-up, with only the length of sample needing to be varied in each case.

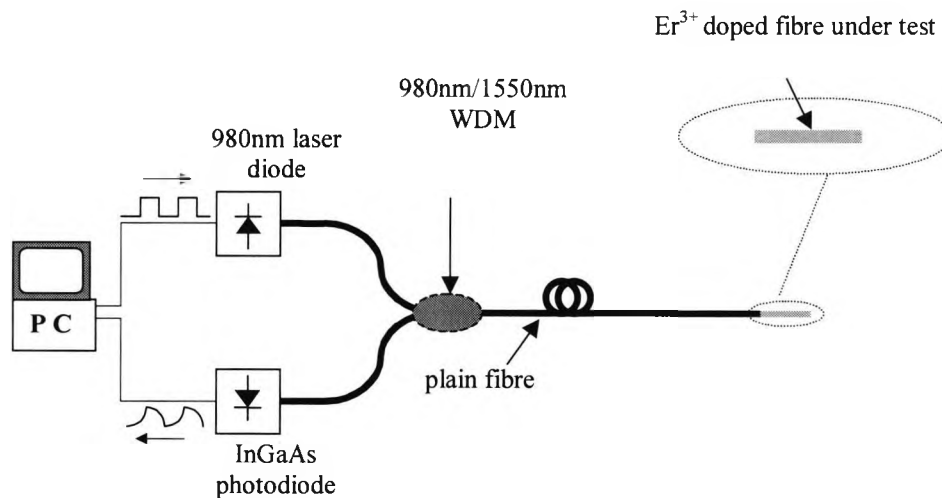


Fig.3.61 Er^{3+} doped fibre experimental set-up for sensor length testing.

A long length of fibre sample was initially chosen to be the sensor length in each case, in order to ensure good absorption and achieve a strong signal yield without saturation, and then the sensor lengths were gradually cut shorter. The 980 nm laser diode employed here (maximum power $P_0 = 2$ mW), previously used for many other applications, is conveniently

Chapter 3 Optical fibre temperature and strain sensors based on fluorescence lifetime monitoring

well suited to the broadened absorption band of this doped material, and it was modulated via an external electronic source. Excitation of the single mode Er^{3+} fibres was achieved by coupling the output of the laser diode to the 980 nm port of a 2x1 980 nm/1550 nm WDM coupler arrangement. An InGaAs photodiode was used to measure the fluorescence emission from Er^{3+} ions and this was connected to the other input port of the WDM coupler. The lifetime from the fibres was measured using an analogue-to-digital card connected to a PC, which sampled the output of the photodiode, this being triggered by the falling edge of the excitation pulse. The value of the fluorescence lifetime was subsequently obtained using Prony's method [8].

B) Results

i) 192 ppm doped Er^{3+} fibre (4 μm /125 μm core/cladding)

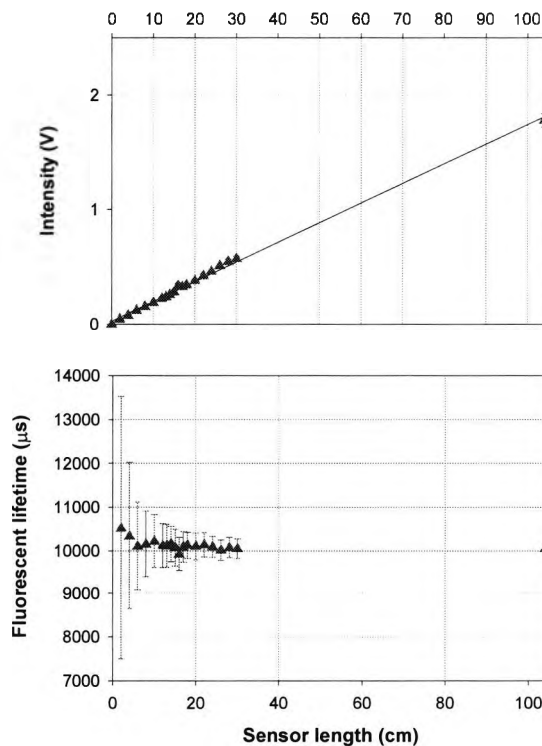


Fig.3.62 192 ppm Er^{3+} doped fibre sensor length effects at 26.2°C.

Chapter 3 Optical fibre temperature and strain sensors based on fluorescence lifetime monitoring

The results obtained for 192 ppm Er^{3+} doped fibre are shown in Fig.3.62, with standard deviation error bars (σ), and are given a linear fit to the intensity data. The fluorescent lifetime signal from this low-doped fibre can be seen to degrade at short lengths (< 8 cm) but stays constant over the range (even up to 104 cm in length - σ therefore very small), whilst the signal intensity reduces proportionally with length.

ii) 1000 ppm doped Er^{3+} fibre (5.2 μm /125 μm core/cladding)

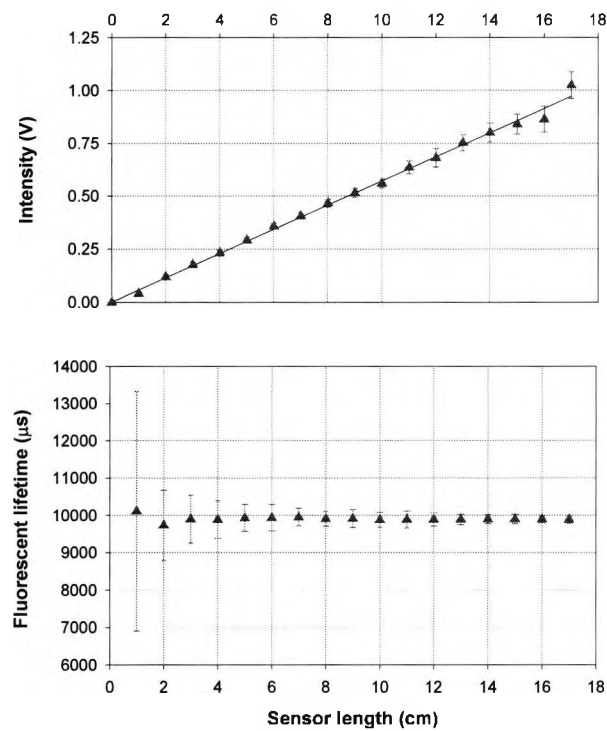


Fig.3.63 1000 ppm Er^{3+} doped fibre sensor length effects at 26.2°C.

The results obtained for 1000 ppm Er^{3+} doped fibre are shown in Fig.3.63 with standard deviation error bars and given a linear fit to the intensity data. The signal can be seen to degrade at very short lengths (< 2 cm) but stays constant over the range, whilst the signal intensity again reduces proportionally with length.

Chapter 3 Optical fibre temperature and strain sensors based on fluorescence lifetime monitoring

iii) 4500 ppm doped Er^{3+} fibre (6.2 μm /125 μm core/cladding)

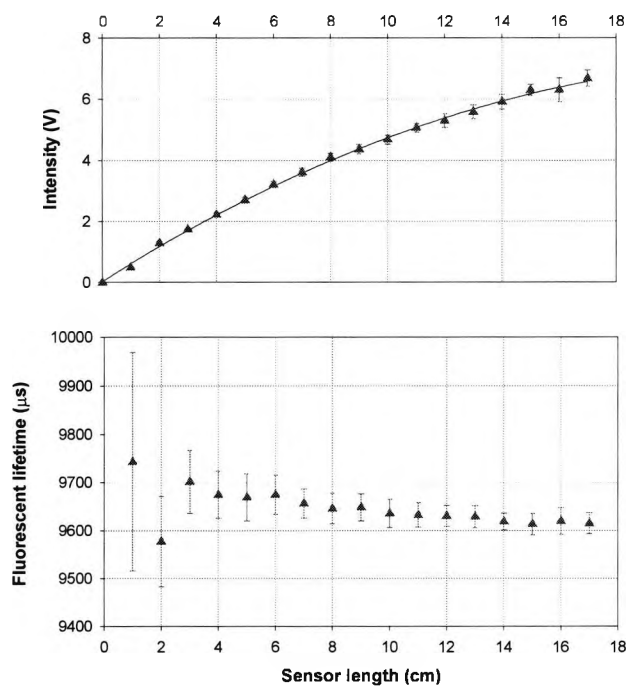


Fig.3.64 4500 ppm Er^{3+} doped fibre sensor length effects at 26.2°C.

The results obtained for 4500 ppm Er^{3+} doped fibre are shown in Fig.3.64 with standard deviation error bars, and given a 2nd order polynomial fit to the intensity data. Here, the lifetime seems to drift upwards slightly with decreasing sensor length, and again the S/N ratio becomes poor as the sensor length is shortened to less than ~2 cm.

3.8.2.2 Er³⁺ Yb³⁺ co-doped fibre

A) Experimental arrangement used

This was essentially similar to Fig.3.49, as it was conveniently the same absorption region as that for Er³⁺. The test was done at the same ambient temperature as before (26.2°C). The fibre used for this test was a new sample of the same Er³⁺ Yb³⁺ co-doped fibre used in previous temperature tests (section 3.5).

B) Results

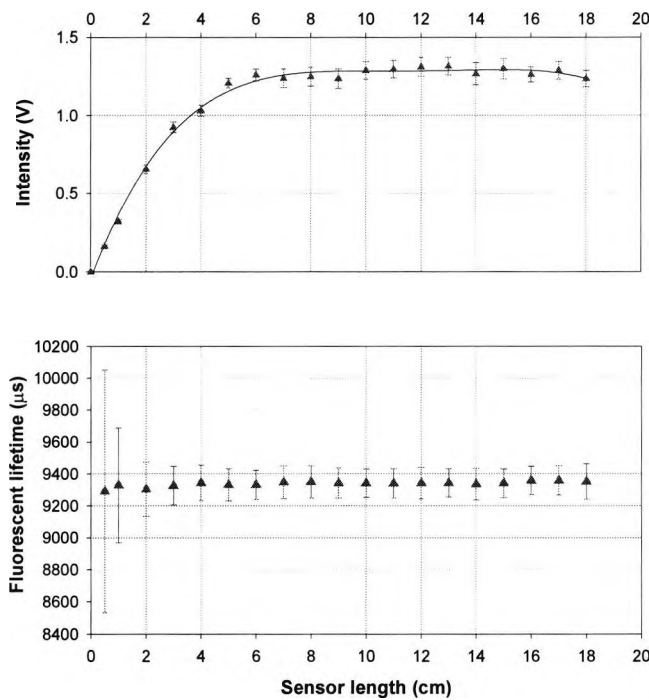


Fig.3.65 Er³⁺ Yb³⁺ co-doped fibre sensor length effects at 26.2°C.

The results obtained for Er³⁺ Yb³⁺ co-doped fibre are shown in Fig.3.65 with standard deviation error bars, and given a 4th order polynomial fit to the intensity data. Here, the lifetime appears to stay constant but, as before, the S/N ratio becomes increasingly poor at sensor lengths < 2 cm. Sensor lengths ≥ 6 cm are favourable.

3.8.2.3 Tm^{3+} Ho^{3+} co-doped fibre

A) Experimental arrangement used

The set-up used for this test was essentially similar to previous work with $\text{Tm}^{3+}/\text{Ho}^{3+}$ co-doped fibre, and is shown below in Fig.3.66.

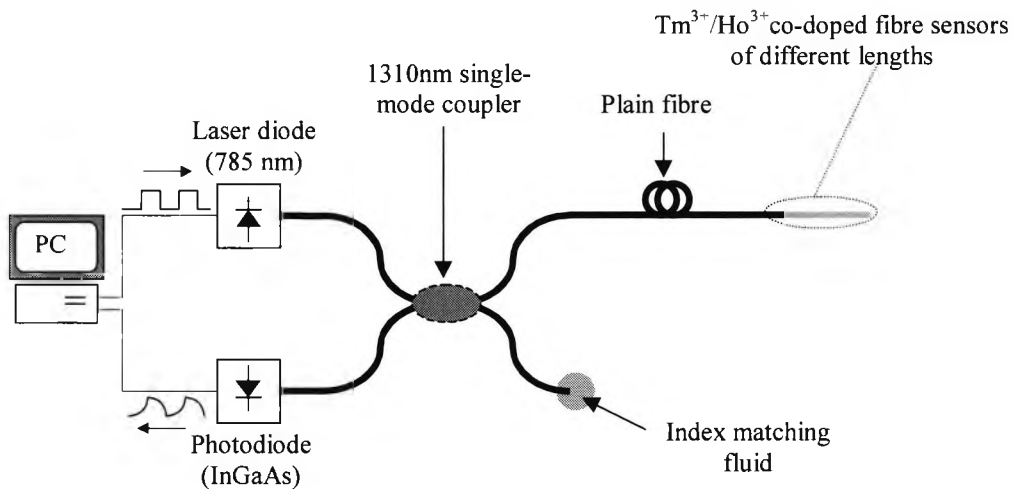


Fig.3.66 $\text{Tm}^{3+}/\text{Ho}^{3+}$ co-doped fibre experimental set-up for sensor length testing.

The fibre used was exactly the same as the $\text{Tm}^{3+}/\text{Ho}^{3+}$ co-doped fibre used in section 3.7, and the constant ambient temperature during these tests was measured to be 26.8°C .

B) Results

Fig.3.67 shows the experimental results obtained on the effect of sensor lengths at 26.8°C for $\text{Tm}^{3+}/\text{Ho}^{3+}$ co-doped fibre, shown with standard deviation error bars. The experiment was repeated using another sample (i.e probe 2), but cut to different sensor lengths, with one measurement being taken using index-matching gel on the end of the fibre for lifetime comparison purposes. The extreme case of zero (i.e 0 cm) sensor length = zero fluorescent intensity (and zero lifetime) is also shown.

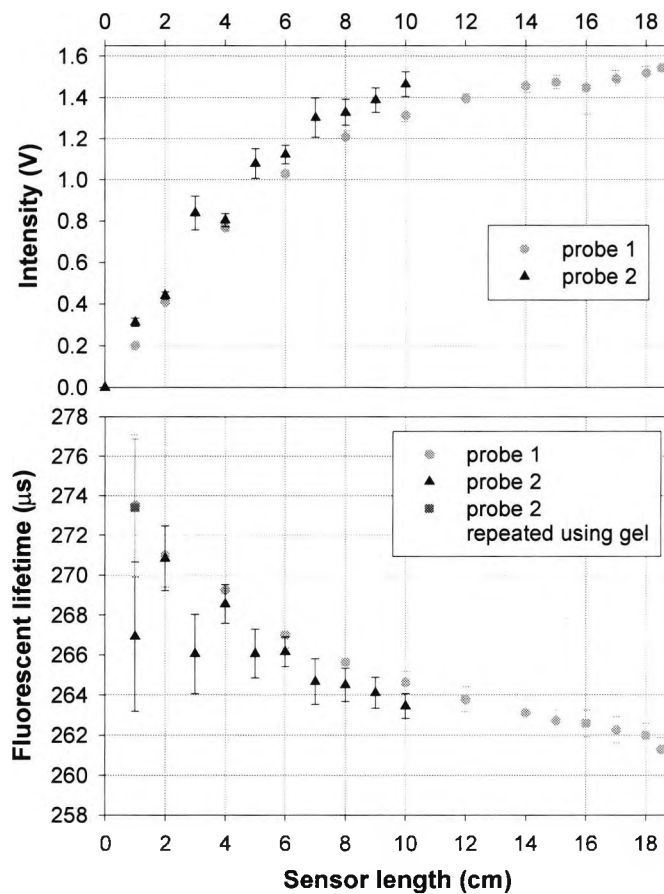


Fig.3.67 Tm^{3+}/Ho^{3+} co-doped fibre experimental results on sensor lengths at 26.8°C.

3.8.2.4 Conclusions

In all cases, and as one would expect, the intensity of the fluorescent signal decreases with sensor length in a manner which is either linear (in the case of the lower doped fibres) or n^{th} order polynomial (higher doped fibres). On the other hand, it is interesting to note that the measured fluorescent lifetime either remains quite constant (lower doped fibres) or drifts upwards slightly with decreasing sensor lengths (higher doped fibres).

3.8.3 Pump power

3.8.3.1 Tm³⁺ Ho³⁺ co-doped fibre

In addition to sensor length testing and using the same experimental set-up, tests on the pump power effect were also performed (at constant temperature) using a constant length (10 cm) of Tm³⁺/Ho³⁺ co-doped fibre after a simple drive current (mA) vs. output power (mW) direct calibration of the 785nm laser diode used (type: Sanyo DL – 7140) was plotted, which enabled the pump power data in Fig 3.68 to be inferred from the gradient of a linear fit to the plot.

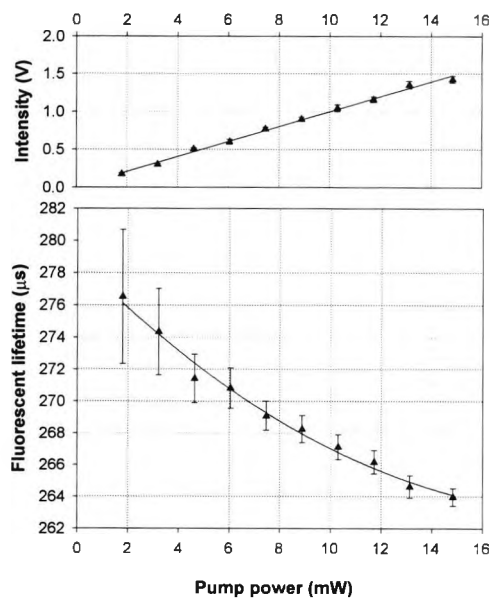


Fig.3.68 Tm³⁺/Ho³⁺ co-doped fibre sensor (~10 cm) experimental results on pump power at 26.2°C.

Fig.3.68 shows the effect of pump power on the fluorescence signal obtained at 26.2°C, shown with a linear fit to the intensity data and a 2nd order polynomial fit to the lifetime data, both with standard deviation error bars.

Chapter 3 Optical fibre temperature and strain sensors based on fluorescence lifetime monitoring

3.8.3.2 Conclusions

The effect of increasing the pump power on $\text{Tm}^{3+}/\text{Ho}^{3+}$ co-doped fibre is seen to increase the intensity in a linear fashion whilst decreasing the lifetime in the manner shown in Fig.3.68. This may have been caused by some ion-ion interactions occurring within the high doped fibre (as mentioned previously the higher doped fibres are more prone to pump power effects) between the dopants. In hindsight, this highly co-doped fibre may not have been the best type of sample to use to investigate this effect.

3.8.4 Summary

Some of the results obtained here on fibre length and pump power effects are similar to those reported by Streck *et al* [28] in recent work on the optical properties of Nd^{3+} -doped silica fibers (of the clad-polymer type) obtained by a sol-gel method. Similarly in that work, they found that the measured fluorescence intensities and lifetimes of Nd^{3+} silica gel fibres were also slightly dependent upon sample fibre lengths, but moreover these measured fluorescence intensities also increased linearly with excitation power (using an argon laser) in a manner similar to that shown in Fig.3.68.

3.9 Chapter summary

The work done in this chapter has measured the fluorescent lifetime strain sensitivities of various rare earth fibre dopants, and has achieved further results on their temperature characteristics and other lifetime influencing parameters, for potential application to the optimisation of temperature and strain sensors based on fluorescent lifetime techniques. The fluorescent lifetime strain sensitivity of a given fibre is seen to be both very small and possibly non-linear in nature, potentially causing large strain errors ($1\sigma \sim 50$ to $100 \mu\epsilon$) if used singularly for strain sensing at a particular temperature. It has, however, been shown to be reasonably constant with dopant concentration and temperature. It can be seen from Table 3.9 that the estimated lifetime strain sensitivities of all materials tested so far are generally very small ($\sim 10^{-2}$ to $10^{-4} \mu\text{s}/\mu\epsilon$) when compared to the lifetime temperature sensitivities ($\sim -1 \mu\text{s}/\text{K}$), but can affect thermometric readings significantly (to $\sim 8^\circ\text{C}$ with $1000 \mu\epsilon$) when used in temperature sensing schemes where strain could be a consideration.

Since the measured strain effect is seen as being small when compared to the larger lifetime temperature sensitivity of a given fibre, there is therefore a need to measure it with more reasonable accuracy using perhaps lower noise detection, longer averaging, higher power laser diodes etc. The errors in the strain are also due (but to a lesser extent) to variations in the strain applied to the fibre due to the pulley system used (i.e. user operative repeatability error), and the extensive cycling tests undertaken have only minimised this. All previous work utilising the lifetime technique used arrangements set up primarily for the purposes of temperature measurement only. Also, the Young's modulus ($Y = \text{stress}/\text{strain}$) of fused

Chapter 3 Optical fibre temperature and strain sensors based on fluorescence lifetime monitoring

quartz (silica) used in equation 3.1 is not completely constant with temperature, as has been assumed in this work, and actually varies slightly over the temperature ranges used [29].

The strain sensitivity could be non-linear in nature, which explains why the estimated errors (i.e. calculated from the data obtained in this work) occurring when two different doped fibres are combined for the purposes of simultaneous temperature-strain sensing based on the lifetime technique alone (i.e. using linear deconvolution methods from equations 2.3 and 2.4) are very large. The effect may, however, in the future be shown to be more linear - using perhaps more sophisticated equipment, in which case the above errors in such simultaneous measurement systems may reduce. Also, the deconvolution matrix method assumes perfect linearity of *both* parameters, i.e. strain sensitivity *and* temperature sensitivity, and hence the well-known non-linearity of the latter will also contribute to the large errors obtained. It should be noted that all temperature sensitivity ($\mu\text{s}/\text{K}$) values in Table 3.9 (with the exception of Tm/Ho co-doped fibre which was estimated at 20°C from a polynomial fit to the data, and Nd at 35°C) have been estimated with a *linear* fit to the data over the *short* temperature ranges.

Because the data in Table 3.9 is not “normalised” in the sense that different fits are used on different sets of data, over different ranges etc.- it is perhaps better to re-analyse it using a more consistent method. For example, instead of having linear fits to just *some* of the data we can fit polynomials (which more accurately describe the well-known lifetime-temperature characteristics from previous work) to *all* of the data from all fibres and then re-

Chapter 3 Optical fibre temperature and strain sensors based on fluorescence lifetime monitoring

estimate the lifetime-temperature sensitivity (and therefore the correction for strain) at a particular temperature, e.g. 35°C. This was done and the results are shown in Table 3.10.

The fluorescent lifetime temperature and strain effects can, however, both be exploited to be combined with other types of sensing elements when assumed to be linear. The work in the next chapter reports on the combination of doped fibres with Bragg grating sensors, where the lifetime temperature sensitivity and small strain sensitivity is complimented by the more linear, and greater in magnitude, Bragg wavelength shifts with temperature and strain, all added to the 2D matrix (equation 2.2) for dual temperature/strain sensing.

	Er³⁺ 200ppm	Er³⁺ 960ppm	Er³⁺ 1050ppm	Er³⁺ 4370ppm	Nd³⁺ 1460ppm	Tm/Ho (Prony's)	Tm/Ho (³H₄)	Tm/Ho (³F₄)
s/p method	A/D	A/D	A/D	A/D	PLD	A/D	A/D	A/D
LD pump (nm)	813	813	980	980	785	785	785	785
Typical lifetime @25°C (μs)	10350	10100	10480	9800	440	265	31.7	274
Strain sensitivity (μs/με)	(1.0 ± 0.2) ×10⁻²	(1.2 ± 0.3) ×10⁻²	(7.15 ± 2.1) ×10⁻³	(1.14 ± 0.1) ×10⁻²	6.64×10⁻⁴	(2.34 ± 0.3) ×10⁻⁴	1.2×10⁻⁴	4.2×10⁻⁴
Temperature sensitivity (μs/K)	-2.45 ± (0.2)	-2.53 ± (0.3)	-1.67 ± (0.04)	-1.48 ± (0.02)	-0.19	-0.08	0.03	-0.10
K/με	0.0040	0.0047	0.0043	0.0077	0.0034	0.0029	0.0040	0.0042
ΔT@1000με	4.0	4.7	4.3	7.7	3.4	2.9	4.0	4.2

Table 3.9 Comparative data from fibres tested so far.

	Er³⁺ 200ppm	Er³⁺ 960ppm	Er³⁺ 1050ppm	Er³⁺ 4370ppm	Nd³⁺ 1460ppm	Tm/Ho (Prony's)	Tm/Ho (³H₄)	Tm/Ho (³F₄)
s/p method	A/D	A/D	A/D	A/D	PLD	A/D	A/D	A/D
LD pump (nm)	813	813	980	980	785	785	785	785
Typical lifetime @25°C (μs)	10350	10100	10480	9800	440	265	31.7	274
Strain sensitivity (μs/με)	(1.0 ± 0.2) ×10⁻²	(1.2 ± 0.3) ×10⁻²	(7.15 ± 2.1) ×10⁻³	(1.14 ± 0.1) ×10⁻²	6.64×10⁻⁴	(2.34 ± 0.3) ×10⁻⁴	1.2×10⁻⁴	4.2×10⁻⁴
Temperature sensitivity @35°C (μs/K)	-3.1574	-1.5182	-1.8278	-1.4596	-0.1948	-0.0821	0.0238	-0.1079
K/με	0.0032	0.0079	0.0039	0.0078	0.0034	0.0029	0.0051	0.0039
ΔT@1000με	3.2	7.9	3.9	7.8	3.4	2.9	5.1	3.9

Table 3.10 Re-analysed comparative data from fibres tested so far.

3.10 References

- [1] K.T.V. Grattan and B.T.Meggitt, *Optical Fiber Sensor Technology*, Vols 1-5, Kluwer Academic Publishers (2000)
- [2] K.T.V.Grattan and Z.Y.Zhang, *Fiber Optic Fluorescence Thermometry*, Chapman & Hall, London (1995)
- [3] Z.Y.Zhang, K.T.V.Grattan, A.W.Palmer, T.Sun and B.T.Meggitt, Fluorescence decay-time characteristics of erbium-doped optical fiber at elevated temperatures, *Rev. Sci. Instrum.*, 68, 2764 (1997)
- [4] T.Sun, Z.Y.Zhang, K.T.V.Grattan and A.W.Palmer, Intrinsic doped fluorescence decay-time based measurements – strain and temperature characteristics for sensor purposes *Rev. Sci. Instrum.*, 69, 4186 (1998)
- [5] T.Sun, Z.Y.Zhang, K.T.V.Grattan and A.W.Palmer, Intrinsic strain and temperature characteristics of Yb-doped silica-based optical fibers, *Rev. Sci. Instrum.*, 70, 1447 (1999)
- [6] B.J.Ainslie, S.P.Craig and S.T.Davey, The absorption and fluorescence spectra of rare earth ions in silica based monomode fiber, *IEEE Journal of Lightwave Technology* 6, No.2, 287 (1988)
- [7] Z.Y.Zhang, K.T.V.Grattan and A.W.Palmer, Phase-locked detection of fluorescence lifetime, *Rev. Sci. Instrum.* 64, 2531 (1993)
- [8] Z.Y.Zhang, K.T.V.Grattan, Y.Hu, A.W.Palmer and B.T.Meggitt, Prony's method for exponential lifetime estimations in fluorescence-based thermometers, *Rev. Sci. Instrum.*, 67, 2590 (1996)

Chapter 3 Optical fibre temperature and strain sensors based on fluorescence lifetime monitoring

- [9] Z.Y.Zhang, K.T.V.Grattan, A.W.Palmer, B.T.Meggitt and T.Sun, Characterization of erbium-doped intrinsic optical fiber sensor probes at high temperatures, *Rev. Sci. Instrum.*, 69, 2924 (1998)
- [10] D.I.Forsyth, S.A.Wade, D.Perciante and K.T.V.Grattan, Temperature and Strain Characteristics of the 3F_4 and 3H_4 Energy levels of Tm:Ho Co-Doped Fibre, in *Proceedings of Sensors and their Applications XI*, K. T. V. Grattan and S. H. Khan, eds. (IOP Publishing Ltd, London), pp. 365-370 (2001)
- [11] M.J.F.Digonnet, *Rare Earth Doped Fiber Lasers and Amplifiers*, 2nd edition, Marcel Dekker, Inc (2001)
- [12] K.A.Winick and G.L.Vossler, Erbium:ytterbium planar waveguide laser in ion-exchanged glass, *Proc. of the SPIE, The International Society for Optical Engineering*, Vol. 2996, 121 (1997)
- [13] M.Karasek, Optimum design of erbium-ytterbium codoped fibres for large-signal, high pump power applications, *Czech. J. Physics*, 49, 5, 895 (1999)
- [14] D.Pacheco and B.Di-Bartolo, Energy transfer and fluorescence characteristics of erbium-doped ytterbium aluminium garnet, *Journal of Luminescence*, Vol. 14, no.1, 19 (1976)
- [15] T.Sun, Z.Y.Zhang, K.T.V.Grattan, Erbium/ytterbium fluorescence based fiber optic temperature sensor system, *Rev. Sci. Instrum.*, 71, 4017 (2000)
- [16] S.J.Zhang, D.I.Forsyth, T.Sun, Z.Y.Zhang and K.T.V.Grattan, Tm/Ho co-doped optical fibre sensor - strain and temperature characteristics of a sensor probe, in *Proceedings of 14th International Conference on Optical Fibre Sensors, Venice, Italy*, SPIE Vol. 4185, 154 (2000)

Chapter 3 Optical fibre temperature and strain sensors based on fluorescence lifetime monitoring

- [17] X.Zou, H.Toratini, Spectroscopic properties and energy transfers in Tm^{3+} singly- and $\text{Tm}^{3+}/\text{Ho}^{3+}$ doubly-doped glasses, *J. Non-Crystal. Solids*, 195, 113 (1996)
- [18] Z.Y.Zhang, K.T.V.Grattan and B.T.Meggitt, Thulium-doped fiber optic decay-time temperature sensors - characterization of high temperature performance, *Rev. Sci. Instrum.*, 71, 1614 (2000)
- [19] J.Morel, A.Woodtli and R.Dändliker, Characterization of the Fluorescent Lifetime of Doped Fibers by Measuring the Frequency Transfer Function, *J. Lightwave Tech.*, 14, 739 (1996)
- [20] A.A.Istratov and O.F.Vyvenko, Exponential analysis in physical phenomena, *Rev. Sci. Instrum.*, 70, 1233 (1999)
- [21] Z.Y.Zhang, K.T.V.Grattan, A.W.Palmer and B.T.Meggitt, Thulium-doped intrinsic fiber optic sensor for high temperature measurements ($>1100^\circ\text{C}$), *Rev. Sci. Instrum.*, 69, 3210 (1998)
- [22] T.Sun, Z.Y.Zhang, K.T.V.Grattan, A.W.Palmer and S.F.Collins, Temperature dependence of the fluorescence lifetime in $\text{Pr}^{3+}:\text{ZBLAN}$ glass for fiber optic thermometry, *Rev. Sci. Instrum.*, 68, 3447 (1997)
- [23] Report #5, LUMITHERM INTERSECT Faraday Partnership Project, *City University, London, UK* (2001)
- [24] K.T.V.Grattan and A.W.Palmer, A fiber optic temperature sensor using fluorescence decay, *SPIE Proc.* 492, 535 (1984)
- [25] K.T.V.Grattan, A.W.Palmer and Z.Y.Zhang, Development of a high-temperature fiber-optic temperature probe using fluorescent decay, *Rev. Sci. Instrum.*, 62, 1210 (1991)

Chapter 3 Optical fibre temperature and strain sensors based on fluorescence lifetime monitoring

- [26] Z.Y.Zhang, T.Sun, K.T.V.Grattan and A.W.Palmer, Optical fiber temperature sensor scheme using Tm: doped yttrium oxide powder-based probe, *Proc. 13th Int. Conf. on Optical Fibre Sensors & Workshop on Device and System Technology toward Future Optical Fiber Communication and Sensing* (SPIE Vol. 3746) 422 (1999)
- [27] Report #2, LUMITHERM INTERSECT Faraday Partnership Project, *City University, London, UK* (1999)
- [28] W.Strek, E.Pawlik, P.Deren, A.Bednarkiewicz, J.Wojcik, V.E.Gaishun and G.I.Malashkevich, Optical properties of Nd³⁺ -doped silica fibers obtained by sol-gel method, *Journal of Alloys and Compounds*, 300 – 301, 459 (2000)
- [29] GE Quartz Worldwide, www.gequartz.com/en/mech.htm (©1997 - 2001)

Chapter 4

Fluorescence based temperature and strain measurement by the incorporation of Fibre Bragg gratings (FBGs)

4.1 Abstract

The work in this chapter reports and compares results obtained from various experimental schemes containing a range of different rare-earth doped sensing materials using fluorescent techniques combined with fibre Bragg gratings (FBGs) for the first time. These novel sensors can be used for the dual measurement of temperature and strain, and their performance is contrasted and compared with the reports from other fibre-based T, ϵ sensors examined previously. The chapter also reports on high temperature endurance effects on FBG performance.

4.2 Introduction

The fluorescence lifetime strain sensitivity has been shown, from extensive work discussed in the previous chapter, to be generally $\sim 10^{-2}$ to 10^{-4} $\mu\text{s}/\mu\epsilon$ for silica based rare earth doped fibres, but its origin remains the subject of some discussion. It may possibly be due to shifts in the energy levels as a function of strain, as has been previously reported in crystals for high pressure tests [1]. A more detailed analysis is required but simple calculations, using a two level model, have indicated [2] that the energy gap need only change very slightly to result in the lifetime change which was observed for applied strains in the region of those used in that work. On the other hand, the physical origin of the strain sensitivity of fluorescence from rare earth doped fibre has also been suggested in other recent work [3] to be due to a temporary volumetric distortion of the energy transfer rates between the dopant ions, caused by a slight decrease in the dopant concentration within a fibre when subjected to strain. Modelling of the latter [4] has been shown to account well for the fluorescent lifetime temperature and strain dependence using Nd^{3+} -doped fibres and this likely can be extrapolated for other doped rare earth dopants.

Therefore, rather than use the change in the fluorescence parameters to determine strain (complicated by being convoluted with the temperature change with high errors involved) it was decided to investigate potentially simpler and more compact optical fibre sensor configurations utilising the familiar properties of Bragg gratings. Experimental systems comprising relatively simple and inexpensive equipment have been created to exploit this

Chapter 4 Fluorescence based temperature and strain measurement incorporating FBG experimental results

unique relationship, to enable dual measurements of strain and temperature, and are described herein.

4.3 FBG background and sensing mechanism

4.3.1 Background

Before combining the FBG with the fluorescence lifetime technique, we can remind ourselves of FBG capabilities how it works. Fibre Bragg grating (FBG) [5, 6] sensors have long been recognised as important fibre optic elements in both sensor and telecommunication applications. The wavelength-encoded nature of the signal, which responds to strain and temperature changes, among others, allows absolute measurement of the measurand, independent of intensity changes which could arise from source fluctuation or fibre bending losses which may be attributed to harsh environments. Furthermore, the dielectric nature of optical fibres means that FBG sensors can be used in applications where EM interference prohibits reliable use of resistive strain gauges. With such clear advantages offered over conventional strain sensors, a FBG sensor system is expected to be cost-effective when large numbers of sensors are multiplexed. Several researchers have demonstrated the use of FBG sensors in applications ranging from civil engineering applications, such as mines [7], to aerospace composites and medical monitoring [8]. FBG sensors may be either attached to the structure or embedded (smart structures) to obtain a quasi-distributed strain at the sensing points along the structure. Such measurements are taken either continuously or at regular intervals, depending on the requirements of the application.

Chapter 4 Fluorescence based temperature and strain measurement incorporating FBG experimental results

A typical recent example FBG capabilities has been shown in an application on the Mjosund road bridge in central Norway by Gebremichael *et al* [9]. Here, the test bridge was instrumented with FBG sensors for structural health analysis and condition evaluation as part of a condition maintenance programme. A key issue in this application of a FBG sensor system was measuring static as well as dynamic data periodically with high-resolution, repeatability and large absolute measurement range. The FBG system utilised a WDM (wavelength division multiplexing) interrogation technique [10, 11] to de-multiplex the return signals from the array of gratings, which in the first phase had 32 attached grating sensors with a capability of multiplexing up to ~100 field sensors. The work advanced the art of instrumentation and monitoring of civil engineering structures with fibre Bragg grating sensor system. A simplified diagram of the system is shown in Fig.4.1.

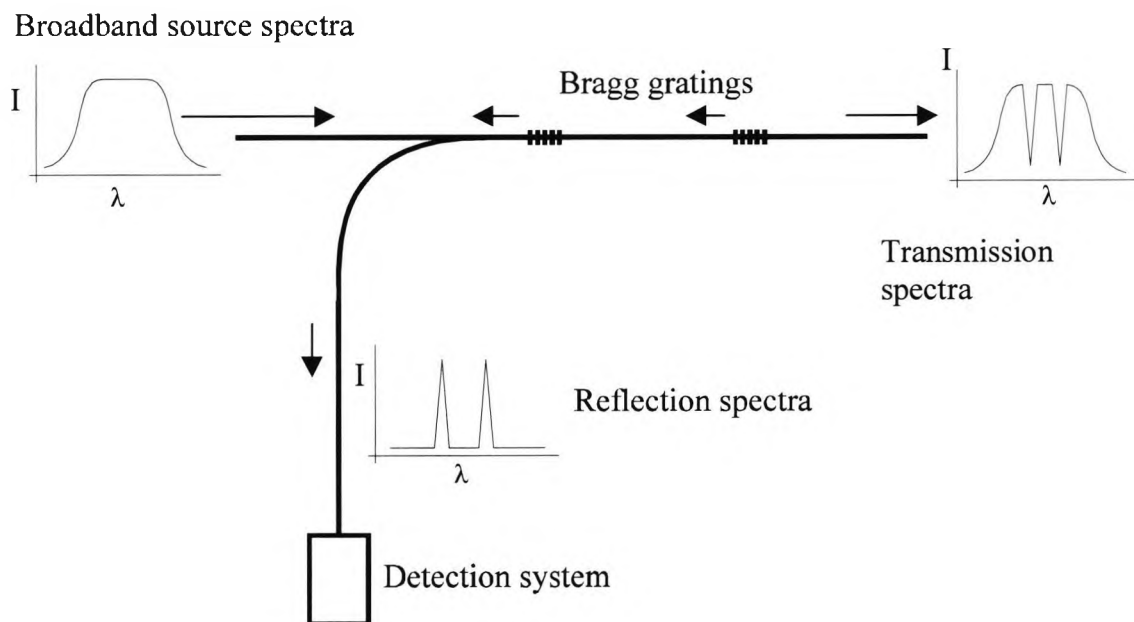


Fig.4.1 An example of a WDM system - the number of gratings depends on the FWHM of the source used.

4.3.2 FBG sensing mechanism

A narrow-band portion of a broadband light propagating in a fibre with a Bragg grating will be reflected with a centre wavelength, λ_B , given by $2n_e\Lambda$ [9]. The strain and temperature sensitivity, and thus the sensor applications, arise from the induced change in the pitch length (Λ) of the grating and the change in the effective refractive index, n_e of the core. It can be seen (equation 4.1 below) that any change in the periodic modulation or the refractive index causes a change in the Bragg wavelength. This allows any strain ($\Delta\varepsilon$) or temperature (ΔT) induced changes to be determined from the corresponding wavelength shift, $\Delta\lambda$.

$$\Delta\lambda = \lambda_B(\alpha + \xi)\Delta T + \lambda_B(1 - \rho_e)\Delta\varepsilon \quad (4.1)$$

where λ_B is the nominal wavelength of the grating, ξ is thermo-optic coefficient of the fibre, α is thermal expansion of the fibre and ρ_e is effective photo-elastic constant.

4.4 Doped fibre based sensors combined with FBGs

4.4.1 4370ppm Erbium doped fibre with FBG as separate component

In this work a unique sensor scheme has been developed, involving the close coupling of a fibre Bragg grating (FBG) and a short length of Er^{3+} -doped fibre, to create a novel dual strain and temperature measurement system. Such a sensing scheme takes advantage of the wide availability and well known sensing properties of fibre Bragg gratings as well as the

Chapter 4 Fluorescence based temperature and strain measurement incorporating FBG experimental results

fluorescence properties of the doped fibre (including the relatively large lifetime strain sensitivity of erbium doped fibre $\rightarrow 10^{-2} \mu\text{s}/\mu\text{e}$), both over short sensor lengths, at relatively low cost and creating a self-referenced sensing technique.

4.4.1.1 Experimental arrangement

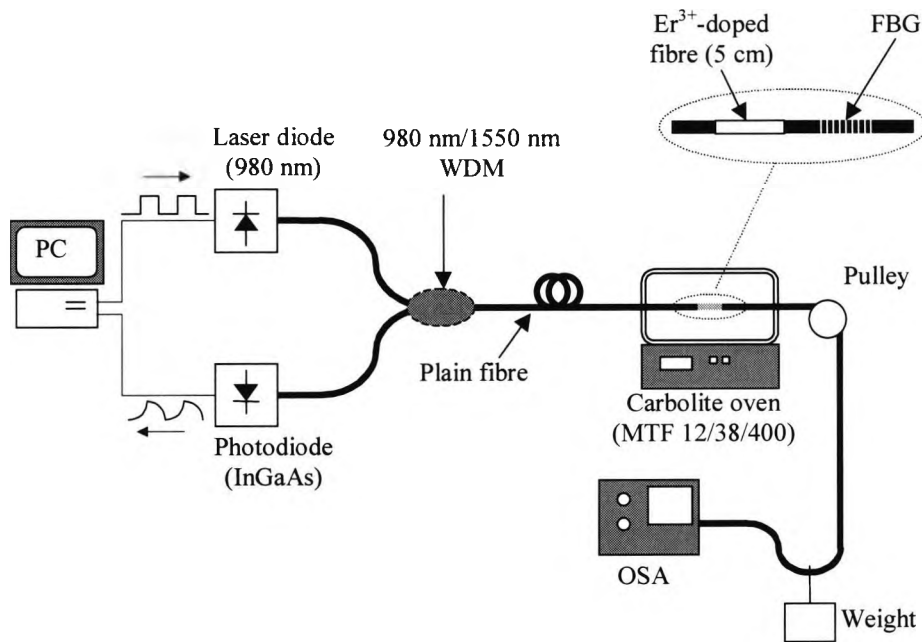


Fig.4.2 Simplified schematic of the experimental arrangement used for the temperature and strain test of the combined Er³⁺-doped fibre/FBG sensor.

The sensor itself was created using a small length (5 cm) of single mode 4370 ppm-wt Er³⁺-doped fibre, fusion spliced in very close proximity to a FBG (center wavelength ~ 1548 nm), to enable the dual element sensor to be compact (overall length < 8 cm), and this was centered within the controlled zone of a temperature stabilized oven (Carbolite, type: MTF 12/38/400) for calibration tests. The experimental arrangement, as shown in Fig.4.2, additionally allowed a range of strains to be applied to the sensor at the various achievable

Chapter 4 Fluorescence based temperature and strain measurement incorporating FBG experimental results

temperatures, from ambient to a maximum of 120°C during these calibration tests (i.e., without damaging the FBG). Extensive strain cycling was undertaken to minimise experimental errors. The 980 nm laser diode was chosen for its output to couple well to the absorption of the $^4I_{11/2}$ energy level of Er^{3+} and its output was modulated via a computer-generated trigger pulse. Excitation of the Er^{3+} -doped fibre (4370 ppm-wt doping concentration) was achieved by coupling the output of the laser diode to the 980 nm port of a 2×1 980 nm/1550 nm WDM coupler arrangement. The length of the Er^{3+} -doped fibre sensor used was chosen to achieve adequate absorption and fluorescence signal yield. Strain was applied to the dual fibre sensor using a pulley system where weights were added, thus progressively increasing or decreasing in a controlled and reproducible way, the overall strain exerted on the test fibre. Care was taken to prevent the fibre from touching the tube oven glass and to lubricate the pulley in order to minimize friction, for better repeatability of the test measurements. The optical detector used, an InGaAs photodiode, was chosen to cover the well known 1.5 μm spectral fluorescence emission from Er^{3+} and was connected to the other input port of the WDM coupler. In this work, for simplicity, the measurement of the FBG wavelength shift was achieved using a commercial optical spectrum analyzer (OSA). FBG wavelength shift measurement schemes using tunable Fabry-Perot filters have been reported on previously in some schemes [11], for example, and this type of detection could be incorporated in a more mature sensing scheme.

Measurements of the fluorescence lifetime and the FBG wavelength were obtained for applied strain values in the region of 22 to 1860 $\mu\epsilon$, with care being taken to stay below the

Chapter 4 Fluorescence based temperature and strain measurement incorporating FBG experimental results

level of fibre fracture, at the range of stable temperatures of 25°C, 40°C, 60°C, 80°C, 100°C and 120°C chosen for this calibration test. This applied strain, ε , was calculated in the same way as before for the work in Chapter 3 using:

$$\varepsilon = \frac{mg/A}{Y} \quad (4.2)$$

where A is the cross-sectional area of the fibre, calculated for the 125 μm diameter sample used, and Y is Young's Modulus ($7.31 \times 10^{10} \text{ N/m}^2$ for fused quartz at room temperature).

In a dual sensor scheme of this nature, it is necessary to measure both the fluorescence lifetime of the Er^{3+} -doped fibre element of the combined sensor, and also the Bragg wavelength shift. For ease of use here, an optical switch was used to alternate between the two. For the lifetime measurement, an analog-to-digital card connected to a PC was used to sample the output of the photodiode, this being triggered by the falling edge of the excitation pulse. The value of the fluorescence lifetime was subsequently obtained using Prony's method, from work done previously [12]. In the sensor tests, measurements of the center wavelength of the FBG were made by recording the fluorescence spectra of the Er^{3+} -doped fibre, which contained an associated and easily observable feature of the spectrum corresponding to the FBG. This represents a particularly attractive feature of the sensor in that the fluorescence generated acts as the interrogation light for the FBG, removing the need for a second optical source. By choosing, as was done in this case, the wavelength of the FBG to lie within the fluorescence band of the doped fibre, the system incorporates its own 'fluorescence fibre source', and this measurement does not interfere with the measurement

Chapter 4 Fluorescence based temperature and strain measurement incorporating FBG experimental results

of the change in the fluorescence lifetime, important for the temperature correction. An example of the fluorescence spectrum of the Er^{3+} -doped fibre and the spectral feature due to the FBG is shown at three temperatures in Fig.4.3.

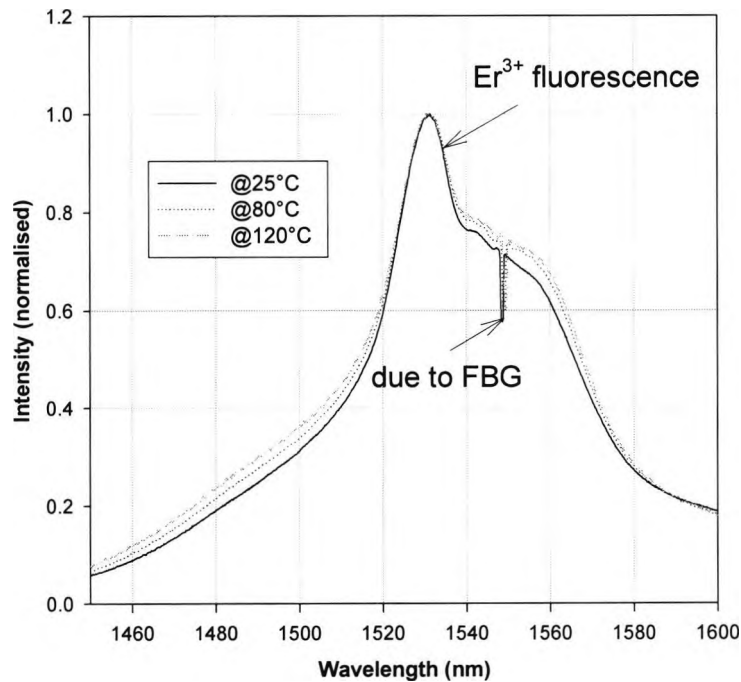


Fig.4.3 Typical fluorescence spectrum and spectral feature due to the reflection by the FBG shown at three of the temperatures (note: OSA resolution of 1 nm for graph shown).

In the calibration tests, fluorescence spectra were recorded using an Agilent OSA, with a resolution bandwidth of 0.1 nm.

4.4.1.2 Experimental results

A series of calibration tests was performed, to assess the performance of the dual temperature-strain sensor system. Fig.4.4 shows the results of a temperature calibration of the Er^{3+} -fluorescence lifetime element, over the range 25–120°C (i.e. with effectively zero applied strain).

Chapter 4 Fluorescence based temperature and strain measurement incorporating FBG experimental results

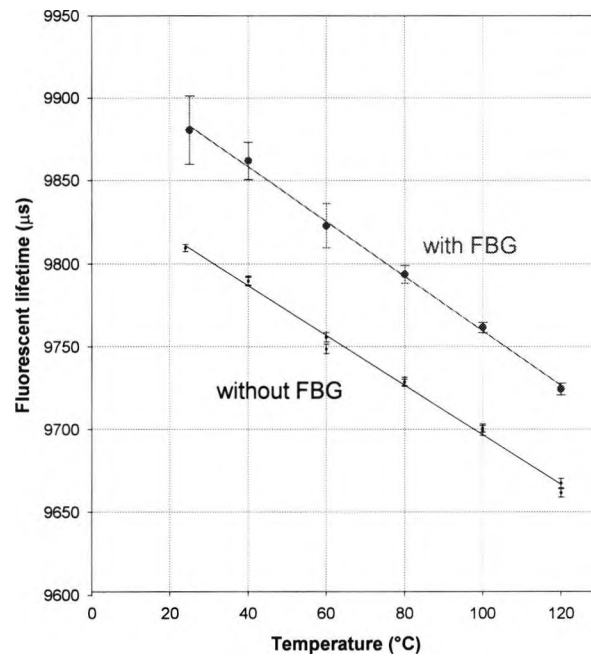


Fig.4.4 Temperature calibration of the Er^{3+} -doped fibre element of the combined Er^{3+} -doped fibre/FBG sensor (i.e. with zero strain) compared with previous results from the same fibre without grating, both shown over the same temperature range.

The familiar calibration feature is seen, as reported previously [13], and also investigated earlier in Chapter 3 for exactly the same fibre, sensor length, range and experimental conditions - but then without the addition of a FBG (results also added in Fig.4.4). It is interesting here to note that the comparison between the lifetimes shown in Fig.4.4 reveals that the addition of a separate FBG component to exactly the same fibre appears to have a very small effect on the measured Er^{3+} -fluorescence lifetime (i.e. it increases a little) but this would not, however, in itself affect the performance of a doped fibre element when used in a combined sensor scheme such as this where the linear sensitivity is more paramount.

Chapter 4 Fluorescence based temperature and strain measurement incorporating FBG experimental results

Strain tests were then carried out and Fig.4.5 shows the effect of strain on the fluorescence lifetime of the Er^{3+} doped fibre element of the dual sensor, at stable temperatures of 25°C, 60°C and 120°C.

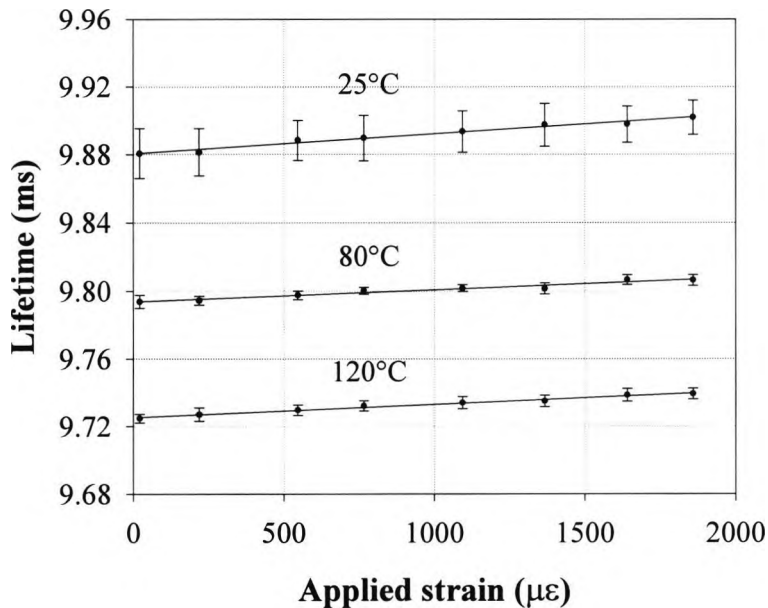


Fig.4.5 Strain effect on the lifetime of Er^{3+} -doped fibre element of the combined Er^{3+} -doped fibre/FBG sensor at 25°C, 60°C and 120°C.

Similar data, obtained at temperatures of 40°C, 80°C and 100°C and showing similar trends, were obtained but have not been displayed for reasons of clarity. The strain sensitivities of the Er^{3+} -doped fibre, obtained from a straight line fit to graphs of fluorescence lifetime versus strain at each of the temperatures tested, are plotted as a function of temperature in Fig.4.6. The high level of scatter of these points and the relatively large error bars shown indicate the relatively low strain sensitivity. The average value of the strain sensitivity over the range 25 - 120°C has been used in this work.

Chapter 4 Fluorescence based temperature and strain measurement incorporating FBG experimental results

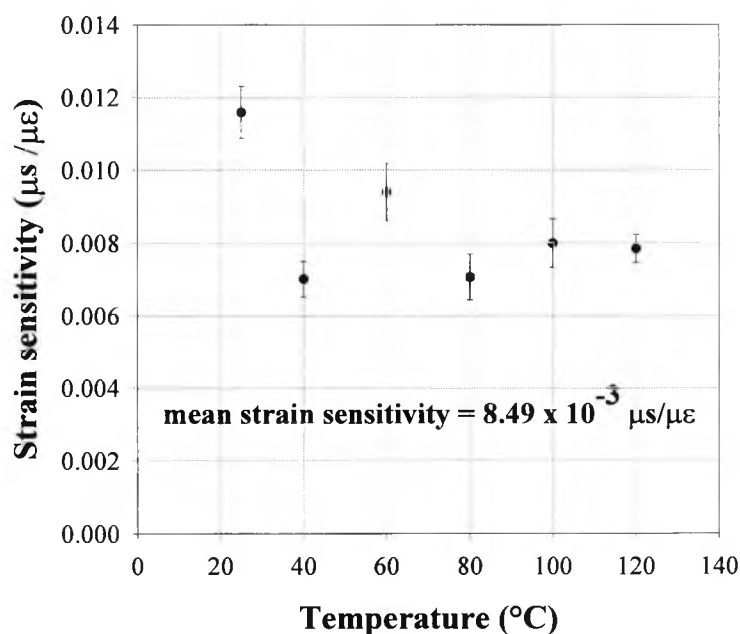


Fig.4.6 Strain sensitivity of the Er^{3+} -doped fibre lifetime versus temperature.

Measurements of the centre wavelength of the FBG were obtained for applied strains between 22 and 1860 $\mu\epsilon$ at temperatures between 20°C and 120°C. Examples of the shift in the FBG wavelength with temperature and strain are given in Fig.4.7 and Fig.4.8 showing both the significant change in the FBG wavelength due to the temperature *and* the strain changes. This shows clearly the relative and indeed comparable magnitudes of both these effects (in contrast to the dominance of the temperature effect on the observed fluorescence lifetime) and, of course, the need for effective temperature compensation for any meaningful strain measurements to be obtained. Both Fig.4.7 and Fig.4.8 also show the high degree of linearity of the shift in FBG wavelength with changes in strain and temperature.

Chapter 4 Fluorescence based temperature and strain measurement incorporating FBG experimental results

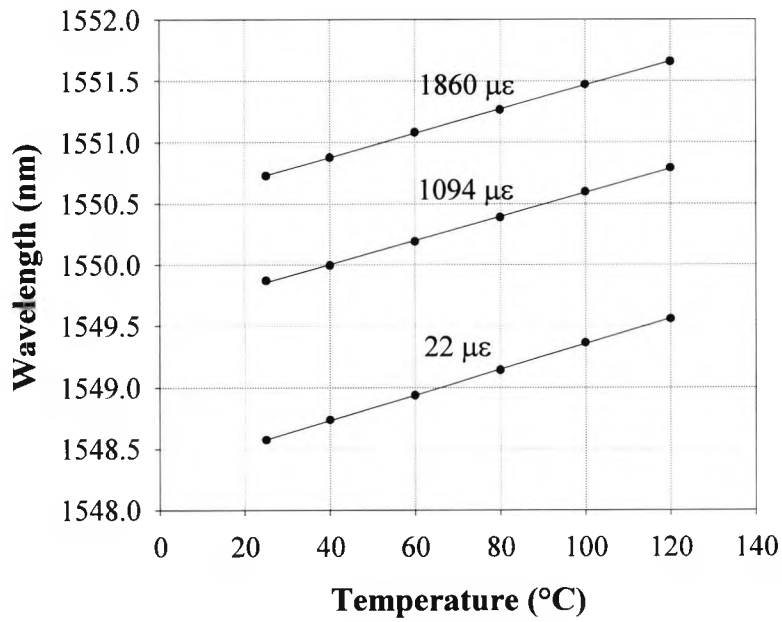


Fig.4.7 Wavelength change as a function of temperature for the FBG at three different applied strains.

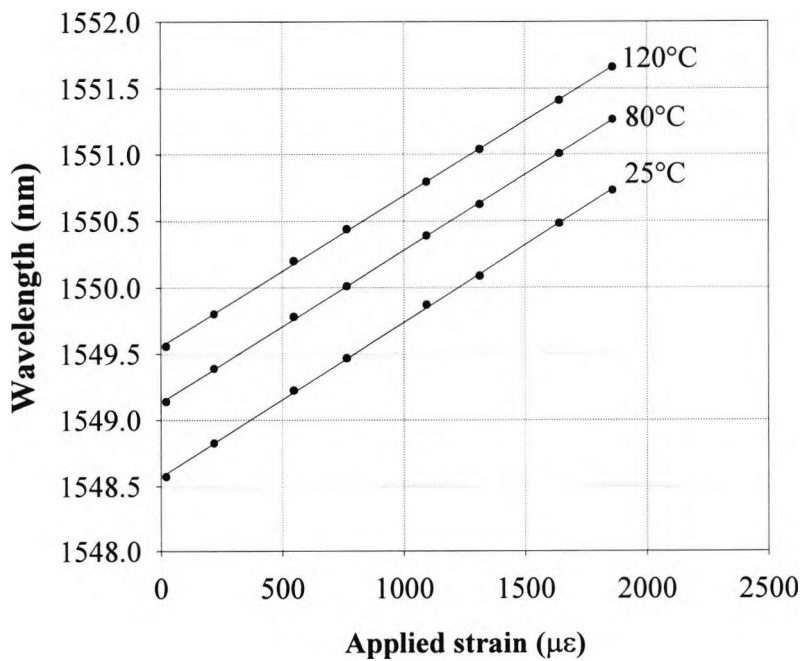


Fig.4.8 Wavelength change as a function of applied strain for the FBG at three different temperatures.

Chapter 4 Fluorescence based temperature and strain measurement incorporating FBG experimental results

Values of the calibration constants (i.e.. the changes in fluorescence lifetime and FBG wavelength with temperature and strain) were obtained by fitting straight lines to the data, and an analysis shows the following:

$$K_{1T} = -1.65 \pm 0.04 \mu\text{s}/^\circ\text{C}$$

$$K_{1\varepsilon} = (8.49 \pm 1.75) \times 10^{-3} \mu\text{s}/\mu\varepsilon$$

$$K_{2T} = (1.03 \pm 0.03) \times 10^{-2} \text{ nm}/^\circ\text{C}$$

$$K_{2\varepsilon} = (1.15 \pm 0.01) \times 10^{-3} \text{ nm}/\mu\varepsilon$$

Using equation (2.2) the following relationships are obtained:

$$T = -0.579\Delta\tau + 4.272\Delta\lambda \quad (4.3)$$

$$\varepsilon = 4.161\Delta\tau + 830.82\Delta\lambda \quad (4.4)$$

where $\Delta\tau$ and $\Delta\lambda$ are the shifts in the lifetime and the FBG wavelength from the values extrapolated from the data obtained for 0°C and zero strain. Using the data obtained in the calibrations, values of temperature T and strain ε were calculated using equations (4.3) and (4.4) and then compared, using a knowledge of the conditions applied during the calibration tests. Fig.4.9 and Fig.4.10 show the results of these calculations for temperature and strain, which give standard deviations of 1.2°C and $20.4 \mu\varepsilon$ for temperature and strain measurement respectively, over the ranges considered.

Chapter 4 Fluorescence based temperature and strain measurement
incorporating FBG experimental results

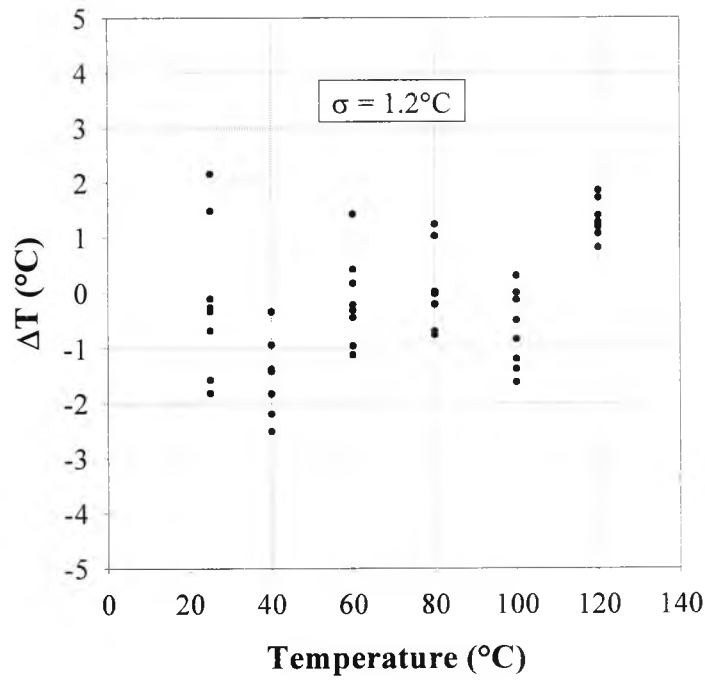


Fig.4.9 Temperature error in the combined Er^{3+} -doped fibre/FBG strain sensor.

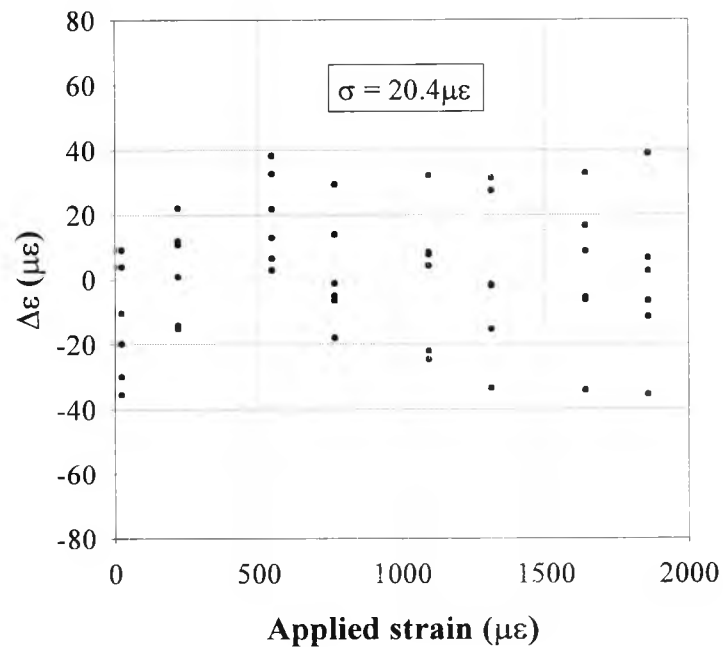


Fig.4.10 Strain error in the combined Er^{3+} -doped fibre/FBG strain sensor.

Chapter 4 Fluorescence based temperature and strain measurement incorporating FBG experimental results

4.4.1.3 Discussion

In this work, a unique dual strain and temperature sensor, using a single laser source and exploiting fully the fluorescence emission from a doped fibre, has been developed and results reported. This relatively low cost, simple sensor has demonstrated that the dual measurement of temperature and strain can be achieved with adequate accuracy for many industrial situations by measuring the fluorescent lifetime decay and the FBG wavelength shift respectively. Calibration results obtained from this simple, low cost, intrinsic sensor scheme show standard deviation errors of 20.4 $\mu\epsilon$ and 1.2°C over strain and temperature ranges of 22-1860 $\mu\epsilon$ and 25-120°C respectively. The sensor is compact, requiring a total system length of < 8 cm (the combined lengths of the doped fibre used and the FBG), contrasting very favourably with sensors using optical amplification which have been reported with considerably greater lengths. The technique reported could be used on large scale, multiple strain applications, e.g. damage detection in civil engineering, maritime or aerospace applications, eliminating the need for a separate temperature compensation element such as the use of a further FBG in compensation. The scheme is not only applicable to Er³⁺-doped fibre – any of the fluorescence species in doped fibre studied by the authors (and others) may be used, although the ready commercial availability FBGs in the 1550 nm region is a considerable incentive for the use of this particular combination of sensor elements. Further work on sensor schemes of this type is continuing.

Chapter 4 Fluorescence based temperature and strain measurement incorporating FBG experimental results

4.4.2 Doped fibres with FBGs written in

Results obtained previously, using the separate FBG spliced to a short length of Er^{3+} -doped fibre for the first time for dual measurement, are now compared with results from two new sensor configurations (under similar experimental conditions) in which the FBGs are directly written into the doped fibres; thus eliminating the need for two separate components in one sensor system and enabling a co-location of the sensor elements. These comprise two unique sensor schemes where the same combination of a FBG and the fluorescence decay within short lengths (a few cm) of doped fibre are used. They again take advantage of the intrinsic properties of FBGs as well as exploiting the fluorescence properties (i.e. lifetime change with temperature *and* strain) of short lengths of doped fibre, which have previously proved to yield satisfactory results.

4.4.2.1 Experimental Arrangement

The previously reported sensor in section 4.4.1 is labelled sensor 1 here for consistency. Two more sensing elements were developed in this particular work. The first sensor was made with the FBG at a centre wavelength of 1551.5 nm, this being chosen because of the ready availability of a phase mask and the Er^{3+} -doped fibre which fluoresces in this spectral region. This is, of course, the wavelength favoured for optical communications purposes. The FBG was written into a 16 cm length of (5/125 μm core/cladding diameter) 1050 ppm Er^{3+} -doped fibre (termed sensor 2) using a KrF excimer laser centred at 248 nm, before which the Er^{3+} -doped fibre was hydrogen-loaded for 1 week to enhance its photosensitivity. The grating was therefore written into exactly the same 1050 ppm Er^{3+} -doped fibre used for

Chapter 4 Fluorescence based temperature and strain measurement incorporating FBG experimental results

high temperature tests earlier in this thesis so that comparisons could be made (i.e. with and without FBG). The second sensor was designed with the FBG (1549.7 nm centre wavelength) written into a 12cm length of single mode $\text{Er}^{3+}:\text{Yb}^{3+}$ co-doped fibre (termed sensor 3). For sensor 3, the co-doped fibre was of unique construction in that it had been designed with a photosensitive ring (during the manufacturing process), and the grating was written using a frequency-doubled argon ion laser (244 nm), thus without requiring prior hydrogen loading of the fibre. This fibre had a cladding diameter of 125 μm , a numerical aperture of 0.2 and core dopants of Er^{3+} , Yb^{3+} and aluminum. Thus, this fibre sensor was chosen to be exactly the same length of the same $\text{Er}^{3+}:\text{Yb}^{3+}$ co-doped fibre used for high temperature tests earlier in this thesis (thus comparisons can again be made with and without FBG). Results from both these schemes are compared with those obtained previously from sensor 1.

During the sensor calibration tests, the sensing elements were centred within the temperature controlled zone of a stabilized oven (Carbolite, type MTF 12/38/400), as shown schematically in Fig.4.11, which essentially and conveniently amounted to the arrangement used in the previous section. In addition to the temperature control, the experimental arrangement again allowed a range of strains to be applied to the sensors at various temperatures (those from ambient to a maximum of 150°C were used during these calibration tests to avoid thermal damage to the FBG). The same 980 nm laser diode, with an output power of approximately 2 mW, was employed to “pump” each doped fibre under test and its output was modulated via a computer-generated trigger pulse. Excitation of the

Chapter 4 Fluorescence based temperature and strain measurement incorporating FBG experimental results

doped fibre sensors was achieved by coupling the output of the laser diode to the 980 nm input port of a 2×1 980 nm/1550 nm wavelength division multiplexing (WDM) coupler

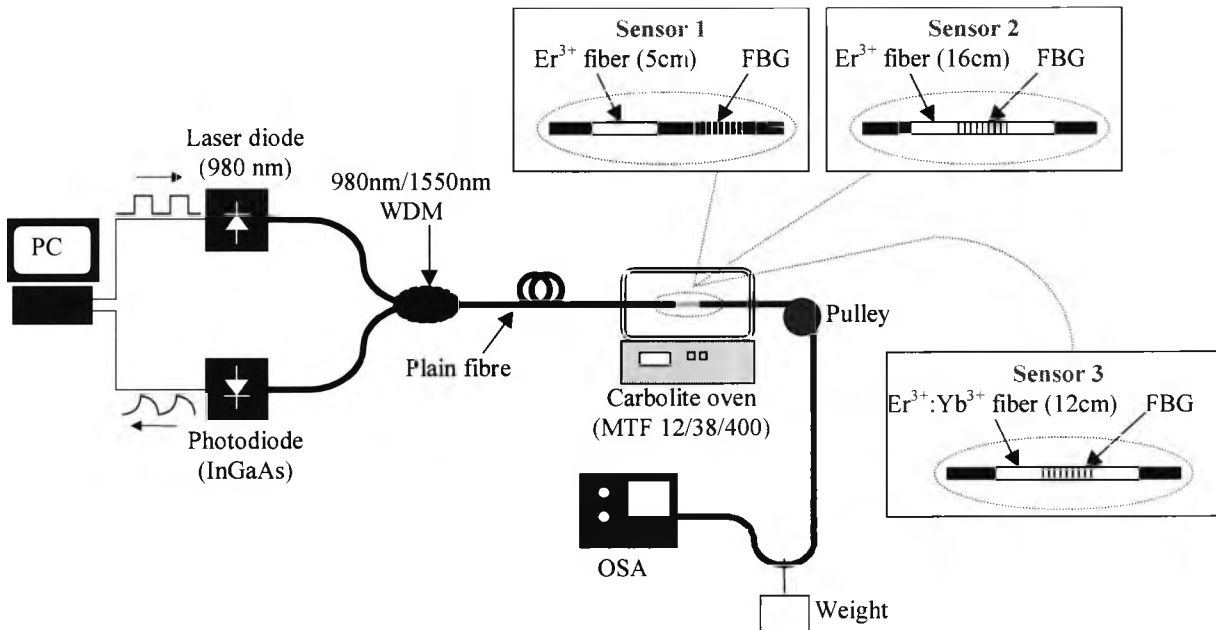


Fig.4.11 Experimental arrangement used for the temperature and strain calibration of the sensors (sensors 1, 2 and 3 shown as insets).

arrangement while fluorescence in the 1550 nm region was detected using the output port. As in previous work, a simple pulley system was used to apply strain to the dual fibre sensors. An InGaAs photodiode was employed in each case to measure the fluorescence emission at the 1550 nm wavelength from both the Er³⁺ and the Er³⁺:Yb³⁺ co-doped fibre sensors (in the latter case enhanced by the direct energy transfer from the Yb³⁺ to the Er³⁺ ions present [14]) by connecting it to the other input port of the WDM coupler. In this work, for simplicity, the measurement of the FBG wavelength shift was achieved using a commercial (Agilent) optical spectrum analyzer (OSA) with a resolution bandwidth of 0.1

Chapter 4 Fluorescence based temperature and strain measurement incorporating FBG experimental results

nm. It should be noted that several relatively inexpensive dedicated systems for measurement of these FBG wavelength changes have been discussed in the literature [9, 11].

The fluorescence lifetime of the doped fibres was measured using an analogue-to-digital card connected to a PC, which sampled the output of the photodiode, this being triggered by the falling edge of the excitation pulse. The value of the fluorescence lifetime was subsequently obtained using Prony's method, as discussed in previous work [12].

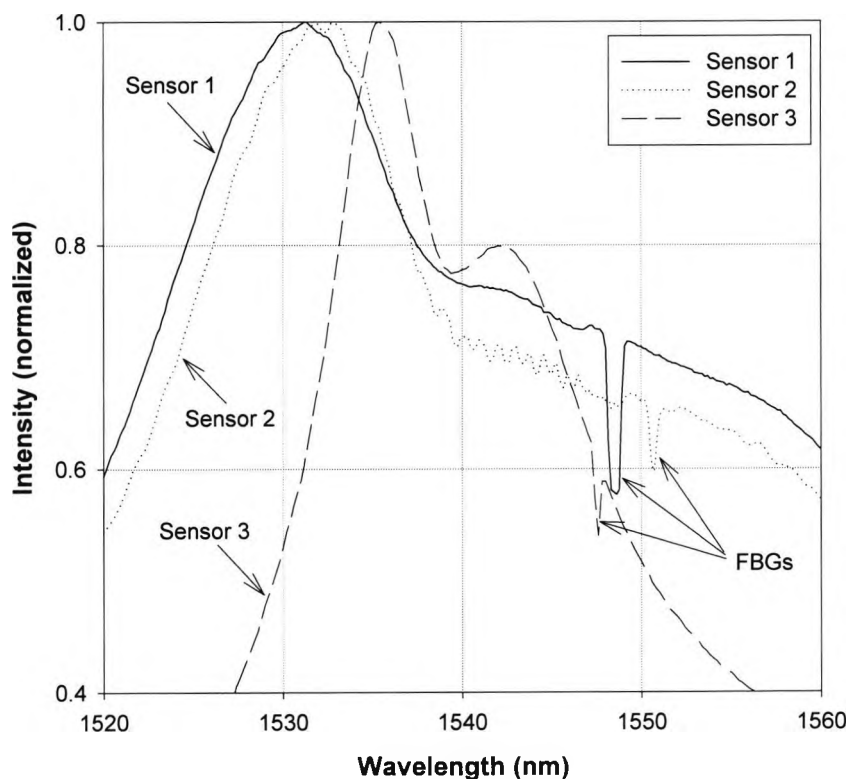


Fig.4.12 Fluorescence spectra from all three sensors showing intensity dips due to the FBG reflection.

Chapter 4 Fluorescence based temperature and strain measurement incorporating FBG experimental results

Measurements of the centre wavelength of the FBG were made by recording and analyzing the transmission dip in the fluorescence spectra of the doped fibres. This emphasises a particularly attractive aspect of this approach in that these spectra contain an associated and easily observable feature corresponding to the FBG (as shown in Fig.4.12) and thus a second source at a wavelength around 1550 nm is not required.

Hence the fluorescence itself which is generated acts as the interrogation light for the FBG, removing the need for additional components. Thus by choosing, as was done in this case, the wavelength of the FBG to lie within the fluorescence band of the doped fibre, the system incorporated its own 'fluorescence fibre source'. This wavelength measurement using the FBG does not interfere with the measurement of the change in the fluorescence lifetime, which provides the temperature correction.

4.4.2.2 Results and discussion

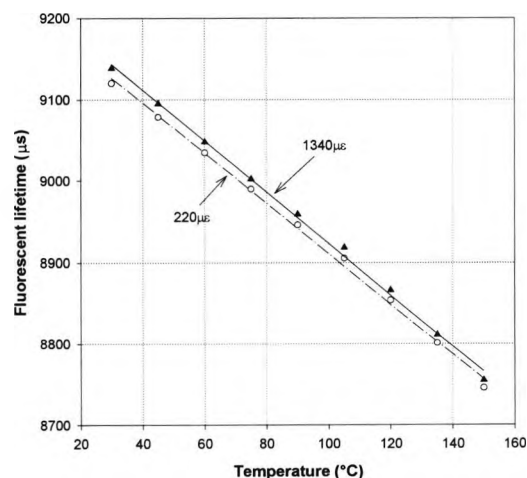


Fig.4.13 Fluorescent lifetime versus temperature calibration data for sensor 3 at minimum and maximum applied strains together with linear fits to the data.

Chapter 4 Fluorescence based temperature and strain measurement incorporating FBG experimental results

A series of calibration tests, involving extensive cycling, was performed to assess the performance of the two dual temperature-strain sensor systems (sensor 2 and sensor 3) and compare with the results previously obtained from sensor 1. Measurements of the fluorescence lifetime and the FBG wavelength for both sensors were taken for a range of applied strains from 221 to 1328 $\mu\epsilon$, at temperatures between 30°C and 150°C. Measurements of the centre wavelength of the FBGs as a function of both temperature and strain resulted in linear wavelength shifts over the ranges measured for both of the sensor configurations, as expected. Fig.4.13 shows an example of the change in the fluorescence lifetime with temperature at two different applied strains, obtained using sensor 3.

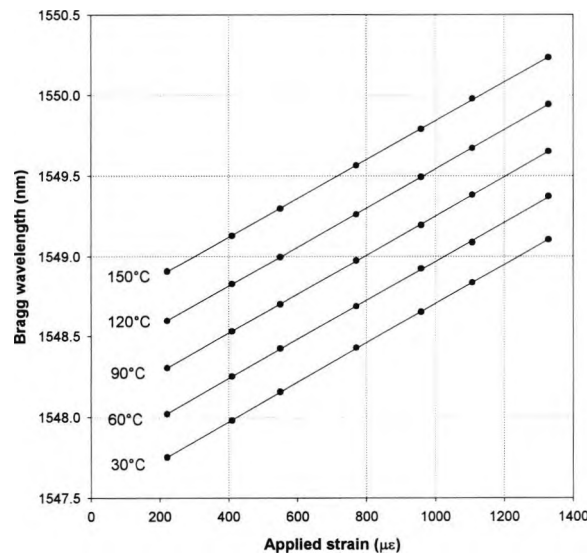


Fig.4.14 Shifts in the fibre Bragg grating wavelength with strain for sensor 3 for a range of temperatures tested.

An example of the shift in the FBG wavelength as a function of applied strain is given in Fig.4.14 for results obtained using sensor 3 at a range of temperatures. The values of the

Chapter 4 Fluorescence based temperature and strain measurement incorporating FBG experimental results

temperature and strain coefficients of the fluorescence lifetime and the FBG wavelength, obtained by fitting straight lines to the data, are given in Table 4.1.

Parameter	Sensor 1	Sensor 2	Sensor 3
K_{1T} ($\mu\text{s}/^\circ\text{C}$)	-1.65 ± 0.04	-1.76 ± 0.01	-3.11 ± 0.06
$K_{1\epsilon}$ ($\mu\text{s}/\mu\epsilon$)	$(8.49 \pm 1.75) \times 10^{-3}$	$(8.08 \pm 1.28) \times 10^{-3}$	$(1.12 \pm 0.01) \times 10^{-2}$
K_{2T} ($\text{nm}/^\circ\text{C}$)	$(1.03 \pm 0.03) \times 10^{-2}$	$(1.09 \pm 0.01) \times 10^{-2}$	$(0.96 \pm 0.01) \times 10^{-2}$
$K_{2\epsilon}$ ($\text{nm}/\mu\epsilon$)	$(1.15 \pm 0.01) \times 10^{-3}$	$(1.22 \pm 0.01) \times 10^{-3}$	$(1.21 \pm 0.01) \times 10^{-3}$

Table 4.1 Temperature and strain coefficients of the fluorescence lifetime and the FBG wavelength for all three sensors.

It can generally be seen from Table 4.1 that the:

- Bragg grating coefficients K_{2T} and $K_{2\epsilon}$ are essentially similar, therefore
 - Bragg grating in doped fibre performs in the same way as in plain fibre
 - it does not interfere with the temperature measurement
- K_{1T} and $K_{1\epsilon}$ coefficients are similar for sensor 1, 2
- K_{1T} and $K_{1\epsilon}$ coefficients are larger for sensor 3
 - different fibre used, therefore different doping concentration.

The strain sensitivities (in units of $\mu\text{s}/\mu\epsilon$) of all the doped fibres, obtained from straight line fits to graphs of fluorescence lifetime versus strain at each of the temperatures tested, are

Chapter 4 Fluorescence based temperature and strain measurement incorporating FBG experimental results

plotted as a function of temperature in Fig.4.15. The results indicate that the strain sensitivities of the three fibres are essentially similar. It is interesting to note, however, that the strain sensitivity of the $\text{Er}^{3+}:\text{Yb}^{3+}$ device (sensor 3), as a function of temperature, appears to be less constant than was seen for the others. The reason this may occur could be due to the presence of one of the dopants (the added Yb^{3+}) which is used in the manufacture of this fibre to enhance the pumping efficiency. The presence of these materials may then have some effect on the strain sensitivity, but this will require further work.

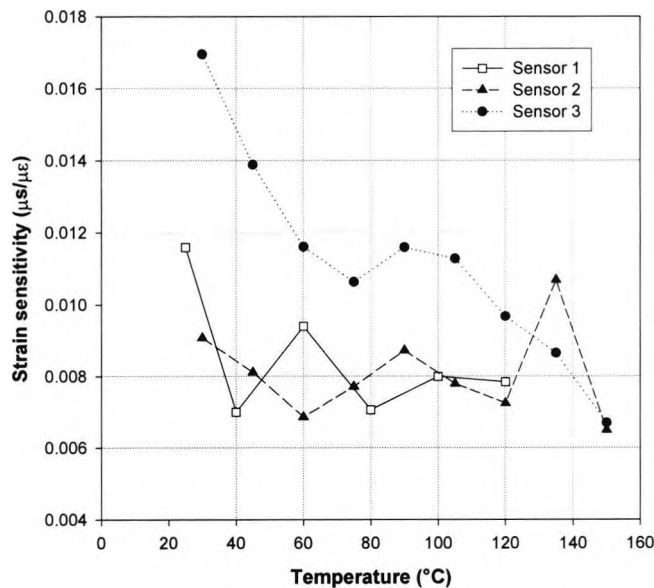


Fig.4.15 Comparison of the strain sensitivities of fluorescent lifetimes over the full temperature ranges for all three sensors.

Using coefficients determined from equation 2.2 and putting them into equations similar to 4.3 and 4.4 in the same way as was done in the previous section, measured values of temperature and strain were calculated for the data obtained from the optical sensors and then these were compared with the known conditions applied during these tests. The

Chapter 4 Fluorescence based temperature and strain measurement incorporating FBG experimental results

standard deviation of the differences between the values calculated from the optical data and those applied in the full range tests for all the sensors studied are recorded in Table 4.2 and are discussed below.

	Temperature range	ΔT ($^{\circ}\text{C}$)	$\Delta \epsilon$ ($\mu\epsilon$)
Sensor 1	25 – 120 $^{\circ}\text{C}$	1.2	20.4
Sensor 2	30 – 120 $^{\circ}\text{C}$	1.5	21.1
	30 – 150 $^{\circ}\text{C}$	1.8	24.7
Sensor 3	30 – 120 $^{\circ}\text{C}$	0.8	7.0
	30 – 150 $^{\circ}\text{C}$	1.9	10.7

Table 4.2 The standard deviation of differences between temperature (ΔT) and strain ($\Delta \epsilon$) values calculated using measurements from the optical sensors and the known parameters applied during the tests.

From Table 4.2 it can be generally seen that the sensors have been tested over a strain range from about 100 to 2000 $\mu\epsilon$ and the temperature resolution (1σ) yields:

- 1 to 2 $^{\circ}\text{C}$ for sensors 1, 2
- $\sim 1^{\circ}\text{C}$ between 30-120 $^{\circ}\text{C}$ for sensor 3
- $\sim 1.5^{\circ}\text{C}$ between 30-150 $^{\circ}\text{C}$ for sensor 3

There is therefore good strain resolution (1σ), $\sim 10 \mu\epsilon$ between 30-150 $^{\circ}\text{C}$, and clearly all the results yield very acceptable levels of uncertainty in both measurands (e.g rms errors of 7 $\mu\epsilon$ and 0.8 $^{\circ}\text{C}$ achieved over strain and temperature ranges of up to 1860 $\mu\epsilon$ and 150 $^{\circ}\text{C}$).

Chapter 4 Fluorescence based temperature and strain measurement incorporating FBG experimental results

One of the potential sources of error lies in the assumption in equations 4.3 and 4.4 that the measured parameters (i.e.. lifetime and FBG wavelength) will have a linear dependency on the measurands (temperature and strain in this case). Previous work [15] has shown this to be a valid assumption for FBGs over the ranges measured here, but work on the fluorescence lifetime however suggests a non-linear temperature dependence when wide temperature ranges are of interest. Fig.4.16 (a) and (b) show an example of a linear fit to the temperature dependence of the fluorescence lifetime of sensor 3 (obtained at minimum applied strain) and the difference between the fit and the actual data, indicating a slight non-linearity. In order to obtain a more detailed understanding of the effect of this on the errors in the data shown in Table 4.2, an estimate of the linearity of the fluorescence lifetime versus temperature data was undertaken for the temperature ranges investigated. The calculated values of \hat{N} (i.e the maximum *non-linearity* expressed as a percentage of f.s.d) obtained from linear fits to the data are listed in Table 4.3 to provide a measure of the linearity of the experimental data. It can be seen from Table 4.3 that a value of 4.28% (for sensor 1) corresponds to the best degree of linearity achieved for temperature measurement using the lifetime alone.

temperature range	sensor 1	sensor 2	sensor 3
25 – 120°C	4.28	–	–
30 – 120°C	–	8.03	5.52
30 – 150°C	–	7.91	15.19

Table 4.3 Average maximum (\hat{N}) non-linearity values (%) obtained from linear fits to lifetimes versus temperature data for all three sensors.

Chapter 4 Fluorescence based temperature and strain measurement incorporating FBG experimental results

The value of 15.19% (for sensor 3) corresponding to an error value of 1.9°C, is the least good in terms of linearity, although satisfactory for a number of measurement situations. Another factor affecting the temperature measurement accuracy is the temperature sensitivity of the fluorescence lifetime, and the errors inherent in the measurement using an erbium-doped fibre system have been discussed previously, in some detail [13], and are not reproduced here. It is expected that the high temperature sensitivity of the fibre used for sensor 3 ($\text{Er}^{3+}:\text{Yb}^{3+}$) (which as can be seen from Table 4.1 is almost twice that of the other two sensors) can enhance its potential performance in practical sensor systems.

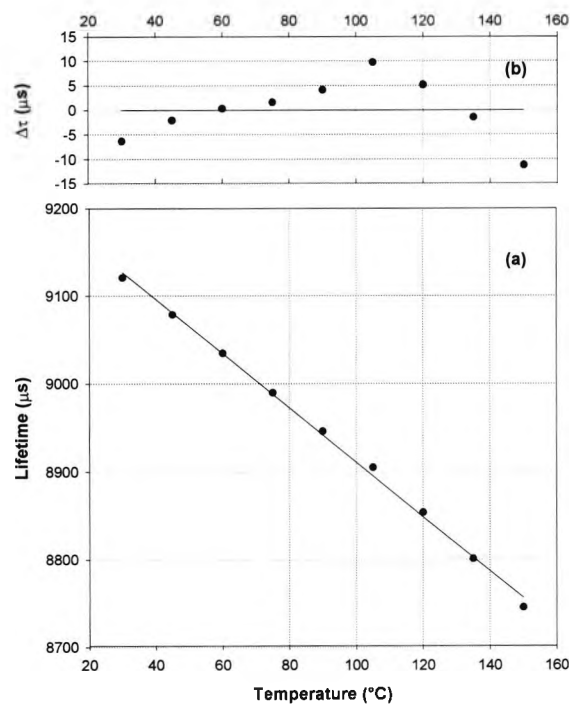


Fig.4.16 (a) Fluorescent lifetime versus temperature data obtained at minimum applied strain (221 $\mu\epsilon$) (b) difference between experimental data and linear fit for sensor 3.

Chapter 4 Fluorescence based temperature and strain measurement incorporating FBG experimental results

Fig.4.17 shows how the fluorescent lifetime dependence on temperature can be exploited, for dual temperature/strain sensor purposes, within the linear region over the lower temperature ranges. The lifetime/temperature dependence of the Er^{3+} 1050 ppm fibre material used for sensor 2 is much more linear (but the response is less sensitive) over a larger temperature range than for the $\text{Er}^{3+}:\text{Yb}^{3+}$ co-doped fibre material used for sensor 3. These graphs display how the performance of the sensor can be customized to meet the demands for high temperature sensitivity, measurement range and good reproducibility.

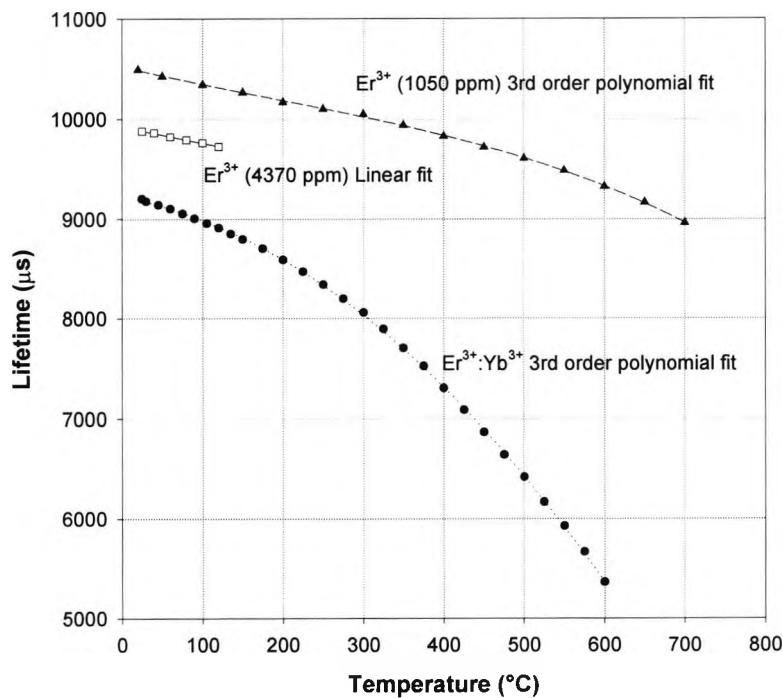


Fig.4.17 Graph showing the temperature characteristics of the fluorescent lifetime of all sensors for an extended temperature range.

As previously mentioned, the dual sensors tested here make use of temperature/strain discrimination techniques. Fig.4.18 (a) and (b) show the importance of the compensation approach by considering temperature and strain measurements from the $\text{Er}^{3+}:\text{Yb}^{3+}$ co-doped

Chapter 4 Fluorescence based temperature and strain measurement incorporating FBG experimental results

fibre dual sensor (sensor 3) both with and without the compensation provided by the fluorescence lifetime measurements. The values obtained from FBG data alone are displayed as filled triangles while the values obtained using the combined FBG/fluorescence lifetime approach are shown as filled circles. The straight lines in the plot show the constant temperature (30°C) and strain (221 $\mu\epsilon$) values to which the sensor was exposed. The graphs illustrate the significance of applying the corrections to the FBG wavelength shift readings which were obtained for a constant temperature (30°C in this case for Fig.4.18 (a)) and a constant strain measurement of

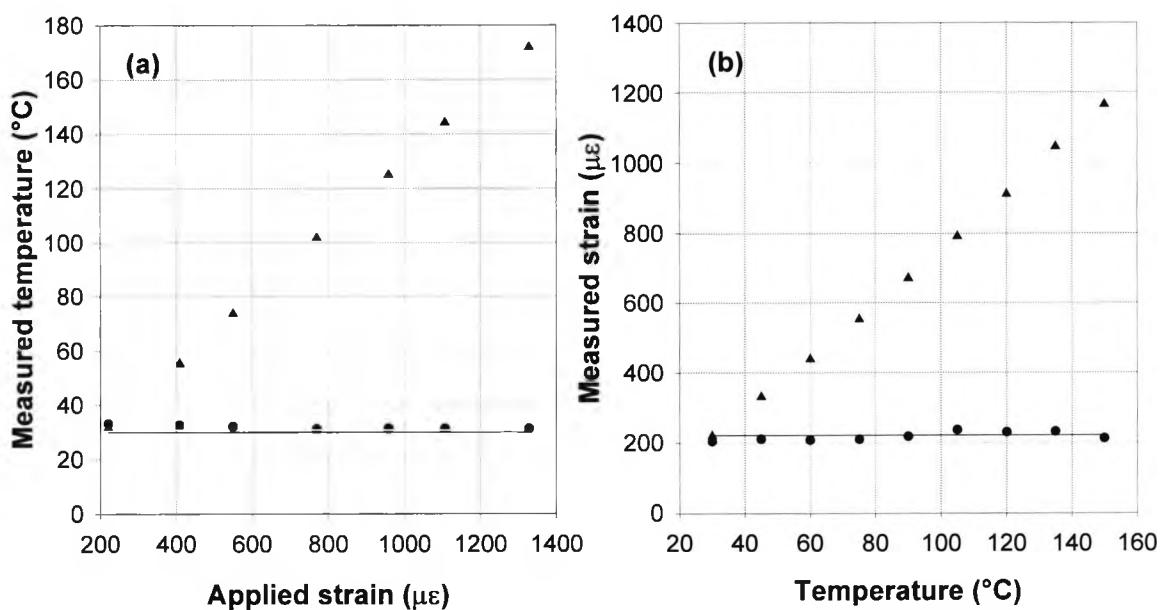


Fig.4.18 (a) Fluorescent lifetime correction of Bragg shifts at constant temperature (30°C) and (b) at constant strain (221 $\mu\epsilon$) for sensor 3.

221 $\mu\epsilon$ respectively (for Fig.4.18 (b)). It is obvious from the graphs that without compensation provided by the lifetime measurement these types of sensors would show a serious measurement error, e.g. adding a strain of 1000 $\mu\epsilon$ would cause the temperature to be

Chapter 4 Fluorescence based temperature and strain measurement incorporating FBG experimental results

read as about 125°C instead of the actual 30°C (as shown in Fig.4.18 (a)) and similarly at 125°C a strain value of about 1000 $\mu\epsilon$ would be recorded instead of the real applied value of 221 $\mu\epsilon$ (as shown in Fig.4.18 (b)). Similarly, Fig.4.19 (a) and (b) show the lifetime corrections by the Bragg element of the sensor scheme.

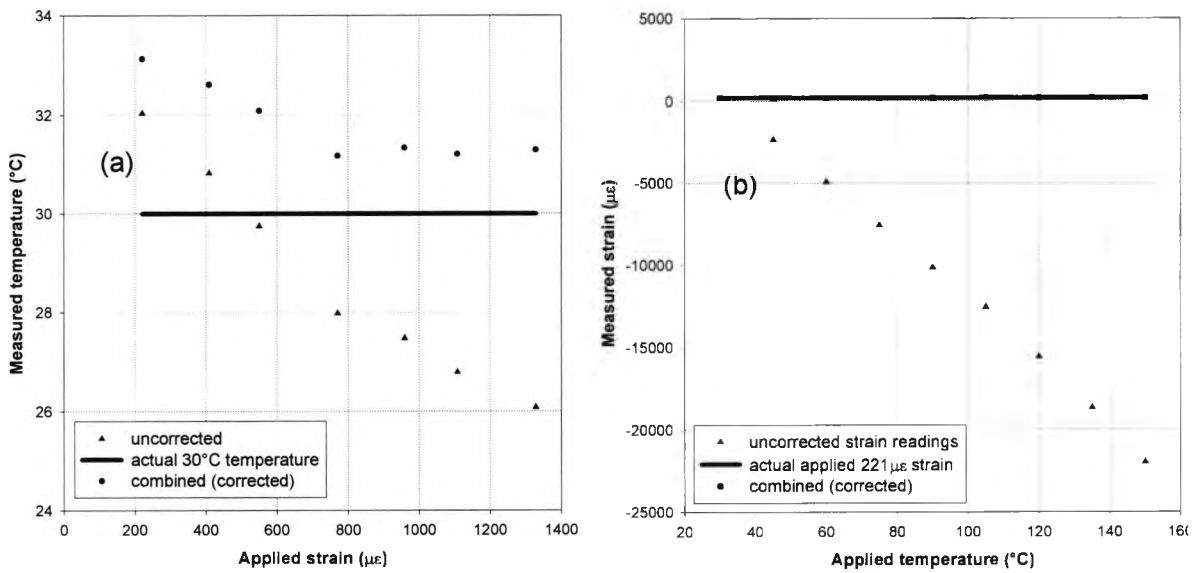
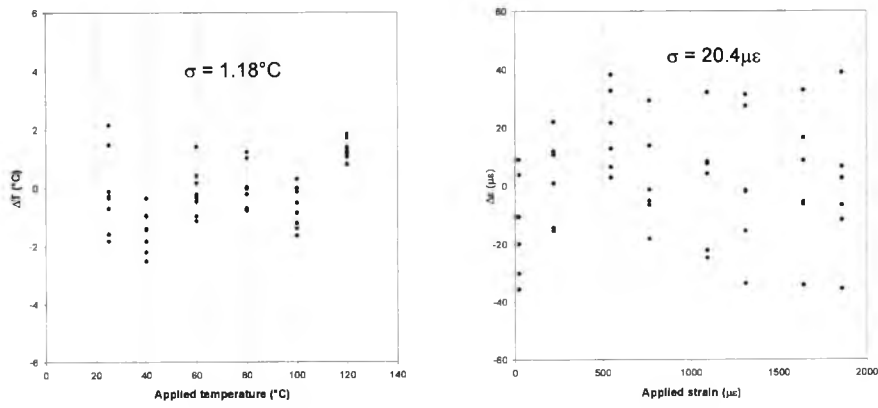


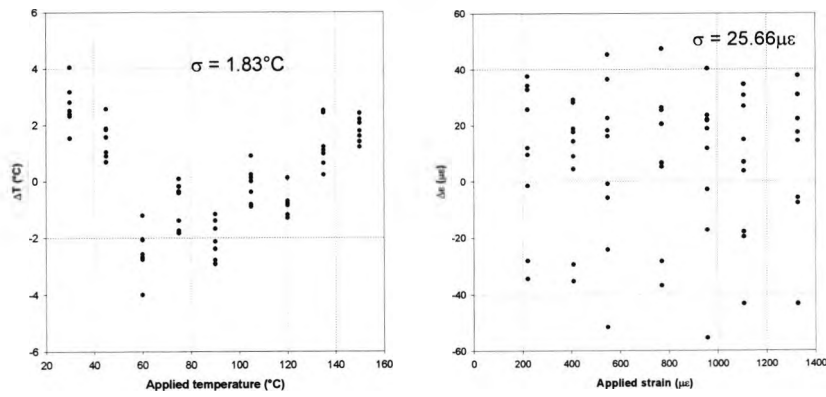
Fig.4.19 (a) Fluorescent lifetime correction by Bragg shifts at constant temperature (30°C) and (b) at constant strain (221 $\mu\epsilon$) for sensor 3.

Fig.4.20 shows the principle output from this work - comparing the standard deviation (rms) accuracies (σ) achieved from all three sensor schemes.

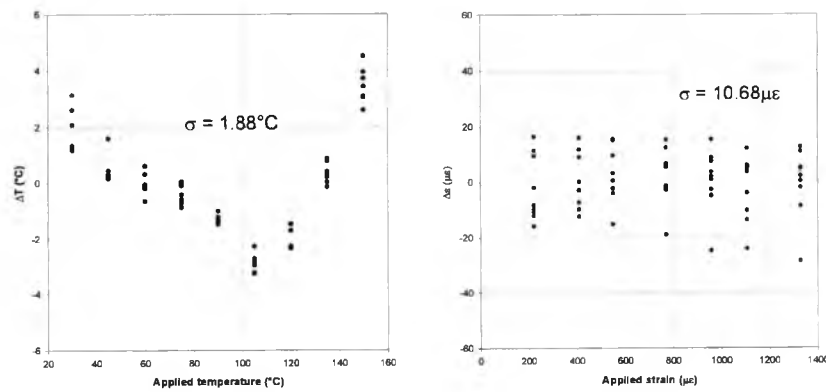
Chapter 4 Fluorescence based temperature and strain measurement incorporating FBG experimental results



a) sensor 1



b) sensor 2



c) sensor 3

Fig.4.20 Comparison of all sensor outputs over full temperature and strain ranges.

Chapter 4 Fluorescence based temperature and strain measurement incorporating FBG experimental results

Table 4.4 shows the lifetime standard deviation (rms) values and the corresponding maximum non-linearity (\hat{N} %) values for *all* lifetime measurements at *all* applied strains.

Temperature range	sensor 1		sensor 2		sensor 3	
	rms	\hat{N} %	rms	\hat{N} %	rms	\hat{N} %
25 – 120°C	2.85	6.51				
	2.30	6.80				
	1.47	4.34				
	1.34	3.99				
	1.45	3.68				
	1.95	4.32				
	1.26	3.08				
	1.12	1.53				
30 – 120°C			3.11	6.80	2.09	7.23
			2.53	7.02	1.79	3.58
			3.51	8.67	1.60	4.47
			2.22	5.13	1.57	5.24
			3.43	10.47	1.93	6.71
			2.64	7.30	1.47	4.40
			3.55	10.81	2.29	7.00
30 – 150°C			3.67	7.88	6.26	15.94
			2.74	6.76	4.83	14.03
			3.80	8.50	6.07	14.71
			3.13	6.54	6.29	15.43
			3.65	9.36	4.97	15.24
			3.75	7.06	6.14	14.66
			3.85	9.28	6.39	16.32

Table 4.4 Lifetime standard deviation (rms) values and corresponding maximum non-

linearity (\hat{N} %) values for all lifetime measurements at all applied strains.

**Chapter 4 Fluorescence based temperature and strain measurement
incorporating FBG experimental results**

Table 4.5 shows the temperature standard deviation (rms) values and the corresponding maximum non-linearity (\hat{N} %) values for *all* lifetime measurements at *all* applied strains.

Temperature range	sensor 1		sensor 2		sensor 3	
	rms	\hat{N} %	rms	\hat{N} %	rms	\hat{N} %
25 – 120°C	1.73	6.51				
	1.40	6.80				
	0.87	4.34				
	0.80	3.99				
	0.87	3.68				
	1.15	4.32				
30 – 120°C	0.76	3.08				
	0.66	1.53				
			1.70	6.80	0.72	7.23
			1.42	7.02	0.60	3.58
			1.94	8.67	0.54	4.47
			1.22	5.13	0.53	5.24
30 – 150°C			1.88	10.47	0.64	6.71
			1.43	7.30	0.49	4.40
			1.97	10.81	0.76	7.00
			2.08	7.88	2.03	15.94
			1.57	6.76	1.88	14.03
			2.16	8.50	1.95	14.71
		1.77	6.54	2.00	15.43	
		2.06	9.36	1.89	15.24	
		2.12	7.06	1.94	14.66	
		2.21	9.28	2.03	16.32	

Table 4.5 Temperature standard deviation (rms) values and corresponding maximum non-

linearity (\hat{N} %) values for all lifetime measurements at all applied strains.

Chapter 4 Fluorescence based temperature and strain measurement incorporating FBG experimental results

4.4.2.3 Means offset modelling

Since these sensors are basically offset sensors (i.e. they work on the *difference* between values of lifetime and Bragg shift at given temperatures and strain from some calculated baseline values) they have to be initialised to make sure that any offset in their means (and therefore any possibility of a biased systematic error) is minimised (temperature and strain means will then both ~ 0) - thereby giving a good spread of measured values around zero (random errors) as shown in the plots in Fig.4.20. One way to do this is to extrapolate from the experimental data obtained over a particular temperature range to estimate these baseline values, as was done in the case of sensor 1, to obtain lifetime and Bragg shift values for the “zero” case or the minimum. Another way is to model the sensor as

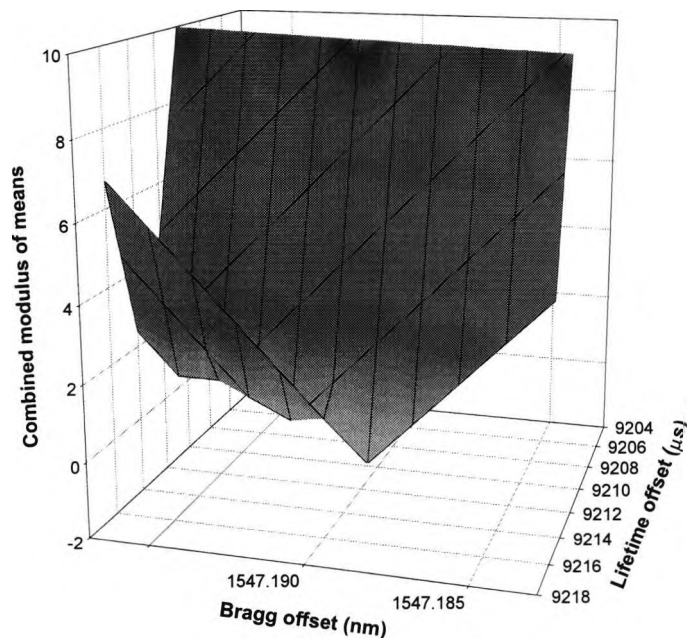


Fig.4.21 Sensor 3 – means modelling of baseline values to achieve a combined minima for optimisation of use (over the range 30 –120°C).

Chapter 4 Fluorescence based temperature and strain measurement incorporating FBG experimental results

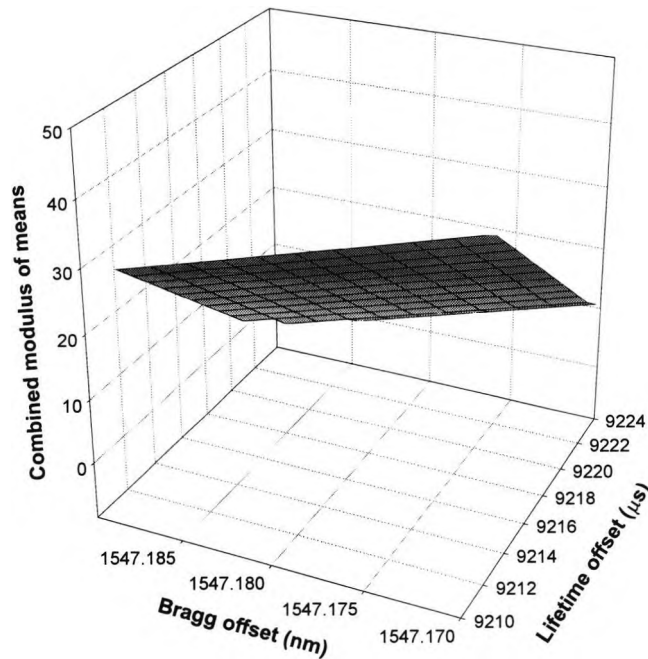


Fig.4.22 Sensor 3 – means modelling of baseline values to achieve a combined minima for optimisation of use (over the range 30 –150°C).

shown in Fig.4.21 and Fig.4.22 which was done for sensor 3, shown here over two different temperature ranges.

From these graphs, the baseline values of lifetime (μs) and Bragg shift (nm) necessary for the combined means minima to approach a value of zero were estimated for sensor 3, i.e. it will be at these values that the sensor baselines are set so that the dual temperature/strain sensor will not suffer from offset. For the range 30-150°C these are estimated as 9222.16 μs and 1547.19 nm, and for 30-120°C range are 9216.00 μs and 1547.19 nm – these values give the modulus of the sum of the temperature and strain mean values to be equal to almost zero in both cases.

Chapter 4 Fluorescence based temperature and strain measurement incorporating FBG experimental results

4.4.2.4 OSA spectra

Extra data concerning the nature of the fluorescence from the special co-doped fibre used in sensor 3 was recorded using the OSA.

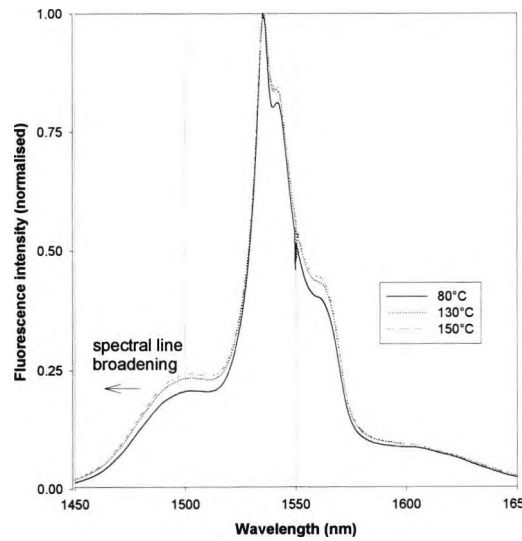


Fig.4.23 Sensor 3 – OSA plots of the fluorescence intensity changes with temperature from 80 – 150°C with 150g mass applied to the fibre (shown at 3 temperatures only).

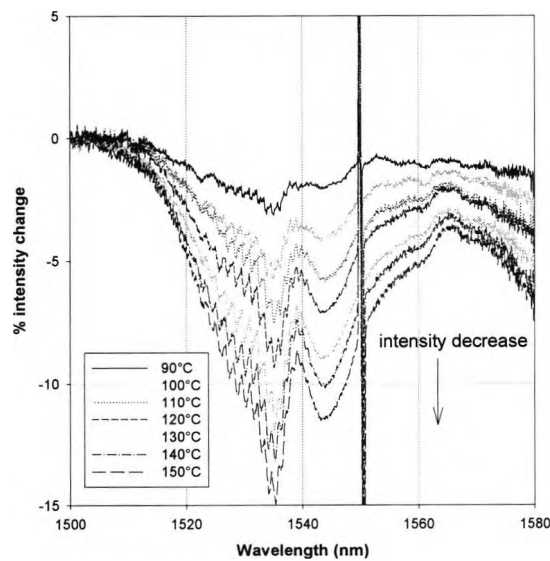


Fig.4.24 Sensor 3 – OSA plots showing the fluorescence intensity % decrease with increasing temperatures from 80°C with 150g mass applied to the fibre.

Chapter 4 Fluorescence based temperature and strain measurement incorporating FBG experimental results

The results in Fig.4.23 show the familiar normalised fluorescence intensity spectral line broadening effect with increasing temperatures at three of the temperatures used from 80°C to 150°C, over a large wavelength range, with a mass of 150 g applied to the fibre. The effect is due to the presence of multiphonons. Fig.4.24 shows these fluorescence intensity changes as a percentage (%) decrease, normalised from 80°C (i.e. “zero” change), over a smaller wavelength range. The lines around 1550 nm are just reflections from the FBG at its centre wavelength.

4.4.2.5 Conclusions

This work has compared the experimental results obtained from three unique and simple sensor schemes, capable of effective temperature-strain discrimination with single sensing elements, which show considerable potential for further development. These sensors utilize the current versatility and effectiveness of Bragg gratings (e.g. ease of WDM, an effective linear temperature/strain response, interrupt immunity and ability for multiplexing) and exploit the temperature/strain dependency of the fluorescence lifetime from doped fibre. Additionally, by using the fluorescence generated within the optical system to interrogate the FBG, these sensors have a major advantage in that no external light source is required. The sensor elements are conveniently co-located on one fibre, for ease of installation and use, and the size of the active region is very small, facilitating both point sensor use and offering the potential for multiplexing of the sensors along a single fibre for distributed measurement. Applications such as in large-scale civil engineering monitoring (e.g. the structural integrity of a bridge) are therefore possible. Research is continuing to determine which materials are best to use for optimisation in a range of different practical compromises, e.g. “smart

Chapter 4 Fluorescence based temperature and strain measurement incorporating FBG experimental results

structures” where sensors need to be embedded and coated for such use, and also to achieve an improvement in the resolution of both parameters. In addition, the issues of long term stability and wider utility are being considered.

4.4.3 High temperature FBG performance

With current research trends looking at FBG thermal stability to produce gratings which will be stable up to 600°C [16] there was a need to know how well our FBG would cope with use in higher temperature sensing devices, used on perhaps oil well monitoring or smart structures, for long-term applications. To this end, a series of further tests were carried out on the same grating used in the experimental set-up previously (then at low temperatures) in section 4.4.2 (i.e. written into the $\text{Er}^{3+}:\text{Yb}^{3+}$ co-doped photosensitive fibre - sensor 3) to test the reflective quality with increasingly ramped temperatures. The irreversible results obtained on the FBG reflectivity (from up to almost 1300 hrs of damaging heat treatments) are shown in Fig.4.25. Since the nature of the data revealed a stepped exponential form, the graph is shown with time constants (τ) estimated from single exponential fits to a series of non-isochronal [17] decay curves (i.e. *different* durations at different temperatures) obtained at increasing annealing temperatures (shown in brackets).

Chapter 4 Fluorescence based temperature and strain measurement incorporating FBG experimental results

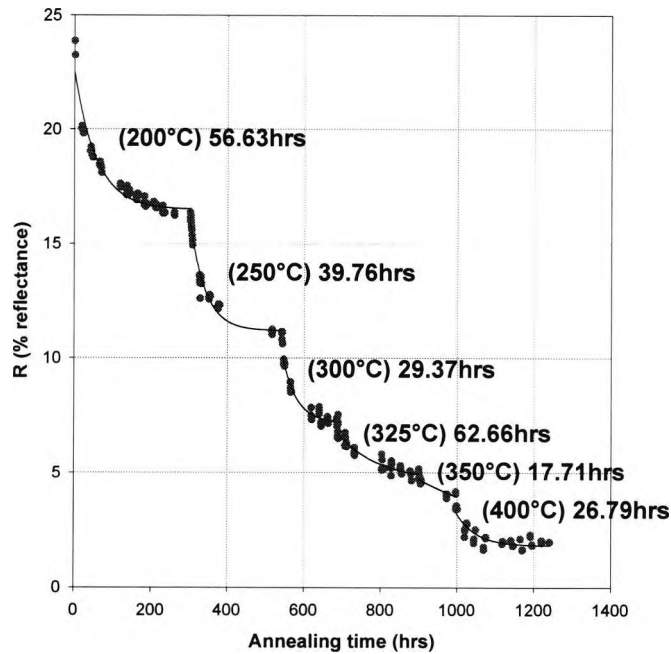


Fig.4.25 Long term thermally induced decay effects on FBG performance.

The observed % reflectance (R) in this case was determined from the OSA transmission spectra data using the relationship $R = 100 * [(I_{max} - I_{min}) / I_{max}]$, where I_{max} and I_{min} are the maximum and minimum transmission intensities around and at the Bragg wavelength separately.

From Fig.4.25, it can be seen that in the longer term usage from using the percentage reflectivity of the grating as an indicator of performance, then this decreases from about 24% initially observed (i.e. before any treatment) to about 2% after almost 1300 hrs of various heat treatments. This decrease in FBG efficiency is clearly observed to be sharper at first and, as can be seen from the fitted time constants (τ) in the brackets in Fig.4.25, the rate of decay generally accelerates with steadily increasing temperatures ramped up to a maximum

Chapter 4 Fluorescence based temperature and strain measurement incorporating FBG experimental results

of 400°C, where the measured % reflectance eventually becomes an absolute value of only ~ 2%, rendering the grating useless for sensor purposes. These results draw clear similarities with previous work reported in the literature [17 - 20] from various types of fibres, and the measured reflectivity can be displayed as an *integrated coupling constant* (ICC) normalised to the starting value to show a series of isothermals [17] as in Fig.4.26.

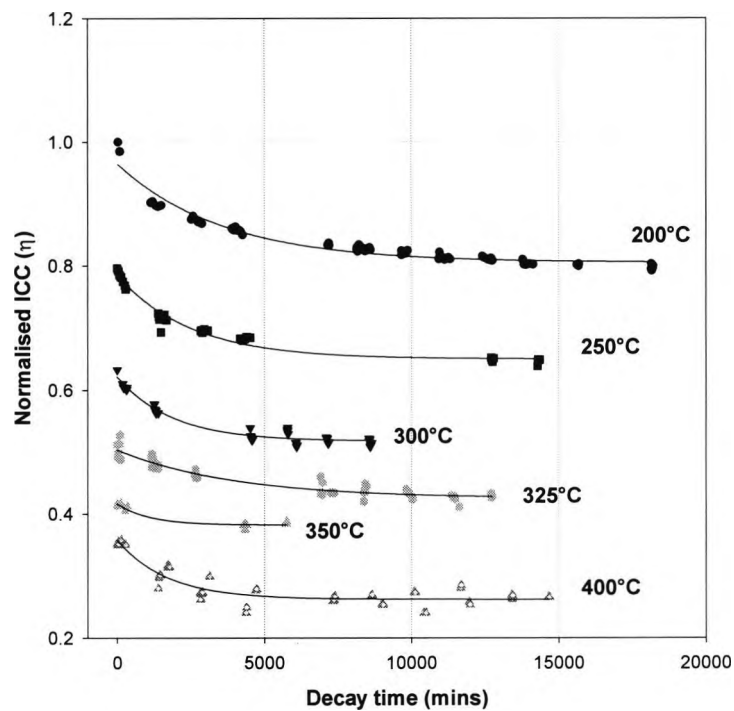


Fig.4.26 Normalised ICC of FBG at each annealing temperature with time.

Decay characteristics of gratings written into non-hydrogen loaded fibres, such as the one used here, have been modelled in previous work [21, 22] to predict the likely performance (and hence their lifetime) in sensor use at a particular temperature, using information from plots similar to Fig.4.26. However, the experimental data obtained here was found not to fit that particular model very well. This could have been due to the fact that the exact

Chapter 4 Fluorescence based temperature and strain measurement incorporating FBG experimental results

composition of the host fibre was not known (e.g. the relative amounts of germanium and boron) and therefore the assumptions of that model used previously were possibly not valid in this case. However, the fitted exponentials shown in Fig.4.25 and Fig.4.26 are good indicators of the would-be sensor lifetime of this particular FBG, written into this particular fibre host material, at a given temperature. Work is continuing to model more gratings, in different fibre hosts, to even higher temperatures [20].

4.4.4 High temperature annealing effects of Er³⁺:Yb³⁺ co-doped photosensitive fibre

In addition to the harsh regime of heat treatments already suffered by the unique Er³⁺:Yb³⁺ co-doped photosensitive fibre FBG host (sensor 3) as reported above, and before discarding this invaluable fibre away, it was decided to test for thermal annealing properties and compare results to those obtained previously in Chapter 3 (see section 3.4.2) using an identical sample length (i.e. 12 cm) of the same fibre. With the grating now “burned” off (i.e. down to 2% reflection), the fibre was subjected to the regime of heat treatments shown in Fig.4.27, shown with standard deviation error bars. Fig.4.28 shows more closely the annealing process, observed before in Fig.3.20, but this time for twice the duration (48 hrs) at the same temperature (800°C). The results obtained compare closely with those in section 3.4.2 of this thesis using the same fibre, and confirm the existence of the “cross-over” point at higher temperatures (i.e. closer to 800°C), from which temperature the lifetime can be seen to increase.

Chapter 4 Fluorescence based temperature and strain measurement incorporating FBG experimental results

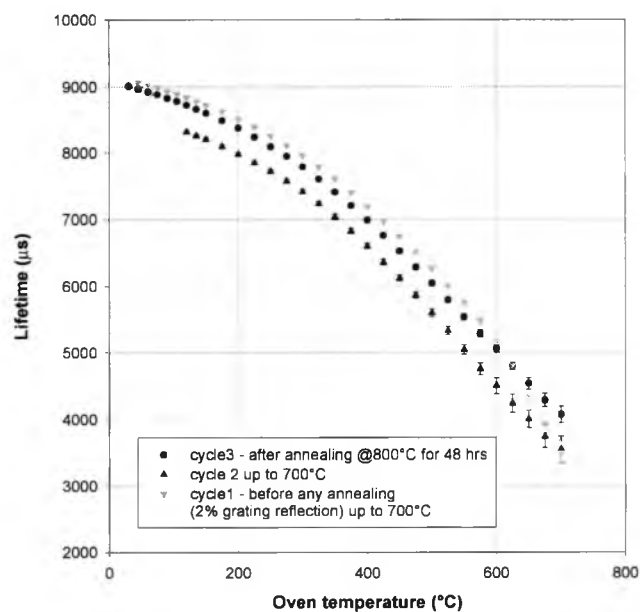


Fig.4.27 $\text{Er}^{3+}:\text{Yb}^{3+}$ co-doped photosensitive fibre annealing effects.

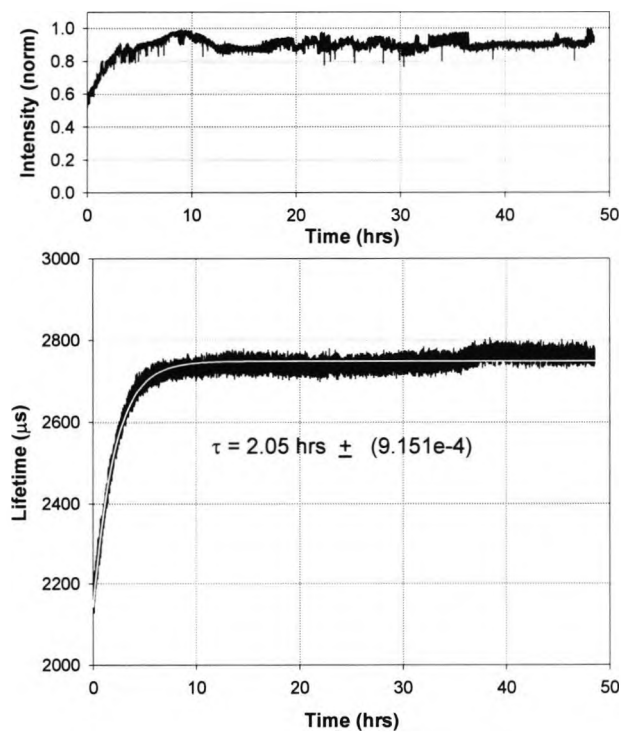


Fig.4.28 $\text{Er}^{3+}:\text{Yb}^{3+}$ co-doped photosensitive fibre annealing at 800°C for 48 hrs.

4.5 Conclusions

The work done in this chapter has introduced the idea of a new type of dual temperature/strain fibre-optic based sensor, based on the combination of fluorescence lifetime and FBG which could easily be developed into a “true” simultaneous temperature/strain sensor, and which also has the potential to be developed into a commercial sensor. Devices tested have shown that very reasonable temperature and strain measurement uncertainties can be achieved from these simple, compact in-fibre sensor schemes over quite large temperature and strain measurement ranges, when compared to reported data from most other similar fibre optic-based sensors in the literature. These are shown in bold in Table 4.6, which compares our results to some from the other work (shown previously in Table 2.1). Work is now underway to develop the sensor scheme with a view to achieving true simultaneous temperature-strain discrimination at higher temperatures (up to $\sim 700^{\circ}\text{C}$) from a single sensing element i.e. a FBG written into more thermally-durable germanium (Ge) doped silica fibre.

Table 4.7 shows data obtained from this thesis added to previous knowledge to provide a fuller analysis of the fluorescent lifetime strain effect, i.e. the principal output of the work. Table 4.7 also compliments the information gained earlier from some of the fibres tested individually, i.e. the same fibres but not combined with FBG (Tables 3.2, 3.9 and 3.10). The results again confirm the existence of the small, but significant, strain effect on the measured fluorescence lifetime which has been successfully exploited for purposes of dual temperature/strain sensing by combining with FBG.

**Chapter 4 Fluorescence based temperature and strain measurement
incorporating FBG experimental results**

T (°C)	ϵ ($\mu\epsilon$)	technique	source and range
0.4	12	Dispersive Fourier transform spectroscopy (DFTS)	Flavin <i>et al</i> Opt Letters 19 1994 (over 25°C, over 1500 $\mu\epsilon$)
5	10	Dual wavelength gratings	Xu <i>et al</i> Electronic Letters 30 1994 1085 (10 - 60°C, 0 - 600 $\mu\epsilon$)
5	10	Two-mode fibres	Vengsarkar <i>et al</i> J Light Tech. 12 1994 (over 90°C, over 500 $\mu\epsilon$)
1.5	9	Different Gratings	Patrick <i>et al</i> IEEE Phot Tech. Letts 8 1996 1223 (25 - 50°C, 290 - 1270 $\mu\epsilon$)
1	17	Two Bragg Gratings	James <i>et al</i> Electronic Letters 32 1996 12 (25 - 150°C, 0 - 2500 $\mu\epsilon$)
4	100	Spontaneous Brillouin Backscatter	Parker <i>et al</i> IEEE Phot Tech. Letts 9 1997 7 (22 - 70°C, 0 - 5350 $\mu\epsilon$)
1	58	Long period grating	Bhatia <i>et al</i> Opt Letters 22 1997 648 (over 125°C, over 2100 $\mu\epsilon$)
1.7/pm	17/pm	Dual wavelength gratings	Brady <i>et al</i> IEE Proc. Optoelectronics, 144, 3, 1997 (37 - 57°C, 1800 $\mu\epsilon$)
0.9	32	Combined fluorescence/Extrinsic Fabry-Perot interferometric (EFPI)	Liu <i>et al</i> Proc SPIE 3330 1998 p332-341 (20 - 90°C, 0 - 1800 $\mu\epsilon$)
0.7	40	Two-mode fibre scanning interferometer	Sinha <i>et al</i> Proc SPIE 3541 1999 p82 (20 - 60°C, over 1600 $\mu\epsilon$)
1.9	22	Bragg gratings + Brillouin OTDA	Posey <i>et al</i> Proc SPIE 3746 1999 p341-4 (0 - 60°C, 200 - 2400 $\mu\epsilon$)
0.7	18.2	ASE	Jung <i>et al</i> Applied Optics 38 1999 13 (45 - 150°C, 0 - 1200 $\mu\epsilon$)
4	35	Two Bragg Gratings	Frank <i>et al</i> Proc SPIE 3860 1999 p89-97 (2 - 95°C, 0 - 3500 $\mu\epsilon$)
1.6	8.5	single Bragg Grating	Guan <i>et al</i> Electronic Letters 36 2000 12 (40 - 100°C, 0 - 500 $\mu\epsilon$)
1.2	20	Superstructure Bragg grating	Guan <i>et al</i> IEEE Phot Tech. Letts 12 2000 6 (20 - 120°C, 0 - 1200 $\mu\epsilon$)
8	54.8	ASE	Jung <i>et al</i> Applied Optics 39 2000 7 (50 - 180°C, 0 - 1100 $\mu\epsilon$)
2.5	26	Interferometric interrogated FBG	Ferriera <i>et al</i> Optical Eng. 39 2000 8 (20 - 140°C, 0 - 1000 $\mu\epsilon$)
1.8	32	stimulated Brillouin scattering	Posey <i>et al</i> IEICE T-on-E E83-C 3 2000 p413-17 (10 - 60°C, 178 - 1245 $\mu\epsilon$)
1.3	23	Long period Gratings	Younggeun <i>et al</i> IEICE T-on-E E83-C 3 2000 p282-6 (20 - 70°C, 0 - 3000 $\mu\epsilon$)
1.2	20.4	Fluorescence + Bragg	Wade <i>et al</i> RSI August 2001 (25 - 120°C, 22 - 1860 $\mu\epsilon$)
1.8	24.7	Fluorescence + Bragg	Wade <i>et al</i> M & C 34 2001 (30 - 150°C, 221 - 1328 $\mu\epsilon$)
1.5	21.1	Fluorescence + Bragg	Wade <i>et al</i> M & C 34 2001 (30 - 120°C, 221 - 1328 $\mu\epsilon$)
0.8	7	Fluorescence + Bragg	Forsyth <i>et al</i> Applied Optics - accepted for publication June 2002 (30 - 120°C, 221 - 1328 $\mu\epsilon$)
1.9	10.7	Fluorescence + Bragg	Forsyth <i>et al</i> Applied Optics - accepted for publication June 2002 (30 - 150°C, 221 - 1328 $\mu\epsilon$)

Table 4.6 Accuracies (rms) from the dual T, ϵ fibre-based sensor schemes tested here

(shown in bold) compared with some others.

Chapter 4 Fluorescence based temperature and strain measurement incorporating FBG experimental results

	<i>Forsyth et al</i>	<i>Forsyth et al</i>	<i>Forsyth et al</i>	<i>Forsyth et al</i>	<i>Forsyth et al</i>	<i>Forsyth et al</i>	<i>Forsyth et al</i>	<i>Sun et al [23]</i>	<i>Sun et al [24]</i>
	Er 200ppm	Er 960ppm	Er 1050ppm*	Er 4370ppm*	Tm/Ho #	Er/Yb*	Nd 1460ppm	Nd wt 7.5%	Yb wt 2.5%
mp method	A/D	A/D	A/D	A/D	A/D	A/D	PLD	PLD	PLD
LD pump (nm)	813	813	980	980	785	980	785	830	980
Typical lifetime @25°C (µs)	10350	10100	10375	9880	280	9120	440	365	875
Strain sensitivity (µs/µε)	$(1.0 \pm 0.2) \times 10^{-2}$	$(1.2 \pm 0.3) \times 10^{-2}$	$(8.08 \pm 1.3) \times 10^{-3}$	$(8.48 \pm 1.8) \times 10^{-3}$	$(2.34 \pm 0.32) \times 10^{-4}$	$(1.12 \pm 0.3) \times 10^{-2}$	$6.64 \times 10^{-4}@$	$(5.36 \pm 0.27) \times 10^{-4}$	$(4.32 \pm 0.71) \times 10^{-4}$
Temperature sensitivity (µs/K)	$-2.45 \pm (0.2)$	$-2.53 \pm (0.3)$	$-1.76 \pm (0.01)$	$-1.65 \pm (0.04)$	-0.08	$-3.10 \pm (0.06)$	-0.15#	$-0.28 \pm (0.03)$	$-0.07 \pm (0.01)$
K/µε	0.0040	0.0047	0.0046	0.0051	0.0029	0.0036	0.0034	0.0019	0.0062
ΔT @1000µε	4.0	4.7	4.6	5.1	2.9	3.6	3.4	1.9	6.2

Table 4.7 Comparison of the performances of all fibres.

@ estimated at 35°C

* with grating written in

Prony's at 20°C

4.6 References

- [1] Th.Troster, T.Gregorian and W.B.Holzapfel, Energy levels of Nd^{3+} and Pr^{3+} in RCL_3 under pressure, *Physical Review B*, 48, 5 (1993)
- [2] D.I.Forsyth, S.A.Wade, D.Perciante and K.T.V.Grattan, Temperature and Strain Characteristics of the $^3\text{F}_4$ and $^3\text{H}_4$ Energy levels of Tm:Ho Co-Doped Fibre, in *Proceedings of Sensors and their Applications XI*, K. T. V. Grattan and S. H. Khan, eds. (IOP Publishing Ltd, London), pp. 365-370 (2001)
- [3] P.M.Farrell, S.A.Wade, G.W.Baxter, S.F.Collins, A.J.Stevenson, and K.T.V.Grattan, On the physical origin of strain sensitivity in optical fibre rare earth fluorescence sensors, in *Proceedings of Sensors and their Applications XI*, K. T. V. Grattan and S. H. Khan, eds. (IOP Publishing Ltd, London), pp. 231-236 (2001)
- [4] S.F.Collins, P.M.Farrell, S.A.Wade, G.W.Baxter, D.A.Simpson, A.J.Stevenson, K.T.V.Grattan and D.I.Forsyth, Modelling Strain Dependence of Fluorescence from Doped Optical Fibres: Application to Neodymium, in *Proceedings of 15th Optical Fiber Sensors Conference Technical Digest (published by IEEE), Portland, USA*, pp. 439 - 442 (2002)
- [5] A.D.Kersey, M.A.Davis, H.J.Patrick, M.LeBlanc, K.P.Koo, C.G.Askins, M.A.Putnam and E.J.Friebele, Fiber Grating Sensors, *J. Lightwave Tech.* 15, 8, 1442 (1997)
- [6] K.T.V.Grattan and B.T.Meggitt, *Optical Fiber Sensor Technology: Advanced Applications*, Kluwer Academic Publishers, Dordrecht, The Netherlands, pp. 79 - 80 (2000)
- [7] P.Ferdinand, O.Ferragu, J.L.Lechien, B.Lescop, V.Marty, V.S.Rougeault, G.Pierre, C.Renouf, B.Jarret, G.Kotrotsios, V.Neuman, Y.Depeursings, J.B.Michel, M.V.Uffelen, Y.Verbandt, M.R.H.Voet and D.Toscano, Mine operating accurate stability control with

Chapter 4 Fluorescence based temperature and strain measurement incorporating FBG experimental results

optical fibre sensing and Bragg grating technology, BRITE-EURam STABILOS project, *Proc SPIE* 2360, 162 (1994)

[8] Y.J.Rao, D.J.Webb, D.A.Jackson, L.Zhang and I.Bennion, In-fibre Bragg grating temperature sensor system for medical applications, *J. Lightwave Technol.* 15 (1996)

[9] Y.M.Gebremichael, B.T.Meggitt, W.J.O. Boyle, W.Li, K.T.V.Grattan, L.Boswell, B.McKinley, K.A.Aarnes, L.Kvenild, Multiplexed Fibre Bragg Grating Sensor System for Structural Integrity Monitoring in Large Civil Engineering Applications, in *Proceedings of Sensors and their Applications XI*, K.T.V.Grattan and S.H.Khan, eds. (IOP Publishing Ltd, London), pp. 341-345 (2001)

[10] A.D.Kersey, T.A.Berkoff and W.W.Morey, Multiplexed fiber Bragg grating strain-sensor system with fiber Fabry-Perot wavelength filter, *Optics Letters* 18, 16, 1370 (1993)

[11] Y.N.Ning, A.Meldrum, W.J.Shi, B.T.Meggitt, A.W.Palmer, K.T.V.Grattan and L.Li, Bragg grating sensing instrument using a tuneable Fabry-Perot filter to detect wavelength variations, *Meas. Sci. Technol.* 9, 599-606 (1998)

[12] Z.Y.Zhang, K.T.V.Grattan, Y.Hu, A.W.Palmer and B.T.Meggitt, Prony's method for exponential lifetime estimations in fluorescence-based thermometers, *Rev. Sci. Instrum.* 67, 2590 (1996)

[13] Z.Y.Zhang, K.T.V.Grattan, A.W.Palmer, B.T.Meggitt, and T.Sun, Characterization of erbium-doped intrinsic optical fiber sensor probes at high temperatures, *Rev. Sci. Instrum.* 69, 2924 (1998)

[14] T.Sun, Z.Y.Zhang and K.T.V.Grattan, Erbium/ytterbium fluorescence based fiber optic temperature sensor system, *Rev. Sci. Instrum.* 71, 4017-22 (2000)

Chapter 4 Fluorescence based temperature and strain measurement incorporating FBG experimental results

- [15] A.Othonos, *Fiber Bragg gratings*, in *Optical Fiber Sensor Technology: Advanced Applications*, K.T.V.Grattan and B.T.Meggitt eds., pp. 113 - 115 (Kluwer Academic Publishers, Dordrecht, Netherlands, 2000)
- [16] M.Winz, K.Stump and T.K.Plant, High Temperature, Stable Fiber Bragg Gratings, in *Proceedings of 15th Optical Fiber Sensors Conference Technical Digest (published by IEEE), Portland, USA*, pp. 195 - 198 (2002)
- [17] D.Razafimahatratra, P.Niay, M.Douay, B.Poumellec and I.Riant, Comparison of isochronal and isothermal decays of Bragg gratings written through continuous-wave exposure of an unloaded germanosilicate fiber, *Appl. Opt.* 39, 12, 1924 (2000)
- [18] S.Kannan, J.Z.Y.Guo and P.Lemaire, Thermal Stability Analysis of UV – Induced Fiber Bragg Gratings, *J. Lightwave Tech.* 15, 8, 1478 (1997)
- [19] B.Guan, H.Tam, X.Tao and X.Dong, Highly Stable Fiber Bragg Gratings Written in Hydrogen – Loaded Fiber, *IEEE Photon. Technol. Lett.* 12, 10, 1349 (2000)
- [20] S.Pal, J.Mandal, T.Sun and K.T.V.Grattan, High temperature sensor potential of Bragg gratings fabricated in different photosensitive fibres, to be presented at *Applied Optics and Optoelectronics Conference, Cardiff* (2002)
- [21] R.Kashyap, *Fiber Bragg Gratings*, pp.409 – 446, Academic Press (1999)
- [22] T.Erdogan, V.Mizrahi, P.J.Lemaire and D.Monroe, Decay of ultraviolet-induced fiber Bragg gratings, *J. Appl. Phys.* 76, 1, 73 (1994)
- [23] T.Sun, Z.Y.Zhang, K.T.V.Grattan and A.W.Palmer, Intrinsic doped fluorescence decay-time based measurements - strain and temperature characteristics for sensor purposes *Rev. Sci. Instrum.*, 69, 4186 (1998)

Chapter 4 Fluorescence based temperature and strain measurement incorporating FBG experimental results

[24] T.Sun, Z.Y.Zhang, K.T.V.Grattan and A.W.Palmer, Intrinsic strain and temperature characteristics of Yb-doped silica-based optical fibers, *Rev. Sci. Instrum.*, 70, 1447 (1999)

Chapter 5

Conclusions and future work

5.1 Abstract

This chapter contains a summary of the work presented in this thesis. The author's opinion on the achievements made from the work herein are given. Then, current trends in fluorescence lifetime-based sensing are discussed, both commercially and academically, together with projected work for the future.

5.2 Summary of achievements

The results of work done in this thesis are believed to match well the original aims and objectives, as described at the end of Chapter 1. Major achievements made in this work are seen as:

- the “state-of-the-art” in fibre-optical sensing has been reviewed and reported on, with particular emphasis on developments in temperature and strain measurement techniques so as to be relevant to the work done for this thesis
- a review of current and former fibre temperature-strain discrimination techniques, for application to dual/simultaneous temperature/strain measurement, reported from various groups has been given
- a characterisation of the fluorescent lifetime properties of several rare earth fibre dopants for application to temperature and strain monitoring: Er^{3+} , Nd^{3+} , $\text{Er}^{3+} \text{Yb}^{3+}$, $\text{Tm}^{3+} \text{Ho}^{3+}$, and $\text{Y}_2\text{O}_3:\text{Tm}^{3+}$ powder
- the strain sensitivity of the fluorescence lifetimes of these materials has been quantified, using linear analyses, over the region from 0 to 2000 $\mu\epsilon$, and has been discussed extensively in this work. The subsequent correction factors for intended thermometric applications in environments which may be affected by strain have been analysed for each material case

- a greater understanding of the strain effect on the measured fluorescent lifetime for the purposes of possible simultaneous temperature-strain sensing using deconvolution methods, e.g. in systems with two differently doped fibres. Since both the temperature and possibly the strain effect are non-linear, the error propagation has been shown to be very large for this type of approach and therefore more effective and complimentary use can be made by combining fluorescent lifetime with another type of highly linear sensor to achieve this end (i.e. FBG)
- modelling of some of the experimental results obtained for the temperature dependence of the fluorescence lifetime (using data from $\text{Y}_2\text{O}_3:\text{Tm}^{3+}$ powder probe) and also modelling of the strain dependence of fluorescence lifetime (in conjunction with the *Optical Technology Research Laboratory, Victoria University, Melbourne, Australia* [1]) using Nd^{3+} to better understand these dependencies, and suggested reasons for the occurrence of the latter have been given
- unique combinations of fluorescence lifetime with FBG, utilising generated fluorescence to act as interrogation source to an FBG, have been successfully achieved for the first time, thus laying the foundations for future work using more compact and effective similar schemes
- high temperature effects on FBG performance have been observed over a very long period of almost 7 weeks and results reported

- effects of thermal annealing, sensor lengths and pump power on the measured fluorescence intensity and lifetime have been investigated for a range of materials, and the results reported.

5.3 Current and future exponents of the fluorescent lifetime

5.3.1 Commercial uses

In the last twenty years, fluorescence spectroscopy has evolved into a powerful tool for the study of chemical, semiconductor, photochemical, and biochemical species [2]. Using a measure of fluorescent lifetime of various materials in a variety of situations, it can provide insight into such intimate processes as solvent-solute interactions, the structure and dynamics of nucleic acids, and the permeability of membranes.

Time-resolved fluorescence measurements are now routine in many laboratories [3]. Modern time-domain and frequency-domain instrumentation, combined with laser light sources, provides resolution of complex intensity and anisotropy decays. Advances in instrumentation, laser technology, fibre-optics and especially selective and sensitive probes can result in the rapid migration of time-resolved fluorescence to clinical chemistry, environmental remote sensing and industrial applications. To date, lifetime probes for analyte recognition (binding) have been identified for Ca^{2+} , Mg^{2+} , Na, K, and pH. Fluorescence lifetime imaging (FLIM) can reveal the local chemical composition and properties of the molecular environment that surrounds the probe in 2D chemical image.

Chapter 5 Conclusions and future work

The fluorescence lifetime method allows the sensing of analytes for which there are no direct probes, like glucose, antigens, or any affinity or immunoassays based on fluorescence energy transfer as a transduction mechanism. Recent development of probes based on transition metal-ligand fluorophores can result in an inexpensive instrumentation with light-emitting diodes (LED) as a light sources for several clinical important analytes like O₂, pH, CO₂.

For thermometric applications, *Luxtron* currently produce several commercial devices which utilise the fluorescent lifetime measurement technique (as opposed to the previously mentioned *Accufiber® models 10 and 100* devices which both use black-body radiation methods) for temperature measurement. Their present *Fluoroptic* thermometer product range [4] consists of;

- model 790 (general use)
- model WTS-11 (power transformers)
- model 3100 (biomedical)
- series 500 (OEM industrial, microwave).

These instruments feature patented fibre-optic probes that use the fluorescence of phosphor materials at their tips to sense temperatures. They are described as being highly accurate, intrinsically safe devices, immune to electromagnetic interference, and operate within the -200°C to 450°C range. For example, the 790 model - in the basic patented technology a temperature sensitive phosphor is affixed to the end of a quartz optical fibre, which is connected to the instrument. Blue-violet light pulses are sent down the fibre causing the phosphor to glow. The decay of the fluorescence after each pulse varies with temperature, providing the basis for the measurement at the sensor to a reported accuracy of $\pm 0.1^\circ\text{C}$. The

fluorescent decay time is measured by a multi-point digital integration of the decay curve method. The same optical fibre transmits the excitation pulses and returns of the fluorescent signal.

5.3.2 Academic uses

Fernicola and co-workers [5] continue to use fluorescent lifetime measurement applied to fibre optic thermometry and, more recently, to surface temperature measurement [6]. Fluorescent decay times are also currently being used by several groups in chemical sensing to detect pH, with the lifetimes being used tending to be much smaller than those used in temperature sensing [7, 8]. Since the termination of the practical work for this thesis, there are now several projects underway at City University, London, UK which use (or will use) the fluorescent lifetime measurement technique, some of which are continuing certain achievements in this thesis. These include on-going work on:

- **fire alarm development** – this work is developing from the previously published work [9] which uses the lifetime technique to monitor a “fire alarm”. The main features of this system are:
 - an “on” condition of an excursion of 50°C above ambient, which itself can rise to 300°C
 - the use of Prony's method [10] to extract the two decay times from a signal received from a 1 m length of Nd³⁺ doped fibre pumped by a 785 nm source

- the two separated signals represent the two lifetimes and temperatures \therefore the ambient and the hot spot temperature can be received
 - the system does not locate the hot spot exactly, since there is no need to, therefore it is much cheaper than Raman distributed systems [11]
 - future work is focused on extending the sensing length of the doped fibre from 1 m to 3 m (there is also currently a problem with the absorption of the fibre at 785 nm) and to improve the resolution.
- **Tm³⁺: YAG crystal fibre** - work has been done on extending the range of a Tm³⁺ doped YAG crystal fibre sensor, which utilises a cross detection technique for the fluorescent decay and background radiation, from room temperature to over 1600°C. The detection system uses a PLD signal processing system [12] for the fluorescence and a compensation current for the background radiation. Preliminary results [13] show a resolution better than 1°C in the range up to 1200°C after an annealing of the probe was undertaken.
 - **chemical sensors** - one of the aims of on-going current work is to combine the lifetime technique with a sol-gel coated fibre optic chemical sensor in order to measure the ambient pH of concrete. When the pH of the concrete changes, the lifetime of an embedded sol-gel smart sensor will change [7, 14].
 - **FBGs** - one of the major achievements of the work using FBG in this thesis has been to combine it with the fluorescent lifetime technique for the first time to achieve dual

temperature/strain sensing. This work will be continued to develop the sensor scheme into a more “truly” simultaneous sensor in the sense that a more direct and synchronous recovery of the two variables may be instantaneously taken, possibly with more resolution (perhaps achieved through non-linear data analysis techniques) than before. Also from work in this thesis, there is a continuation of the FBG high temperature work: my colleagues are now fabricating type-I and IIA gratings into different photosensitive fibres such as B-Ge co-doped silica fibre, Ge-doped silica fibre, Sn-doped germanosilicate fibre and Er, Sn-doped germanosilicate fibres. So far [15, 16] they have tested thermal decays of type-I and IIA in B-Ge co-doped and Ge-doped fibres and observed that the type-I and IIA FBGs of the B-Ge co-doped fibre survived up to 250 and 400°C, after which the rapid decays started. Type-I and IIA FBGs of Ge-doped fibre survived up to 600 and 650°C, with approx. 50% of their NICC (i.e. normalised integrated coupling constant – see Chapter 4), and are being further tested for repeatability. They will also be looking at the high temperature potential of the Sn-doped samples.

5.4 References

- [1] S.F.Collins, P.M.Farrell, S.A.Wade, G.W.Baxter, D.A.Simpson, A.J.Stevenson, K.T.V.Grattan and D.I.Forsyth, Modelling Strain Dependence of Fluorescence from Doped Optical Fibres: Application to Neodymium, in *Proceedings of 15th Optical Fiber Sensors Conference Technical Digest (published by IEEE), Portland, USA*, pp. 439 - 442 (2002)
- [2] About Fluorescence Index, <http://www.pti-nj.com>, Photon Technology International (1999)

- [3] Fluorescence Lifetime Technology: Application to Clinical and Biological Chemical Sensing and Imaging, <http://www.spie.org>, The International Society for Optical Engineering (2000)
- [4] Data sheet from Orbis Technologies Ltd, www.orbitech.co.uk/lux10.html (2002)
- [5] L.Rosso, V.Fernicola and Y.Shen, Cr-doped Sapphire Fibre Sensor for Fluorescence Thermometry, in Proc. 8th International Symposium on Temperature and Thermal Measurements in Industry and Science (TEMPMEKO 2001), Vol. 2, pp. 949-954, Berlin, Germany (2001)
- [6] V.Fernicola *et al*, to be presented at the Temperature Symposium, Chicago (2002)
- [7] V.Misra, H.Mishra, H.C.Joshi and T.C.Pant, An optical pH sensor based on excitation energy transfer in Nafion® film, *Sensors and Actuators B*, 82, 133 (2002)
- [8] E.A.Austin, J.P.Dakin and A.P.Strong, Use of transition-metal-doped sapphire crystals to calibrate and thermally compensate fluorescent-lifetime chemical detectors, Europt(R)ode V Lyon 16-19 Apr 2000 PKC9 (published by ORC, University of Southampton)
- [9] T.Sun, K.T.V.Grattan and W.M.Sun, Fluorescence based optical fibre fire alarm system, in *Proceedings of 15th Optical Fiber Sensors Conference Technical Digest (published by IEEE), Portland, USA*, pp. 471 - 474 (2002)
- [10] Z.Y.Zhang, K.T.V.Grattan, Y.Hu, A.W.Palmer and B.T.Meggitt, Prony's method for exponential lifetime estimations in fluorescence-based thermometers, *Rev. Sci. Instrum.*, 67, 2590 (1996)
- [11] R.M.Odic, R.I.Jones and R.P.Tatam, Distributed Temperature Sensor for Aeronautic Applications, in *Proceedings of 15th Optical Fiber Sensors Conference Technical Digest (published by IEEE), Portland, USA*, pp. 459 - 462 (2002)

Chapter 5 Conclusions and future work

- [12] Z.Y.Zhang, K.T.V.Grattan and A.W.Palmer, Phase-locked detection of fluorescence lifetime, *Rev. Sci. Instrum.* 64, 2531 (1993)
- [13] Y.Shen, W.Zhao, J.He, T.Sun and K.T.V.Grattan, to be presented at *APOC2002, Shanghai, PRC* (October 2002)
- [14] O.S.Wolfbeis, Novel Techniques and Materials for Fiber Optic Chemical sensing, *Optical Fiber Sensors: Proceedings of the 6th International Conference*, eds. H.J.Arditty, J.P.Dakin and R.Th.Kersten, Springer-Verlag Berlin Heidelberg, pp. 416 - 424 (1989)
- [15] T.Sun, D.I.Forsyth, S.A.Wade, S.Pal, J.Mandal, W.D.N.Pritchard, G.Garnham and K.T.V.Grattan, Fibre Bragg Grating coupled fluorescent optical fibre sensors, to be presented at *1st International Conference on Optical and Laser Diagnostics (ICOLAD 2002)*, 16-20 December 2002, City University, London, UK
- [16] S.Pal, J.Mandal, T.Sun and K.T.V.Grattan, High temperature sensor potential of Bragg gratings fabricated in different photosensitive fibres, to be presented at *Applied Optics and Optoelectronics Conference, Cardiff* (2002)

Publications arising from thesis

Journal papers

1. A.Arnaud, **D.I.Forsyth**, T.Sun, Z.Y.Zhang and K.T.V.Grattan, Strain and temperature effects on Erbium-doped fiber for decay-time based sensing, *Rev. Sci. Instrum.*, 71, 104 (2000)
2. S. A.Wade, **D.I.Forsyth**, Q.Guofu and K.T.V.Grattan, Fiber optic sensor for dual measurement of temperature and strain using a combined fluorescence lifetime decay and fiber Bragg grating technique, *Rev. Sci. Instrum.*, 72, 3186 (2001)
3. S.A.Wade, **D.I.Forsyth**, Q.Guofu, X.Chen, T.S.Chuan, W.Yong, T.Sun and K.T.V.Grattan, Dual measurement of strain and temperature using the combination of Er³⁺-doped fibre fluorescence lifetime and a fibre bragg grating, *Meas. Control*, 34, 175 (2001)
4. **David I. Forsyth**, Scott A. Wade, Tong Sun, Xiaomei Chen and Kenneth T. V. Grattan, Dual temperature and strain measurement using the combined fluorescence lifetime and Bragg wavelength shift approach in doped optical fiber, accepted for publication (June 2002) in *APPLIED OPTICS*

Conference papers

1. A.Arnaud, **D.I.Forsyth**, T.Sun, Z.Y.Zhang and K.T.V.Grattan, Er-doped fibre based fluorescence thermometry - effects of fibre strain on system performance, in *Proceedings of Sensors and their Applications X*, N.M.White and A.T.Augousti eds. (IOP Publishing Ltd, London), pp. 63 - 68 (1999)

Publications arising from thesis

2. S.J.Zhang, **D.I.Forsyth**, T.Sun, Z.Y.Zhang and K.T.V.Grattan, Tm/Ho co-doped optical fibre sensor - strain and temperature characteristics of a sensor probe, in *Proceedings of 14th International Conference on Optical Fibre Sensors, Venice, Italy*, SPIE Vol. 4185, pp. 154 - 167 (2000)
3. S.A.Wade, **D.I.Forsyth**, Q.Guofu, X.Chen, T.S.Chuan, W.Yong, T.Sun and K.T.V.Grattan, Dual measurement of strain and temperature using the combination of Er³⁺-doped fibre fluorescence lifetime and a fibre Bragg grating, in *Proceedings of Sensors and their Applications XI*, K.T.V.Grattan and S.H.Khan eds. (IOP Publishing Ltd, London), pp. 309 - 314 (2001)
4. **D.I.Forsyth**, S.A.Wade, D.Perciante and K.T.V.Grattan, Temperature and strain characteristics of the ³F₄ and ³H₄ energy levels of Tm:Ho co-doped fibre, in *Proceedings of Sensors and their Applications XI*, K.T.V.Grattan and S.H.Khan eds. (IOP Publishing Ltd, London), pp. 365 - 370 (2001)
5. K.T.V.Grattan, S.A.Wade, **D.I.Forsyth**, T.Sun and X.Chen, Combined fluorescence decay-time and fiber Bragg grating temperature and strain sensing, in Proceedings of SPIE Vol 4596, *Advanced Photonic Sensors and Applications II, 27-30 November, Singapore* pp. 90 - 96 (2001)
6. T.Sun, K.T.V.Grattan, S.A.Wade, **D.I.Forsyth**, Silica optical fiber based rare-earth doped sensors, in Proceedings of SPIE Vol 4596, *Advanced Photonic Sensors and Applications II, 27-30 November, Singapore* pp. 219 - 229 (2001)

Publications arising from thesis

7. K.T.V.Grattan, T.Sun, S.A.Wade, Z.Y.Zhang, **D.I.Forsyth** and W.M.Sun, Optical fiber fluorescence-based sensor techniques for high temperature measurement, in *Proceedings of 1st International Symposium on Optical and Quantum Technology*, 7-8th December, Department of Applied Physics, Faculty of Science, KMITL, Bangkok, Thailand, pp. 8 – 16 (2001)

8. T.Sun, K.T.V.Grattan, S.A.Wade, **D.I.Forsyth** and W.M.Sun, Silica optical fibre based temperature and strain sensors, in *Proceedings of 1st International Symposium on Optical and Quantum Technology*, 7-8th December, Department of Applied Physics, Faculty of Science, KMITL, Bangkok, Thailand, pp. 24 - 34 (2001)

9. S.F.Collins, P.M.Farrell, S.A.Wade, G.W.Baxter, D.A.Simpson, A.J.Stevenson, K.T.V. Grattan and **D.I.Forsyth**, Modelling Strain Dependence of Fluorescence from Doped Optical Fibres: Application to Neodymium, in *Proceedings of 15th Optical Fiber Sensors Conference Technical Digest (published by IEEE), Portland, USA*, pp. 439 - 442 (2002)

10. T.Sun, **D.I.Forsyth**, S.A.Wade, S.Pal, J.Mandal, W.D.N.Pritchard, G.Garnham and K.T.V.Grattan, Fibre Bragg Grating coupled fluorescent optical fibre sensors, to be presented at *1st International Conference on Optical and Laser Diagnostics (ICOLAD 2002)*, 16-20 December 2002, City University, London, UK

Publications arising from thesis

Others

D.I.Forsyth, S.A.Wade, T.Sun and K.T.V.Grattan, Dual temperature and strain measurement using combined Bragg grating and fluorescence characteristics in optical fibres, in Abstracts and Programme of *In-Fibre Bragg Gratings and Special Fibres*, meeting organised by the Institute of Physics (IOP) UK, 17 October 2001, Coventry, UK